

Design and evaluation of a vibration ore flow restore machine

BJ Meiring

 orcid.org/0000-0001-8129-4407

Dissertation accepted in fulfilment of the requirements for the degree *Master of Engineering in Mechanical Engineering* at the North-West University

Supervisor: Prof. Martin van Eldik

Co-supervisor: Dr. Barend Botha

Graduation: December 2021

Student number: 24309869

ABSTRACT

Ore passes provide a low cost method for gravitational transport of broken ore and waste rock through long vertical distances to lower levels of an underground mine. A hang-up or blockage in an ore pass is undesirable as it may lead to loss of productivity and a heavy financial cost to restore flow. This study focuses on methods to restore the flow of ore after a blockage occurs, specifically by designing an ore flow restoring machine that use vibration and building a physical machine to test the design.

Mathematical models were developed to analyse the design of the proposed ore flow restore machine. This was regarded necessary to investigate whether the ore flow restore machine is capable of unblocking a blockage in an ore pass. Two three-degree-of-freedom mathematical models were developed to predict the dynamic displacements, dynamic forces and system natural frequencies for the ore flow restore machine for different operating conditions. These mathematical models were implemented in computer programs.

A Finite Element Analysis (FEA) approach was used to analyse whether the design was free of structural resonance. An FEA approach was also used to determine the dynamic material stresses of the design when operating with and without steel cables. The design was deemed acceptable to build and evaluate experimentally.

The input parameters required for the computer programs were characterised. Different mathematical models were developed for characterisation of the machine rubber mount vertical and horizontal dynamic properties. Measured data served as inputs and references for these mathematical models. The axial stiffness of the steel cable combination was validated with in-situ measured data. The operating frequency of the machine was also characterised, as was the size of the sample rocks used for experimental evaluation.

The unblocking of interlocking and cemented blockages was evaluated for two possible unblocking methods: steel cables and a hammer. The underlying three-degree-of-freedom mathematical models for the ore flow machine were experimentally validated. The predicted response, transmitted forces and natural frequencies were compared to the respective corresponding measured values. This was done for the stand-alone machine, where the steel cables were removed from the machine, and for the machine when the steel cables were caught in a blockage.

Keywords: Ore pass, blockage, unblocking, Ore Flow Restore Machine, characterization, Finite Element Analysis, resonance, evaluation, response, dynamic forces.

OPSOMMING

Ertsgange dien as 'n lae-koste metode om erts en afvalklip deur middel van gravitasie oor lang vertikale afstande te vervoer na laer vlakke in ondergrondse myne. 'n Opeenhoping of blokkasie in 'n ertsgang is ongewens omdat dit lei tot verliese en hoë finansiële koste om weer die vloei van erts te herstel. Hierdie studie sal fokus op metodes om die vloei van erts te herstel nadat 'n blokkasie plaasgevind het, spesifiek deur die ontwerp van 'n masjien wat ertsvloei herstel d.m.v. vibrasie en die validasie daarvan deur die masjien prakties te bou en te toets.

Wiskundige modelle is ontwikkel om die ontwerp van die Ertsvloei Herstel Masjien te analiseer. Dis was nodig om dit bepaal of die masjien in staat sou wees om 'n blokkasie in 'n ertspas te ontblok. Twee drievryheidsgraad wiskundige modelle is ontwikkel om die dinamiese verplasinge, dinamiese kragte en die natuurlike frekwensies van die sisteem, vir twee verskillende operasionele kondisies, te voorspel. Hierdie wiskundige modelle is geïmplementeer in rekenaarprogramme.

'n Eindige Element Analise (EEA) benadering is gevolg om te bepaal of die ontwerp vry is van strukturele resonansie. 'n EEA benadering is ook gevolg om die dinamiese materiaal stres te bepaal van die ontwerp tydens bedryf, met en sonder staal kables. Die ontwerp was voldoende om gebou en eksperimenteel geëvalueer te word.

Die inset parameters wat benodig word deur die rekenaarprogramme is gekarakteriseer. Verskillende wiskundige modelle is ontwikkel vir die karakterisering van die monterestukke se vertikale en horisontale dinamiese eienskappe. Gemete data het gedien as inset en verwysingswaardes vir die genoemde wiskundige modelle. Die aksiale styfheid van die staalkabel kombinasie is gevalideer teenoor in-situ gemete data. Die operasionele frekwensie van die masjien is ook gekarakteriseer, sowel as die grootte van die proefklippe wat gebruik is vir eksperimentele evaluering.

Die ontblokking van aaneengeskakelde en gesementeerde blokkasies is getoets met twee moontlike ontblokkingsmetodes: staalkables en 'n hamer. Die onderliggende drievryheidsgraad wiskundige modelle vir die Ertsvloei Herstel Masjien is eksperimenteel gevalideer. Die voorspelde respons, oordraagbare kragte en natuurlike frekwensies is vergelyk met die ooreenstemmende gemete waardes. Dit is gedoen vir die alleenstaande masjien, wanneer die staal kables van die masjien ontkoppel was, en ook vir wanneer die staalkables in 'n blokkasie vasgevang is.

Sleutelwoorde: Ertsgang, blokkasie, ontblokking, Erts Vloei Herstel Masjien, karakterisering, Eindige Element Analise, resonansie, evaluering, respons, dinamiese kragte

DECLARATION

I, Barend Jacobus Meiring, hereby declare that the material used in this study is my own original work, except where specifically referred to by name, or in the form of a reference. This work has not been submitted to any other university.

Barend Meiring

Student number: 24309869

Identity number: 9401215020083

ACKNOWLEDGEMENTS

- Prof Martin van Eldik and Dr Barend Botha for their guidance to complete my masters
- Mr Sarel Naudé, Mr Thabo Diobe and Mr Willem van Tonder with their assistance in and around the laboratory
- Mr Bartlo van der Merwe and Mr André Fourie for their aid with manufacturing
- Mr Johann Bloem, Mr Johan de Beer and Mr Braam Labuschagne for their assistance and guidance
- Mr Christo Botes and Mr Werner Greyling for their help in the laboratory
- Miss Heleen Vermeulen with financial admin assistance
- OMV Crushers for sponsoring rock samples
- Potch Rubber for sponsoring conveyer belts
- Vesco Plastics Sales for sponsoring a Vesconite cylinder

TABLE OF CONTENTS

Abstract	i
Opsomming	ii
Declaration	iii
Acknowledgements	iv
Table of contents	v
List of tables	ix
List of figures	xi
Nomenclature	xx
1 Introduction and literature overview	1-1
1.1 Background	1-1
1.1.1 Hang-ups and blockages	1-1
1.1.2 Hang-ups in ore passes.....	1-2
1.1.3 Blockages in ore passes.....	1-3
1.2 Problem statement	1-4
1.3 Purpose of the study.....	1-4
1.4 Scope of work.....	1-4
2 Literature survey	2-6
2.1 Introduction.....	2-6
2.2 Methods to prevent hang-ups and blockages	2-6
2.3 Methods for restoring flow.....	2-7
2.3.1 Water methods	2-7
2.3.2 Explosive methods	2-11
2.3.3 Mechanical methods.....	2-18
2.4 Vibration ore-drawing on ore passes	2-18
2.5 Conclusion.....	2-19
3 Concept design	3-21
3.1 Introduction.....	3-21
3.2 Brief concept evaluation description and selection.....	3-21
3.3 Mathematical modelling	3-23

3.3.1	Three-degree-of-freedom mathematical model - stand-alone machine	3-24
3.3.1.1	Natural frequencies of machine as rigid body supported by elastic mounts	3-27
3.3.1.2	Dynamic forces transmitted through rubber mounts.....	3-27
3.3.1.3	Force exerted by hammer.....	3-29
3.3.2	Three-degree-of-freedom mathematical model – steel cables	3-30
3.3.2.1	Natural frequencies of machine as rigid body supported by elastic mounts with steel cables.....	3-31
3.3.2.2	Force transmitted through steel cables	3-32
3.3.3	Characterization of dynamic mount properties	3-33
3.3.3.1	Bump test	3-33
3.4	Computer implementation.....	3-34
3.4.1	Introduction.....	3-34
3.4.2	Three-degree-of-freedom mathematical model - stand-alone machine	3-34
3.4.3	Three-degree-of-freedom mathematical model - steel cables	3-35
3.4.4	Characterization of mount dynamic properties	3-36
3.5	Concluding remarks.....	3-37
4	Finite element analysis.....	4-38
4.1	Introduction.....	4-38
4.2	Modal analysis.....	4-38
4.3	Dynamic stress analysis	4-41
4.3.1	Stand-alone machine.....	4-42
4.3.2	Steel cables acting as springs	4-44
4.4	Conclusion.....	4-47
5	Experimental characterisation	5-48
5.1	Introduction.....	5-48
5.2	Machine mass	5-48
5.3	Rubber mounts dynamic properties	5-51
5.4	Stiffness of extension spring and steel cable	5-56
5.5	Motor excitation force	5-57
5.6	Rock sample size	5-59

5.7	Conclusion.....	5-62
6	Experimental evaluation	6-63
6.1	Introduction.....	6-63
6.2	Vibration measurements.....	6-63
6.3	Stand-alone machine response	6-64
6.3.1	Steady state response	6-65
6.3.2	Comparison between predicted and measured responses.....	6-67
6.4	Steel cables acting as springs	6-68
6.4.1	Steady state response	6-71
6.4.2	Comparison between predicted and measured responses.....	6-73
6.5	Hammer operation response	6-74
6.6	Stand-alone machine forces	6-78
6.6.1	Steady state dynamic forces.....	6-78
6.6.2	Comparison between predicted and measured dynamic forces	6-79
6.7	Steel cables acting as springs forces.....	6-79
6.7.1	Steady state dynamic forces.....	6-80
6.7.2	Comparison between predicted and measured dynamic forces	6-80
6.8	Hammer operation forces	6-81
6.9	Machine natural frequencies.....	6-82
6.9.1	Stand-alone machine - natural frequencies.....	6-82
6.9.2	Steel cables acting as springs - natural frequencies	6-86
6.9.3	Comparison between predicted and measured natural frequencies.....	6-90
6.10	Machine operation	6-91
6.10.1	Steel cables.....	6-91
6.10.1.1	Dry interlocking blockage.....	6-91
6.10.1.2	Cemented blockage.....	6-96
6.10.2	Hammer.....	6-103
6.10.2.1	Dry interlocking blockage.....	6-103
6.10.2.2	Cemented blockage.....	6-106
6.10.3	Constant load unblocking method.....	6-110
6.10.3.1	Constant load method with addition of water	6-115
6.11	Conclusion and discussion of results	6-119

7	Conclusions	7-120
7.1	Suggestions for further study	7-121
	References.....	7-123
	Appendix A – Matlab® computer programs	7-124
	Appendix B – Photos of experimental work	7-136
	Appendix C – Rubber mount specifications.....	7-142
	Appendix D – Excitation motor specifications	7-144
	Appendix E – Permission to use figures from articles	7-145
	Appendix F – Detailed drawings.....	7-148
	Appendix G – Language editing declaration	7-188

LIST OF TABLES

Table 4.1: Summary of the calculated and simulated natural frequencies for the stand-alone machine..... 4-41

Table 5.1: Summary of the horizontal characterised properties for the rubber mounts..... 5-53

Table 5.2: Summary of the vertical characterized properties for the rubber mounts..... 5-55

Table 5.3: Comparison of natural frequencies for machine when steel cables are caught in a blockage. 5-57

Table 6.1: Summary of the predicted and measured response amplitudes of the stand-alone machine..... 6-67

Table 6.2: Summary of the predicted and measured response amplitudes of the machine when steel cables act as additional springs. 6-73

Table 6.3: Summary of the measured response amplitudes of the machine while operating the hammer with and without being in contact with the blocked sample rock. 6-78

Table 6.4: Comparison of predicted and measured horizontal steady state dynamic forces..... 6-78

Table 6.5: Comparison of predicted and measured vertical steady state dynamic forces..... 6-79

Table 6.6: Summary of the predicted and measured dynamic forces during steady state operation for stand-alone machine. 6-79

Table 6.7: Comparison of predicted and measured horizontal steady state dynamic forces for steel cables. 6-80

Table 6.8: Comparison of predicted and measured vertical steady state dynamic forces for steel cables. 6-80

Table 6.9: Summary of the predicted and measured dynamic forces during steady state operation for the machine when the steel cables act as springs. 6-81

Table 6.10:	Measured horizontal and vertical steady state dynamic forces with hammer not in contact with rock.....	6-81
Table 6.11:	Measured horizontal and vertical steady state dynamic forces with hammer in contact with rock.....	6-82
Table 6.12:	Comparison of the measured dynamic forces during steady state operation for the machine when the hammer is in contact with, and not in contact with blocked sample rock.	6-82
Table 6.13:	Summary of natural frequencies for stand-alone machine.....	6-91
Table 6.14:	Summary of natural frequencies for machine when steel cables act as additional springs.	6-91
Table 6.15:	Summary of dry interlocking unblocking tests for steel cables.	6-96
Table 6.16:	Summary of cemented unblocking tests for the steel cables.	6-103
Table 6.17:	Summary of dry interlocking unblocking tests for the hammer.....	6-106
Table 6.18:	Summary of the cemented unblocking tests for the hammer.	6-110
Table 6.19:	Summary of the constant load unblocking tests for dry interlocking blockages.....	6-114
Table 6.20:	Summary of the constant load tests for unblocking wet interlocking blockages.....	6-118

LIST OF FIGURES

Figure 1-1:	A schematic illustration of impediments to flow in an ore pass due to: left: Interlocking arching, right: Cohesive arching (Hadjigeorgiou & Lessard, 2010).	1-2
Figure 1-2:	A photo of a large rock blocking an ore pass and causing a restriction to the flow of ore and waste rock (Szwedzicki, 2007).	1-3
Figure 2-1:	Presentation of different screening methods: a) Grizzly, b) Scalper, c) Mantle and d) No screening (Hadjigeorgiou & Lessard, 2007).	2-6
Figure 2-2:	Representation of the introduction of water from above the hang-up or blockage (Hadjigeorgiou & Lessard, 2010).	2-9
Figure 2-3:	Representation of the introduction of water below the blockage. (Hadjigeorgiou & Lessard, 2010).	2-10
Figure 2-4:	Presentation of drilling holes into a boulder wedge at the tipping point of a finger raise (Hadjigeorgiou & Lessard, 2010).	2-12
Figure 2-5:	Representation of a Sputnik (Hadjigeorgiou & Lessard, 2010).	2-13
Figure 2-6:	Presentation of manual positioning of a Sputnik when the workers are protected by control chains (Hadjigeorgiou & Lessard, 2010).	2-13
Figure 2-7:	Presentation of remote positioning of a Sputnik by means of a loading-hauling-dumping (LHD) unit (Hadjigeorgiou & Lessard, 2010). .	2-14
Figure 2-8:	Presentation of launching a Sputnik where the tipping point is used as a launch pad (Hadjigeorgiou & Lessard, 2010).	2-14
Figure 2-9:	Presentation of positioning explosives near the hang-up by means of a pushing rod (Hadjigeorgiou & Lessard, 2010).	2-15
Figure 2-10:	Presentation of a rudimentary cart used to assist in the positioning of explosives close to the hang-up (Hadjigeorgiou & Lessard, 2010).	2-16
Figure 2-11:	Presentation of a “Blasting Star” used to assist in the positioning of explosives close to the hang-up (Hadjigeorgiou & Lessard, 2010).	2-16
Figure 2-12:	A photo displaying a Quickdraw cannon (Szwedzicki, 2007).	2-17

Figure 2-13:	Presentation of a long-hole drilling design to clear a hang-up within a long ore pass (Szwedzicki, 2007).....	2-18
Figure 2-14:	Presentation of a VOM installed at an ore pass (Wu & Sun, 2008).....	2-19
Figure 3-1:	Representation of the first concept design.	3-22
Figure 3-2:	Representation of the second concept design.....	3-23
Figure 3-3:	Three-degree-of-freedom model for stand-alone machine.....	3-26
Figure 3-4:	Three-degree-of-freedom model for main steel structure when the steel cables act as an additional spring.	3-30
Figure 3-5:	Representation of the flowchart for the computer implementation of the three-degree-of-freedom mathematical model for the machine.	3-35
Figure 3-6:	Representation of the flowchart for the computer implementation of the three-degree-of-freedom mathematical model for the machine when the steel cables are caught in a blockage.	3-36
Figure 3-7:	Representation of the flowchart for the computer implementation of the characterization of the rubber mounts.	3-37
Figure 4-1:	Representation of the translation mode shape along the y-axis at 5,89 Hz.	4-39
Figure 4-2:	Representation of the translation mode shape along the x-axis at 7,80 Hz.	4-39
Figure 4-3:	Representation of the rotational mode shape around the z-axis at 9,51 Hz.	4-39
Figure 4-4:	Representation of the rotational mode shape around the x-axis at 16,19 Hz.	4-40
Figure 4-5:	Representation of the translation mode shape along the z-axis at 18,92 Hz.	4-40
Figure 4-6:	Representation of the rotational mode shape along the y-axis at 22,82 Hz.	4-40
Figure 4-7:	Representation of the structural mode shape at 69,40 Hz.	4-41

Figure 4-8:	Representation of the meshed SOLIDWORKS® CAD model for static load analysis.	4-42
Figure 4-9:	Representation of the result obtained from static load analysis.	4-43
Figure 4-10:	Representation of the point of where the maximum stress is located. ...	4-43
Figure 4-11:	Zoomed-in representation of the point of where the maximum stress is located.....	4-44
Figure 4-12:	Section view of machine to represent the position where the cable force is located.....	4-45
Figure 4-13:	Representation of the meshed SOLIDWORKS® CAD model static load analysis where the steel cables exert force onto machine.	4-45
Figure 4-14:	Representation of the result obtained from the static load analysis where the steel cables exert force onto machine.....	4-46
Figure 4-15:	Representation of the point of where the maximum stress is located. ...	4-46
Figure 4-16:	Zoomed-in representation of the point of where the maximum stress is located.....	4-47
Figure 5-1:	Representation of the process utilised to weigh the machine.	5-49
Figure 5-2:	Representation of weights weighed to determine the accuracy of the load cell.....	5-50
Figure 5-3:	Representation of the turnbuckle, shackles and extension spring weighed by a household scale.	5-51
Figure 5-4:	Representation of the hammer, sleeve and Vesconite bush weighed with a household scale.....	5-51
Figure 5-5:	Stand-alone machine with Diagnostic Instrument coupled, with accelerometers.	5-52
Figure 5-6:	Placement of the accelerometer at the fixing point of the left rubber mounts.....	5-52
Figure 5-7:	Measured horizontal natural frequency for the stand-alone machine.....	5-53

Figure 5-8:	Measured vertical natural frequency for the stand-alone machine.....	5-54
Figure 5-9:	Vertical displacement at different frequencies for the stand-alone machine with a motor inclination of 0° and unbalance of 35%.	5-55
Figure 5-10:	Measured horizontal natural frequency for the machine when steel cables are caught in a blockage.....	5-56
Figure 5-11:	Measured vertical natural frequency for the machine when steel cables are caught in a blockage.....	5-57
Figure 5-12:	One excitation motor of the machine with end caps removed.....	5-58
Figure 5-13:	Close up of the discs forming the unbalance mass of the excitation motor.....	5-59
Figure 5-14:	Representation of the size of the large sample rocks.	5-60
Figure 5-15:	Representation of the size of the large medium sample rocks.....	5-60
Figure 5-16:	Representation of the size of the small medium sample rocks.	5-61
Figure 5-17:	Representation of the size of the small sample rocks.....	5-61
Figure 5-18:	Representation of the size of the fine segregate sample rocks.....	5-61
Figure 6-1:	Experimental test setup of the machine and chute.	6-64
Figure 6-2:	Placement of the accelerometers on the machine.....	6-64
Figure 6-3:	Predicted horizontal steady state response at Mount 2 for the stand-alone machine.....	6-65
Figure 6-4:	Predicted vertical steady state response at Mount 2 for the stand-alone machine.....	6-66
Figure 6-5:	Measured horizontal steady state response at Mount 2 for the stand-alone machine.....	6-66
Figure 6-6:	Measured vertical steady state response at Mount 2 for the stand-alone machine.....	6-67
Figure 6-7:	Representation of cables laid down in the scaled chute.	6-69

Figure 6-8:	Representation of the steel cables attached to the machine.....	6-69
Figure 6-9:	Machine with steel cables attached while caught in a blockage.....	6-70
Figure 6-10:	Representation of the gate removed from the scaled chute.....	6-70
Figure 6-11:	Predicted horizontal steady state response at Mount 2 when steel cables act as springs.....	6-71
Figure 6-12:	Predicted vertical steady state response at Mount 2 when steel cables act as springs.....	6-72
Figure 6-13:	Measured horizontal steady state response at Mount 2 when steel cables act as springs.....	6-72
Figure 6-14:	Measured vertical steady state response at Mount 2 when steel cables act as springs.....	6-73
Figure 6-15:	Machine with M24 threaded rod (hammer) attached.	6-75
Figure 6-16:	Representation of the two hammer conditions.....	6-75
Figure 6-17:	Measured horizontal response at Mount 2 when hammer is not in contact with rock.	6-76
Figure 6-18:	Measured vertical response at Mount 2 when hammer is not in contact with rock.	6-76
Figure 6-19:	Measured horizontal steady state response at Mount 2 hammer is in contact with rock.	6-77
Figure 6-20:	Measured vertical steady state response at Mount 2 when hammer is in contact with rock.....	6-77
Figure 6-21:	Representation of the machine with the side of the machine removed. .	6-83
Figure 6-22:	Measured horizontal natural frequency for the stand-alone machine.....	6-84
Figure 6-23:	Measured vertical natural frequency for the stand-alone machine.....	6-85
Figure 6-24:	Measured rotational natural frequency for the stand-alone machine.	6-86
Figure 6-25:	Representation of the machine with the cables attached and the side of the machine removed.....	6-87

Figure 6-26:	Measured horizontal natural frequency for the machine with cables acting as springs.	6-88
Figure 6-27:	Measured vertical natural frequency for the machine with cables acting as springs.	6-89
Figure 6-28:	Measured rotational natural frequency for the machine with cables acting as springs.	6-90
Figure 6-29:	Blockage created for the first test frequency with the gate of the chute removed.	6-92
Figure 6-30:	Partial unblocking occurred at 18.25 Hz and an unbalance of 77%.	6-93
Figure 6-31:	Measured horizontal response at Mount 2 when steel cables are caught in between rock at an input frequency of 22 Hz and 87% unbalance.	6-94
Figure 6-32:	Measured vertical response at Mount 2 when steel cables are caught in between rock at an input frequency of 22 Hz and 87% unbalance.	6-94
Figure 6-33:	Measured horizontal response at Mount 2 when steel cables are caught in between rock at an input frequency of 20.25 Hz and 94% unbalance.	6-95
Figure 6-34:	Measured vertical response at Mount 2 when steel cables are caught in between rock at an input frequency of 20.25 Hz and 94% unbalance.	6-96
Figure 6-35:	Representation of the mud as poured over the sample rocks.	6-97
Figure 6-36:	Representation of the fine segregated powder with which the mud was created.	6-97
Figure 6-37:	Representation of the mud created to add to the sample rocks.	6-98
Figure 6-38:	Representation of test setup for the first test where steel cables are caught in a cemented blockage.	6-99
Figure 6-39:	Top view of the scaled chute where mud was added and left to dry.	6-99
Figure 6-40:	Blockage created for the first test where cables are caught in a cemented blockage.	6-100

Figure 6-41:	Partial unblocking for the first test at 50% excitation unbalance.	6-100
Figure 6-42:	Partial unblocking for the first test at 64% excitation unbalance.	6-101
Figure 6-43:	Measured horizontal response at Mount 2 when steel cables are caught in a cemented blockage at an input frequency of 20.25 Hz and 77% unbalance.	6-102
Figure 6-44:	Measured vertical response at Mount 2 when steel cables are caught in a cemented blockage at an input frequency of 20.25 Hz and 77% unbalance.	6-102
Figure 6-45:	Blockage created for the first hammer test with the gate of the chute removed.	6-104
Figure 6-46:	Representation of how the hammer made contact with the sample rock.	6-104
Figure 6-47:	Representation of a small partial unblocking at an unbalance of 77%.	6-104
Figure 6-48:	Measured horizontal response at Mount 2 for hammer operation at an input frequency of 18.25 Hz and 94% unbalance.	6-105
Figure 6-49:	Measured vertical response at Mount 2 for hammer operation at an input frequency of 18.25 Hz and 94% unbalance.	6-106
Figure 6-50:	Representation of the mud as poured over the sample rocks.	6-107
Figure 6-51:	Representation of test setup for the first test where the hammer is used for unblocking a cemented blockage.	6-108
Figure 6-52:	Blockage created for the first test where the hammer is used for unblocking a cemented blockage.	6-108
Figure 6-53:	Small partial unblocking for the first test at 94% excitation unbalance.	6-109
Figure 6-54:	Measured horizontal response at Mount 2 for hammer operation at an input frequency of 18.25 Hz and 94% unbalance.	6-109
Figure 6-55:	Measured vertical response at Mount 2 for hammer operation at an input frequency of 18.25 Hz and 94% unbalance.	6-110

Figure 6-56:	Representation of test setup for the constant load test where the steel cables are used for unblocking a dry interlocking blockage.	6-111
Figure 6-57:	Blockage created for the constant load test where the steel cables are used for unblocking a dry interlocking blockage.	6-112
Figure 6-58:	Representation of the blockage after 17 consecutive runs for the constant load method with steel cables.	6-112
Figure 6-59:	Representation of test setup for the constant load test where the hammer is used for unblocking a dry interlocking blockage.	6-113
Figure 6-60:	Blockage created for the constant load test where the hammer is used for unblocking a dry interlocking blockage.	6-113
Figure 6-61:	Representation of a successful unblocking of the blockage by utilizing a constant load method with the hammer operation.	6-114
Figure 6-62:	Representation of test setup for the constant load test where the steel cables are used for unblocking a wet interlocking blockage.	6-115
Figure 6-63:	Blockage created for the constant load test where the steel cables are used for unblocking a wet interlocking blockage.	6-116
Figure 6-64:	Representation of a successful unblocking of the wet interlocking blockage by using a constant load method with the steel cables.	6-116
Figure 6-65:	Representation of test setup for the fatigue based test where the hammer is used for unblocking a wet interlocking blockage.	6-117
Figure 6-66:	Blockage created for the constant load test where the hammer is used for unblocking a wet interlocking blockage.	6-118
Figure 6-67:	Representation of the blockage after 10 consecutive runs.	6-118
Figure 7-1:	Representation of the test setup for the second test frequency where steel cables are caught in a dry interlocking blockage.	7-136
Figure 7-2:	Blockage created for the second test frequency where steel cables are caught in a dry interlocking blockage.	7-136
Figure 7-3:	Representation of the test setup for the third test frequency where steel cables are caught in a dry interlocking blockage.	7-137

Figure 7-4: Blockage created for the third test frequency where steel cables are caught in a dry interlocking blockage. 7-137

Figure 7-5: Partial unblocking occurred at 20.25 Hz and an unbalance of 94 % for the third test frequency where steel cables are used for unblocking a dry interlocking blockage..... 7-138

Figure 7-6: Representation of test setup for the second test where steel cables are caught in a cemented blockage..... 7-138

Figure 7-7: Blockage created for the second test where cables are caught in a cemented blockage. 7-139

Figure 7-8: Partial unblocking for the second test, at 77 % excitation unbalance, where steel cables are used for unblocking a cemented blockage. 7-139

Figure 7-9: Blockage created for the second test where the hammer is for unblocking a dry interlocking blockage..... 7-140

Figure 7-10: Representation of test setup for the second test where the hammer is used for unblocking a cemented blockage. 7-140

Figure 7-11: Blockage created for the second test where the hammer is used for unblocking a cemented blockage. 7-141

Figure 7-12: Small partial unblocking for the second test where the hammer is used for unblocking a cemented blockage at an excitation unbalance of 50 %..... 7-141

NOMENCLATURE

Capital letters

A_c	Cross-section area of steel cable	m^2
E_c	Modulus of elasticity of the steel cable	MPa
F_e	Excitation force produced by excitation motors	N
F_{ex}	Horizontal excitation force	N
F_{ez}	Vertical excitation force	N
ΔF_{sc}	Dynamic force transmitted through the steel cable	N
ΔF_{x1}	Dynamic horizontal force transmitted through Mount 1	N
ΔF_{x2}	Dynamic horizontal force transmitted through Mount 2	N
F_x	Horizontal force amplitude transmitted through mounts	N
F_{x1}	Horizontal force amplitude transmitted through Mount 1	N
F_{x2}	Horizontal force amplitude transmitted through Mount 2	N
ΔF_{z1}	Dynamic vertical force transmitted through Mount 1	N
ΔF_{z2}	Dynamic vertical force transmitted through Mount 2	N
F_z	Vertical force amplitude transmitted through mounts	N
F_{z1}	Vertical force amplitude transmitted through Mount 1	N
F_{z2}	Vertical force amplitude transmitted through Mount 2	N
J_y	Mass moment of inertia about the y axis	kgm^2
K	Stiffness matrix of the system	N/m
L_c	Length of the steel cable	m
M	Mass matrix of the system	kg

M_{ex}	Moment caused by the horizontal excitation force	Nm
M_{ey}	Resultant moment about the y axis	Nm
M_{ez}	Moment caused by the vertical excitation force	Nm
\vec{X}	Mode shape vector	—
ΔX_1	Horizontal response amplitude for Mount 1	m
ΔX_2	Horizontal response amplitude for Mount 2	m
ΔZ_1	Vertical response amplitude for Mount 1	m
ΔZ_2	Vertical response amplitude for Mount 2	m

Lower-case letters

c	Damping in a system	Ns/m
c_c	Critical damping of a system	Ns/m
c_{x1}	Horizontal damping coefficient of Mount 1	Ns/m
c_{x2}	Horizontal damping coefficient of Mount 2	Ns/m
c_{z1}	Vertical damping coefficient of Mount 1	Ns/m
c_{z2}	Vertical damping coefficient of Mount 2	Ns/m
e	Acting point of excitation motors	—
f	Forced frequency	Hz
f_n	Natural frequency	Hz
f_{nx}	Horizontal natural frequency	Hz
f_{nz}	Vertical natural frequency	Hz
g	Centre of gravity of machine	—

g_x	Gravitational constant about x axis	m/s^2
g_z	Gravitational constant about z axis	m/s^2
k	Stiffness	N/m
k_{cable}	Stiffness of steel cables	N/m
k_{spring}	Stiffness of extension springs	N/m
k_{sc}	Axial stiffness of steel cable combination	N/m
k_{scx}	Horizontal stiffness of steel cable combination	N/m
k_{scz}	Vertical stiffness of steel cable combination	N/m
k_{x1}	Horizontal stiffness of Mount 1	N/m
k_{x2}	Horizontal stiffness of Mount 2	N/m
k_{z1}	Vertical stiffness of Mount 1	N/m
k_{z2}	Vertical stiffness of Mount 2	N/m
m	Mass	kg
m_1	Mass of the ore flow restore machine	kg
m_e	Static moment of the excitation motors	kgm
m_u	Unbalance mass of the excitation motors	kg
r_u	Radius at which unbalance mass of the excitation motors are located	m
$\Delta scdisp$	Dynamic deflection of the attachment point of the steel cable	m
t	Time	s
Δx	Dynamic displacement in the horizontal direction	m
Δx_1	Dynamic horizontal displacement at Mount 1	m
Δx_2	Dynamic horizontal displacement at Mount 2	m

Δx_4	Dynamic horizontal displacement of steel cable attachment point	m
$\Delta \dot{x}$	Dynamic velocity in the horizontal direction	m/s
$\Delta \dot{x}_1$	Dynamic horizontal velocity at Mount 1	m/s
$\Delta \dot{x}_2$	Dynamic horizontal velocity at Mount 2	m/s
$\Delta \ddot{x}$	Dynamic acceleration in the horizontal direction	m/s^2
x_1	Horizontal coordinate of Mount 1	m
x_2	Horizontal coordinate of Mount 2	m
x_3	Horizontal coordinate of excitation motors	m
x_4	Horizontal coordinate of steel cable attachment point	m
\ddot{x}_{cg1}	First horizontal acceleration amplitude of the system's centre of gravity	m/s^2
\ddot{x}_{cg2}	Second successive horizontal acceleration amplitude of the system's centre of gravity	m/s^2
Δz	Dynamic displacement in the vertical direction	m
Δz_1	Dynamic vertical displacement at Mount 1	m
Δz_2	Dynamic vertical displacement at Mount 2	m
Δz_4	Dynamic vertical displacement of steel cable attachment point	m
$\Delta \dot{z}$	Dynamic velocity in the vertical direction	m/s
$\Delta \dot{z}_1$	Dynamic vertical velocity at Mount 1	m/s
$\Delta \dot{z}_2$	Dynamic vertical velocity at Mount 2	m/s
$\Delta \ddot{z}$	Dynamic acceleration in the vertical direction	m/s^2
z_1	Vertical coordinate of Mount 1	m

z_2	Vertical coordinate of Mount 2	m
z_3	Vertical coordinate of excitation motors	m
z_4	Vertical coordinate of steel cable attachment point	m
\ddot{z}_{cg1}	First vertical acceleration amplitude of the system's centre of gravity	m/s^2
\ddot{z}_{cg2}	Second successive vertical acceleration amplitude of the system's centre of gravity	m/s^2

Greek symbols

β	Angle of attachment of the excitation motors	<i>degrees</i>
$\Delta\theta_y$	Dynamic rotational displacement about the y axis	<i>rad</i>
$\Delta\dot{\theta}_y$	Dynamic rotational velocity about the y axis	<i>rad/s</i>
$\Delta\ddot{\theta}_y$	Dynamic rotational acceleration about the y axis	<i>rad/s²</i>
ω	Forced rotational speed	<i>rad/s</i>
ω_n	Natural frequency	<i>rad/s</i>
ω_d	Damped frequency	<i>rad/s</i>
φ	Angle of steel cable relative to the z axis	<i>degrees</i>
τ_d	Damped time period	<i>s</i>
ζ	Damping ratio of the rubber mounts	—
ζ_x	Horizontal damping ratio of the rubber mounts	—
ζ_z	Vertical damping ratio of the rubber mounts	—

Abbreviations:

VOM Vibration Ore-drawing Machine

CAD Computer-Aided Design

FEA Finite Element Analysis

NWU North-West University

VSD Variable Speed Drive

1 INTRODUCTION AND LITERATURE OVERVIEW

1.1 Background

Ore passes form part of a system of ore handling. The system of ore handling includes draw points, tips, ore passes and chutes (Stacey & Swart, 1997). Draw points are the location where ore is drawn or extracted, tips are the point where the ore and waste rock are tipped into the ore pass and chutes or boxfronts are used to control flow from ore passes into crushers or trains (Stacey & Swart, 1997). Ore passes provide a low cost method for gravitational transport of broken ore and waste rock through long vertical distances to lower levels of an underground mine (Hadjigeorgiou & Lessard, 2007).

Hang-up and blockage in an ore pass are undesirable as it may lead to loss of productivity and a heavy financial cost to restore flow (Vo *et al.*, 2016). Hang-ups occur anywhere along the length of an ore pass whereas blockages occur at the chute beneath the ore pass (Stacey & Swart, 1997). Hang-ups and blockages can occur either due to interlocking forces, due to cohesion forces or a combination of both (Szwedzicki, 2007).

There are several methods of restoring flow in an ore pass after a hang-up or blockage occur such as those that employ water or air, those that rely on explosives, and mechanical methods (Hadjigeorgiou & Lessard, 2010). Water-based methods are intended to clear cohesive hang-ups, explosive methods are used to clear hang-ups caused by interlocking forces and mechanical methods are used to break large boulders wedged at the tipping point (Hadjigeorgiou & Lessard, 2010). All of the mentioned methods used for removal of hang-ups and blockages can lead to safety problems and/or to a reduction in the life duration of an ore pass (Szwedzicki, 2007).

1.1.1 Hang-ups and blockages

A distinction is made between hang-ups, which occur through the length or at the tipping point of an ore pass, and blockages which occur at the end of an ore pass where the chute is located (Szwedzicki, 2007). Hang-ups and blockages can further be categorized into impediment of flow due to interlocking arching, cohesive arching or a combination of the two (Hadjigeorgiou & Lessard, 2007). Figure 1-1 represents a schematic illustration of a hang-up in an ore pass due to interlocking and cohesive arching.

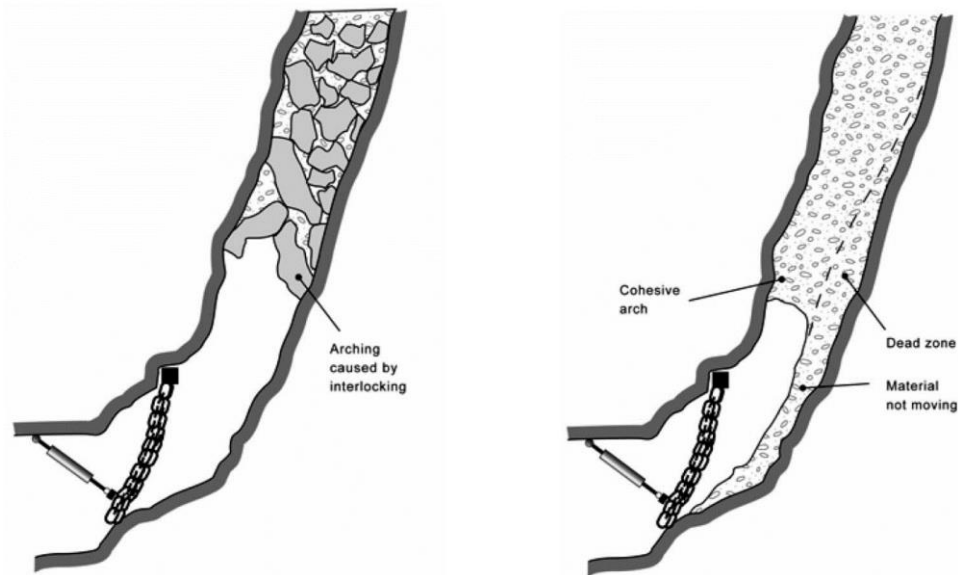


Figure 1-1: A schematic illustration of impediments to flow in an ore pass due to: left: Interlocking arching, right: Cohesive arching (Hadjigeorgiou & Lessard, 2010).

1.1.2 Hang-ups in ore passes

Factors such as cohesion, consolidation and compaction of fines, as well as constrictions within the ore pass contribute to the formation of hang-ups in ore passes. The formation of hang-ups also depends on the percentage of fines and oversize fragments, shape of the fragments, size of the large blocks relative to the size of the ore pass, and the ore pass flowing method (Szwedzicki, 2007).

Fine materials can hold larger particles together and form a continuous arch or dome across the ore pass which leads to a hang-up. Cohesion depends on the size and the fragmentation of the fines, and on the water content. Dry fines and fully saturated fines do not contribute to cohesive arches (Szwedzicki, 2007).

Consolidation and cementation in an ore pass of fine materials and certain sulphide materials occur when the materials dry out due to exposure to water and air. Prolonged time between draws allows for cementation and consolidation within the ore pass (Szwedzicki, 2007).

Compaction of material is caused by the impact of the fall of material from the tipping point or due to the load applied by a high column of fragmented rocks. The fragmented materials develop high frictional forces when compacted and resist free flow of ore and waste rock (Szwedzicki, 2007).

Constrictions or reduction in the cross-sectional flow area of the waste rock and ores result in restriction of flow and hang-ups (Figure 1-2). Constrictions within an ore pass can be caused by a change in the shape of a pass, blockages due to scaling of the ore pass wall or by blockages caused by foreign material. Constrictions resulting from the shape of the ore pass are caused by the roughness of the wall, ore pass enlargement due to blasting and scaling of the ore pass wall, structural features at the bottom of the ore pass such as chutes, and cohesive material sticking to the wall of the ore pass. Constriction within an ore pass can be caused when foreign material such as steel supports, rock bolts, wire mesh, etc. enter the ore pass (Szwedzicki, 2007).

The occurrence of interlocking hang-ups depends on the size distribution as well as on the absolute size of the material. A desirable relative ratio between the dimensions of the material and the ore pass should be determined and maintained to accommodate prevention of interlocking hang-ups (Szwedzicki, 2007). This will be discussed in Paragraph 2.2 “Methods to prevent hang-ups and blockages”.



Figure 1-2: A photo of a large rock blocking an ore pass and causing a restriction to the flow of ore and waste rock (Szwedzicki, 2007).

1.1.3 Blockages in ore passes

The main cause of blockages is a reduction in the cross sectional area between the transition of the ore pass to the chute. Blockages occur when big slabs wedge themselves into the chute. These slabs are large rocks scaling from the wall of the ore pass due to the degradation of the

ore pass. Blockages also occur when fine or sticky material accumulate in or near the chute which leads to a reduction in the cross sectional flow area (Hadjigeorgiou & Lessard, 2007).

1.2 Problem statement

Ore passes are a convenient way to transfer ore and waste rock from higher levels to lower levels in an underground mine, from where the ore and waste rock are hoisted out of the mine. The problem is that many hang-ups and blockages occur in ore passes. The operation of ore-drawing comes to a halt and the mine loses time and incurs a lot of expenses in the process. Hang-ups and blockages are therefore very costly disruptions and need to be minimised or cleared in a quick and efficient way.

1.3 Purpose of the study

Many hang-ups and blockages occur in ore passes of underground mines. The purpose of this study is to develop a vibration method to safely restore the flow after a blockage should occur. A special machine needs to be designed to transfer vibrations to a blockage. Finally, this machine must also be built and experimentally evaluated.

1.4 Scope of work

Research must be done regarding i) the current methods to prevent hang-ups and blockages, ii) existing methods used to restore flow after a hang-up or blockage, and iii) whether vibration is used to prevent- or restore flow after a hang-up or blockage had occurred. With the research in mind, concept designs must be developed and presented to the mine and the design that is chosen will then be used for the final design of a vibration ore flow restore machine. Mathematical models must be developed to analyse the design in terms of response, forces transmitted and natural frequencies.

After mathematical modelling, the machine needs to be designed in a Computer-Aided Design (CAD) environment and Finite Element Analysis needs to be conducted to analyse the stiffness of the machine and stress levels during operation. When the design is deemed sufficient, the machine will be built and the input parameters characterised to validate the accuracy of these parameters. Hereafter the machine must be experimentally evaluated by measuring the response and natural frequencies of the machine. These measured values must be compared with the predicted values to validate the mathematical models. The next phase consists of conducting tests with blockages to determine whether the machine can restore the flow after a blockage had occurred.

Conclusions regarding the validity of the mathematical models and the success of the vibration ore flow restore machine must be drawn from the data obtained during the experimental evaluation. Suggestions for further studies, if any, should also be constructed.

2 LITERATURE SURVEY

2.1 Introduction

The focus of this literature review will be i) on the methods used to prevent hang-ups and blockages, and ii) on methods to restore the flow after a hang-up or blockage had occurred. Finally, iii) the use of vibration in ore passes and to restore the flow will also be researched.

2.2 Methods to prevent hang-ups and blockages

Considering the main causes of hang-ups and blockages, prevention can be accomplished by managing the size of the material, managing the flow arrangement and managing the water content in the material transported by the ore pass (Szwedzicki, 2007).

The size of the rock can be controlled by implementing infrastructure to control the size of the rock entering the ore pass or instructing the crew who works at the tipping point of the ore pass to do so. Figure 2-1 represents the different methods to control the size of the material entering an ore pass.

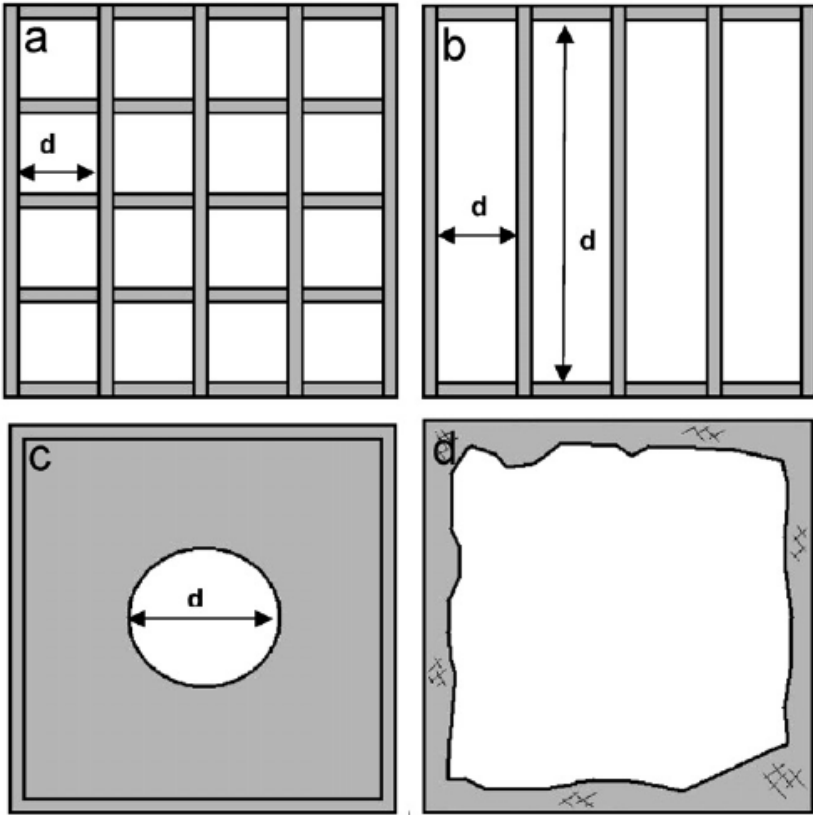


Figure 2-1: Presentation of different screening methods: a) Grizzly, b) Scalper, c) Mantle and d) No screening (Hadjigeorgiou & Lessard, 2007).

Grizzlies are the best screening method of the three because this method restricts large rocks and requires less maintenance than scalpers. Scalpers require more maintenance because large rocks wedge between the bars of the scalpers. Crew often force the large rocks through the bars, which damages the bars and can lead to bars breaking off from the scalper. The broken bars enter the ore pass which leads to obstruction and constriction within the ore pass. Both methods require additional infrastructure to crush large rocks to the required size to enter through the screening method. Another disadvantage of scalpers is that large rocks can still enter the ore pass due to the rectangular shape of the scalper. Mantles are easier to construct and do not require additional infrastructure because mantles allow larger rock fragments. The advantage of mantles is that no additional cost for infrastructure is required, but the flow of large rocks lead to interlocking hang-ups and wall degradation (Hadjigeorgiou, 2005).

Impact and wear induced on ore passes from large rocks lead to scaling where large rock blocks detach from the ore pass wall. These large rock blocks cause a constriction within the ore pass, which leads to hang-ups. To minimise wear- and impact forces on the wall of an ore pass, the level of the ore passes should be kept high (Hadjigeorgiou, 2005; Szwedzicki, 2007). However, the level of the ore pass should be kept low, and the material should constantly be moving when the ore pass is used to transport material with a large number of fines. The continuous flow of material ensures that the fines do not compact and form cohesive arches. The low level ensures that when a cohesive arch forms, the hang-up will be near the bottom of the ore pass and can be easily removed (Szwedzicki, 2007).

Sticky mud is formed when water and fines ores are mixed together and cause blockages in the ore pass. Fully saturated fines and dry fines do not contain cohesive forces so the use of water in an underground mine should be used prudently. Coarser rock should be blended with fine and wet material to decrease the ratio of wetness contained within the mixture (Szwedzicki, 2007).

2.3 Methods for restoring flow

A safe method to restore the flow after a blockage or hang-up requires a procedure where the operator does not enter an area of potential hazard (Szwedzicki, 2007). Methods used to restore the flow in an ore pass can be categorised into three types: methods that employ water, methods that rely on explosives and mechanical methods (Hadjigeorgiou & Lessard, 2010).

2.3.1 Water methods

Water-based methods can be divided into three categories: the introduction of water from above the hang-up or blockage, introduction of water from a point below the blockage and water injected through boreholes at a high pressure. The introduction of water into an ore pass

can lead to catastrophic runaways, mud flow and inundation, therefore operations should be carefully planned before execution (Szwedzicki, 2007; Hadjigeorgiou & Lessard, 2010).

Introduction of water from above the hang-up or blockage entails the dumping of a predetermined amount of water directly into the ore pass (Figure 2-2). The increase in water content of the material cause a reduction in the frictional forces within the hang-up which causes the hang-up to collapse, clearing the restriction within the ore pass. This method does not cause any damage to the ore pass and does not cause any time delays such as the methods based on the usage of explosives. The introduction of excess water into an ore pass may trigger a mud rush which resulted into fatalities in the past. This method should be used in sections where a chute is installed at the end of the ore pass to reduce the impact of a potential mud rush. This method is restricted to clearing hang-ups and blockages caused by cohesive arches because of the high porosity exhibited by coarse material (Hadjigeorgiou & Lessard, 2010).

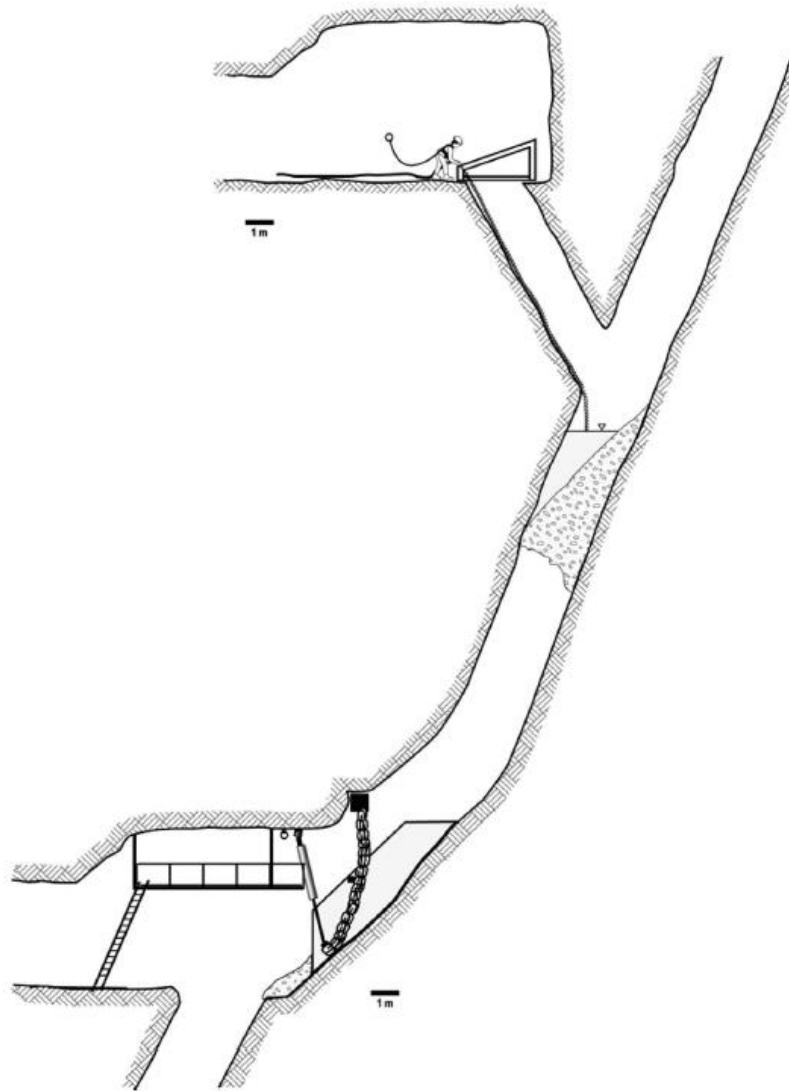


Figure 2-2: Representation of the introduction of water from above the hang-up or blockage (Hadjigeorgiou & Lessard, 2010).

The introduction of water from a point below the blockage is employed when the blockage or accumulation of material is located in the chute of an ore pass (Figure 2-3). This method entails an operator washing out the blockage by means of a hose or a nozzle. The increase of water content of the material leads to the reduction in the frictional forces, as previously mentioned, which leads to the elimination of the blockage or accumulation. This method should only be used when the workers involved in the release of the blockage are positioned in a safe area, such as a catwalk, where a sudden release of material cannot harm any of the workers. Note that the blockage can give way any time during the washing down process. This method is more effective for releasing blockages caused by cohesive arches but can be used to release interlocking arches. The introduction of water washes the fine materials out between the rocks which leaves more room for the movement of the larger rocks and potentially eliminating the

interlocking arches. Adequate time for draining needs to be allowed when water was first introduced from above the blockages before introducing water below the blockage to eliminate the risk of mud rushes (Hadjigeorgiou & Lessard, 2010).

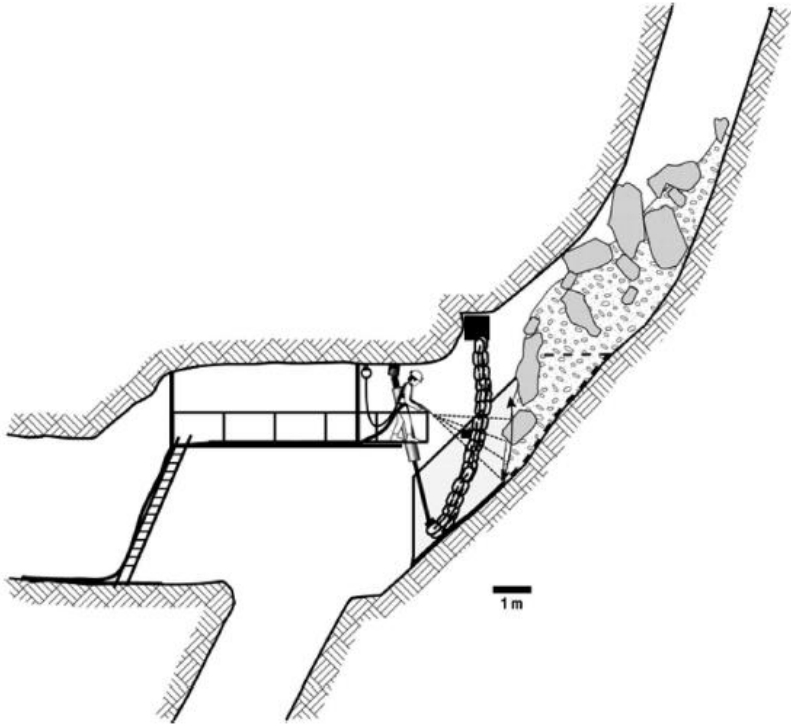


Figure 2-3: Representation of the introduction of water below the blockage. (Hadjigeorgiou & Lessard, 2010).

High pressure injection through bore holes entails drilling holes through to the ore pass from the nearest access point and injecting water under a high pressure. The water can be injected with a pressure of the regular mine water pressure, with compressed air or at a high pressure. As previously mentioned, the increase in water content will remove the fines but the high-pressure water can also loosen blocks which are causing interlocking arches. The drilled boreholes can be reused if the hang-up reoccurs at the same position. A mud rush can still occur when excess water is introduced through the boreholes. The water pressure can reduce due to leakage through cracks and fractured rock and may not be sufficient to remove key blocks from the hang-up. It is very difficult to determine the exact position of a hang-up so the end of the boreholes may not be near the key blocks and the addition of high pressure water will not have any influence on the hang-up (Szwedzicki, 2007).

2.3.2 Explosive methods

The most common method to restore flow in an ore pass after a hang-up or blockage has occurred, is by means of methods that rely on explosives. The big disadvantage of using explosives is that the blasting energy and concussion waves damage the surrounding rock mass of the ore pass and the ore pass infrastructure. Excessive damage to the rock mass surrounding the ore pass leads to wall degradation which result in costly rehabilitation or even abandonment of the ore pass. The usage of explosives is limited to interlocking arches because it can lead to the compaction of fines when used on cohesive arches. A wide variety of methods which rely on the usage of explosives have been developed for different hang-up or blockage conditions (Szwedzicki, 2007).

One method is to drill one or more holes into large blocks of hang-ups situated near the tipping point or into blockages situated near the chute of the ore pass, and filling these holes with explosives to break the large blocks (Figure 2-4). This method consists of two variations where different drilling methods and different strengths of explosives are used to break the large boulders. The advantages of using weak strength explosives are that the explosion emits less gas and rock projectiles, and the surrounding infrastructure is less likely to be damaged. Caution must be applied when drilling into interlocking arches at tipping point with the absence of a grizzly due to the probability of the hang-up collapsing at any time. Excess usage of explosives can lead to wall degradation, damage to surrounding infrastructure and rocks being projected at great velocities which poses a significant threat to workers and infrastructure (Szwedzicki, 2007; Hadjigeorgiou & Lessard, 2010).

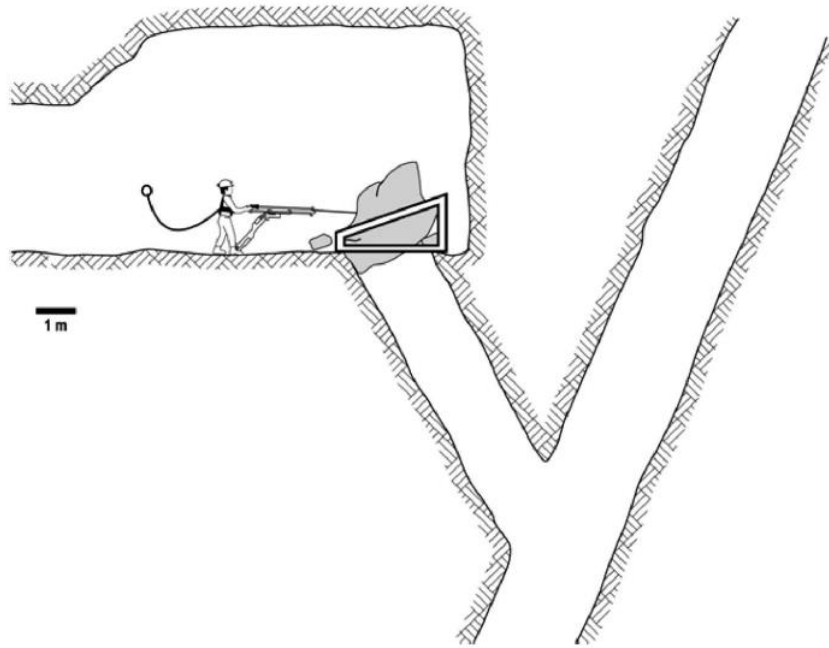


Figure 2-4: Presentation of drilling holes into a boulder wedge at the tipping point of a finger raise (Hadjigeorgiou & Lessard, 2010).

A so-called Sputnik can be used to restore the flow after a hang-up occurs. A Sputnik is a device which employs compressed air as a launch method to lift a 12 kg explosive charge up to a height of 100 m towards the hang-up (Figure 2-5). The height that a Sputnik can reach is dependent on the weight of the charge and the available air pressure. A Sputnik is used when a hang-up is located 20 m to 100 m above a chute or draw point, but a tipping point can also be used as a launching pad when the hang-up is higher than 100 m above the chute or draw point. The use of a Sputnik allows workers to be situated at a safe distance and away from falling material as the hang-up gets released, although the workers must always ensure that they are out of harm's way when utilising the Sputnik. Different areas and launching pads are illustrated by Figure 2-6 to Figure 2-8. Because this method utilizes explosives it can lead to damage to the surrounding rock mass of the ore pass, wall degradation and time delays for dust and blasting fumes to clear out (Szwedzicki, 2007; Hadjigeorgiou & Lessard, 2010).

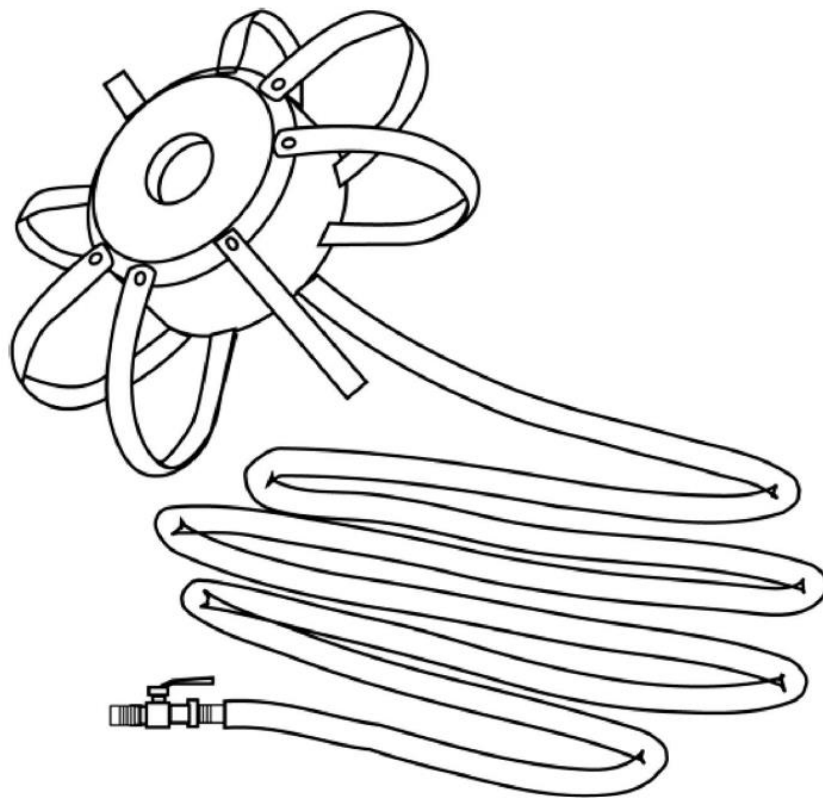


Figure 2-5: Representation of a Sputnik (Hadjigeorgiou & Lessard, 2010).

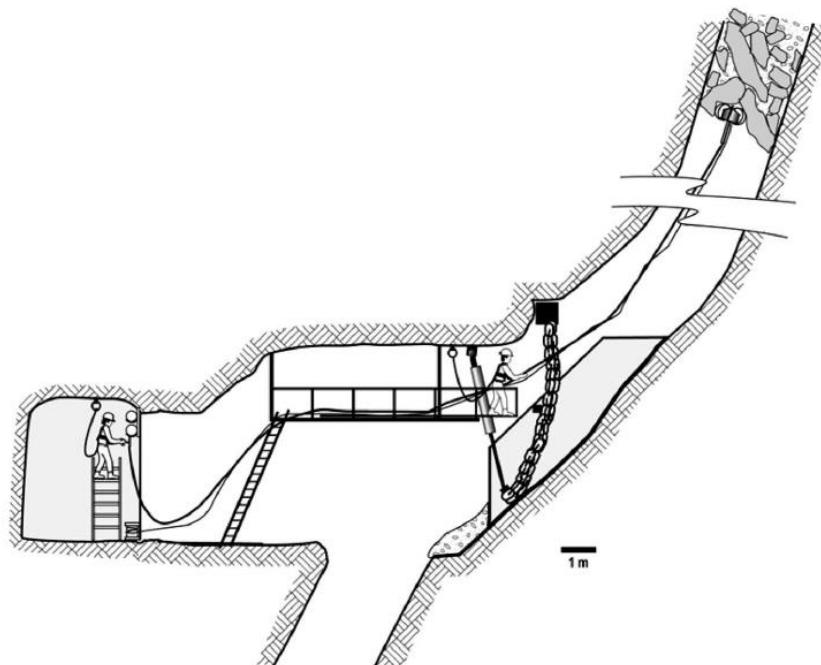


Figure 2-6: Presentation of manual positioning of a Sputnik when the workers are protected by control chains (Hadjigeorgiou & Lessard, 2010).

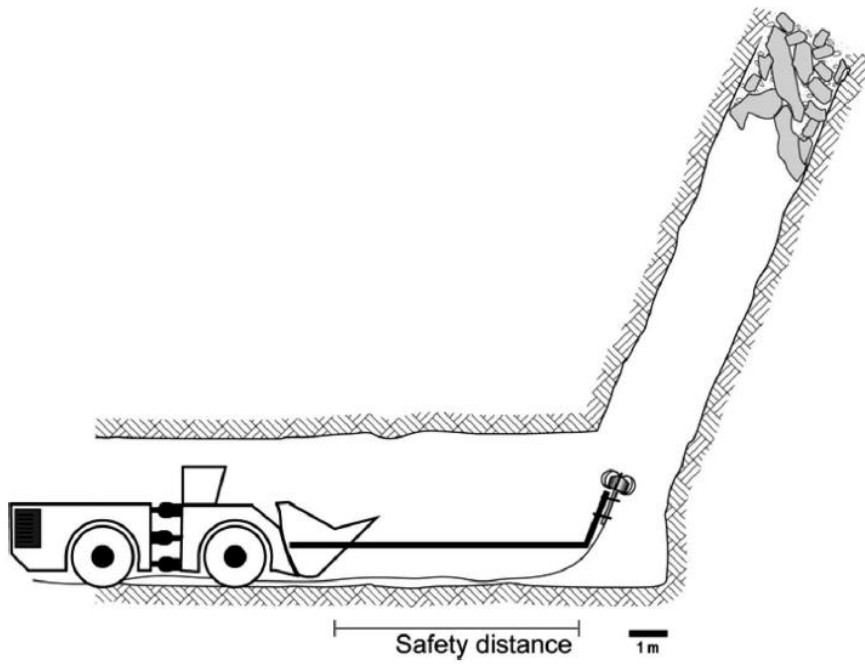


Figure 2-7: Presentation of remote positioning of a Sputnik by means of a loading-hauling-dumping (LHD) unit (Hadjigeorgiou & Lessard, 2010).

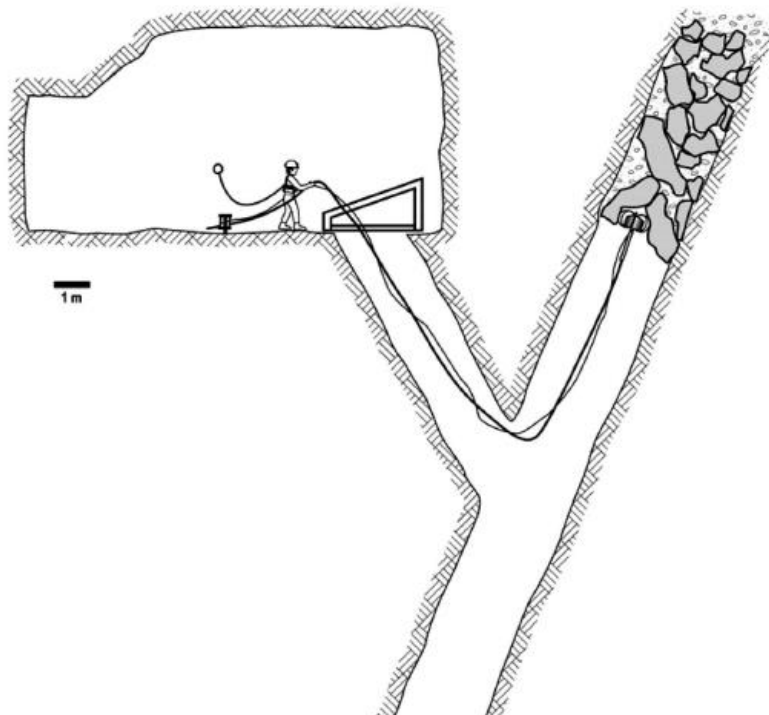


Figure 2-8: Presentation of launching a Sputnik where the tipping point is used as a launch pad (Hadjigeorgiou & Lessard, 2010).

Explosive charges can also be placed near hang-ups by using pushing rods made of aluminium, PVC or wood. This method is limited to hang-ups located a maximum of 20 m above the control chains (Figure 2-9). A rudimentary cart (Figure 2-10) or “Blasting Star” (Figure 2-11) is often used to position the charge close to the hang-up and to prevent the charge from coming into contact with the ore pass wall. The operator utilising this method must ensure that he/she positions himself/herself clear of any falling material should the hang-up collapse during the process of lifting the explosive up to the hang-up. This method can contribute to damaging the mass rock surrounding the ore pass which leads to wall degradation (Szwedzicki, 2007; Hadjigeorgiou & Lessard, 2010).

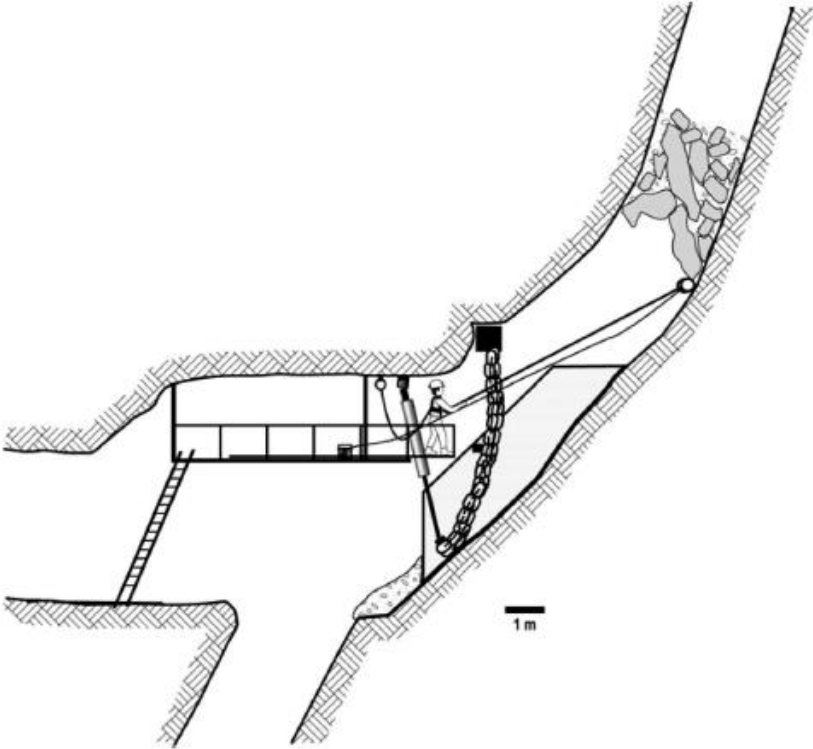


Figure 2-9: Presentation of positioning explosives near the hang-up by means of a pushing rod (Hadjigeorgiou & Lessard, 2010).

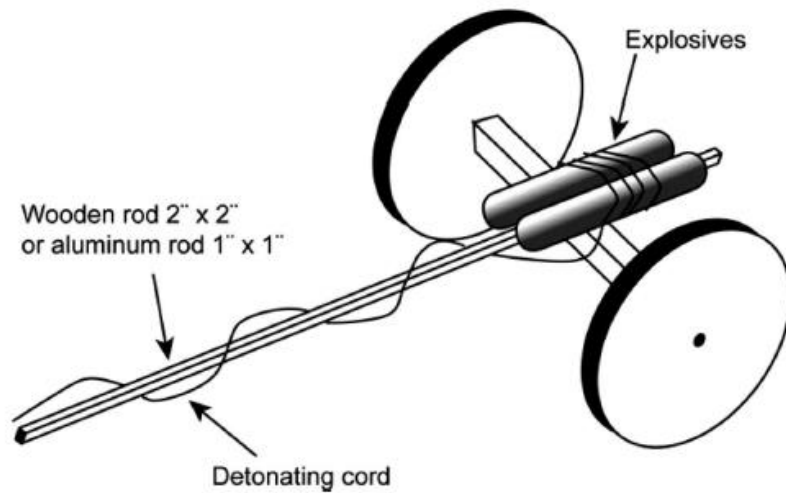


Figure 2-10: Presentation of a rudimentary cart used to assist in the positioning of explosives close to the hang-up (Hadjigeorgiou & Lessard, 2010).

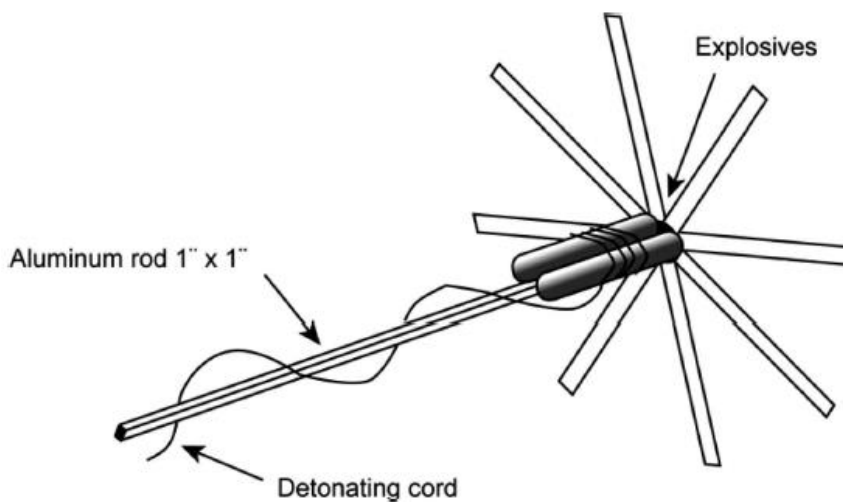


Figure 2-11: Presentation of a “Blasting Star” used to assist in the positioning of explosives close to the hang-up (Hadjigeorgiou & Lessard, 2010).

Projectiles are launched from launching devices towards the hang-up or blockage where shock energy is transferred to the rock at projectile impact. The launching device should be in a safe location to ensure that the worker is clear of falling material when the hang-up or blockage collapses. The shock wave transferred by the impact is similar to the effect of concussion caused by explosives. A ballistic disc can be used to propel a steel slug towards the hang-up or blockage to shatter the rocks causing interlocking arches (Szwedzicki, 2007).

Another option is to use a Quickdraw cannon that fires an explosive projectile which explodes on impact with the hang-up or blockage (Figure 2-12). The energy transferred through the explosion causes the rock to move or to break the interlocking arches. This method requires a precise target location of the hang-up or blockage and this is not always possible in ore passes (Szwedzicki, 2007).

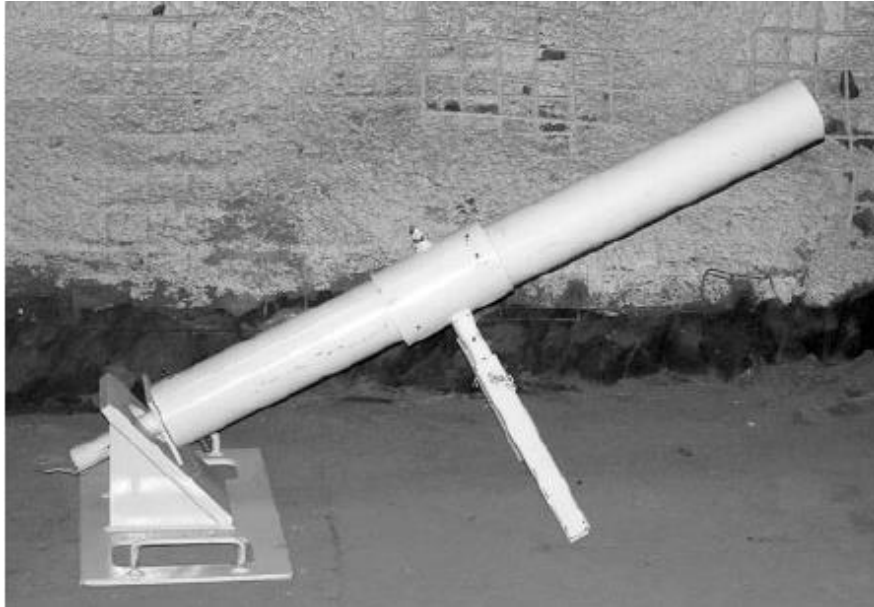


Figure 2-12: A photo displaying a Quickdraw cannon (Szwedzicki, 2007).

Drilling to hang-ups through rock mass and blasting can be used as a last resort when the previously mentioned methods are not applicable or not successful. The method entails drilling a hole or several holes through the rock mass surrounding an ore pass towards the location of a hang-up and transporting explosive charges to the hang-up by means of the holes and detonating the charge (Figure 2-13). This method is the safest method to restore the flow after a hang-up occurred because this method makes use of remote drilling and detonating which does not expose the operators to any danger. The holes should be drilled dipping down, if possible, to minimise the migration of fines into the drilled holes. These drilled holes can be reused if the hang-ups reoccur regularly at the same location in the ore pass. However, this method holds the greatest potential of causing damage to the ore pass wall and contributing to wall degradation. This method is also expensive and consumes a lot of time, and worsen when a trial and error approach is used to locate the exact location of the hang-up (Szwedzicki, 2007; Hadjigeorgiou & Lessard, 2010).

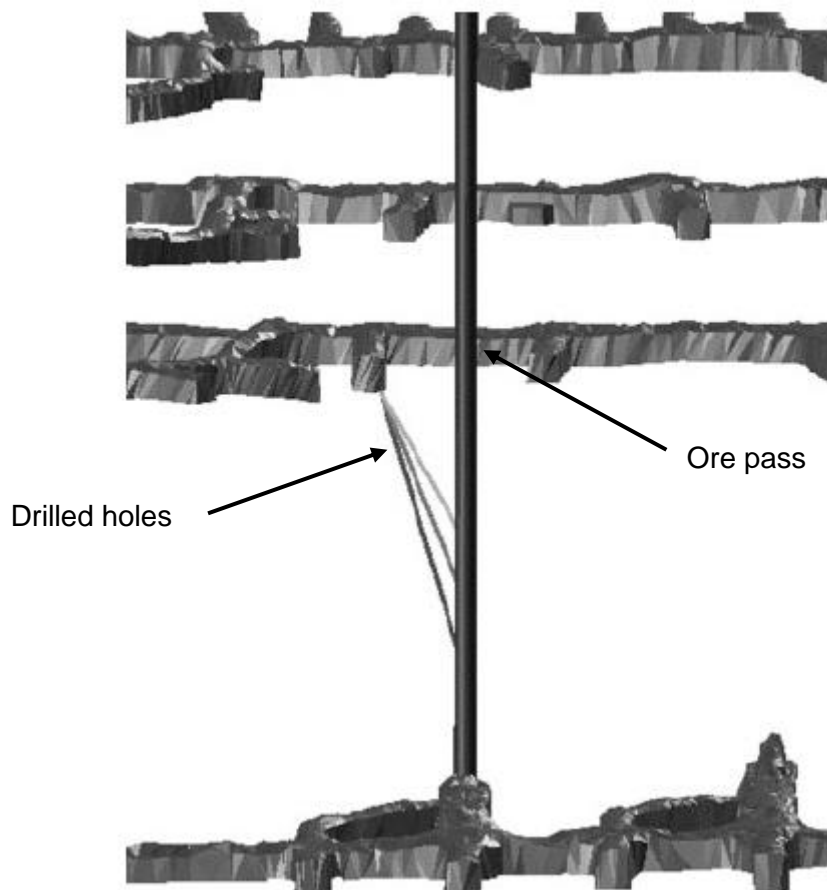


Figure 2-13: Presentation of a long-hole drilling design to clear a hang-up within a long ore pass (Szwedzicki, 2007).

2.3.3 Mechanical methods

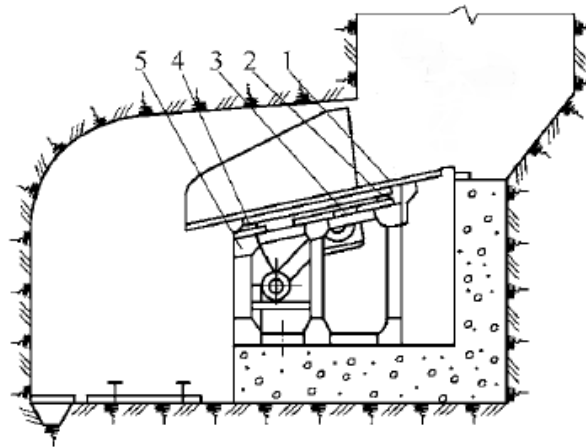
A mechanical method entails the usage of mobile rock breakers to fracture down large rocks which are wedged at the tipping point of the ore pass. The use of this mechanical method is less popular because of the additional capital and maintenance cost involving equipment not used on a regular basis (Hadjigeorgiou & Lessard, 2010).

2.4 Vibration ore-drawing on ore passes

Vibrating Ore-drawing Machines (VOMs) can be applied to ore passes to enhance the productivity of ore-drawing, minimise blockages in the ore pass, and decrease the number of workers required for ore-drawing - rendering it a more successful form of restoring flow in the ore pass. VOMs can be applied to common ore passes, in ore passes where the discharged ores contain a large amount of water and silt, in ore passes discharging cohesive ores, and in ore passes with a large output. A VOM consists of three parts: an operation mechanism, an

elastic system and an excitation system. The application of VOMs in the industry are safe, economical and efficient (Wu & Sun, 2008).

The VOM activates a suitable vibration frequency between the ores in an ore pass by transferring vibration from the VOM to the ores. This vibration frequency between the ores causes a decrease in the frictional and cohesive forces so that the ores can flow more fluently. A VOM mechanism can be created by fixing an exciter (which is driven by an electric motor) or by fixing a vibrating electric machine to the bottom surface of a vibrating table-board (Figure 2-14). In essence, a VOM is a table-board where the vibration is transferred to the table-board by an electric vibration motor. Different examples where VOMs were installed for the application at ore passes are listed in Wu and Sun's *Vibrating Ore-Drawing Technology: Granular Dynamic Theory and Its Applications*, under section 9 (Wu & Sun, 2008).



1—Vibration table-board; 2—Elastic element; 3—Inertial exciter;
4—Base of electric motor and rebounding electric machine; 5—Frame

Figure 2-14: Presentation of a VOM installed at an ore pass (Wu & Sun, 2008).

2.5 Conclusion

Certain precautions and preventative measures can be applied to minimise the occurrence of hang-ups and blockages, such as controlling the size of the rock tipped into an ore pass, managing the amount of fines and water content of the material entering the ore pass and managing the flow arrangement. Even so, hang-ups and blockages still occur when preventative measures are applied and need to be eliminated.

Many methods of releasing hang-ups and blockages and restoring the flow exist, and every method has advantages and disadvantages. The release methods can be grouped into two

sections, being methods which employ water and methods utilising explosives. The methods which employ water are restricted to hang-ups and blockages which are caused by cohesive arches and these methods have the potential to cause mud rushes. Methods which utilise explosives are restricted to hang-ups and blockages caused by interlocking arches and these cause damage to the wall of the ore pass. The damage inflicted on the wall of the ore pass leads to wall degradation and wall scaling.

Vibrating ore-drawing machines (VOMs) have resulted in remarkable success when applied to ore passes. The VOM assists in aiding the flow of ores in ore passes while minimising the occurrence of blockages. A VOM is easy to build and to install but it needs to be designed according to the specific conditions of the ore pass because ore passes can contain different properties. Thus, vibration was proven to be successful in aiding the flow of ore and this study will therefore aim to design a machine which will use vibration to restore flow after a blockage had occurred.

This study's literature overview is limited because there is little research on the application of vibration for the restoration of flow in an ore pass after a blockage or hang up had occurred.

In the next chapter two developed concept designs will be discussed that was also presented to the mine. The design which the mine chose will then be further developed by mathematical modelling and Finite Element Analysis (FEA).

3 CONCEPT DESIGN

3.1 Introduction

This chapter will serve to describe the development of the concept design, through mathematical modelling and the implementation of these models in a computer program. The concept designs will briefly be discussed and the reasons why a certain design was chosen. Thereafter the mathematical models will be discussed which was used to calculate the displacements, forces, natural frequencies and characteristics of the final design. Finally, the implementation of these models in a MATLAB® environment will be discussed.

3.2 Brief concept evaluation description and selection

The first concept design was to implement the same principles of a Vibration Ore-drawing Machine (VOM) to the boxfront of the underground mine as seen in Figure 3-1, with the addition of steel cables that will be strung through ore pass and attached to the VOM. This concept was considered because research revealed that this was a very safe and effective method to restore flow. This concept was turned down because the mine spent too much money over the years on strengthening the boxfronts and don't want to make any alterations to the current boxfronts.

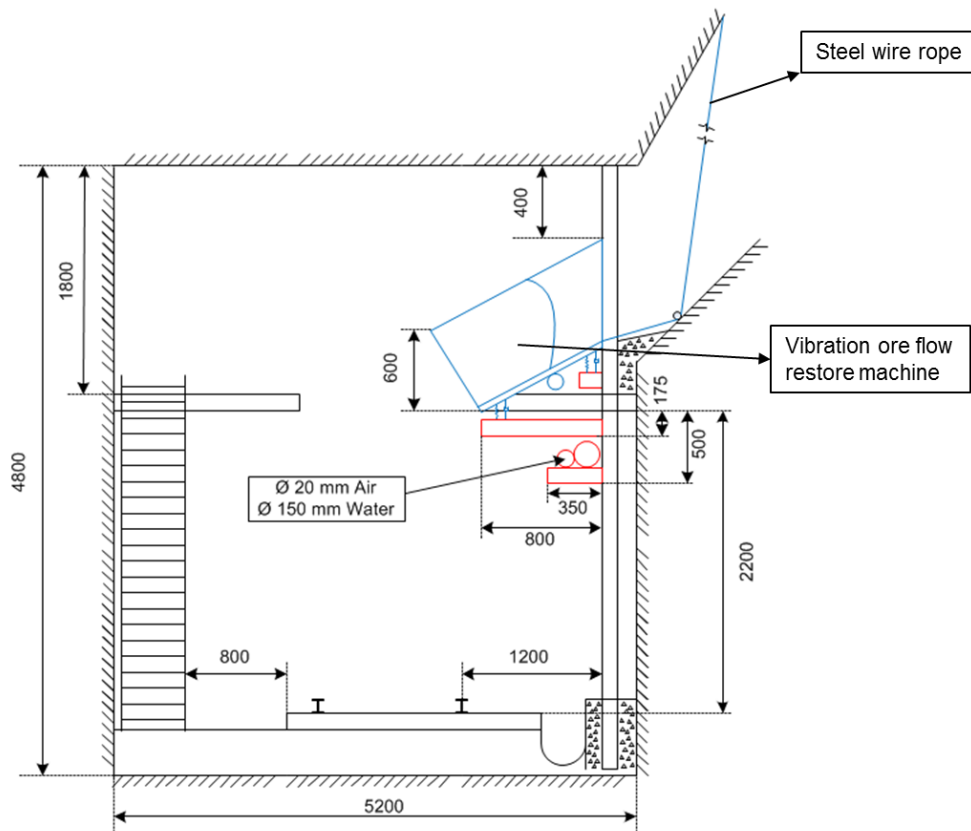


Figure 3-1: Representation of the first concept design.

The second design concept was to transfer vibrations over to a blockage by means of vibrating steel cables as seen in Figure 3-2. The steel cables will initially be strung through the ore pass and when a blockage should occur, the steel cables will be trapped in between the rock. The steel cables will be attached to a mass that is connected on top of the boxfront of an ore pass. The mass will be supported by rubber mounts and oscillated by two excitation motors attached to each side of the mass.

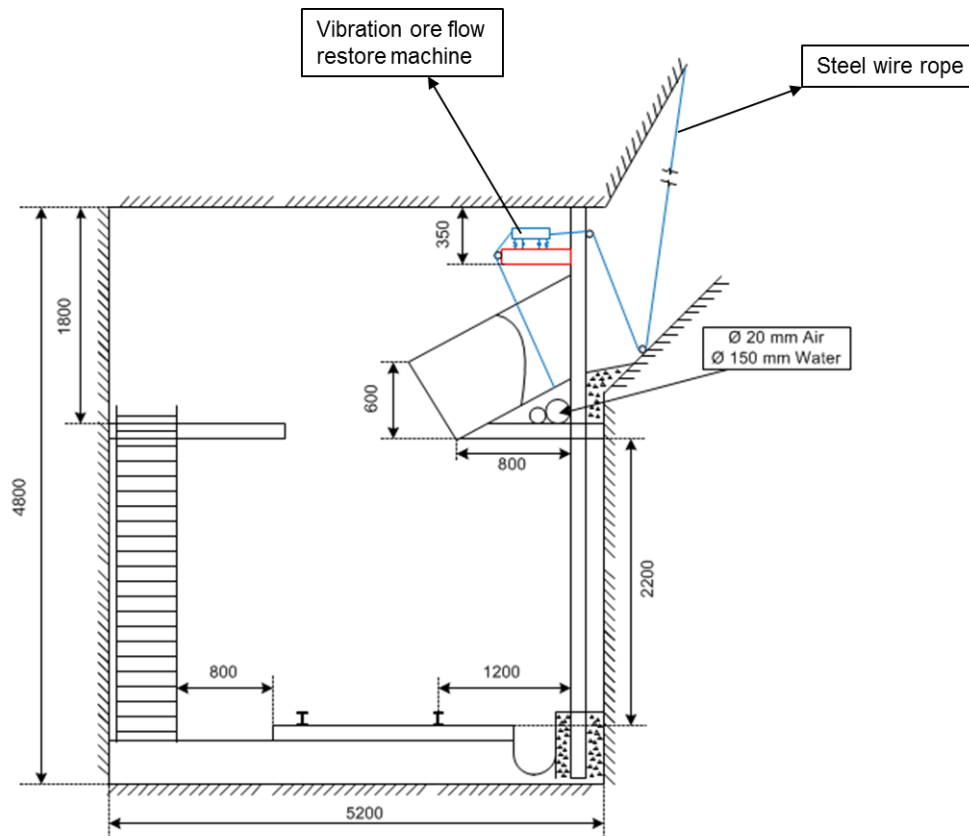


Figure 3-2: Representation of the second concept design.

Additionally to the second design concept, a metal rod will be attached to the mass which could serve as a hammer and transfer energy to the blockage through impact.

This design concept was accepted by the mine and will therefore be the focus of the possible solution. This design will be developed through mathematical models and constructed in SOLIDWORKS® where additional analysis will be conducted to supplement the design.

3.3 Mathematical modelling

This section will serve to describe the three different mathematical models used within this study. The first mathematical model was developed to calculate the static and dynamic displacements, the forces transmitted and the natural frequencies for the main steel structure of the planned ore flow restore machine (machine). The second mathematical model was developed to calculate the same properties as mentioned before but under the condition where the steel cables have been caught between the rocks when a blockage occur and acts like an additional spring. The third mathematical model was developed to calculate the dynamic properties of the rubber mounts supporting the machine.

3.3.1 Three-degree-of-freedom mathematical model - stand-alone machine

For this study, a three-degree-of-freedom model was developed to calculate the response, dynamic forces transmitted and the natural frequencies of the machine. The machine was idealized as a rigid body with a mass m_1 and a mass moment of inertia J_y . The model consists of an orthogonal global coordinate system (xyz) , with the origin positioned at the centre of gravity (g) of the machine. The x-axis is parallel to the horizontal, the z-axis is parallel to the vertical and the y-axis is perpendicular to the x-axis and z-axis. The machine's main structure is attached to a support structure by means of a combination of three elastic rubber mounts at each side of the machine with positions relative to the designated global coordinate system. The rubber mounts contain vertical stiffness coefficients (k_{z1}, k_{z2}) and horizontal stiffness coefficients (k_{x1}, k_{x2}) , respectively. The damping characteristics of the rubber mounts will be modelled as viscous damping. The rubber mounts contain vertical viscous damping coefficients (c_{z1}, c_{z2}) and horizontal viscous damping coefficients (c_{x1}, c_{x2}) , respectively.

The three modes that will be investigated for this study are two translation modes - movement as vertical displacement (Δz) and movement as horizontal displacement (Δx) - and one rotational mode which is movement as rotational displacement about the y-axis ($\Delta \theta_y$).

Two excitation motors will be used to transfer fluctuating forces to the machine. These motors will be identical and attached to opposite sides of the machine. The motors will rotate in opposite directions relative to each other, which results in eliminating the resultant force in the y-direction (Rao, 2011). The motors will be attached at point e , which is the acting point of the unbalance shaking force as seen in Figure 3-3. This leads to eliminating the resultant moments about the x and z axis.

The excitation force F_e produced by the motors at any time t , can be calculated as follow:

$$F_e(t) = m_e \omega^2 \sin(\omega t) \quad (3-1)$$

where m_e is the static moment of the excitation motor and ω is the rotational speed of the motor. The static moment of the excitation motor is the product of the unbalance mass m_u with the radius at which the unbalance mass is positioned r_u and can be describe as follows:

$$m_e = m_u \times r_u \quad (3-2)$$

The motors can rotate about the point e towards an angle of β to obtain an excitation force in the horizontal and vertical direction as seen in Figure 3-3. The excitation force in the horizontal direction can be calculated as follows:

$$F_{ex}(t) = F_e(t) \cos(\beta) \quad (3-3)$$

The excitation force in the vertical direction can be calculated as follows:

$$F_{ez}(t) = F_e(t) \sin(\beta) \quad (3-4)$$

whereas the moment about the y axis caused by the horizontal excitation force can be calculated as follows:

$$M_{ex}(t) = F_{ex}(t)z_3 \quad (3-5)$$

and the moment about the y axis caused by the vertical excitation force can be calculated as follows:

$$M_{ez}(t) = F_{ez}(t)x_3 \quad (3-6)$$

where x_3 and z_3 are the x and z coordinates of the excitation point where the motors are located.

From the two different moments calculated above, the resultant moment about the y axis can be defined as:

$$M_{ey}(t) = M_{ex} - M_{ez} \quad (3-7)$$

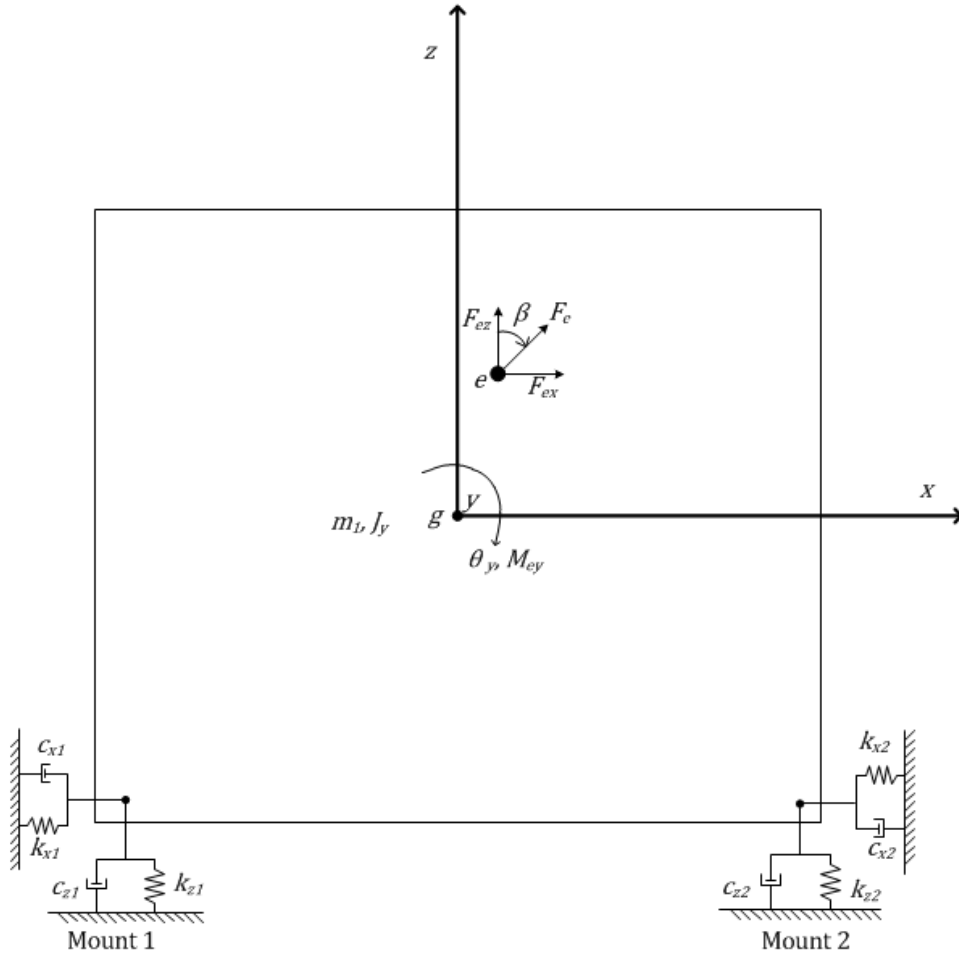


Figure 3-3: Three-degree-of-freedom model for stand-alone machine.

With reference to Figure 3-3 and by utilizing Newton's second law, three differential equations of motion were derived. The equation of motion for the x direction is as follow:

$$m_1 \Delta \ddot{x} = -\Delta x(k_{x1} + k_{x2}) - \Delta \dot{x}(c_{x1} + c_{x2}) - \Delta \theta_y(k_{x1}z_1 + k_{x2}z_2) - \Delta \dot{\theta}_y(c_{x1}z_1 + c_{x2}z_2) + F_{ex}(t) \quad (3-8)$$

where Δx , $\Delta \dot{x}$, and $\Delta \ddot{x}$ are the displacement, velocity and acceleration of the centre of mass in the x direction, and $\Delta \theta_y$ and $\Delta \dot{\theta}_y$ are the rotational displacement and rotational velocity about the y axis. The vertical coordinates of the mounts are described by z_1 and z_2 . The second equation of motion for the direction in the z axis is as follows:

$$m_1 \Delta \ddot{z} = -\Delta z(k_{z1} + k_{z2}) - \Delta \dot{z}(c_{z1} + c_{z2}) - \Delta \theta_y(-k_{z1}x_1 - k_{z2}x_2) - \Delta \dot{\theta}_y(-c_{z1}x_1 - c_{z2}x_2) + F_{ez}(t) \quad (3-9)$$

where Δz , $\Delta \dot{z}$, and $\Delta \ddot{z}$ are the displacement, velocity and acceleration of the centre of mass in the z direction. The horizontal coordinates of the mounts are described by x_1 and x_2 . The third equation of motion for rotation about the y axis is as follow:

$$\begin{aligned} J_y \Delta \ddot{\theta}_y = & -\Delta x(k_{x1}z_1 + k_{x2}z_2) - \Delta \dot{x}(c_{x1}z_1 + c_{x2}z_2) - \Delta z(-k_{z1}x_1 - k_{z2}x_2) \\ & - \Delta \dot{z}(-c_{z1}x_1 - c_{z2}x_2) - \Delta \theta(k_{x1}z_1^2 + k_{x2}z_2^2 + k_{z1}x_1^2 + k_{z2}x_2^2) \quad (3-10) \\ & - \Delta \dot{\theta}(c_{x1}z_1^2 + c_{x2}z_2^2 + c_{z1}x_1^2 + c_{z2}x_2^2) + M_{ey}(t) \end{aligned}$$

where $\Delta \ddot{\theta}_y$ is the rotational acceleration about the y axis.

3.3.1.1 Natural frequencies of machine as rigid body supported by elastic mounts

The three natural frequencies of the machine can be determined by solving the eigenvalue problem (Rao, 2011). The eigenvalue value problem can be defined as:

$$[[k] - \omega_n^2[m]]\vec{X} = \vec{0} \quad (3-11)$$

where $[k]$ is the stiffness matrix of the system and $[m]$ is the mass matrix of the system. The vector \vec{X} is known as the mode shape of the system, ω_n^2 is known as the eigenvalue and ω_n as the natural frequency of the system. The stiffness and mass matrixes of the machine system are derived from equations (3-8) to (3-10). The stiffness matrix for the machine, modelled as a rigid body and supported by elastic mounts, is defined as follows:

$$K = \begin{bmatrix} k_{x1} + k_{x2} & 0 & k_{x1}z_1 + k_{x2}z_2 \\ 0 & k_{z1} + k_{z2} & -k_{z1}x_1 - k_{z2}x_2 \\ k_{x1}z_1 + k_{x2}z_2 & -k_{z1}x_1 - k_{z2}x_2 & k_{x1}z_1^2 + k_{x2}z_2^2 + k_{z1}x_1^2 + k_{z2}x_2^2 \end{bmatrix} \quad (3-12)$$

and the mass matrix for the machine is:

$$M = \begin{bmatrix} m_1 & 0 & 0 \\ 0 & m_1 & 0 \\ 0 & 0 & J_y \end{bmatrix} \quad (3-13)$$

The natural frequency can also be described as:

$$f_n = \frac{\omega_n}{2\pi} \quad (3-14)$$

where ω_n is expressed in rad/s and f_n in Hz .

3.3.1.2 Dynamic forces transmitted through rubber mounts

Dynamic forces are transmitted to the support structure of the machine due to the reaction forces from the rubber mounts. The rubber mounts cause a reaction force resulting from the

stiffness- and damping characteristics. The vertical force transmitted to the support structure through Mount 1 is:

$$\Delta F_{z1} = \Delta z_1 k_{z1} + \Delta \dot{z}_1 c_{z1} \quad (3-15)$$

and the horizontal force transmitted to the support structure through Mount 1 is:

$$\Delta F_{x1} = \Delta x_1 k_{x1} + \Delta \dot{x}_1 c_{x1} \quad (3-16)$$

where Δz_1 and Δx_1 are the dynamic vertical and horizontal displacements at Mount 1, respectively, and $\Delta \dot{z}_1$ and $\Delta \dot{x}_1$ are the dynamic vertical and horizontal velocities at Mount 1, respectively. By assuming small displacements, the dynamic vertical displacement at Mount 1 can be calculated as:

$$\Delta z_1 = \Delta z - x_1 \Delta \theta_y \quad (3-17)$$

and the dynamic horizontal deflection as:

$$\Delta x_1 = \Delta x + z_1 \Delta \theta_y \quad (3-18)$$

where the terms $x_1 \Delta \theta_y$ and $z_1 \Delta \theta_y$ refer to the linear deflection in the z and x directions, respectively, at Mount 1 due to the rotation of the machine. The dynamic vertical velocity can be calculated as:

$$\Delta \dot{z}_1 = \Delta \dot{z} - x_1 \Delta \dot{\theta}_y \quad (3-19)$$

and the dynamic horizontal velocity as:

$$\Delta \dot{x}_1 = \Delta \dot{x} + z_1 \Delta \dot{\theta}_y \quad (3-20)$$

where the terms $x_1 \Delta \dot{\theta}_y$ and $z_1 \Delta \dot{\theta}_y$ refer to the linear velocities in the z and x directions respectively, at Mount 1 due to the rotational velocity of the machine. Similar to the transmitted forces through Mount 1, the vertical force transmitted to the support structure through Mount 2 is:

$$\Delta F_{z2} = \Delta z_2 k_{z2} + \Delta \dot{z}_2 c_{z2} \quad (3-21)$$

and the horizontal force transmitted to the support structure through Mount 2 is:

$$\Delta F_{x2} = \Delta x_2 k_{x2} + \Delta \dot{x}_2 c_{x2} \quad (3-22)$$

where Δz_2 and Δx_2 are the dynamic vertical and horizontal displacements at Mount 2, respectively, $\Delta \dot{z}_2$ and $\Delta \dot{x}_2$ are the dynamic vertical and horizontal velocities at Mount 2, respectively. By assuming small displacements, the dynamic vertical deflection at Mount 2, similar to the deflection at Mount 1, can be calculated as:

$$\Delta z_2 = \Delta z - x_2 \Delta \theta_y \quad (3-23)$$

and the dynamic horizontal deflection at Mount 2 as:

$$\Delta x_2 = \Delta x + z_2 \Delta \theta_y \quad (3-24)$$

Similar to the deflection at Mount 1, the terms $x_2 \Delta \theta_y$ and $z_2 \Delta \theta_y$ refer to the linear deflections in the z and x directions, respectively, at Mount 2 due to the rotation of the machine. The dynamic vertical velocity at Mount 2, similar to Mount 1, can be calculated as:

$$\Delta \dot{z}_2 = \Delta \dot{z} - x_2 \Delta \dot{\theta}_y \quad (3-25)$$

and the dynamic horizontal deflection as:

$$\Delta \dot{x}_2 = \Delta \dot{x} + z_2 \Delta \dot{\theta}_y \quad (3-26)$$

where the terms, similar to the velocity at Mount 1, $x_2 \Delta \dot{\theta}_y$ and $z_2 \Delta \dot{\theta}_y$ refer to the linear velocities in the z and x directions, respectively, at Mount 2 due to the rotational velocity of the machine.

3.3.1.3 Force exerted by hammer

The influence of the hammer on the machine and the force the hammer would experience, were excluded from the mathematical model due to the complexity thereof. The response of the machine while operating the hammer will be measured and used to calculate the dynamic forces transmitted by the machine to the support structure, in the same manner as for the stand-alone machine as described in the previous section.

3.3.2 Three-degree-of-freedom mathematical model – steel cables

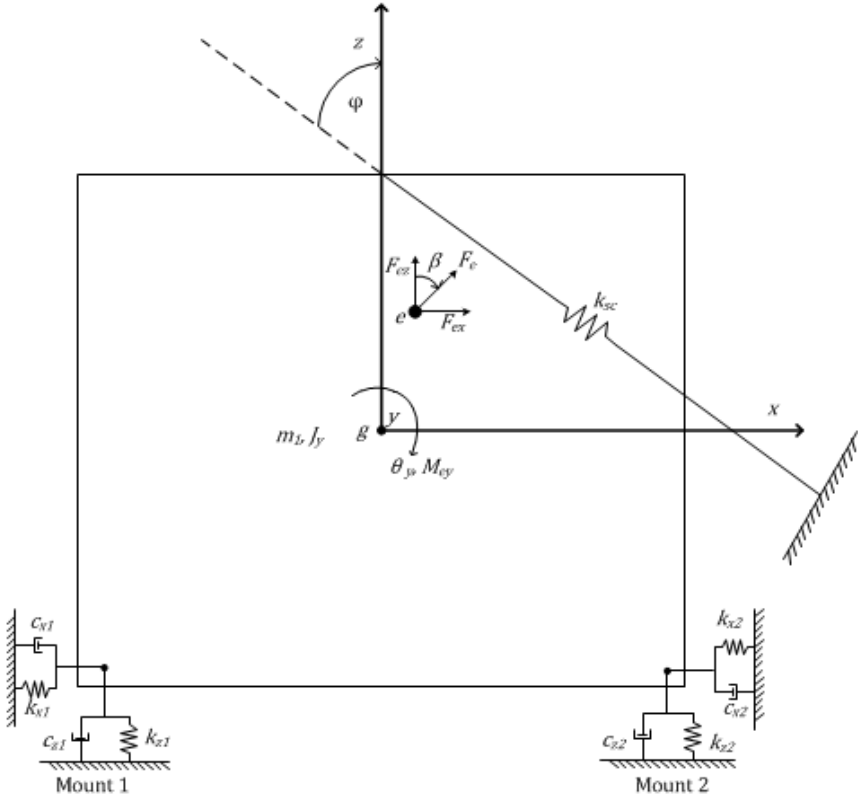


Figure 3-4: Three-degree-of-freedom model for main steel structure when the steel cables act as an additional spring.

The three-degree-of-freedom model where the steel cables are caught between rocks is similar to the previous three-degree-of-freedom model with the exception that the steel cables are acting as an additional spring, as seen in Figure 3-4. This model will be used to calculate the response and natural frequencies when the steel cables act as an additional spring. Extension springs are attached between the machine and the steel cables and the series combination will also be referred to as steel cables hereafter. The steel cables were not evaluated in a single-degree-of-freedom model, also due to the significant difference in mass. The mass of the system increased with a third of the steel cables' mass which also increased the moment of inertia of the system. The axial stiffness of the steel cables is k_{sc} and is attached at an angle φ relative to the z axis. This angle was chosen as 45° . With reference to Figure 3-4 and by applying Newton's second law, the three new differential equations of motion were derived. The equation of motion for the x direction is as follows:

$$\begin{aligned}
m_1 \Delta \ddot{x} = & -\Delta x(k_{x1} + k_{x2} + k_{scx}) - \Delta \dot{x}(c_{x1} + c_{x2}) \\
& - \Delta \theta_y(k_{x1}z_1 + k_{x2}z_2 + k_{scx}z_4) - \Delta \dot{\theta}_y(c_{x1}z_1 + c_{x2}z_2) \\
& + F_{ex}(t)
\end{aligned} \quad (3-27)$$

where k_{scx} is the horizontal component of the stiffness of the steel cables combination and z_4 is the vertical position where the steel cables are attached to the machine. The second equation of motion in the z direction is as follows:

$$\begin{aligned}
m_1 \Delta \ddot{z} = & -\Delta z(k_{z1} + k_{z2} + k_{scz}) - \Delta \dot{z}(c_{z1} + c_{z2}) \\
& - \Delta \theta_y(-k_{z1}x_1 - k_{z2}x_2 - k_{scz}x_4) - \Delta \dot{\theta}_y(-c_{z1}x_1 - c_{z2}x_2) \\
& + F_{ez}(t)
\end{aligned} \quad (3-28)$$

where k_{scz} is the vertical component of the stiffness of the steel cables combination and x_4 is the horizontal position where the steel cables are attached to the machine. The third equation of motion for rotation about the y axis is as follows:

$$\begin{aligned}
J_y \Delta \ddot{\theta}_y = & -\Delta x(k_{x1}z_1 + k_{x2}z_2 + k_{scx}z_4) - \Delta \dot{x}(c_{x1}z_1 + c_{x2}z_2) \\
& - \Delta z(-k_{z1}x_1 - k_{z2}x_2 - k_{scz}x_4) - \Delta \dot{z}(-c_{z1}x_1 - c_{z2}x_2) \\
& - \Delta \theta(k_{x1}z_1^2 + k_{x2}z_2^2 + k_{z1}x_1^2 + k_{z2}x_2^2 + k_{scx}z_4^2 + k_{scz}x_4^2) \\
& - \Delta \dot{\theta}(c_{x1}z_1^2 + c_{x2}z_2^2 + c_{z1}x_1^2 + c_{z2}x_2^2) + M_{ey}(t)
\end{aligned} \quad (3-29)$$

3.3.2.1 Natural frequencies of machine as rigid body supported by elastic mounts with steel cables

The stiffness and mass matrixes for the machine, where the steel cables are caught between the rocks during a blockage, were derived from equations (3-27) to (3-29). The stiffness matrix of the machine where the cables are caught in a blockage is as follows:

$$K = \begin{bmatrix} k_{x1} + k_{x2} + k_{scx} & 0 & k_{x1}z_1 + k_{x2}z_2 + k_{scx}z_4 \\ 0 & k_{z1} + k_{z2} + k_{scz} & -k_{z1}x_1 - k_{z2}x_2 - k_{scz}x_4 \\ k_{x1}z_1 + k_{x2}z_2 + k_{scx}z_4 & -k_{z1}x_1 - k_{z2}x_2 - k_{scz}x_4 & k_{x1}z_1^2 + k_{x2}z_2^2 + k_{z1}x_1^2 + k_{z2}x_2^2 + k_{scx}z_4^2 + k_{scz}x_4^2 \end{bmatrix} \quad (3-30)$$

and the mass matrix of the machine with steel cables is:

$$M = \begin{bmatrix} m_1 & 0 & 0 \\ 0 & m_1 & 0 \\ 0 & 0 & J_y \end{bmatrix} \quad (3-31)$$

The static deflections, static forces and dynamic forces transmitted to the support structure for this three-degree-of-freedom model are the same as calculated in the three-degree-of-freedom model where no steel cables are acting on the machine.

3.3.2.2 Force transmitted through steel cables

The stiffness of the steel cables combination denotes to the force transmitted through the steel cables. The damping of the steel cables was neglected. The force transmitted through the steel cables can be calculated as follows:

$$\Delta F_{sc} = \Delta scdisp \times k_{sc} \quad (3-32)$$

where $\Delta scdisp$ is the displacement of the point where the steel cables are attached to the machine and k_{sc} is the stiffness of the steel cable combination. The steel cables are attached in series with the extension springs and the combined stiffness is calculated as follows:

$$k_{sc} = \frac{k_{cable} \times k_{spring}}{k_{cable} + k_{spring}} \quad (3-33)$$

where k_{cable} is the axial stiffness of the cable and k_{spring} is the stiffness of the extension spring. The axial stiffness of the steel cables can be calculated as follows:

$$k_{cable} = \frac{E_c A_c}{L_c} \quad (3-34)$$

where E is the modulus of elasticity for the steel cables, A is the cross-section area of the steel cables and L is the length of the steel cables. The displacement of the steel cables combination can be calculated as:

$$\Delta scdisp = \sqrt{\Delta x_4^2 + \Delta z_4^2} \quad (3-35)$$

where Δx_4 and Δz_4 are the horizontal and vertical dynamic displacements of the points where the steel cables are attached to the machine, respectively. The dynamic horizontal deflection of the steel cables' attachment point can be calculated as follows:

$$\Delta x_4 = \Delta x + z_4 \Delta \theta_y \quad (3-36)$$

and the dynamic vertical deflection of the steel cables' attachment point as:

$$\Delta z_4 = \Delta z - x_4 \Delta \theta_y \quad (3-37)$$

where the terms $z_4\Delta\theta_y$ and $x_4\Delta\theta_y$ denote the linear displacements in the x and z directions, respectively, due to the rotation of the machine, at the attachment point.

3.3.3 Characterization of dynamic mount properties

The dynamic horizontal and vertical properties of the rubber mounts will be determined by means of a bump test. This entails applying an impact force to the machine as seen in Figure 3-3 in the desired horizontal or vertical direction and measuring the acceleration response. This response will be used to calculate the desired dynamic properties.

3.3.3.1 Bump test

By using two successive acceleration amplitude responses \ddot{x}_{cg1} and \ddot{x}_{cg2} with the damped time period τ_d , between these two amplitudes, the following ratio (Rao, 2011) can be used to aid in the calculation of the dynamic properties:

$$\frac{\ddot{x}_{cg1}}{\ddot{x}_{cg2}} = e^{\zeta\omega_n\tau_d} \quad (3-38)$$

where ζ is the damping ratio of the rubber mounts and ω_n is the undamped natural frequency of the rigid system. The damped frequency ω_d of the rigid system can be calculated as:

$$\omega_d = \frac{2\pi}{\tau_d} \quad (3-39)$$

The damped frequency of the system can also be calculated as:

$$\omega_d = \sqrt{1 - \zeta^2} \omega_n \quad (3-40)$$

By simultaneously solving equations (3-38) to (3-40), the damping ratio and the undamped natural frequency can be determined. From this, the stiffness of the rubber mounts and the amount of damping can be calculated as:

$$\omega_n = \sqrt{\frac{k}{m}} \quad (3-41)$$

where k is the stiffness of the mounts in the desired direction and m is the mass of the machine. The amount of damping in the rubber mounts can be calculated as:

$$c = \zeta c_c \quad (3-42)$$

where c_c is the amount of critical damping for the rigid system, which can be calculated as:

$$c_c = 2m \sqrt{\frac{k}{m}} = 2\sqrt{km} = 2m\omega_n \quad (3-43)$$

These equations can be used in the vertical and the horizontal direction to determine the properties of the rubber mount in the direction investigated in the three-degree-of-freedom models.

The mathematical models described in Paragraph 3.3.1 to Paragraph 3.3.3 are too complex to solve by hand and will be implemented in a MATLAB® environment, for MATLAB® has built-in functions which will be able to solve the equations of motion simultaneously as well as the eigenvalue problem. The implementation of the mathematical models in MATLAB® will be described in Paragraph 3.4.

3.4 Computer implementation

3.4.1 Introduction

The three mathematical models described in Paragraph 3.3 were implemented in a MATLAB® environment and this section will serve to describe the programs used to solve the mathematical models. The first model was implemented to determine the dynamic deflections and forces, and to determine the natural frequency of the system. The second model was implemented to determine the same as previously mentioned but under the condition where the steel cables are caught in a blockage. The third model was implemented to determine the dynamic properties of the rubber mounts supporting the flow restoring machine.

3.4.2 Three-degree-of-freedom mathematical model - stand-alone machine

The flowchart of the MATLAB® program utilised to calculate the response, dynamic forces and the natural frequency of the machine is depicted in Figure 3-5. The inputs consist of the mass and moment of inertia of the machine, the rubber mounts' dynamic properties and coordinates, and the static moment and rotational speed of the excitation motors. The dynamic properties of the rubber mounts and the static moment of the excitation motor were provided by the suppliers of each component.

The equations (3-8) to (3-10) were written as six first order differential equations and were solved in MATLAB® by numerical integration with a built-in MATLAB® function *ode23.m*. The built-in MATLAB® function *eig.m* was used to solve the eigenvalue problem as described in Paragraph 3.3.1.1 to calculate the mode shapes and natural frequencies.

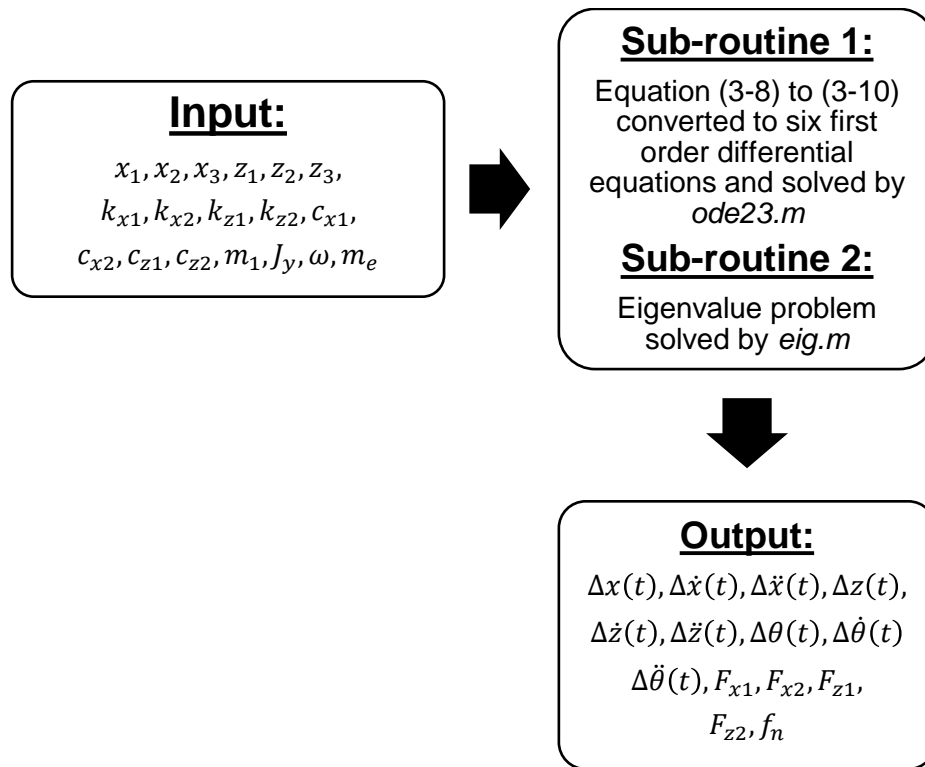


Figure 3-5: Representation of the flowchart for the computer implementation of the three-degree-of-freedom mathematical model for the machine.

3.4.3 Three-degree-of-freedom mathematical model - steel cables

The model implemented to calculate the response, dynamic forces, the dynamic forces transmitted through the steel cables, and the natural frequencies for the machine when the steel cables are caught in a blockage is represented by Figure 3-6.

The inputs consist of the mass and moment of inertia of the machine, the dynamic properties and coordinates of the rubber mounts supporting the machine, the static moment and rotational speed of the excitation motors, and the axial stiffness of the steel cables and the coordinates of the attachment point between the steel cables and the machine. The dynamic properties of the rubber mounts and the static moment of the excitation motor were provided by the suppliers of each component.

The equations (3-27) to (3-29) was written as six first order differential equations and solved by the MATLAB[®] built in function *ode23.m*. The eigenvalue problem was also solved by the *eig.m* MATLAB[®] function to determine the mode shapes and natural frequencies of the machine when the steel cables are caught in a blockage.

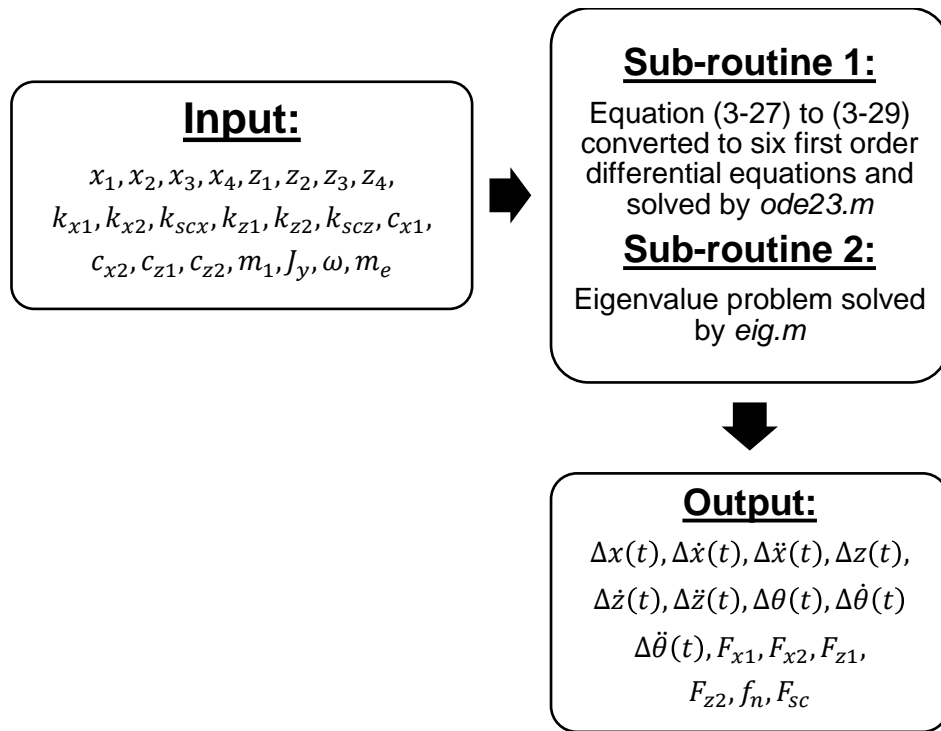


Figure 3-6: Representation of the flowchart for the computer implementation of the three-degree-of-freedom mathematical model for the machine when the steel cables are caught in a blockage.

3.4.4 Characterization of mount dynamic properties

The model implemented to determine the dynamic properties of the rubber mounts by means of a bump test can be seen in Figure 3-7. The inputs consist of two successive acceleration response amplitudes in the horizontal or vertical direction, the time period between these two amplitudes, and the mass of the machine supported by the rubber mounts.

The equations (3-38) to (3-43) are solved simultaneously in MATLAB®.

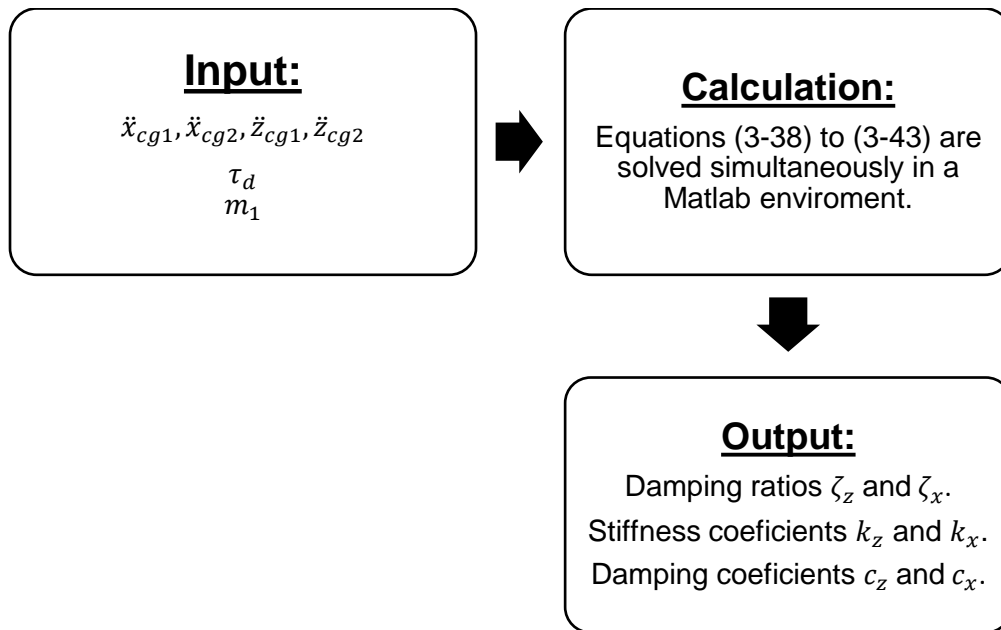


Figure 3-7: Representation of the flowchart for the computer implementation of the characterization of the rubber mounts.

3.5 Concluding remarks

Two mathematical models were developed to calculate the dynamic response, natural frequencies and forces transmitted to the support structure under different conditions for the planned ore flow restore machine. A third mathematical model was developed to calculate the dynamic properties of the rubber mounts supporting the structure.

The three mathematical models were implemented as separate programs in a MATLAB® environment. The characterization of the input parameters for the first two models and the implementation of the third model will be described in detail in Chapter 5. The implementation of the first two mathematical models will be further discussed in Chapter 4 and Chapter 6.

4 FINITE ELEMENT ANALYSIS

4.1 Introduction

Finite element analysis (FEA) was used to analyse the stiffness of the machine and stress levels during operation. The machine was designed in a SOLIDWORKS® environment and this computer aided design (CAD) model was used to perform the FEA. SOLIDWORKS® was chosen to aid in the design phase of the machine, for SOLIDWORKS® have excellent 3D modelling capabilities as well as simulation packages which was used for FEA. The fasteners, hammer and steel cables were neglected to simplify the model for the FEA. The bonded contact feature of SOLIDWORKS® Simulation was used to define the connections of parts within the model. The bottom of the rubber mounts was chosen to be fixed and a solid mesh configuration was used for the FEA. The specification values, as provided by suppliers of the rubber mounts and excitation motors were used as inputs for the FEA.

4.2 Modal analysis

Modal analysis was used to determine and investigate the first seven mode shapes. The first six mode shapes denote the natural frequencies of the rubber mounts and the seventh mode shape is defined as the structural natural frequency. The natural frequencies of the rubber mounts obtained from modal analysis were compared with the predicted natural frequencies as verification. The rubber mounts were modelled in SOLIDWORKS® as rubber tubes and the modified geometry and elastic modulus delivered the same equivalent stiffness as set out by the specifications supplied by the manufacturers of the rubber mounts. The first six modes obtained from modal analysis are shown in Figure 4-1 to Figure 4-6. The seventh mode denotes the structural natural frequency of the machine and needed to be investigated, for the machine was assumed as a rigid body in the mathematical model. The design of the structure was an iterative process to ensure that the structural natural frequency is a scale of 200% above 25 Hz (the operating frequency of the excitation motors) to ensure that the system is operated far below structural resonance. Various stiffener designs were considered to increase the stiffness of the structure which will result in a higher structural natural frequency. The design which resulted in the most stiffness added to the system with a minimal increase in mass was chosen. The seventh mode obtained from modal analysis is represented in Figure 4-7.

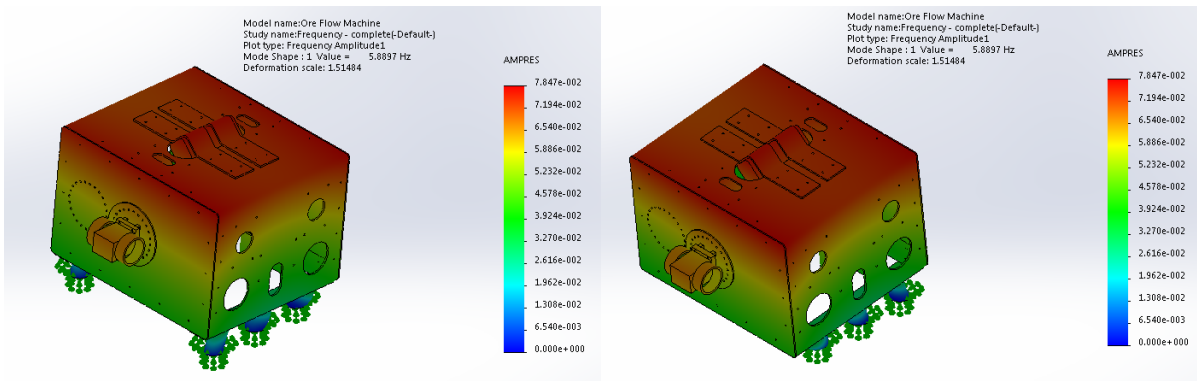


Figure 4-1: Representation of the translation mode shape along the y-axis at 5,89 Hz.

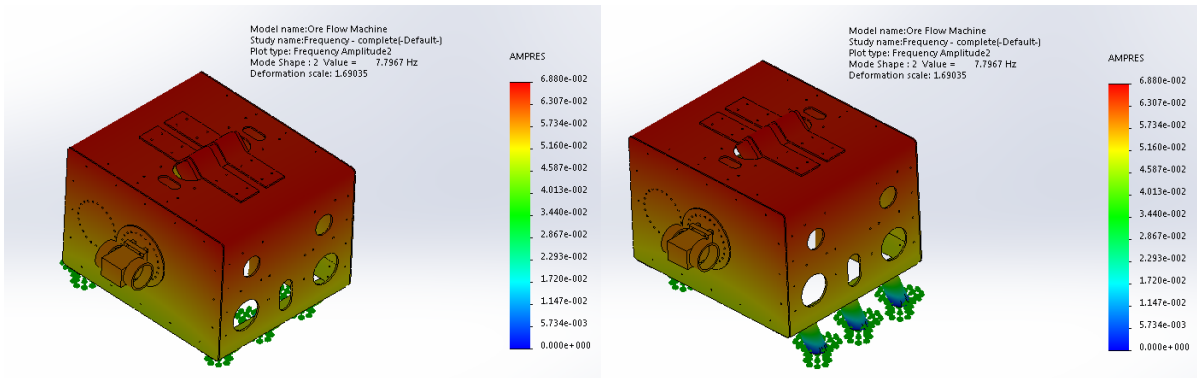


Figure 4-2: Representation of the translation mode shape along the x-axis at 7,80 Hz.

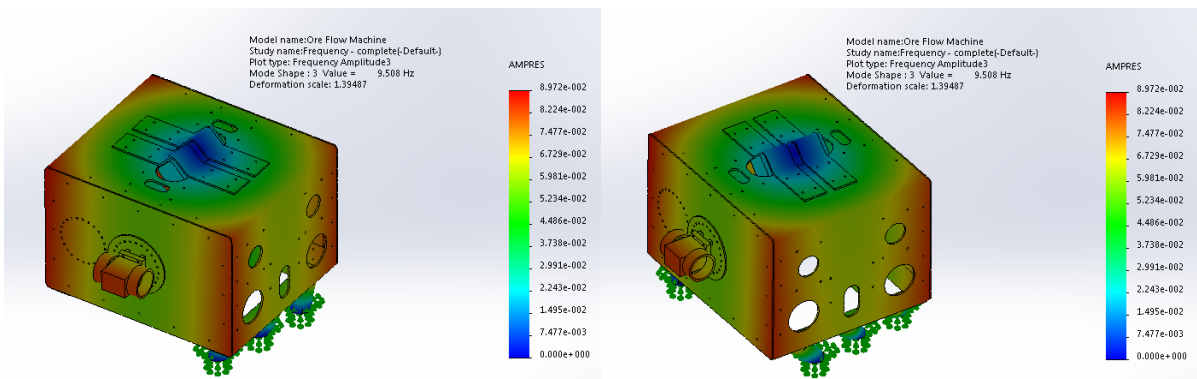


Figure 4-3: Representation of the rotational mode shape around the z-axis at 9,51 Hz.

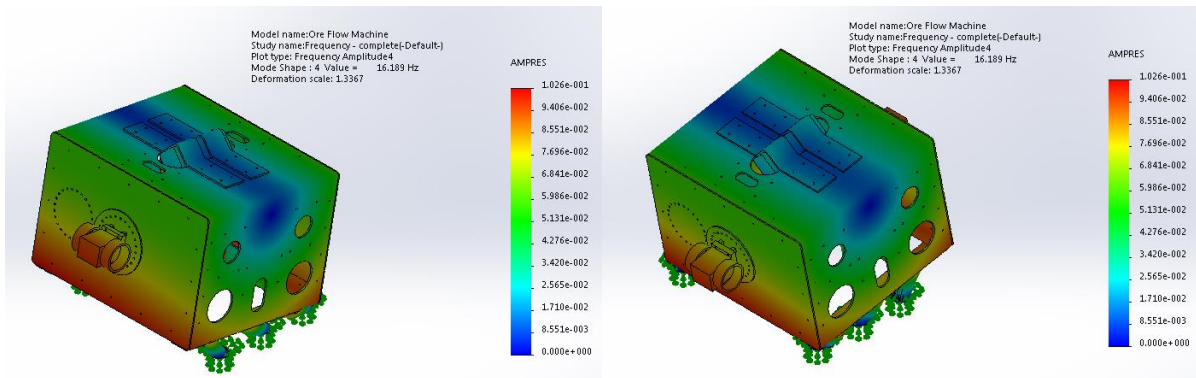


Figure 4-4: Representation of the rotational mode shape around the x-axis at 16,19 Hz.

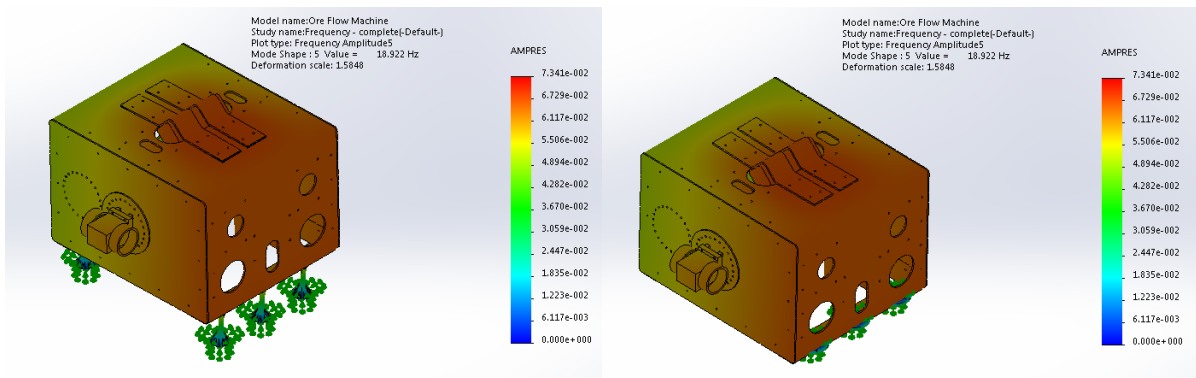


Figure 4-5: Representation of the translation mode shape along the z-axis at 18,92 Hz.

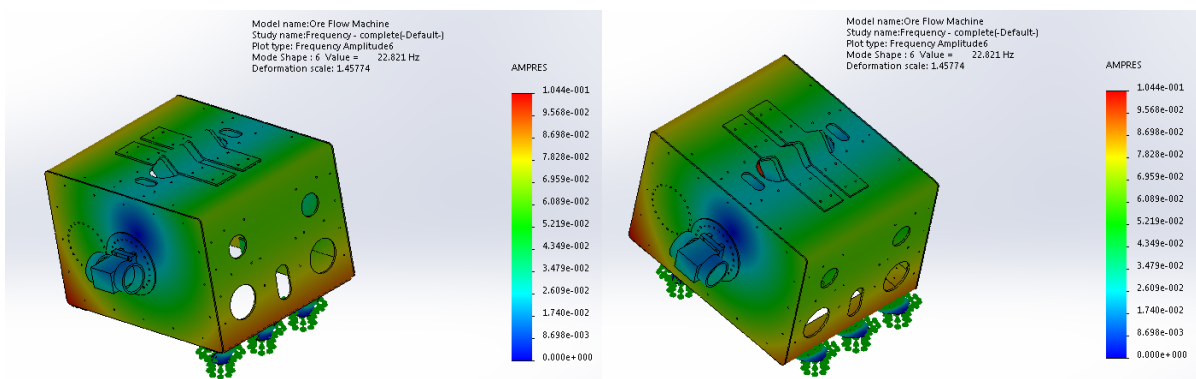


Figure 4-6: Representation of the rotational mode shape along the y-axis at 22,82 Hz.

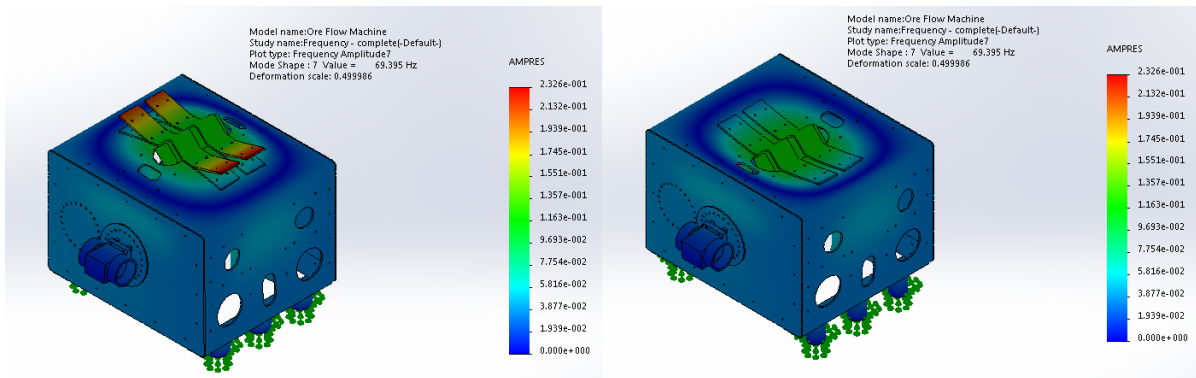


Figure 4-7: Representation of the structural mode shape at 69,40 Hz.

The natural frequencies obtained from FEA were compared with the three natural frequencies (horizontal, vertical and rotational) calculated from MATLAB[®] as provided in Table 4.1. The small difference between these values are contributed to SOLIDWORKS[®] FEA including the coupling of all six modes whereas the three-degree-of-freedom mathematical model only includes the coupling of three modes.

Table 4.1: Summary of the calculated and simulated natural frequencies for the stand-alone machine.

Mode	Simulated frequency [Hz]	Calculated frequency [Hz]
x	7.80	8.89
y	5.89	
z	18.92	18.12
θ_x	16.19	
θ_y	22.82	22.13
θ_z	9.51	
Structural	69.40	

4.3 Dynamic stress analysis

The static load analysis in SOLIDWORKS[®] was used to compute the stress levels in the machine during the two different operating conditions. The gravity load component was adjusted to induce the same maximum reaction forces at the rubber mounts, as the reaction forces obtained from the mathematical models. Supplier specifications were used for inputs of these mathematical models for the FEA as part of the design phase. Thus, by inducing the same reaction forces, the static load analysis determined the maximum stress levels of the

machine when operating. If the operating stress was higher than the yield strength of steel, the machine was redesigned and strengthened at the point where the maximum stress was experienced.

4.3.1 Stand-alone machine

The maximum reaction forces experienced when operating the machine while the steel cables are not caught in the blockage were calculated as $F_x = 1465 N$ and $F_z = 39022 N$ (as described in Paragraph 3.3.1.2). The gravitational load components to induce the reaction forces were computed as $g_x = 5.3 m/s^2$ and $g_z = - 141.6 m/s^2$. The gravitational load components, fixture of rubber tubes and the mesh used for the static load analysis are depicted in Figure 4-8. The maximum von Mises material stress was computed as $374.8 MPa$, as seen in Figure 4-9. The maximum stress observed by the machine is located at a concentrated point, at the edge of the angle iron which connects the side plate and the bent sheet metal, as seen in Figure 4-10. The maximum stress is deemed as an inaccurate stress calculation due to the stress being located at a concentrated point. Thus, an accurate estimated stress lies within the bright green/light yellow region represented in Figure 4-11, which amounts to about $280 MPa$.

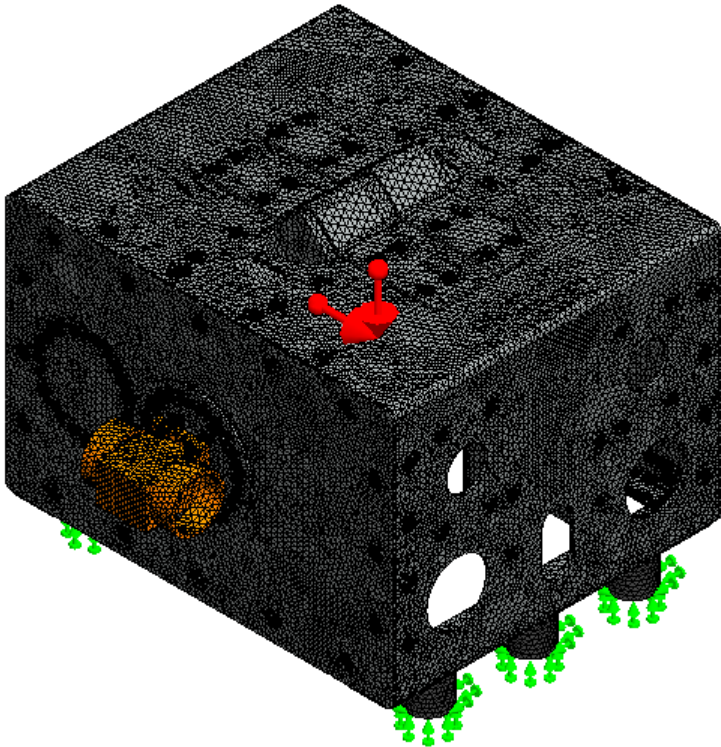


Figure 4-8: Representation of the meshed SOLIDWORKS® CAD model for static load analysis.

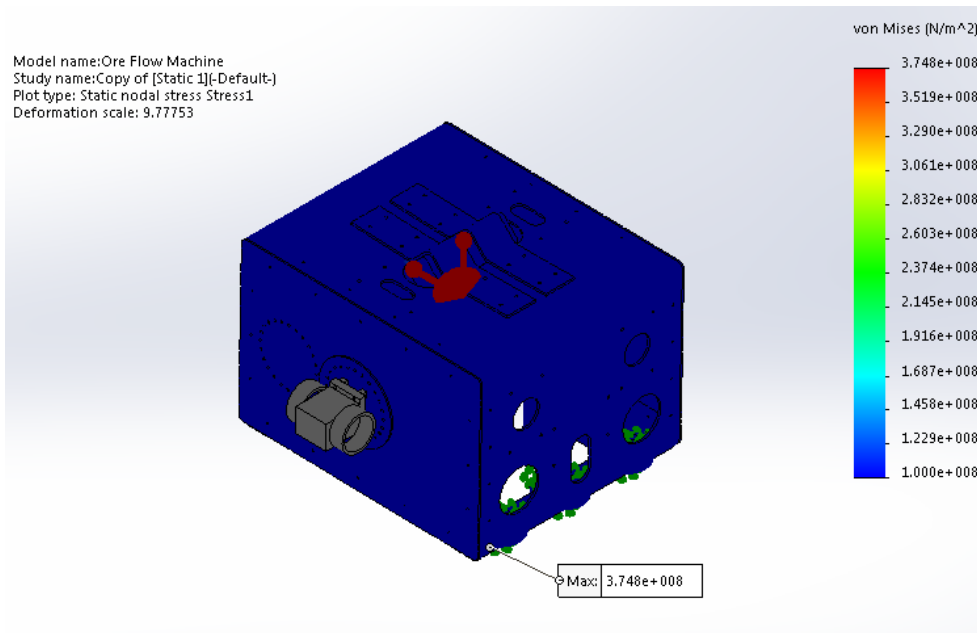


Figure 4-9: Representation of the result obtained from static load analysis.

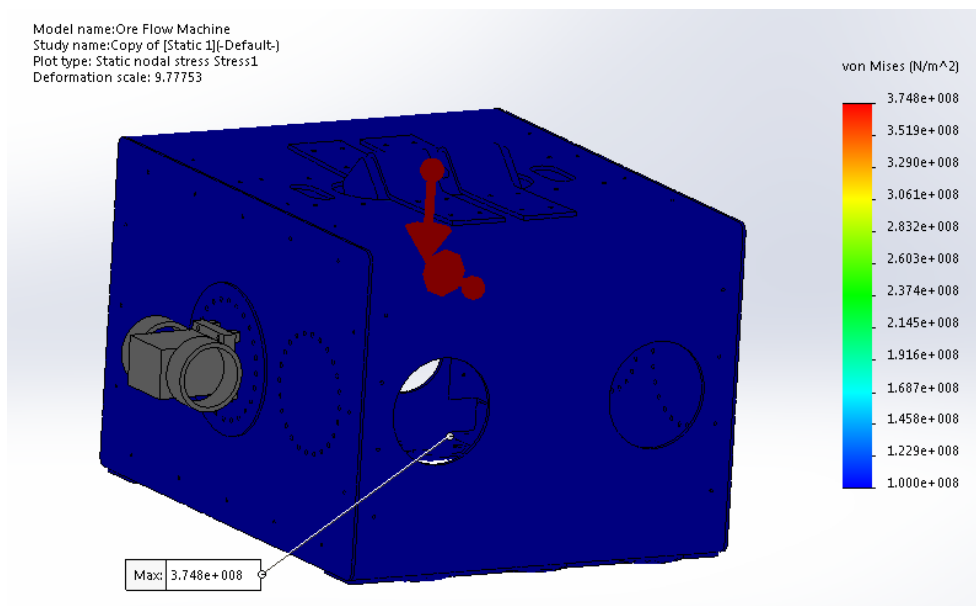


Figure 4-10: Representation of the point of where the maximum stress is located.

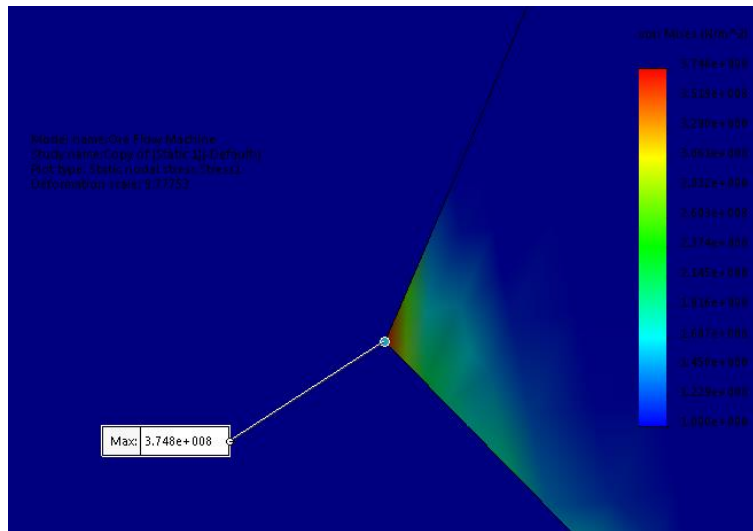


Figure 4-11: Zoomed-in representation of the point of where the maximum stress is located.

4.3.2 Steel cables acting as springs

The maximum reaction forces experienced when operating the machine while the steel cables are caught in a blockage and acting as additional spring, were calculated as $F_x = 2129\text{ N}$ and $F_z = 35890\text{ N}$ (as described in Paragraph 3.3.2). The gravitational load components to induce these reaction forces were $g_x = -15.85\text{ m/s}^2$ and $g_z = -106.58\text{ m/s}^2$. Additional load components of 9215 N were added to the points where the steel cables attach onto the machine as seen from the section views represented in Figure 4-12, to include the force which the steel cables exert on the machine. The gravitational load components, fixture of rubber tubes and the mesh used for the static load analysis can be seen in Figure 4-13. The maximum von Mises material stress was computed as 156.2 MPa , as shown in Figure 4-14. The maximum stress observed by the machine is located at a concentrated point, at the edge of the clamp used to clamp in the square bar located on top of the machine, as represented in Figure 4-15. The maximum stress is deemed as an inaccurate stress calculation due to the stress being located at a concentrated point. Thus, an accurate estimate stress lies within the bright green/light yellow region as represented in Figure 4-16, which amounts to about 100 MPa .

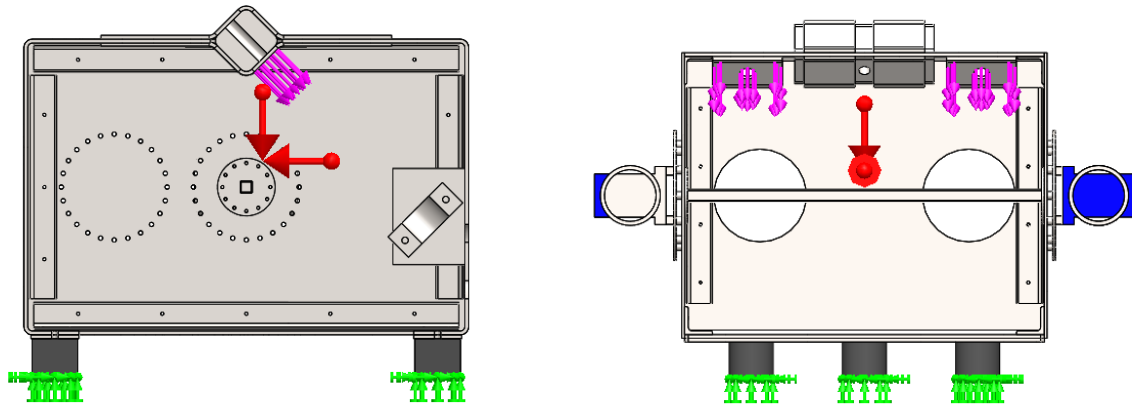


Figure 4-12: Section view of machine to represent the position where the cable force is located.

Left: Left section view.

Right: Front section view.

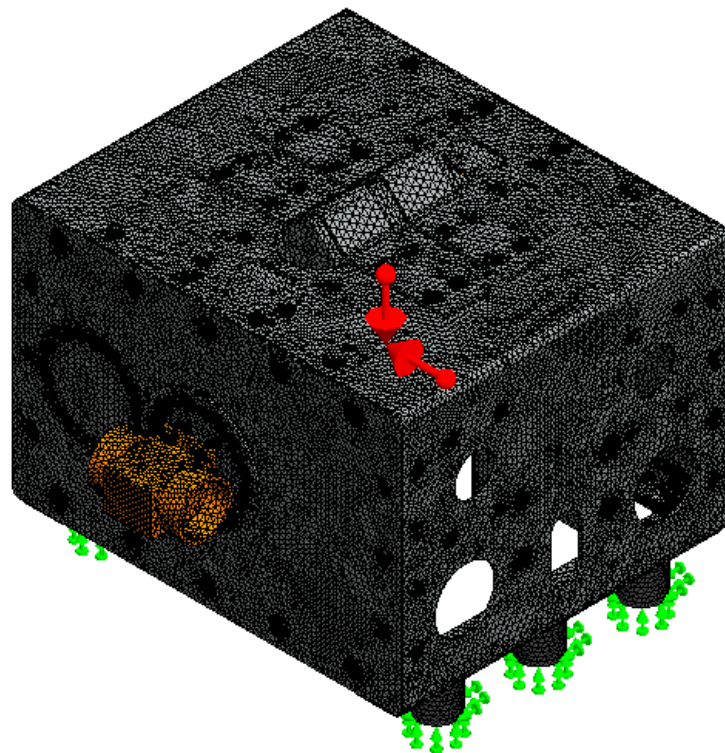


Figure 4-13: Representation of the meshed SOLIDWORKS® CAD model static load analysis where the steel cables exert force onto machine.

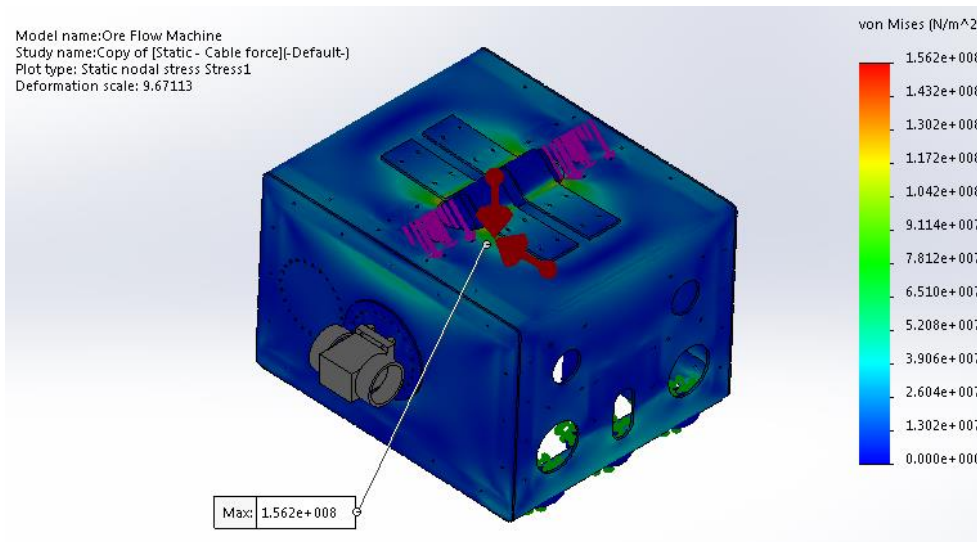


Figure 4-14: Representation of the result obtained from the static load analysis where the steel cables exert force onto machine.

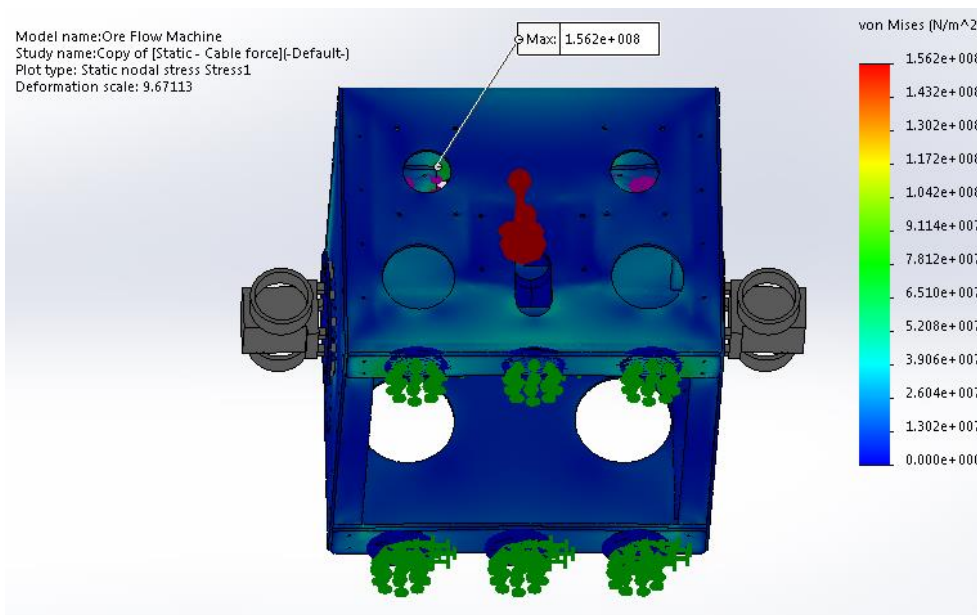


Figure 4-15: Representation of the point of where the maximum stress is located.

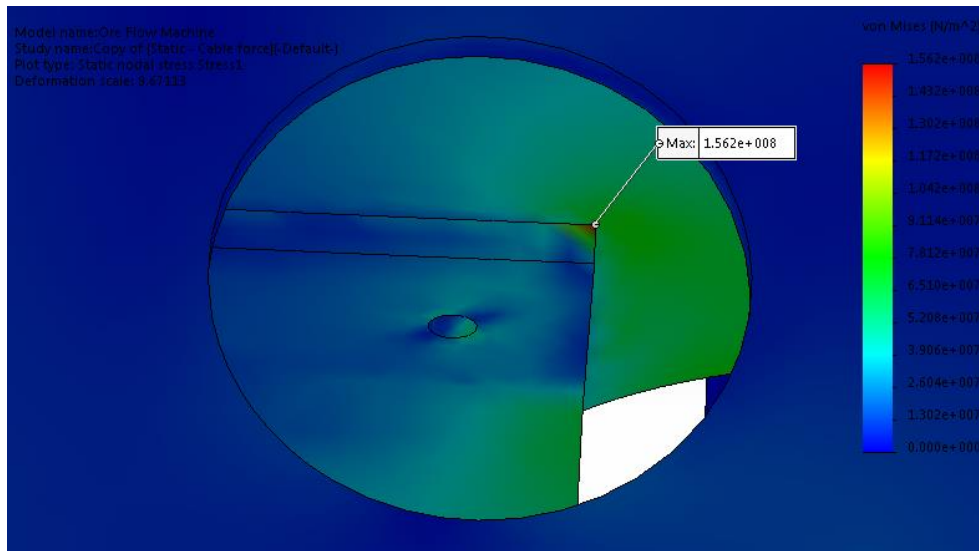


Figure 4-16: Zoomed-in representation of the point of where the maximum stress is located.

4.4 Conclusion

Finite Element Analysis (FEA) was used to determine the different mode shapes driven by the rubber mounts and the structural natural frequency of the machine. The three natural frequencies calculated with the three-degree-of-freedom mathematical model (horizontal, vertical and rotational) correlate well with the corresponding mode shapes determined through FEA. The structural natural frequency of the machine is well above the operating frequency of the unbalance motors which deems the design safe from structural resonance.

FEA was also used to determine the maximum stresses present in the machine when operating with and without steel cables caught in a blockage. The machine was analysed under extreme conditions therefore the machine will be safe from failure when operating, knowing that the machine will never be operated at such extreme conditions.

The design was deemed sufficient and the machine was built and erected in the North West University's laboratory. The drawings can be viewed in Appendix F. The input parameters used for the design of the machine will be characterised in Chapter 5.

5 EXPERIMENTAL CHARACTERISATION

5.1 Introduction

The input parameters (as described in Paragraph 3.4) such as the mass of the ore-flow restore machine, the dynamic- and static properties of the rubber mounts, and the excitation force of the vibration motors will be characterised to ensure that the values provided by suppliers and SOLIDWORKS® (used for design purposes) are correct. The characterisation of these parameters will also be used to verify that the model is built according to the specifications set out by the theoretical models. This chapter will describe the process followed to characterise the parameters.

5.2 Machine mass

The mass of the machine was characterised by lifting the machine with a hydraulic jack. A load cell with an electronic output display was fitted between the hydraulic jack and the machine as seen in Figure 5-1. A 10 *kg* weight and a 20 *kg* weight were weighed by the load cell to determine the accuracy of the load cell. Figure 5-2 (a) shows an output of 9 *kg* for the 10 *kg* mass and Figure 5-2 (b) shows an output of 19 *kg* for the 20 *kg* mass. This concludes that the load cell has a small percentage error but is considered small enough to be deemed accurate.

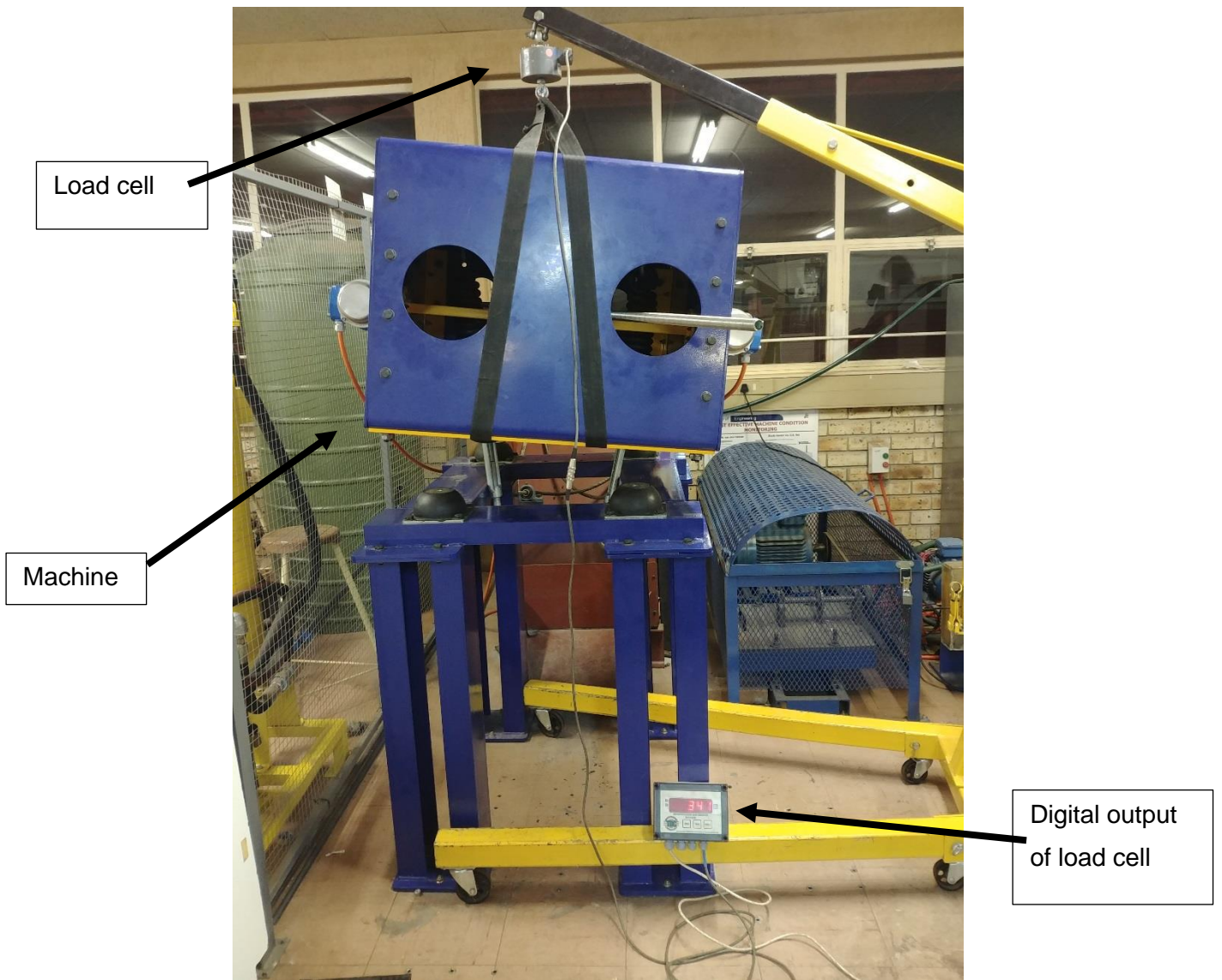


Figure 5-1: Representation of the process utilised to weigh the machine.



Figure 5-2: Representation of weights weighed to determine the accuracy of the load cell.

Left: 10 kg mass

Right: 20 kg mass

The mass of the machine was determined as 342 kg , with reference to Figure 5-1, which corresponds to the mass obtained in SOLIDWORKS[®]. The mass moment of inertia of the machine about the y axis as seen in Figure 3-3 was obtained from SOLIDWORKS[®] and is equal to 46.2733 kgm^2 . The mass moment of inertia was assumed to stay the same when the steel cables are caught in a blockage.

A steel spring, shackles and a turnbuckle was weighed with four different scales as seen in Figure 5-3, and the average mass was determined as 10.85 kg . The hammer, sleeve and Vesconite bush were weighed with four different scales as seen in Figure 5-4, and the average mass was determined as 9.95 kg . Thus the mass of the machine when the steel cables and hammer are disconnected was calculated as 310.35 kg , the mass of the machine with the two steel cables only connected was calculated as 332.05 kg , and the mass of the machine with the hammer connected was calculated as 320.3 kg .



Figure 5-3: Representation of the turnbuckle, shackles and extension spring weighed by a household scale.



Figure 5-4: Representation of the hammer, sleeve and Vesconite bush weighed with a household scale.

5.3 Rubber mounts dynamic properties

The horizontal dynamic properties of the rubber mounts were determined by means of an in-situ bump test as explained in Paragraph 3.3.3.1. An impact load was applied to the machine and the response signals were recorded with an accelerometer coupled with a Diagnostics

Instruments 2200 FFT Analyser as seen in Figure 5-5 and Figure 5-6. The time and frequency domain signals obtained from the bump test can be seen in Figure 5-7. The computer program (MATLAB®) used to calculate the dynamic stiffness, damping ratio and damping coefficient is described in Paragraph 3.4.4.



Figure 5-5: Stand-alone machine with Diagnostic Instrument coupled, with accelerometers.



Figure 5-6: Placement of the accelerometer at the fixing point of the left rubber mounts.

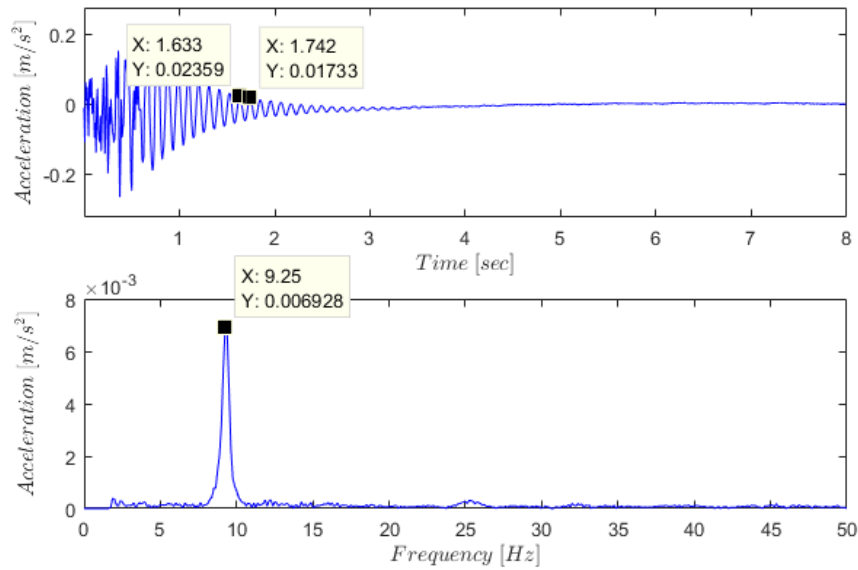


Figure 5-7: Measured horizontal natural frequency for the stand-alone machine.
Top graph: Time domain acceleration signal.
Bottom graph: Frequency domain acceleration signal.

The characterised horizontal dynamic properties for the rubber mounts are listed in Table 5.1 below.

Table 5.1: Summary of the horizontal characterised properties for the rubber mounts.

Property	Characterised value
k_{x1}, k_{x2} [kN/m]	513.322
ζ_x [%]	4.9
f_{nx} [Hz]	9.15
c_{x1}, c_{x2} [Ns/m]	874.801

Note that k_{x1} , k_{x2} and c_{x1} , c_{x2} are the equivalent stiffness and damping for a grouping of three mounts on each side of the machine as stated in Paragraph 3.3.1.

The vertical dynamic properties were characterised by a combination of an in-situ bump test and a sweep test. The bump test was used to characterise the vertical stiffness of the mounts and the sweep test was used to characterise the damping ratio of the rubber mounts. The bump test was conducted in a similar manner as for the horizontal characteristics, where an

impact load was applied to the machine and the response measured with an accelerometer coupled with a Diagnostics Instruments 2200 FFT Analyser. The time and frequency domain signals obtained from the bump test can be seen in Figure 5-8.

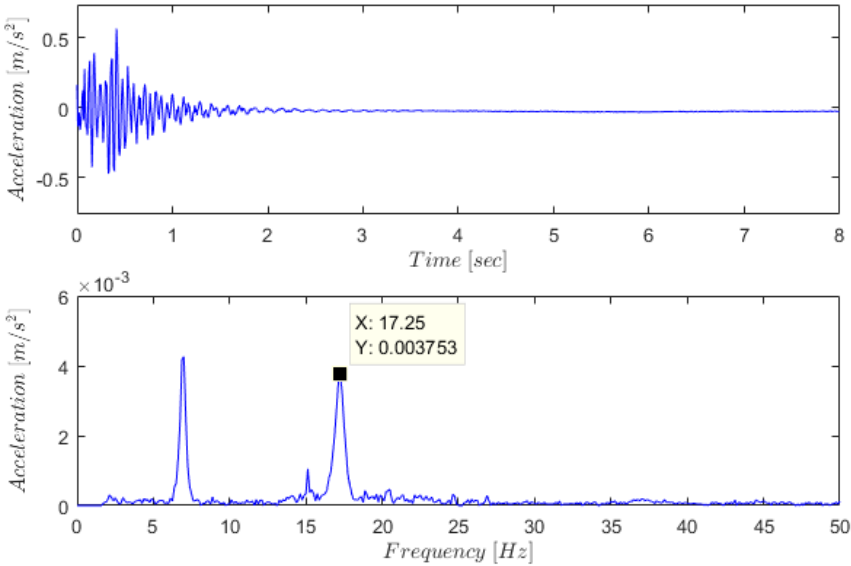
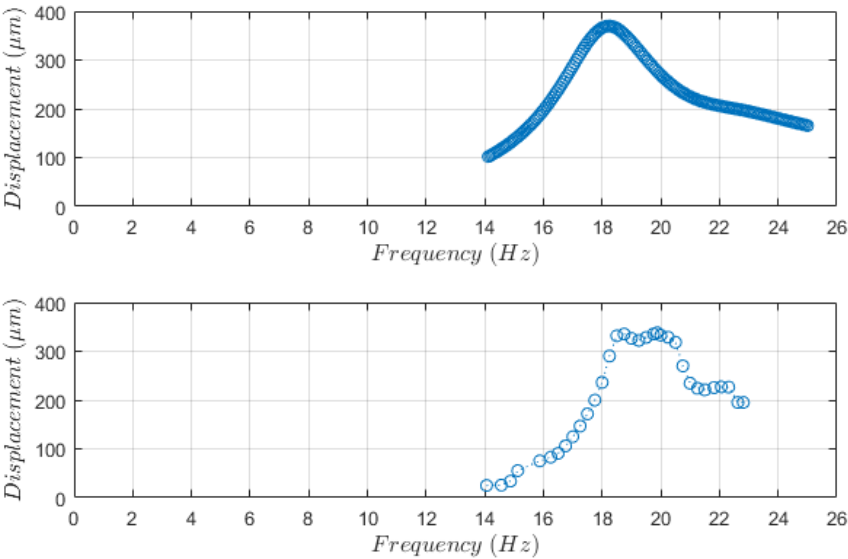


Figure 5-8: Measured vertical natural frequency for the stand-alone machine.
Top graph: Time domain acceleration signal.
Bottom graph: Frequency domain acceleration signal.

Sweep tests were conducted by measuring the response of the machine while the speed of the motors was varied over a range of frequencies, using a variable speed drive (VSD). The unbalance of the motors was set to 35% and the inclination of the motors was set to 0°. The response was measured with an accelerometer and the accelerometer was placed at the fixing point of the left rubber mount to measure vertical displacement. The measured displacement at the different frequencies were tabulated to determine at which frequencies the maximum displacement is achieved. This sweep test was conducted from 14 Hz to 23 Hz. The steel cables were disconnected from the machine and the hammer was removed during the sweep tests for the stand-alone machine.

The theoretical sweep test was calculated and plotted with the use of MATLAB® as explained in Paragraph 3.3.1 and Paragraph 3.4.2 with a motor unbalance of 35% and motor inclination of 0°. The amount of damping was characterized as 9%, to obtain the same theoretical corresponding displacements as the measured displacements during the sweep test for the two resonance conditions, respectively (vertical and rotational). The theoretical sweep test was conducted from 14 Hz to 25 Hz.

Figure 5-9 is a representation of the predicted and measured displacement over the range of different frequencies.



**Figure 5-9: Vertical displacement at different frequencies for the stand-alone machine with a motor inclination of 0° and unbalance of 35%.
 Top graph: Predicted vertical displacement.
 Bottom graph: Measured vertical displacement.**

The characterised vertical dynamic properties for the rubber mounts are listed in Table 5.2 below.

Table 5.2: Summary of the vertical characterized properties for the rubber mounts.

Property		Characterized value
k_{z1}, k_{z2}	[kN/m]	1822.887
ζ_z	[%]	9.0
f_{nz}	[Hz]	17.25
c_{z1}, c_{z2}	[Ns/m]	3027.354

Note that k_{z1}, k_{z2} and c_{z1}, c_{z2} are the equivalent stiffness and damping for a grouping of three mounts on each side of the machine as stated in Paragraph 3.3.1. The actual vertical damping ratio of the machine as seen from Table 5.2 is ten times the estimated damping ratio used for

the design of the machine. This means that the machine will experience smaller vertical displacements during operation than estimated during the design phase.

5.4 Stiffness of extension spring and steel cable

As for the characterisation of the dynamic properties of the rubber mounts, the natural frequencies were determined by conducting in-situ bump tests on the machine when the steel cable combination was caught in a blockage and tensioned. The horizontal bump test results can be seen in Figure 5-10, and the vertical bump test result can be seen in Figure 5-11. A comparison of the predicted and measured natural frequencies is presented in Table 5.3. With reference to Table 5.3, it can be seen that the predicted and measured natural frequencies correspond well despite of the mounts being tensioned under preload of the steel cables. Thus, the calculated theoretical stiffness of the steel cable combination may be deemed as acceptable.

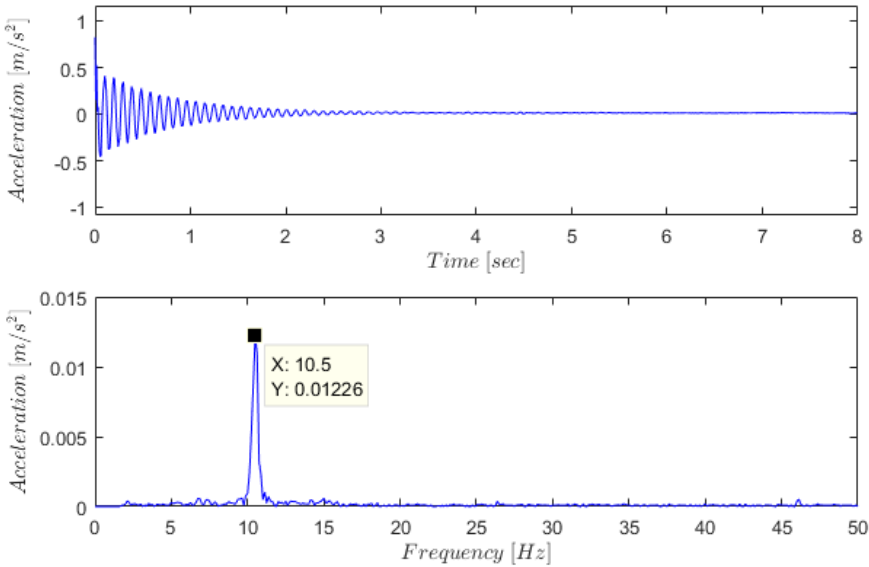


Figure 5-10: Measured horizontal natural frequency for the machine when steel cables are caught in a blockage.

Top graph: Time domain acceleration signal.

Bottom graph: Frequency domain acceleration signal.

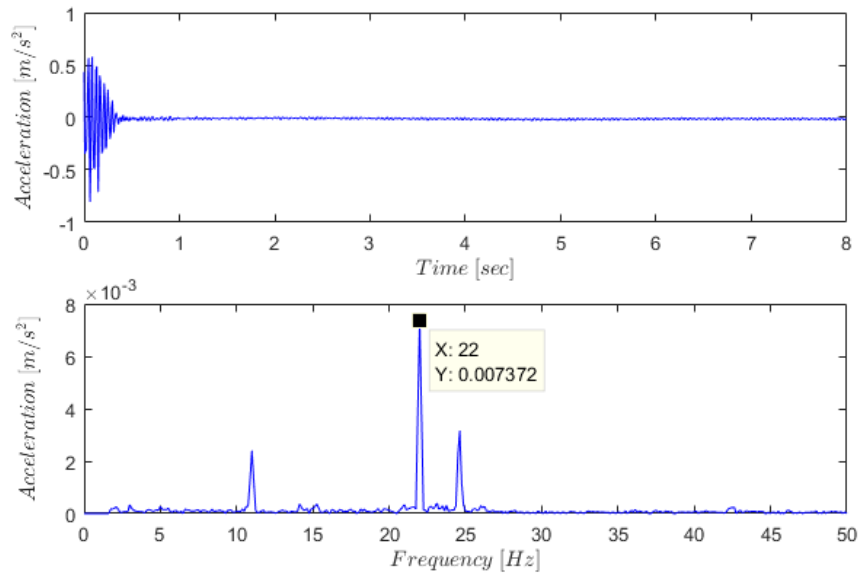


Figure 5-11: Measured vertical natural frequency for the machine when steel cables are caught in a blockage.

Top graph: Time domain acceleration signal.

Bottom graph: Frequency domain acceleration signal.

Table 5.3: Comparison of natural frequencies for machine when steel cables are caught in a blockage.

Mode	Predicted frequency [Hz]	Measured frequency [Hz]
<i>x</i>	12.28	10.5
<i>z</i>	19.45	22.0

5.5 Motor excitation force

Two excitation motors were attached on opposite sides of the machine to achieve linear motion. These motors rotate in opposite directions in order to eliminate the resultant force in the *y*-direction as seen in Figure 3-3. The magnitude of the excitation force was chosen with the criteria that the deflection of the mounts should not exceed 10 *mm*. The maximum allowable deflection of the rubber mounts is 13 *mm* as seen from the specifications of the rubber mounts as indicated in Appendix C. The computer program described in Paragraph 3.4 was used to calculate the magnitude of the excitation force to provide a deflection of 10 *mm*. This magnitude was used to select the size and type of exciter motors. Two Venanzetti

VV05B/4 exciter motors were chosen for this design. These motors operate at 25 Hz (four poles) and provide a maximum excitation force of 300 N. The technical specifications of the excitation motors are provided under Appendix D. The unbalance masses of the motors can be adjusted to achieve different excitation magnitudes. Figure 5-12 displays one of the excitation motors without protection caps. Figure 5-13 displays a close-up of the unbalance mass which consists of a collection of discs. These discs can be rotated to achieve a series of different excitation force magnitudes. The M12 x 1.0 mm nuts which fasten the discs were torqued towards a value of 30 Nm by means of a torque wrench. The excitation force needed to achieve a deflection of 10 mm was calculated as 50 N.

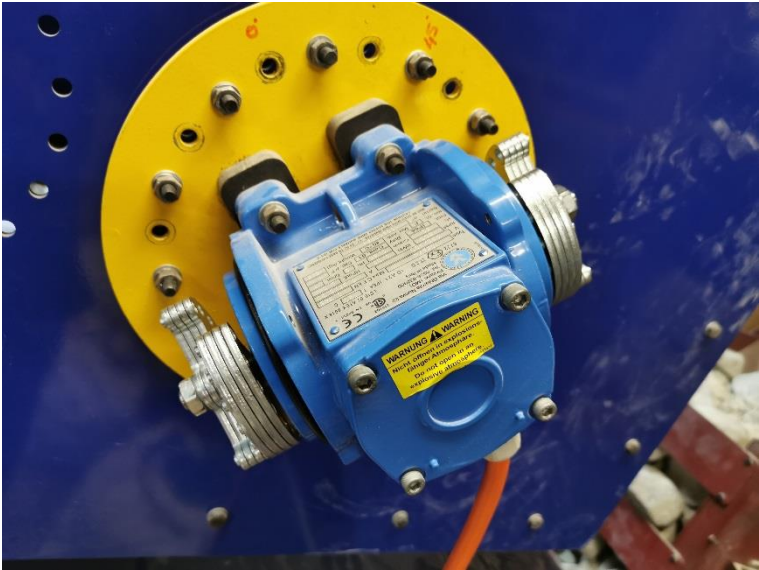


Figure 5-12: One excitation motor of the machine with end caps removed.



Figure 5-13: Close up of the discs forming the unbalance mass of the excitation motor.

The motors will be attached at an angle of 45° which is perpendicular to the steel cables. This ensures that the excitation force is in line with the length of the steel cables. The excitation motors were operated at the natural frequencies of the system during different operating conditions to ensure maximum displacement.

As mentioned in Paragraph 5.3, the actual characterised damping ratio of the rubber mounts was higher than the initial estimated damping ratio used for the design of the machine. Thus, less response is experienced when operating the machine.

5.6 Rock sample size

The largest ore size passing through an ore pass of an underground mine experiencing this problem is approximately 400 mm in diameter (de Beer, 2018). The samples that were used for experimentation was lime rock which is deemed as an acceptable substitute for the ore and rock handled in an underground mine. The samples used in the laboratory of the NWU were scaled by a factor of approximately 2, which is the same factor the test chute was scaled with. Therefore, the largest size of rock samples used in the laboratory was approximately 200 mm . Five different rock sample sizes, as seen in Figure 5-14 to Figure 5-18, were used during the experimental phase which included large ($150\text{ mm} - 250\text{ mm}$), large medium ($100\text{ mm} - 150\text{ mm}$), small medium ($50\text{ mm} - 100\text{ mm}$), small ($20\text{ mm} - 50\text{ mm}$) and fine segregate (less than 20 mm). The scale chute was filled with a ratio of 60% large rock and 40% large medium to fine segregate rock.



Figure 5-14: Representation of the size of the large sample rocks.



Figure 5-15: Representation of the size of the large medium sample rocks.



Figure 5-16: Representation of the size of the small medium sample rocks.



Figure 5-17: Representation of the size of the small sample rocks.



Figure 5-18: Representation of the size of the fine segregate sample rocks.

5.7 Conclusion

The mass of the machine was successfully characterised by using a load cell. The dynamic properties of the rubber mounts were successfully characterised by means of in-situ bump tests and a sweep test on the machine. The theoretical stiffness of the extension springs and steel cables were deemed as acceptable. The motor excitation force was successfully characterised to ensure that the rubber mounts' limits will not be exceeded. The sizes of sample rock were characterised to ensure that proportional sizes are used for experimental evaluation.

The tests conducted on the machine to determine whether the machine functions as predicted by the mathematical models and serves the purpose of unblocking a blockage will be discussed in Chapter 6.

6 EXPERIMENTAL EVALUATION

6.1 Introduction

The machine was experimentally evaluated by means of vibration measurements. Accelerometers were placed at the fixing points of the mounts and the response in the vertical and horizontal directions, and the natural frequencies were recorded. The response was recorded during steady state operational conditions. The dynamic transmitted forces were determined with the measured response and experimentally characterised mount properties. The measured vertical and horizontal response, natural frequencies and dynamic transmitted forces were compared to the predicted values calculated as described in Paragraph 3.3.

This chapter will first present all the tests and test results, followed by a short discussion thereof in Paragraph 6.11.

6.2 Vibration measurements

Two accelerometers were placed at the fixing points of the two mounts of the machine and coupled to a Diagnostics Instruments 2200 FFT Analyser. This setup was used to record the time domain and frequency signals for steady state operational conditions. Just the time domain and frequency graphs of Mount 2 will be represented in this chapter, but the predicted and measured data of both mounts will be represented in tables. This will eliminate the representation of unnecessary and repetitive graphs. The angle of the excitation motors was set to 45° relative to the horizontal axis. This angle was chosen to ensure maximum transmission of forces through the steel cables and hammer which are at an angle of 45° relative to the horizontal axis. The excitation motor unbalance was set to different percentages for the stand-alone machine, when the steel cables are caught in a blockage and when the hammer is used for unblocking.

Figure 6-1 displays the machine located in the vibration laboratory at the NWU. The placement of the accelerometers is displayed in Figure 6-2. A variable speed drive (VSD) was used to power the excitation motors which means that the rotational speed of the excitation motors could be varied. The tests were conducted at an excitation motor frequency which resulted in the maximum displacement at the rubber mounts for the different operating conditions. Larger displacement will ensure that more energy is transferred via the steel cables or hammer, and more energy could lead to a better possibility of unblocking a blockage.



Figure 6-1: Experimental test setup of the machine and chute.

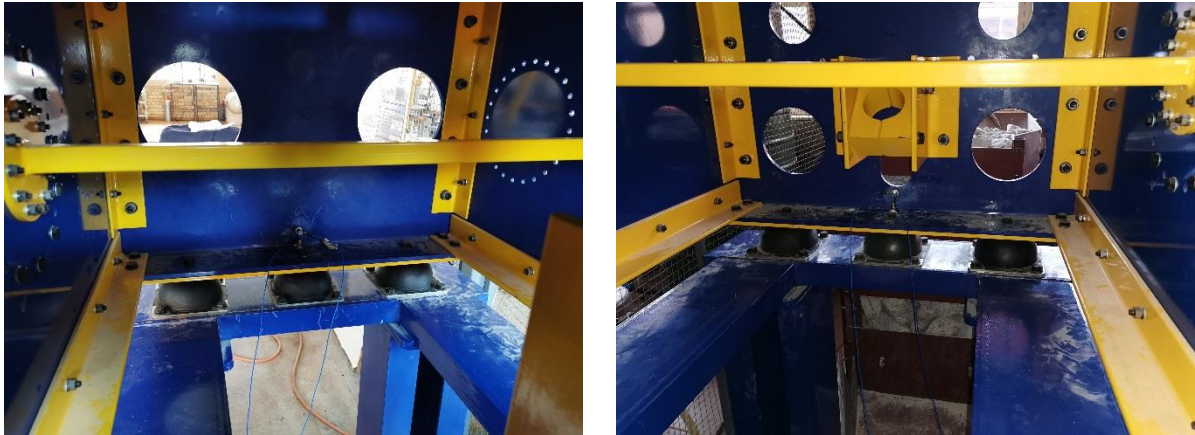


Figure 6-2: Placement of the accelerometers on the machine.

Left: Placement at Mount 1.

Right: Placement at Mount 2.

6.3 Stand-alone machine response

The responses of the stand-alone machine were measured at the fixing points of the two mounts in the horizontal and vertical directions, respectively. These measurements were taken during steady state operation. The predicted responses of the stand-alone machine were

calculated as described in Paragraph 3.4.2. The input values used to calculate the predicted responses were characterised as seen in Chapter 5. The horizontal dynamic stiffness ($k_{x1} = k_{x2}$) of the mounts is 513322 N/m and the horizontal damping coefficient ($c_{x1} = c_{x2}$) is 875 Ns/m . The vertical dynamic stiffness ($k_{z1} = k_{z2}$) is 1822887 N/m and the vertical damping coefficient ($c_{z1} = c_{z2}$) is 3027 Ns/m . The mass of the stand-alone machine is characterised as 310.35 kg and the moment of inertia J_{yy} is obtained from SOLIDWORKS® as 46.2733 kgm^2 . The frequency of the excitation motors was set to 18.25 Hz , which is the frequency at which the machine experiences maximum displacement according to the sweep test as described in Paragraph 5.3. The unbalance of the excitation motors was set to 50% in order to compare the measured and predicted responses of the system. The steel cables were disconnected from the machine and the hammer was removed while measuring the response for the stand-alone machine.

6.3.1 Steady state response

Figure 6-3 to Figure 6-6 show the predicted and measured steady state response at Mount 2 in the horizontal and vertical directions, respectively, of the stand-alone machine. A comparison between the predicted and measured values is presented in Table 6.1.

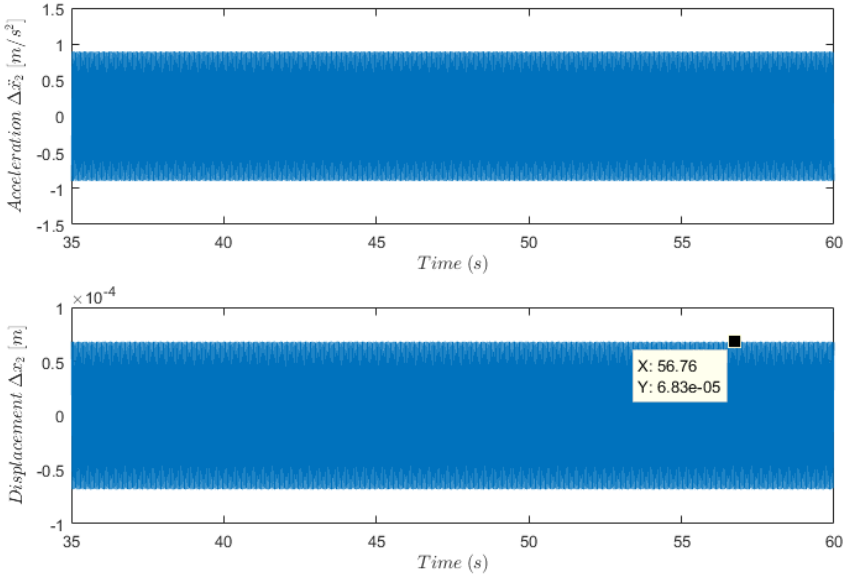


Figure 6-3: Predicted horizontal steady state response at Mount 2 for the stand-alone machine.

Top graph: Time domain acceleration signal.

Bottom graph: Time domain displacement signal.

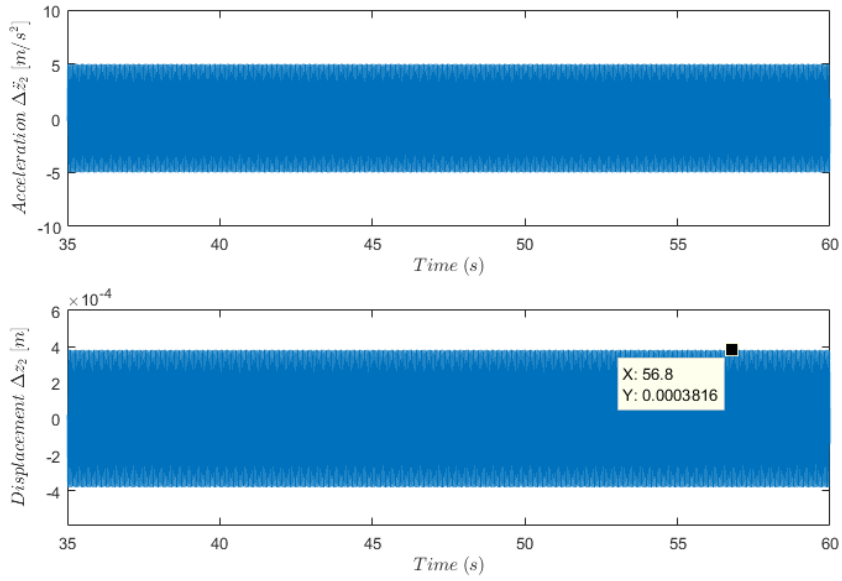


Figure 6-4: Predicted vertical steady state response at Mount 2 for the stand-alone machine.

Top graph: Time domain acceleration signal.

Bottom graph: Time domain displacement signal.

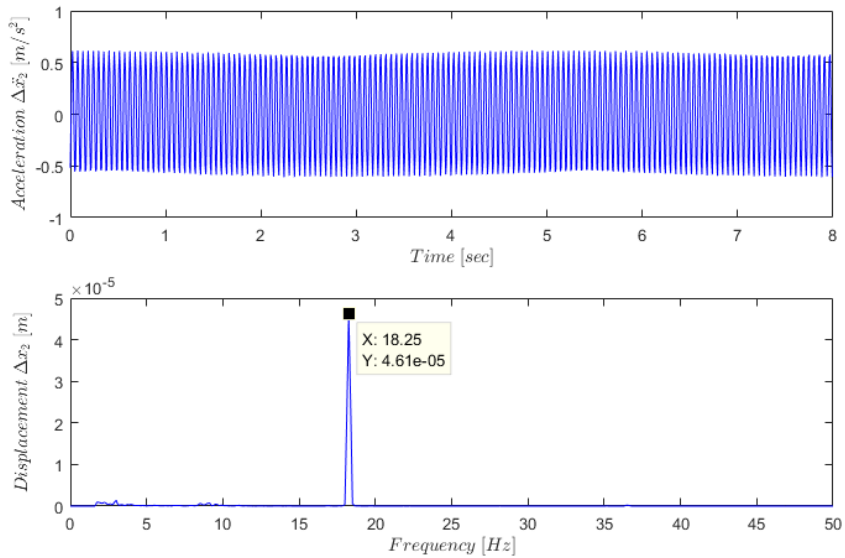


Figure 6-5: Measured horizontal steady state response at Mount 2 for the stand-alone machine.

Top graph: Time domain acceleration signal.

Bottom graph: Frequency domain displacement signal.

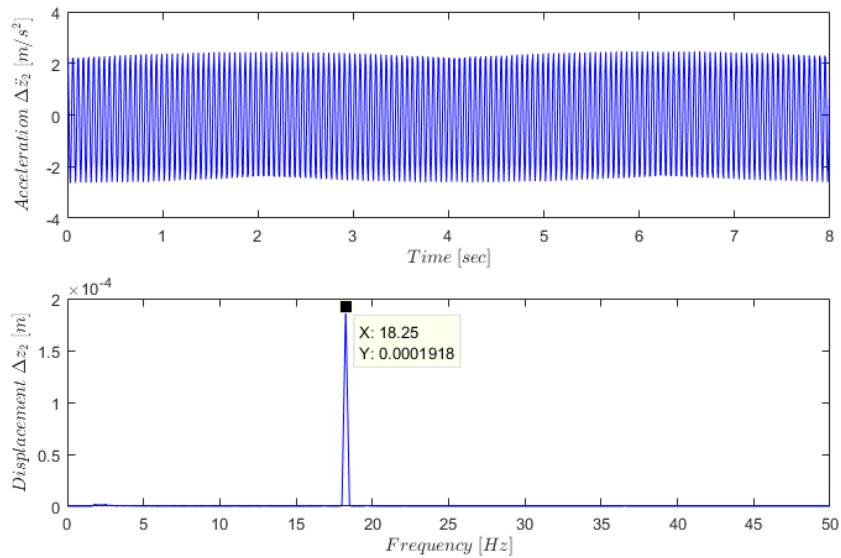


Figure 6-6: Measured vertical steady state response at Mount 2 for the stand-alone machine.

Top graph: Time domain acceleration signal.

Bottom graph: Frequency domain displacement signal.

6.3.2 Comparison between predicted and measured responses

Table 6.1 presents a comparison between the predicted and measured response amplitudes of the stand-alone machine during steady state operation.

Table 6.1: Summary of the predicted and measured response amplitudes of the stand-alone machine.

Response parameter	Predicted displacement amplitude [mm]	Measured displacement amplitude [mm]
ΔX_1	0.0683	0.0612
ΔX_2	0.0683	0.0461
ΔZ_1	0.3357	0.2629
ΔZ_2	0.3816	0.1918

The difference between the predicted and measured vertical response as seen in Table 6.1 is due to the method how the vertical damping ratio of the mounts were characterised. The damping ratio of the rubber mounts was characterised during a sweep test so that the vertical response

from the mathematical model were relative similar to the actual response for both the vertical- and rotational mode. The vertical response had a larger difference for the vertical mode as for the rotational mode during characterisation and this comparison test was conducted at the vertical mode which leads to the difference. The predicted and measured horizontal response is quite similar and the small difference is due to imperfections resulting from manufacturing and construction of the machine. This may lead to a small shift in the centre of gravity and to asymmetry.

6.4 Steel cables acting as springs

The steel cables were laid down into the scale chute as illustrated in Figure 6-7. The chute was filled with sample rock thereafter and the steel cables were attached to the machine. The steel cables were tightened by tightening the turnbuckles attached between the steel cables and the extension springs as seen in Figure 6-8 and Figure 6-9. The gate of the chute was removed (Figure 6-10) to allow rock to flow should the blockage collapse. The dynamic properties for the rubber mounts were characterised in the same manner as for the stand-alone machine, as described in Paragraph 5.3. The horizontal dynamic stiffness ($k_{x1} = k_{x2}$) of the mounts is 513322 N/m and the horizontal damping coefficient ($c_{x1} = c_{x2}$) is 1157 Ns/m . The vertical dynamic stiffness ($k_{z1} = k_{z2}$) is 1822887 N/m and the vertical damping coefficient ($c_{z1} = c_{z2}$) is 3355 Ns/m . The increase in the damping is due to the increase of the system's stiffness with the addition of the steel cables. The mass of the machine with steel cables attached is characterized as 317.583 kg and the moment of inertia J_{yy} is calculated as 47.3518 kgm^2 . The response of the machine with steel cables caught in a blockage was measured at a frequency of 20.25 Hz , where the machine experienced the maximum displacement. The excitation unbalance was set to 50% for a comparison between measured and predicted.



Figure 6-7: Representation of cables laid down in the scaled chute.
Left: Top view.
Right: Front view.



Figure 6-8: Representation of the steel cables attached to the machine.
Left: Inside the machine.
Right: Between the machine and scale chute.



Figure 6-9: Machine with steel cables attached while caught in a blockage.



Figure 6-10: Representation of the gate removed from the scaled chute.

6.4.1 Steady state response

Figure 6-11 to Figure 6-14 shows the predicted and measured steady state response at Mount 2 in the horizontal and vertical directions, respectively. Table 6.2 represents a comparison between the predicted and measured response for the machine when the steel cables act as springs.

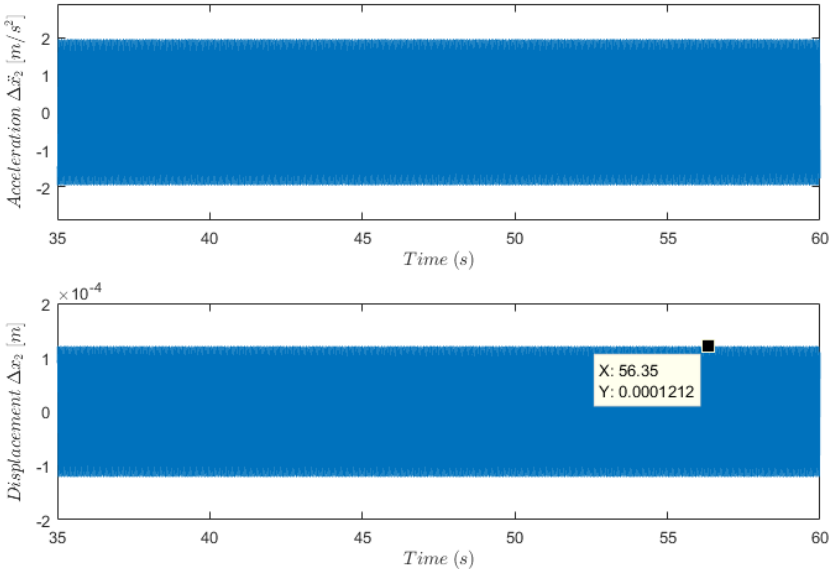


Figure 6-11: Predicted horizontal steady state response at Mount 2 when steel cables act as springs.

Top graph: Time domain acceleration signal.

Bottom graph: Time domain displacement signal.

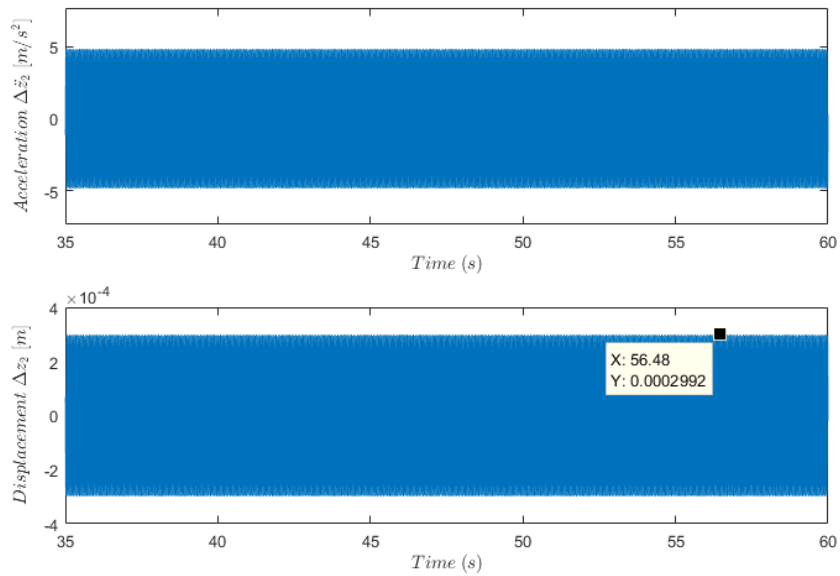


Figure 6-12: Predicted vertical steady state response at Mount 2 when steel cables act as springs.

Top graph: Time domain acceleration signal.

Bottom graph: Time domain displacement signal.

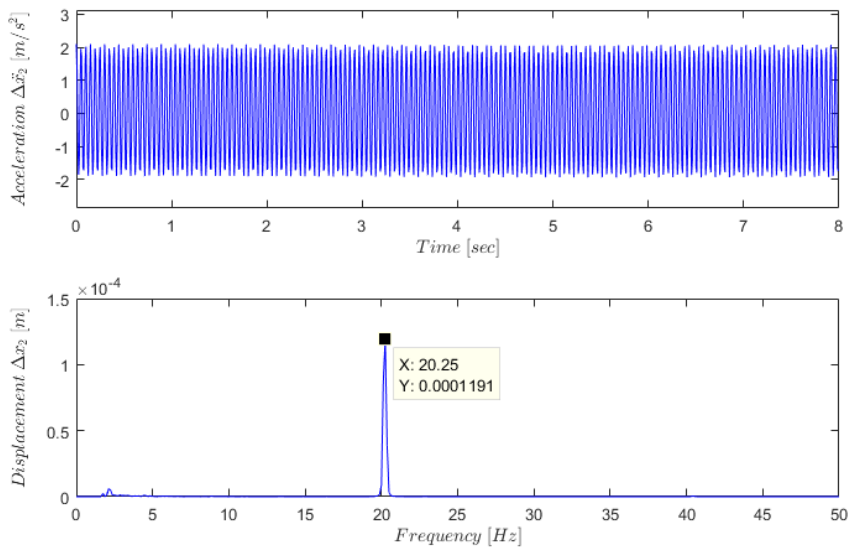


Figure 6-13: Measured horizontal steady state response at Mount 2 when steel cables act as springs.

Top graph: Time domain acceleration signal.

Bottom graph: Frequency domain displacement signal.

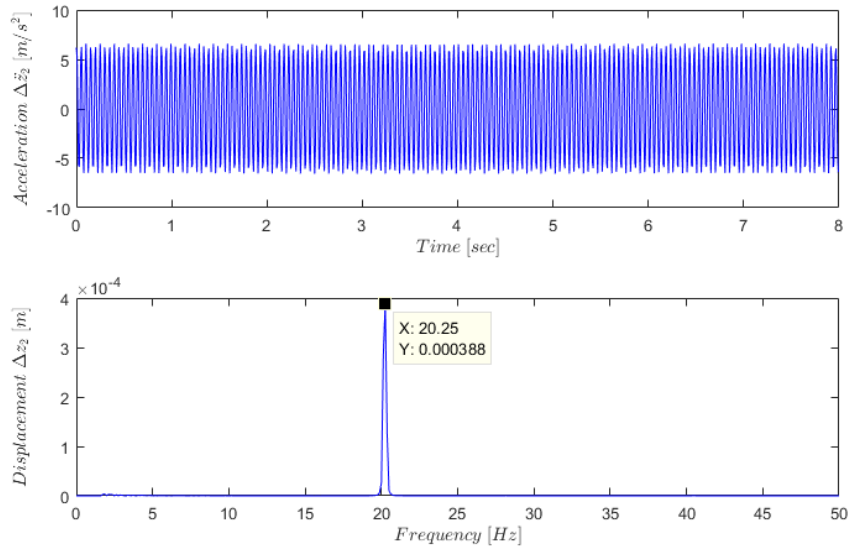


Figure 6-14: Measured vertical steady state response at Mount 2 when steel cables act as springs.
Top graph: Time domain acceleration signal.
Bottom graph: Frequency domain displacement signal.

6.4.2 Comparison between predicted and measured responses

Table 6.2 represents a comparison between the predicted and measured response amplitudes, when the steel cables act as additional springs under steady state operation.

Table 6.2: Summary of the predicted and measured response amplitudes of the machine when steel cables act as additional springs.

Response parameter	Predicted displacement amplitude [mm]	Measured displacement amplitude [mm]
ΔX_1	0.1212	0.0774
ΔX_2	0.1212	0.1191
ΔZ_1	0.3666	0.4484
ΔZ_2	0.2992	0.3880

The difference between the predicted and measured response as seen in Table 6.2 are caused by the same reason as for the stand-alone machine (Paragraph 6.3.2) but the pre-tension in the rubber mounts, when the steel cables are tightened, also contributes. The pre-tension in

the rubber mounts was not included in the mathematical model for this was too complex. The small difference between the predicted and measured horizontal response is due to same reasons as the stand-alone machine as mentioned in Paragraph 6.3.2.

6.5 Hammer operation response

Similar to Paragraph 6.4.1 where the response was measured after the chute was filled with sample rock, the response was also measured when the machine was used to hammer the rock in a blockage. An M24 threaded rod, which serves as a hammer, was screwed into the machine as shown in Figure 6-15. The response was measured for two conditions where the threaded rod made contact with the rock and where the rod did not make contact, as illustrated in Figure 6-16. The excitation frequency of the motors was set to 18.25 Hz, which is the frequency at which the stand-alone machine experience maximum displacement (as described in Paragraph 6.3). The same frequency was chosen because the small mass of the hammer in relation to the complete machine, will lead to a negligible change in the frequency where maximum displacement will be experienced. The unbalance of the excitation motors was set to 50% for both conditions so that the response of the two conditions could be compared. The response was measured with an accelerometer, placed at the fixing points of the rubber mounts and coupled with a Diagnostic Instrument. The hammer operation of the machine was too complicated to include in the mathematical model. The responses recorded for these two conditions are shown in Figure 6-17 to Figure 6-20. Table 6.3 lists the measured responses for the two conditions during operation of the machine.



Figure 6-15: Machine with M24 threaded rod (hammer) attached.

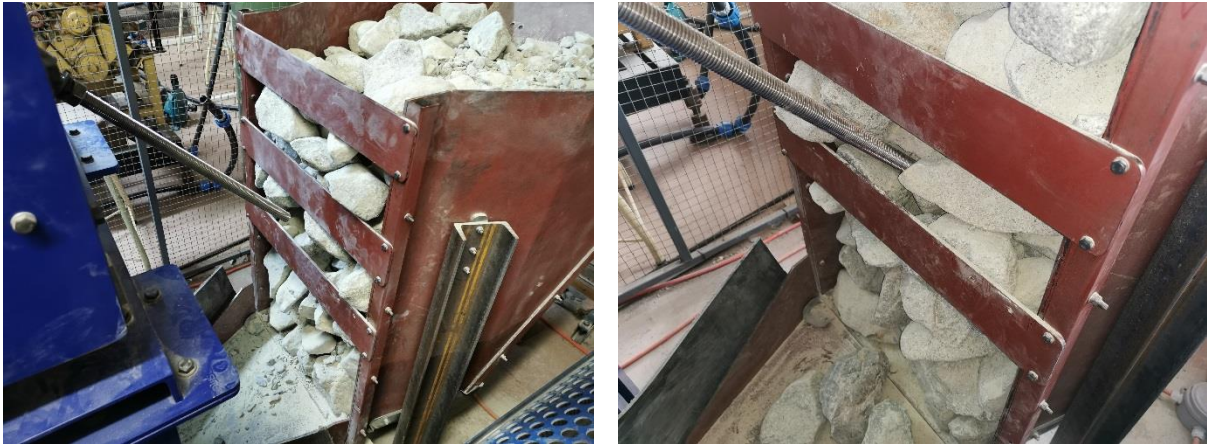


Figure 6-16: Representation of the two hammer conditions.

Left: Hammer is not in contact with the rock.

Right: Hammer is in contact with the rock.

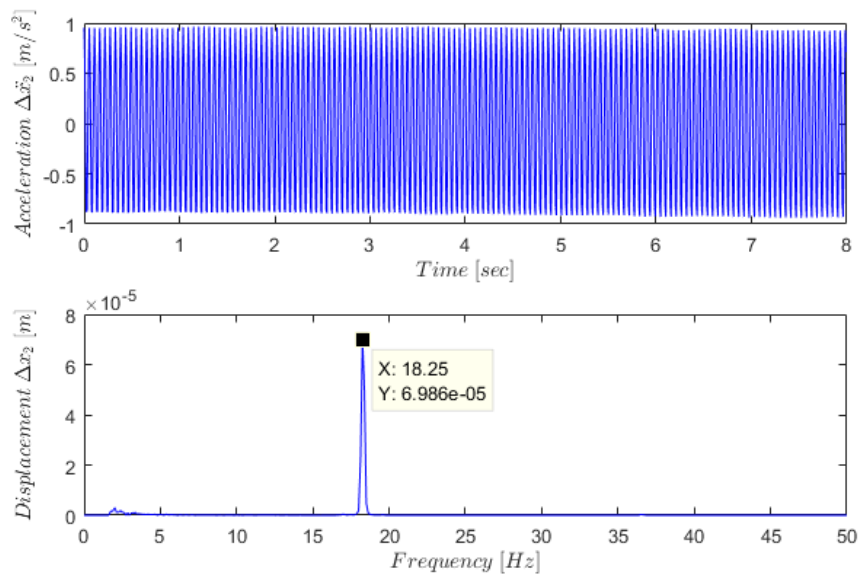


Figure 6-17: Measured horizontal response at Mount 2 when hammer is not in contact with rock.

Top graph: Time domain acceleration signal.

Bottom graph: Frequency domain displacement signal.

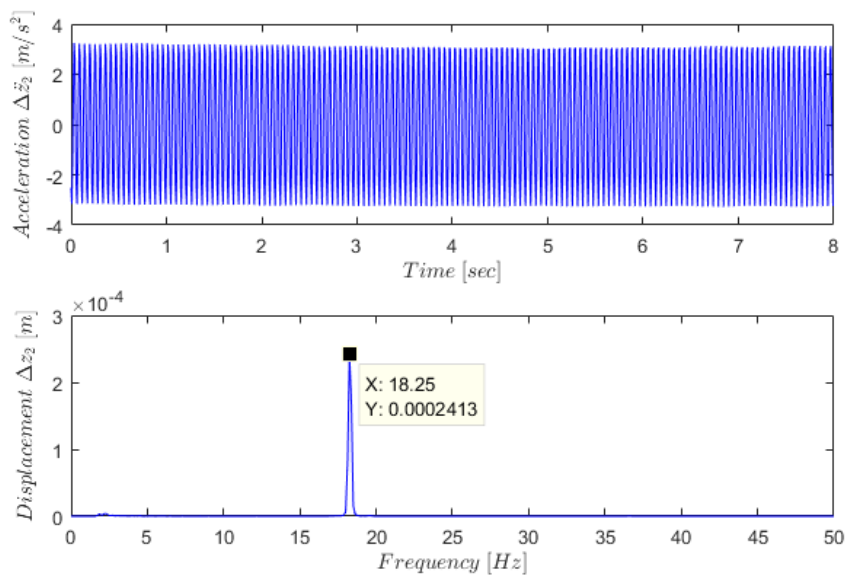


Figure 6-18: Measured vertical response at Mount 2 when hammer is not in contact with rock.

Top graph: Time domain acceleration signal.

Bottom graph: Frequency domain displacement signal.

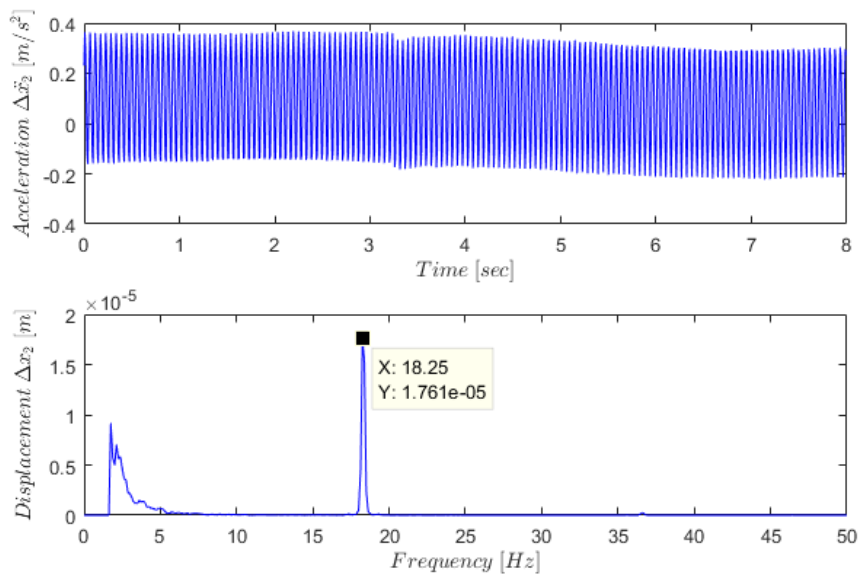


Figure 6-19: Measured horizontal steady state response at Mount 2 hammer is in contact with rock.

Top graph: Time domain acceleration signal.

Bottom graph: Frequency domain displacement signal.

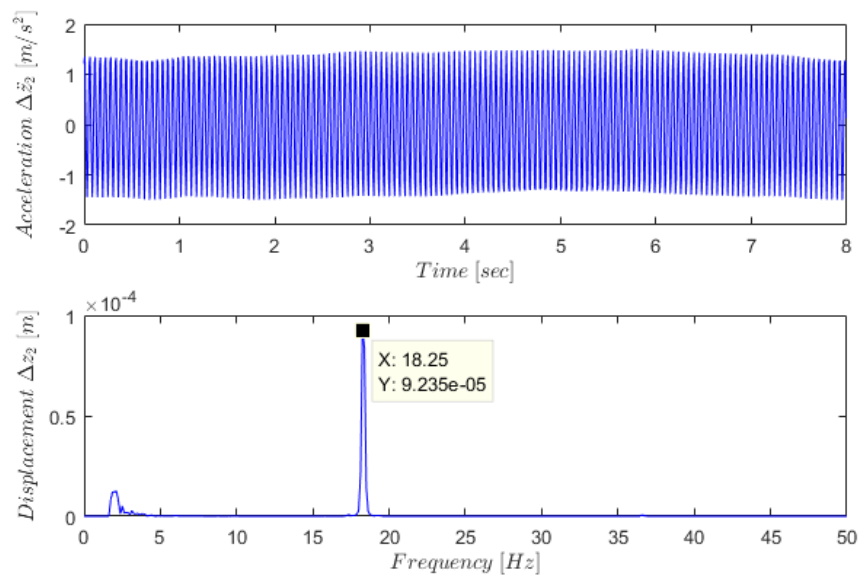


Figure 6-20: Measured vertical steady state response at Mount 2 when hammer is in contact with rock.

Top graph: Time domain acceleration signal.

Bottom graph: Frequency domain displacement signal.

Table 6.3: Summary of the measured response amplitudes of the machine while operating the hammer with and without being in contact with the blocked sample rock.

Response parameter	Hammer not in contact [mm]	Hammer in contact [mm]
ΔX_1	0.0905	0.0184
ΔX_2	0.0699	0.0176
ΔZ_1	0.2503	0.1995
ΔZ_2	0.2413	0.0924

6.6 Stand-alone machine forces

The dynamic forces transmitted to the support structure and surroundings were determined with the measured responses and the characterized dynamic properties of the rubber mounts. The dynamic forces transmitted to the support structure were calculated for steady state operation as described in Paragraph 3.3.1.2 and compared to the measured dynamic forces.

6.6.1 Steady state dynamic forces

As described in Paragraph 3.3.1.2, the dynamic forces exerted to the support structure result from the stiffness- and damping characteristics of the rubber mounts . The dynamic stiffness- and damping properties characterized in Chapter 5 were used to calculate the dynamic forces. Table 6.4 and Table 6.5 represent a comparison of the predicted and measured steady state dynamic forces in the horizontal and vertical directions, respectively.

Table 6.4: Comparison of predicted and measured horizontal steady state dynamic forces.

Mount	Maximum displacement [mm]	Stiffness coefficient [kN/m]	Damping coefficient [kNs/m]	Spring force [N]	Damping force [N]	Resultant force [N]
Predicted						
1	0.0683	513.322	0.875	35.061	6.851	35.724
2	0.0683	513.322	0.875	35.061	6.851	35.724
Measured						
1	0.0612	513.322	0.875	31.390	6.134	31.983
2	0.0461	513.322	0.875	23.666	4.625	24.113

Table 6.5: Comparison of predicted and measured vertical steady state dynamic forces.

Mount	Maximum displacement [mm]	Stiffness coefficient [kN/m]	Damping coefficient [kNs/m]	Spring force [N]	Damping force [N]	Resultant force [N]
Predicted						
1	0.3357	1822.887	3.027	611.873	116.522	622.869
2	0.3816	1822.887	3.027	695.529	132.453	708.029
Measured						
1	0.2629	1822.887	3.027	479.171	91.251	487.783
2	0.1918	1822.887	3.027	349.551	66.567	355.833

6.6.2 Comparison between predicted and measured dynamic forces

Table 6.6 represents a summary of the predicted and measured dynamic forces for the stand-alone machine.

Table 6.6: Summary of the predicted and measured dynamic forces during steady state operation for stand-alone machine.

Force	Predicted resultant force amplitudes [N]	Measured resultant force amplitudes [N]
F_{x1}	35.724	31.983
F_{x2}	35.724	24.113
F_{z1}	622.869	487.783
F_{z2}	708.029	355.833

The predicted and measured forces differ because the predicted and measured response differ. The forces transmitted has a direct relationship with the machine's response thus when the predicted and measured response differ, the predicted and measured forces will also differ.

6.7 Steel cables acting as springs forces

The same process to calculate the dynamic forces for the stand-alone machine as described in Paragraph 3.3.1.2 was followed to calculate the dynamic forces when the steel cables act as springs.

6.7.1 Steady state dynamic forces

The dynamic stiffness- and damping properties characterised in Chapter 5 were used to calculate the dynamic forces. Table 6.7 and Table 6.8 represent a comparison of the predicted and measured steady state dynamic forces in the horizontal and vertical directions, respectively.

Table 6.7: Comparison of predicted and measured horizontal steady state dynamic forces for steel cables.

Mount	Maximum displacement [mm]	Stiffness coefficient [kN/m]	Damping coefficient [kNs/m]	Spring force [N]	Damping force [N]	Resultant force [N]
Predicted						
1	0.1212	513.322	1.158	62.236	17.859	64.748
2	0.1212	513.322	1.158	62.236	17.859	64.748
Measured						
1	0.0774	513.322	1.158	39.726	11.399	41.329
2	0.1191	513.322	1.158	61.137	17.543	63.604

Table 6.8: Comparison of predicted and measured vertical steady state dynamic forces for steel cables.

Mount	Maximum displacement [mm]	Stiffness coefficient [kN/m]	Damping coefficient [kNs/m]	Spring force [N]	Damping force [N]	Resultant force [N]
Predicted						
1	0.3666	1822.887	3.355	668.252	156.508	686.335
2	0.2992	1822.887	3.355	545.414	127.738	560.172
Measured						
1	0.4484	1822.887	3.355	817.383	191.435	839.501
2	0.3880	1822.887	3.355	707.280	165.648	726.419

6.7.2 Comparison between predicted and measured dynamic forces

Table 6.9 represents a summary of the predicted and measured dynamics forces for the machine when the steel cables act as springs.

Table 6.9: Summary of the predicted and measured dynamic forces during steady state operation for the machine when the steel cables act as springs.

Force	Predicted resultant force amplitudes [N]	Measured resultant force amplitudes [N]
F_{x1}	64.748	41.329
F_{x2}	64.748	63.604
F_{z1}	686.335	839.501
F_{z2}	560.172	726.419

As described in Paragraph 6.6.2, the predicted and measured forces differ because the predicted and measured response differ.

6.8 Hammer operation forces

The measured response recorded in Paragraph 6.5 was used to compute the reaction forces exerted through the rubber mounts as described in Chapter 2. The maximum measured response was used to calculate the corresponding maximum dynamic force amplitude resulting from the stiffness- and damping characteristics of the rubber mounts. Table 6.10 displays the dynamic forces exerted through the rubber mounts when the hammer is not in contact with the rock and

Table 6.11 displays the dynamic forces when the hammer is in contact with the blocked sample rock. Table 6.12 displays the comparison between the dynamic forces of the machine when the hammer is not in contact with, and is in contact with the blocked sample rock, respectively.

Table 6.10: Measured horizontal and vertical steady state dynamic forces with hammer not in contact with rock.

Mount	Maximum displacement [mm]	Stiffness coefficient [kN/m]	Damping coefficient [kNs/m]	Spring force [N]	Damping force [N]	Resultant force [N]
Horizontal						
1	0.0905	513.322	0.875	46.456	9.078	47.334
2	0.0699	513.322	0.875	35.881	7.012	36.560
Vertical						
1	0.2503	1822.887	3.027	456.269	86.889	464.468

2	0.2413	1822.887	3.027	439.863	83.765	447.767
---	--------	----------	-------	---------	--------	---------

Table 6.11: Measured horizontal and vertical steady state dynamic forces with hammer in contact with rock.

Mount	Maximum displacement [mm]	Stiffness coefficient [kN/m]	Damping coefficient [kNs/m]	Spring force [N]	Damping force [N]	Resultant force [N]
Horizontal						
1	0.0184	513.322	0.875	9.445	1.846	9.624
2	0.0176	513.322	0.875	9.034	1.765	9.205
Vertical						
1	0.1995	1822.887	3.027	363.666	69.255	370.201
2	0.0924	1822.887	3.027	168.435	32.076	171.462

Table 6.12: Comparison of the measured dynamic forces during steady state operation for the machine when the hammer is in contact with, and not in contact with blocked sample rock.

Force	Hammer not in contact [N]	Hammer in contact [N]
F_{x1}	47.334	9.624
F_{x2}	36.560	9.205
F_{z1}	464.468	370.201
F_{z2}	447.767	171.462

6.9 Machine natural frequencies

Bump tests were conducted in order to measure the horizontal, vertical and rotational natural frequencies of the machine. The bump tests consisted of applying an impact force and measuring the acceleration with an accelerometer coupled with a DI 2200 FFT Analyser. The natural frequencies were also calculated as described in Paragraph 3.3.1.1 and will be compared with the measured natural frequencies.

6.9.1 Stand-alone machine - natural frequencies

Figure 6-21 is a summary of points where the impact force and accelerometer are located on the machine. The steel cables were disconnected from the machine and the hammer was

removed during the bump tests for the stand-alone machine. Figure 6-22 to Figure 6-24 are representations of the graphs obtained after conducting the bump tests. The mass of the stand-alone machine is characterized as 310.35 kg and the moment of inertia J_{yy} is obtained from SOLIDWORKS® as 46.2733 kgm^2 .

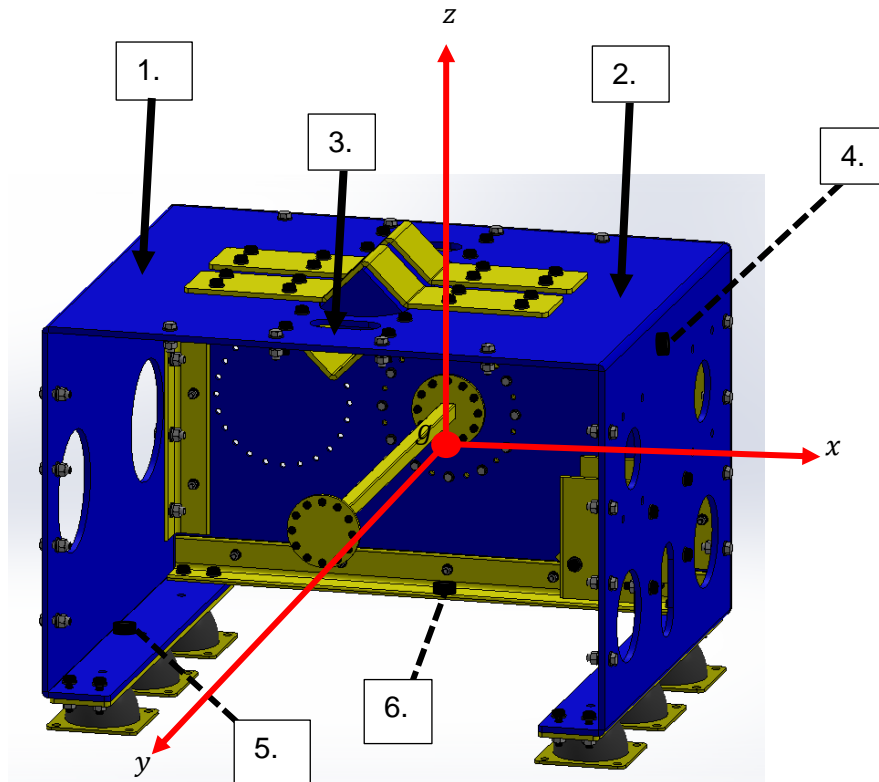


Figure 6-21: Representation of the machine with the side of the machine removed.

Horizontal bump test: With reference to Figure 6-21, the horizontal bump test was conducted by implying an impact force at No. 1, in a vertical direction as depicted by the arrow, in the middle, near the left-top edge of the machine. The accelerometer was placed perpendicular to the middle of the vertical side of the machine to measure horizontal acceleration as depicted by No. 4, near the top of the machine, in between the holes and the top edge of the machine. The result obtained from this bump test is represented by Figure 6-22 below.

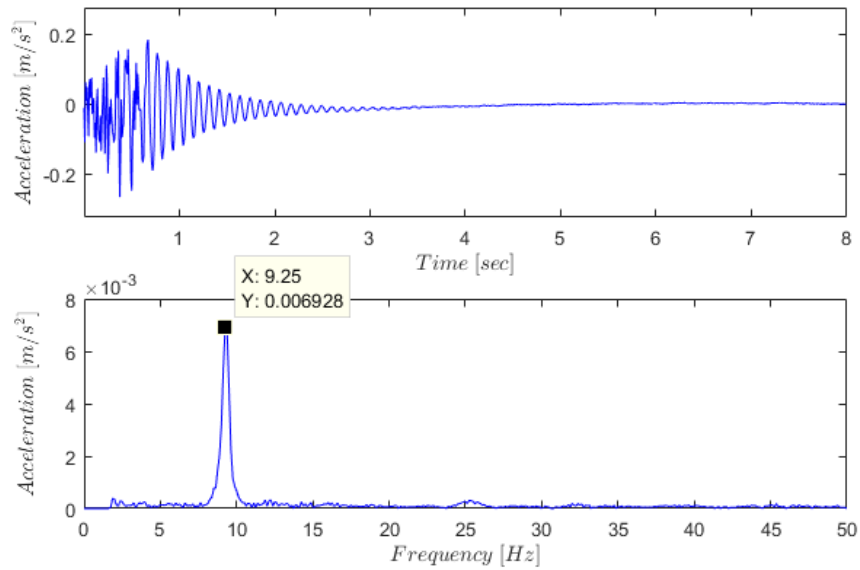


Figure 6-22: Measured horizontal natural frequency for the stand-alone machine.
Top graph: Time domain acceleration signal.
Bottom graph: Frequency domain acceleration signal.

Vertical bump test: With reference to Figure 6-21, the vertical bump test was conducted by implying an impact force at No. 3, in a vertical direction as depicted by the arrow, in the middle, in line with the square bar, near the edge of the side plate of the machine. The accelerometer was placed perpendicular to the horizontal angle iron of the machine to measure vertical acceleration as depicted by No. 6, in line with the middle bolt that connects the side plate and the angle iron. The result obtained from this bump test is represented by Figure 6-23 below.

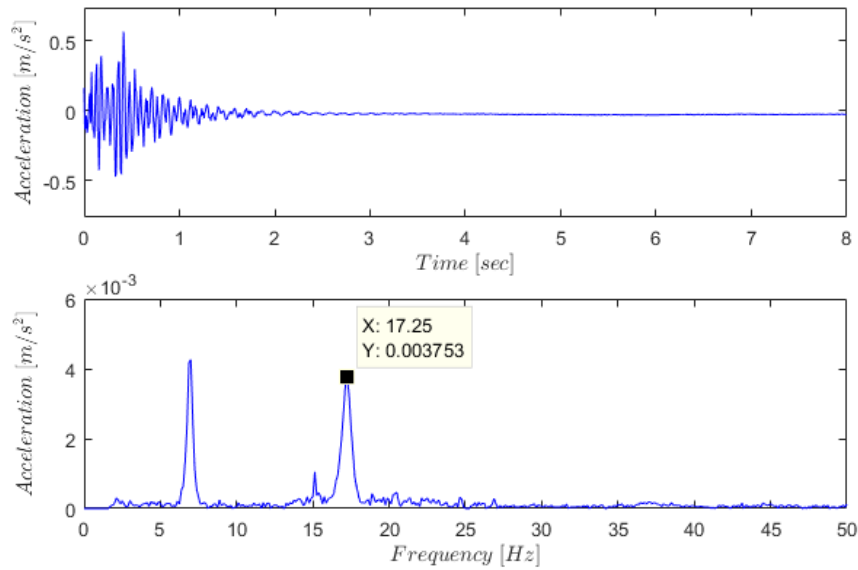


Figure 6-23: Measured vertical natural frequency for the stand-alone machine.
Top graph: Time domain acceleration signal.
Bottom graph: Frequency domain acceleration signal.

Rotational bump test: With reference to Figure 6-21, the rotational bump test was conducted by implying an impact force at No. 2, in a vertical direction as depicted by the arrow, in the middle, near the top-right edge of the machine. The accelerometer was placed perpendicular to the horizontal plate of the machine to measure vertical acceleration as depicted by No. 5, in between and in line with the bolt that attaches the middle rubber mount to the machine and the bend of the sheet metal. The result obtained from this bump test is represented by Figure 6-24 below.

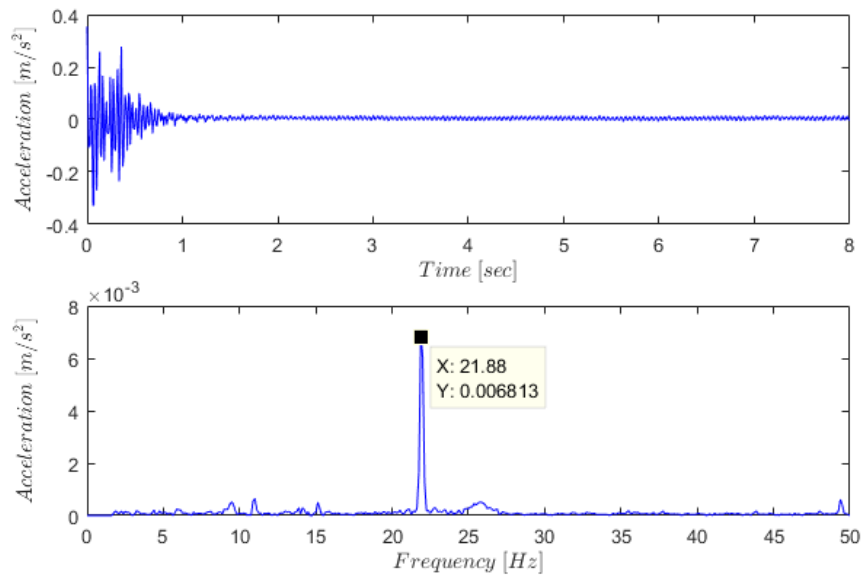


Figure 6-24: Measured rotational natural frequency for the stand-alone machine.
Top graph: Time domain acceleration signal.
Bottom graph: Frequency domain acceleration signal.

A summary of the predicted and measured natural frequencies for the stand-alone machine is presented in Table 6.13 below.

6.9.2 Steel cables acting as springs - natural frequencies

The bump tests were conducted when the steel cables were caught between rocks which leads to the cables acting as additional springs. The bump tests for the three mode shapes when the steel cables are acting as springs were conducted in the same manner as the tests for the stand-alone machine, as describe under Section 1.1. The hammer was removed during the bump tests when the steel cables are caught in a blockage. Figure 6-25 is a summary of points where the impact force and accelerometer are located on the machine when the steel cables act as additional springs. The mass of the machine with steel cables attached is characterized as 317.583 kg and the moment of inertia J_{yy} is calculated as 47.3518 kgm^2 .

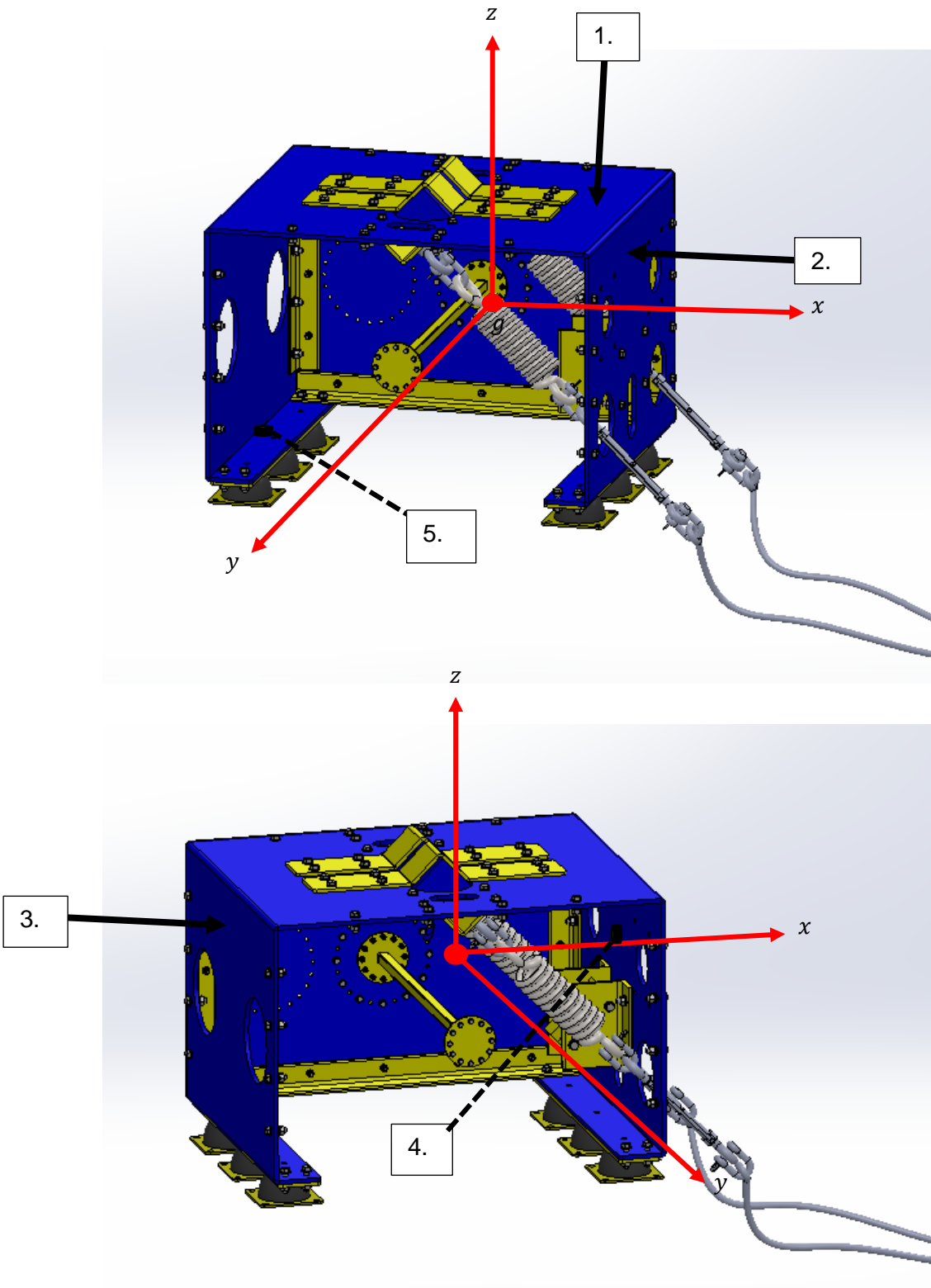


Figure 6-25: Representation of the machine with the cables attached and the side of the machine removed.

Top: Left view of machine.

Bottom: Right view of machine.

Horizontal bump test: With reference to Figure 6-25, the horizontal bump test was conducted by implying an impact force at No. 3, in a horizontal direction as depicted by the arrow, in the middle, near the edge of the machine. The accelerometer was placed perpendicular to the vertical side of the machine to measure horizontal acceleration as depicted by No. 4, in line with the bolt that attaches the middle rubber mount to the machine. The result obtained from this bump test is represented by Figure 6-26 below.

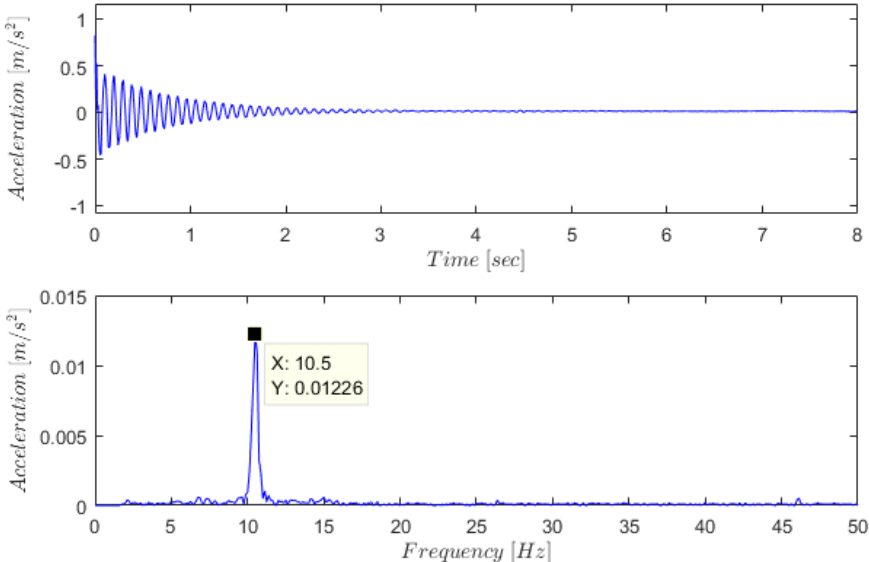


Figure 6-26: Measured horizontal natural frequency for the machine with cables acting as springs.

Top graph: Time domain acceleration signal.

Bottom graph: Frequency domain acceleration signal.

Vertical bump test: With reference to Figure 6-25, the vertical bump test was conducted by implying an impact force at No. 1, in a vertical direction as depicted by the arrow, in the middle, near the top-right edge of the machine. The accelerometer was placed perpendicular to the horizontal plate of the machine to measure vertical acceleration as depicted by No. 5, in between and in line with the bolt that attaches the middle rubber mount to the machine and the bend of the sheet metal. The result obtained from this bump test is represented by Figure 6-27 below.

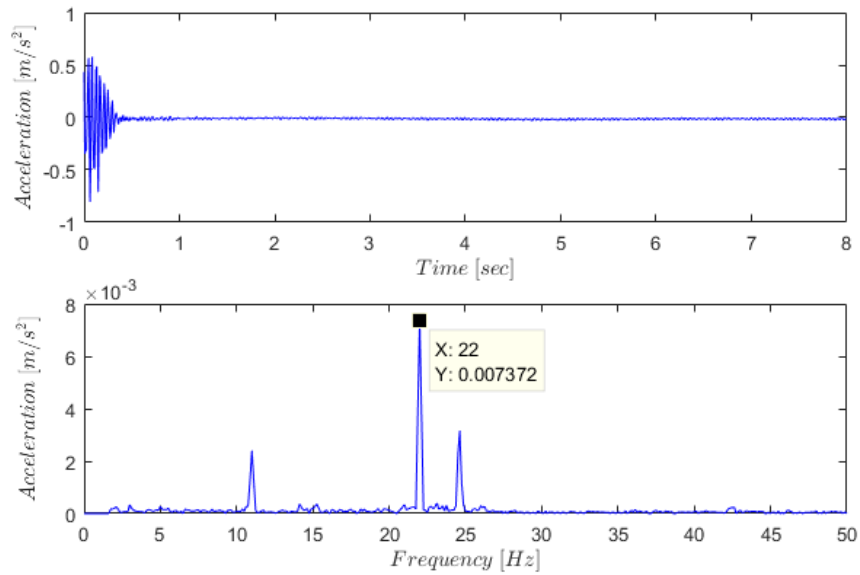


Figure 6-27: Measured vertical natural frequency for the machine with cables acting as springs.

Top graph: Time domain acceleration signal.

Bottom graph: Frequency domain acceleration signal.

Rotational bump test: With reference to Figure 6-25, the rotational bump test was conducted by implying an impact force at No. 2, in a horizontal direction as depicted by the arrow, in the middle, near the top-right edge of the machine. The accelerometer was placed perpendicular to the horizontal plate of the machine to measure vertical acceleration as depicted by No. 5, in between and in line with the bolt that attaches the middle rubber mount to the machine and the bend of the sheet metal. The result obtained from this bump test is represented by Figure 6-28 below.

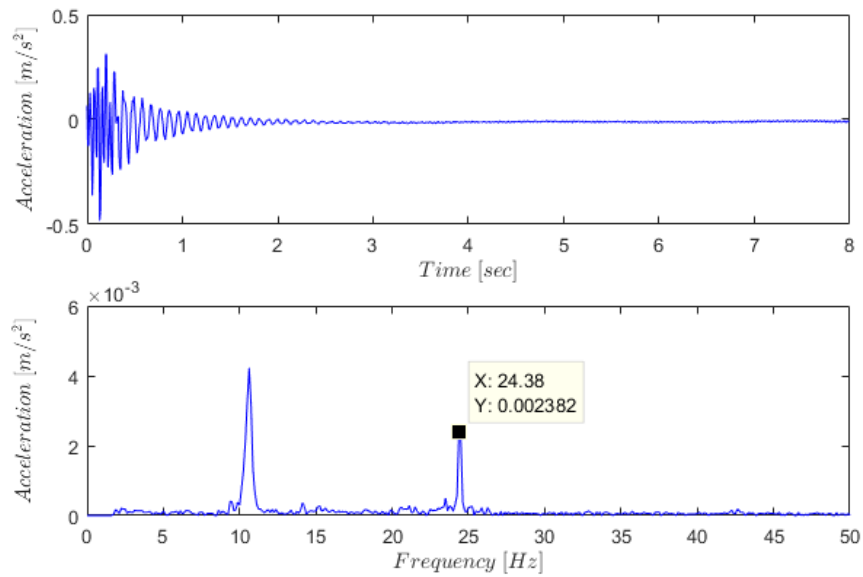


Figure 6-28: Measured rotational natural frequency for the machine with cables acting as springs.

Top graph: Time domain acceleration signal.

Bottom graph: Frequency domain acceleration signal.

A summary of the predicted and measured natural frequencies when the steel cables act as springs is shown in

Table 6.14 below.

6.9.3 Comparison between predicted and measured natural frequencies

Table 6.13 displays a summary of the predicted and measured natural frequencies for the stand-alone machine.

Table 6.14 displays a summary of the predicted and measured natural frequencies of the machine when the steel cables act as additional springs.

The predicted and measured natural frequencies of the stand-alone machine as seen in Table 6.13, differ with a small percentage. The predicted and measured natural frequencies of the machine when the steel cables act as additional springs as seen in Table 6.14, shows a larger variance. This is due to the pre-tension in the rubber mounts when the steel cables are tightened, which was not included in the mathematical model for it was too complex to describe it mathematically.

Table 6.13: Summary of natural frequencies for stand-alone machine.

Mode	Predicted frequency [Hz]	Measured frequency [Hz]
x	8.89	9.25
z	18.12	17.25
θ_y	22.13	21.88

Table 6.14: Summary of natural frequencies for machine when steel cables act as additional springs.

Mode	Predicted frequency [Hz]	Measured frequency [Hz]
x	12.28	10.5
z	19.45	22.0
θ_y	22.14	24.38

6.10 Machine operation

The steel cables and hammer operation of the machine were tested against two types of blockages: a dry interlocking blockage and a cemented blockage. The dry interlocking blockage was created in the laboratory by filling the scaled chute with 60% large sample rock and 40% large medium to fine segregate sample rock. The cemented blockage was created by filling the scale chute with the exact same ratio as for a dry interlocking blockage but mud, created from the fine segregated powder, was poured into the top of the scaled chute afterwards. The mud was left to dry which created the cemented blockage. After the two types of blockages were created, the gate of the scale chute was opened and the two different operations were tested against the blockages.

6.10.1 Steel cables

6.10.1.1 Dry interlocking blockage

As described in Paragraph 6.4, the steel cables were laid into the scaled chute before the chute was filled with sample rock. After the chute was filled with approximately 500 kg sample rock, the steel cables were tightened by means of turnbuckles and the gate of the chute was removed to start conducting tests. The test with steel cables was conducted at three different frequencies: the frequency where the stand-alone machine experiences maximum

displacement (18.25 Hz), the vertical natural frequency obtained from bump tests when the steel cables are caught in between rocks (22 Hz) and the frequency where maximum displacement was experienced while the steel cables are caught in between rocks (20.25 Hz). For each testing frequency, the unbalance of the excitation motors was set to the lowest setting (18%) and increased each time when the blockage was not disturbed. This was repeated until an unblocking occurred at a specific unbalance or until the unbalance could not be increased any further. If a partial unblocking occurred at a specific unbalance, the steel cables would be tightened again, and the machine would be switched on at the same unbalance at which the partial unblocking occurred and the test was continued.

Figure 6-29 represents the blockage created for the steel cable test at a frequency of 18.25 Hz. Figure 6-30 represents a partial unblocking which occurred at 77% unbalance. The steel cables were tightened thereafter and the test was continued but no unblocking occurred for higher unbalances.



Figure 6-29: Blockage created for the first test frequency with the gate of the chute removed.



Figure 6-30: Partial unblocking occurred at 18.25 Hz and an unbalance of 77%.

As mentioned above, the same test was repeated for an input frequency of 22 Hz. The excitation motors were switched on and the Diagnostic Instrumentation was used to ensure that the machine operates at 22 Hz. The frequency input on the VSD was kept the same and as the unbalance increased, the frequency displayed by the diagnostic instrumentation decreased due to increased slip in the induction motors. The unbalance of the excitation motors was increased from 18% up to 87%, but no unblocking occurred at this frequency. As the unbalance increased, the severity of an unknown mode shape the machine was experiencing increased and the measured response for the machine decreased. Figure 6-31 to Figure 6-32 represents the measured horizontal and vertical response, respectively, at an unbalance of 87% and an input frequency of 22 Hz. Representation of the test setup and blockage created for the second unblocking test for steel cables can be viewed in Appendix B.

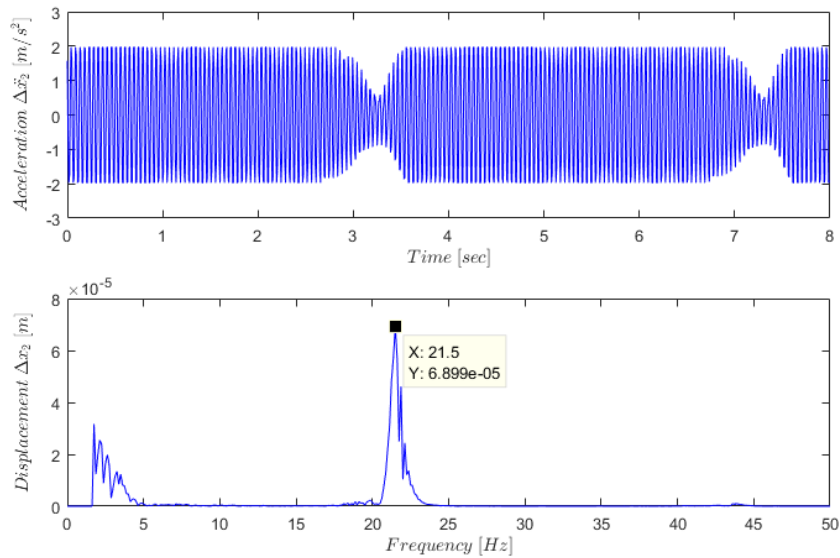


Figure 6-31: Measured horizontal response at Mount 2 when steel cables are caught in between rock at an input frequency of 22 Hz and 87% unbalance.

Top graph: Time domain acceleration signal.

Bottom graph: Frequency domain displacement signal.

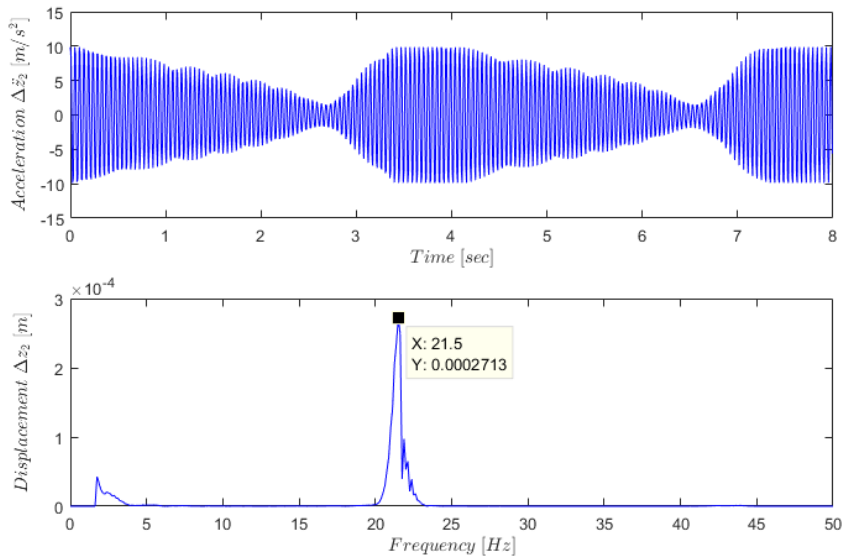


Figure 6-32: Measured vertical response at Mount 2 when steel cables are caught in between rock at an input frequency of 22 Hz and 87% unbalance.

Top graph: Time domain acceleration signal.

Bottom graph: Frequency domain displacement signal.

Another test was conducted in the same manner as the previous two tests at an input frequency of 20.25 Hz. The excitation motors were switched on and the Diagnostic Instrumentation was used to ensure that the machine operates at 20.25 Hz. The frequency input on the VSD was kept the same and as the unbalance increased, the frequency displayed by the diagnostic instrumentation decreased due to an increase in slip of the induction motors. A partial unblocking occurred at an excitation unbalance of 94%. The steel cables were tightened thereafter and the test was continued but no further unblocking occurred. Figure 6-33 to Figure 6-34 represent the measured horizontal and vertical responses, respectively, at Mount 2 for an input frequency of 20.25 Hz and an unbalance of 94%. Representation of the test setup, blockage created and partial unblocking can be viewed in Appendix B.

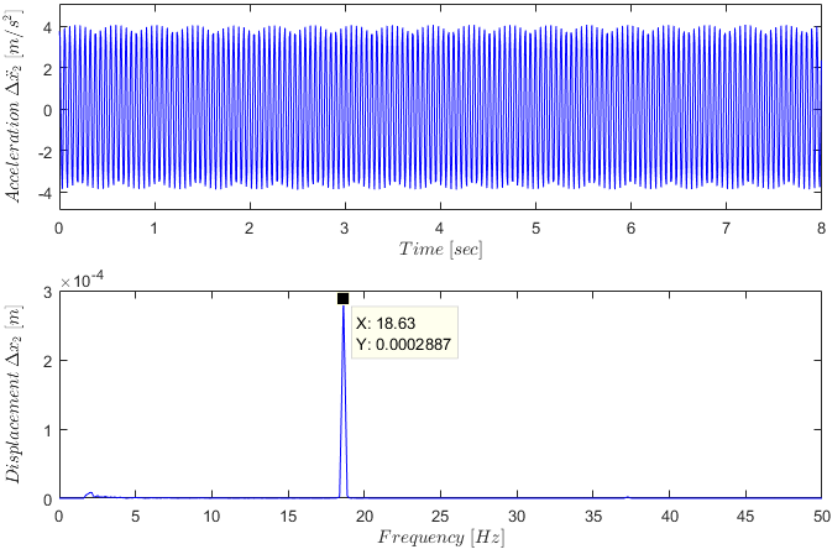


Figure 6-33: Measured horizontal response at Mount 2 when steel cables are caught in between rock at an input frequency of 20.25 Hz and 94% unbalance.

Top graph: Time domain acceleration signal.

Bottom graph: Frequency domain displacement signal.

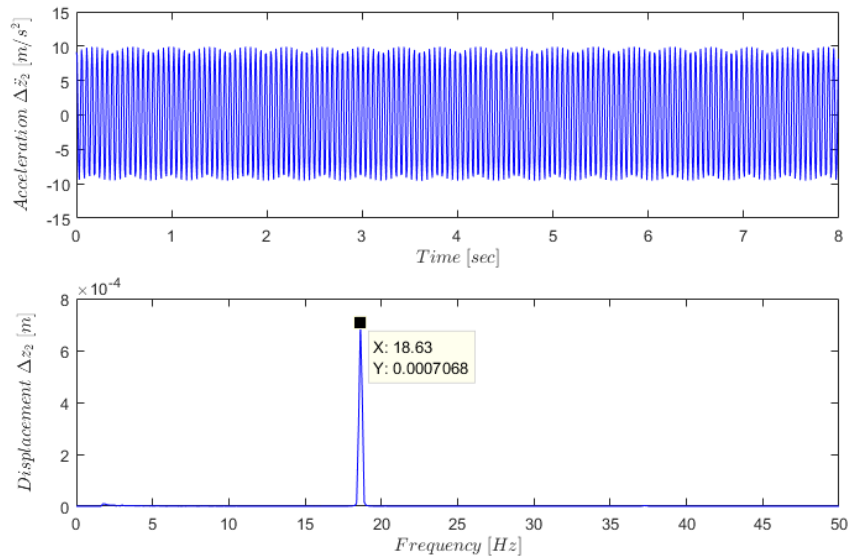


Figure 6-34: Measured vertical response at Mount 2 when steel cables are caught in between rock at an input frequency of 20.25 Hz and 94% unbalance.
Top graph: Time domain acceleration signal.
Bottom graph: Frequency domain displacement signal.

Table 6.15 summarises the results obtained after conducting the dry interlocking unblocking tests for the steel cables. With reference to the second test at an input frequency of 22 Hz, it is possible that no unblocking occurred due the unknown mode shape which led to smaller displacements.

Table 6.15: Summary of dry interlocking unblocking tests for steel cables.

Test no.	VSD input frequency [Hz]	Unblocking test result
1	18.25	Partially at 77 % unbalance
2	22	No unblocking
3	20.25	Partially at 94 % unbalance

6.10.1.2 Cemented blockage

Tests for a cemented blockage were conducted in the same manner as for a dry interlocking blockage as described in Paragraph 6.10.1.1, but after the scale chute was filled with sample rock, approximately 12 L mud was poured over the rocks inside of the scaled chute as illustrated in Figure 6-35. The mud was made from fine segregated powder as shown in Figure

6-36 and Figure 6-37. The mud was left to dry so that cementation could occur, the steel cables were tightened and the gate of the chute was opened. The unbalance of the excitation motors was initially set to 18 % and increased until an unblocking occurred. The machine was operated at an input frequency of 20.25 Hz because larger displacement was experienced at this frequency. If a partial unblocking occurred, the steel cables were tightened thereafter and the test was continued.



Figure 6-35: Representation of the mud as poured over the sample rocks.



Figure 6-36: Representation of the fine segregated powder with which the mud was created.



Figure 6-37: Representation of the mud created to add to the sample rocks.

Figure 6-38 represents the test setup for the first steel cable unblocking test with a cemented blockage. Figure 6-39 represents a top view of the scaled chute where mud was poured over the sample rock and left to dry. Figure 6-40 represents the blockage created for the first cemented blockage test where the steel cables are caught in the blockage. Figure 6-41 represents a partial unblocking which occurred at 50% excitation unbalance. The cables were tightened again and the test was continued where another partial unblocking occurred at 64%, as shown in Figure 6-42. No further unblocking occurred for the remaining excitation unbalances.



Figure 6-38: Representation of test setup for the first test where steel cables are caught in a cemented blockage.



Figure 6-39: Top view of the scaled chute where mud was added and left to dry.



Figure 6-40: Blockage created for the first test where cables are caught in a cemented blockage.



Figure 6-41: Partial unblocking for the first test at 50% excitation unbalance.



Figure 6-42: Partial unblocking for the first test at 64% excitation unbalance.

Another test was conducted in the same manner as the previous test and partial unblocking occurred at 77% excitation unbalance. Figure 6-43 to Figure 6-44 represents the measured horizontal and vertical responses, respectively, at Mount 2 for an input frequency of 20.25 Hz and an unbalance of 77%. The cables were tightened again and the test was continued. No further unblocking occurred for the remaining excitation unbalances. Representation of the test setup, blockage created and partial unblocking for the second cemented test can be viewed in Appendix B.

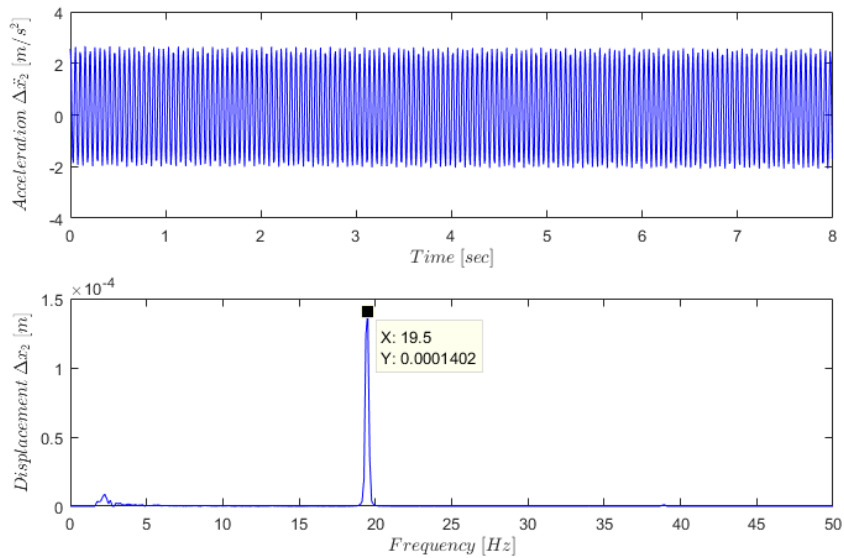


Figure 6-43: Measured horizontal response at Mount 2 when steel cables are caught in a cemented blockage at an input frequency of 20.25 Hz and 77% unbalance.

Top graph: Time domain acceleration signal.

Bottom graph: Frequency domain displacement signal.

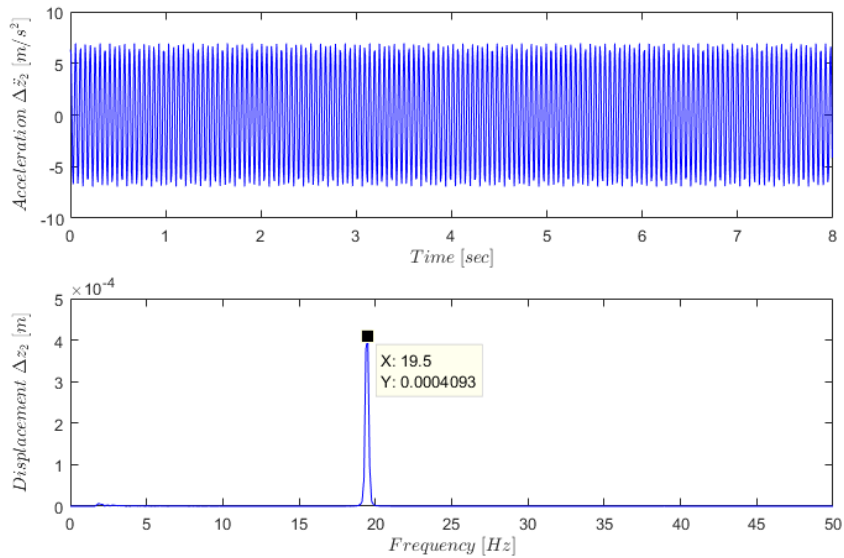


Figure 6-44: Measured vertical response at Mount 2 when steel cables are caught in a cemented blockage at an input frequency of 20.25 Hz and 77% unbalance.

Top graph: Time domain acceleration signal.

Bottom graph: Frequency domain displacement signal.

Table 6.16 summarises the results obtained from the two unblocking tests for cemented blockages by utilizing steel cables.

Table 6.16: Summary of cemented unblocking tests for the steel cables.

Test no.	VSD input frequency [Hz]	Unblocking test result
1	20.25	Partially at 50% and 64% unbalance
2	20.25	Partially at 77% unbalance

6.10.2 Hammer

6.10.2.1 Dry interlocking blockage

As described in Paragraph 6.5, the hammer was screwed into the machine and the scaled chute was filled with approximately 500 kg sample rock. The gate of the chute was removed, the hammer was turned until it made contact with the sample rock and could not be turned any further. The unbalance of the excitation motors was set to 18% and increased until an unblocking occurred. Two tests were conducted for the machine with the hammer connected at 18.25 Hz, the same frequency at which the stand-alone machine experiences maximum displacement. This frequency was chosen because the change in mass and change in the moment of inertia due to the addition of the hammer is negligibly small, and will only lead to a small change in frequency. The influence of the hammer on the change of frequency could be neglected because the mass of the hammer relative to the machine is very small. If a partial unblocking occurred at a specific unbalance, the hammer would be turned into the rocks again and the machine was switched on at the same unbalance at which the partial unblocking occurred and the test was continued.

Figure 6-45 represents the blockage created for the first hammer test at 18.25 Hz. Figure 6-46 displays how the hammer made contact with the sample rock for this particular blockage. Figure 6-47 represents a small partial unblocking at an excitation motor unbalance of 77% where some of the sample rock shifted within the chute.



Figure 6-45: Blockage created for the first hammer test with the gate of the chute removed.



Figure 6-46: Representation of how the hammer made contact with the sample rock.



Figure 6-47: Representation of a small partial unblocking at an unbalance of 77%.

The second test was conducted in the same manner as the first test with a constant input frequency of 18.25 Hz. The increase in excitation unbalance led to an increase in slip for the induction motors which resulted in a decrease in measured frequency. No unblocking occurred for the second hammer test for the range of excitation motor unbalances. Figure 6-48 to Figure 6-49 represents the horizontal and vertical measured response, respectively, at Mount 2 for an unbalance of 94%. Representation of the blockage created for the second test can be viewed in Appendix B.

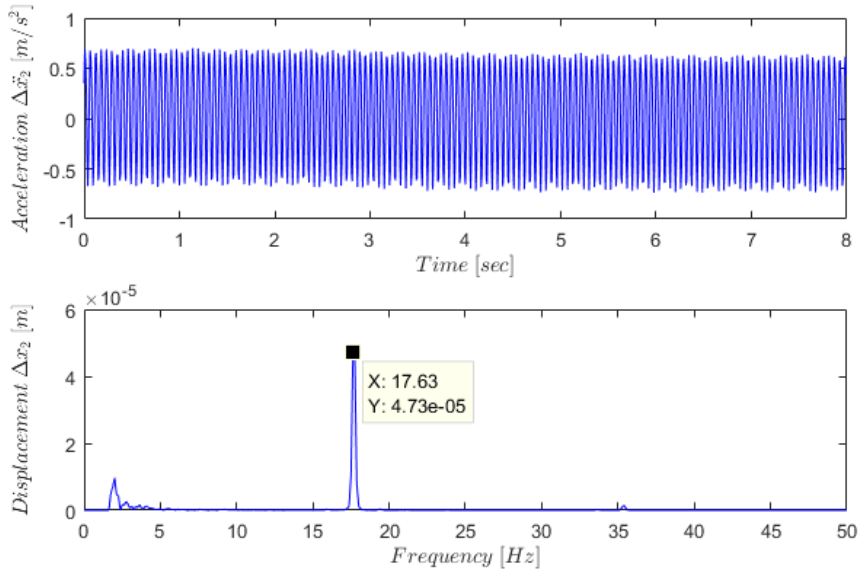


Figure 6-48: Measured horizontal response at Mount 2 for hammer operation at an input frequency of 18.25 Hz and 94% unbalance.
Top graph: Time domain acceleration signal.
Bottom graph: Frequency domain displacement signal.

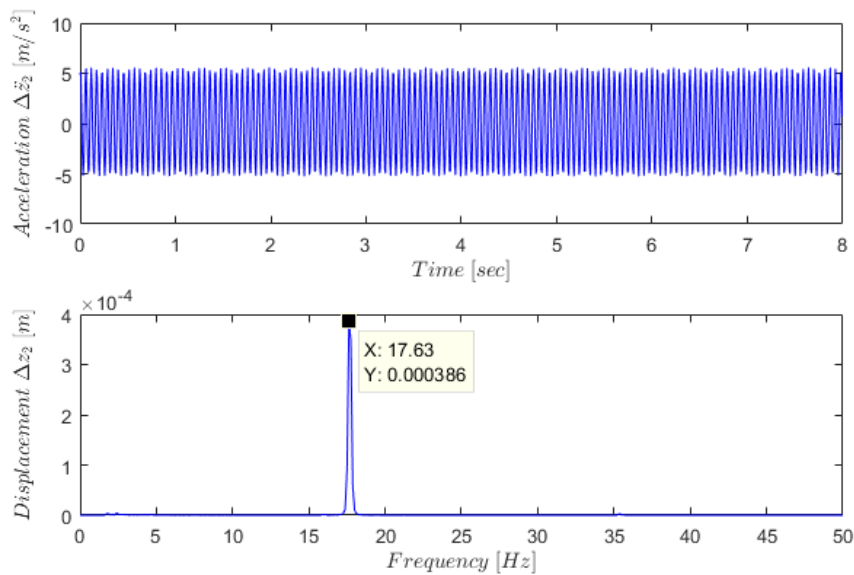


Figure 6-49: Measured vertical response at Mount 2 for hammer operation at an input frequency of 18.25 Hz and 94% unbalance.

Top graph: Time domain acceleration signal.

Bottom graph: Frequency domain displacement signal.

Table 6.17 summarises the results obtained from the two dry interlocking unblocking tests for the hammer operation.

Table 6.17: Summary of dry interlocking unblocking tests for the hammer.

Test no.	VSD input frequency [Hz]	Unblocking test result
1	18.25	Partially small at 77% unbalance
2	18.25	No unblocking

6.10.2.2 Cemented blockage

Tests for a cemented blockage was conducted in the same manner as for a dry interlocking blockage (as described in Paragraph 6.10.2.1), but after the scaled chute was filled with sample rock, about 12 L of mud made from fine segregate powder were poured over the top of the rock into the chute as seen in Figure 6-50. The mud was left to dry so that cementation could occur. The hammer was turned until it made contact with the rock and the gate of the chute was removed. The unbalance of the excitation motors was set to 18% and increased until an unblocking occurred. The machine was operated at an input frequency of 18.25 Hz as

described in Paragraph 6.10.2.1. If a partial unblocking occurred, the hammer was turned until it made contact with the rocks again and the test was continued.



Figure 6-50: Representation of the mud as poured over the sample rocks.

Figure 6-51 represents the test setup for the first hammer unblocking test with a cemented blockage. Figure 6-52 represents the blockage created for the first cemented blockage test where the hammer is used for unblocking. The hammer was turned into the rocks again after the 50% and 87% unbalance tests because the rock, which the hammer made contact with, shifted. Figure 6-53 represents a small partial unblocking where a few rocks were shuffled, which occurred at 94% excitation unbalance. Figure 6-54 to Figure 6-55 represents the horizontal and vertical measured response, respectively, at Mount 2 for an unbalance of 94%.



Figure 6-51: Representation of test setup for the first test where the hammer is used for unblocking a cemented blockage.



Figure 6-52: Blockage created for the first test where the hammer is used for unblocking a cemented blockage.

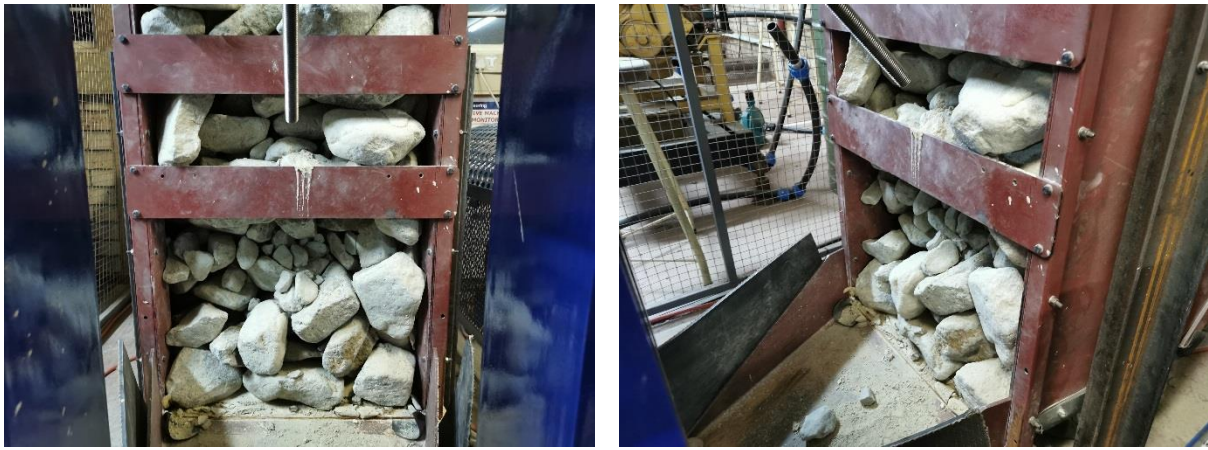


Figure 6-53: Small partial unblocking for the first test at 94% excitation unbalance.

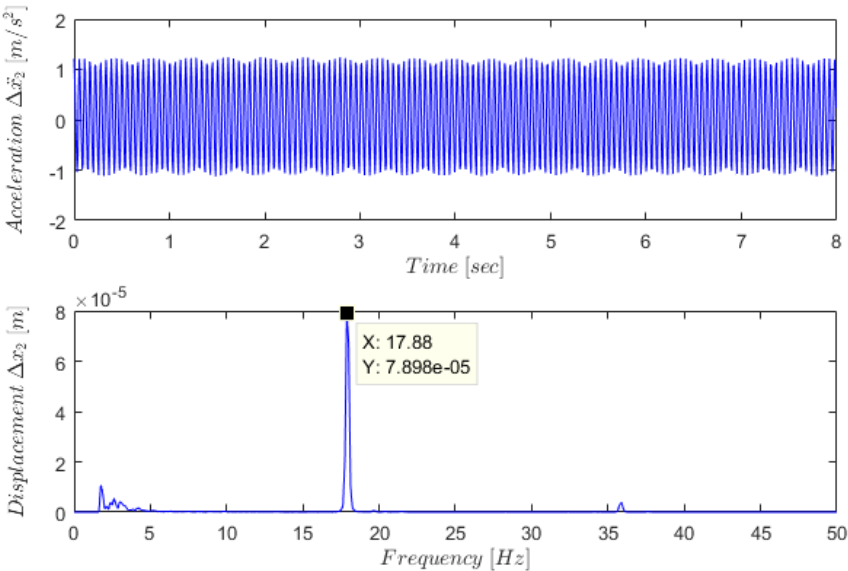


Figure 6-54: Measured horizontal response at Mount 2 for hammer operation at an input frequency of 18.25 Hz and 94% unbalance.

Top graph: Time domain acceleration signal.
Bottom graph: Frequency domain displacement signal.

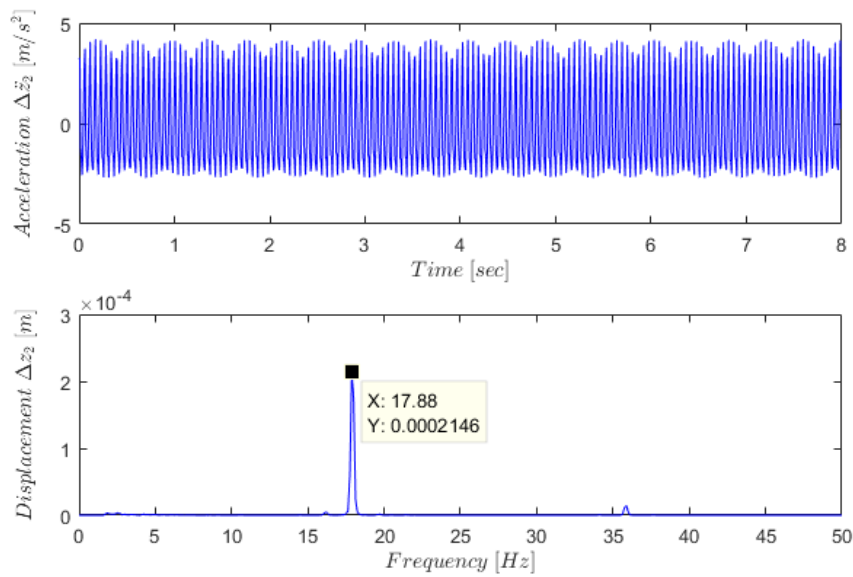


Figure 6-55: Measured vertical response at Mount 2 for hammer operation at an input frequency of 18.25 Hz and 94% unbalance.

Top graph: Time domain acceleration signal.

Bottom graph: Frequency domain displacement signal.

The second test for unblocking a cemented blockage for the hammer was conducted in the same manner as the previous test. A partial unblocking occurred at 50% excitation unbalance and no further unblocking occurred. The test setup, blockage created and partial unblocking for the second cemented unblocking test can be viewed in Appendix B.

Table 6.18 summarises the results obtained for the two tests for unblocking a cemented blockage with the hammer operation.

Table 6.18: Summary of the cemented unblocking tests for the hammer.

Test no.	VSD input frequency [Hz]	Unblocking test result
1	18.25	Partially small at 94% unbalance
2	18.25	Partially at 50% unbalance

6.10.3 Constant load unblocking method

A constant load method was tested for unblocking a blockage where the steel cables or hammer was tightened, the machine was operated at a predetermined excitation unbalance for a period of time, the machine was shut off, the steel cables or hammer was tightened again,

and the machine started up again. This was repeated for numerous times or until an unblocking occurred. This method was to ensure that a constant load was exerted onto the blockage because the rocks shift during runs, reducing the load which the steel cables and hammer exert onto the blockage. This test method was utilized for the steel cables and hammer operations separately.

Figure 6-56 represents the constant load test setup for the steel cables operation. Figure 6-57 represents the dry interlocking blockage created for the constant load test. The excitation unbalance was set to 64% (the average unbalance at which partial unblocking had occurred) and the machine was operated at a frequency of 20.25 Hz. The steel cables were tightened and the constant load test was conducted. A few rocks fell out while tightening the steel cables in between runs and when operating. No unblocking had occurred after 17 consecutive runs for the dry interlocking blockage as seen in Figure 6-58.



Figure 6-56: Representation of test setup for the constant load test where the steel cables are used for unblocking a dry interlocking blockage.



Figure 6-57: Blockage created for the constant load test where the steel cables are used for unblocking a dry interlocking blockage.



Figure 6-58: Representation of the blockage after 17 consecutive runs for the constant load method with steel cables.

Figure 6-59 represents the constant load test setup for the hammer operation. Figure 6-60 represents the dry interlocking blockage created for the constant load test. The excitation unbalance was set to 64 % and the machine was operated at a frequency of 18.25 Hz. The hammer was turned into the blockage and the constant load test was conducted. A few rocks fell out while turning the hammer in between runs and when operating. The hammer was turned out of the blockage after the fifth run and a successful unblocking occurred as seen in Figure 6-61.



Figure 6-59: Representation of test setup for the constant load test where the hammer is used for unblocking a dry interlocking blockage.



Figure 6-60: Blockage created for the constant load test where the hammer is used for unblocking a dry interlocking blockage.



Figure 6-61: Representation of a successful unblocking of the blockage by utilizing a constant load method with the hammer operation.

Table 6.19 summarize the results obtained for the two constant load tests for unblocking a dry interlocking blockage.

Table 6.19: Summary of the constant load unblocking tests for dry interlocking blockages.

Test	VSD input frequency [Hz]	Unblocking test result
Steel cables	20.25	Unsuccessful after 17 runs
Hammer	18.25	Successful after 5 runs

6.10.3.1 Constant load method with addition of water

Additional to applying the constant load method, water was added to the top of the chute to, in theory, reduce the friction within the blockage. The scaled chute was filled with sample rock and about 6 L water was poured over the top of the sample rocks. As explained in the previous section, the machine will be operated for a set amount of time and the steel cables or hammer will be tightened again each time in between runs. This test was conducted for using either steel cables or the hammer for unblocking a blockage separately.

Figure 6-62 represents the constant load test setup for the steel cable operation where water was introduced to the top of the scaled chute. Figure 6-63 represents the wet interlocking blockage created for the test. The excitation unbalance was set to 64% and the machine was operated at a frequency of 20.25 Hz. The steel cables were tightened and the constant load test was conducted. A few rocks fell out while tightening the steel cables in between runs and when operating. The steel cables were loosened after 17 consecutive runs and a successful unblocking occurred as seen in Figure 6-64.



Figure 6-62: Representation of test setup for the constant load test where the steel cables are used for unblocking a wet interlocking blockage.

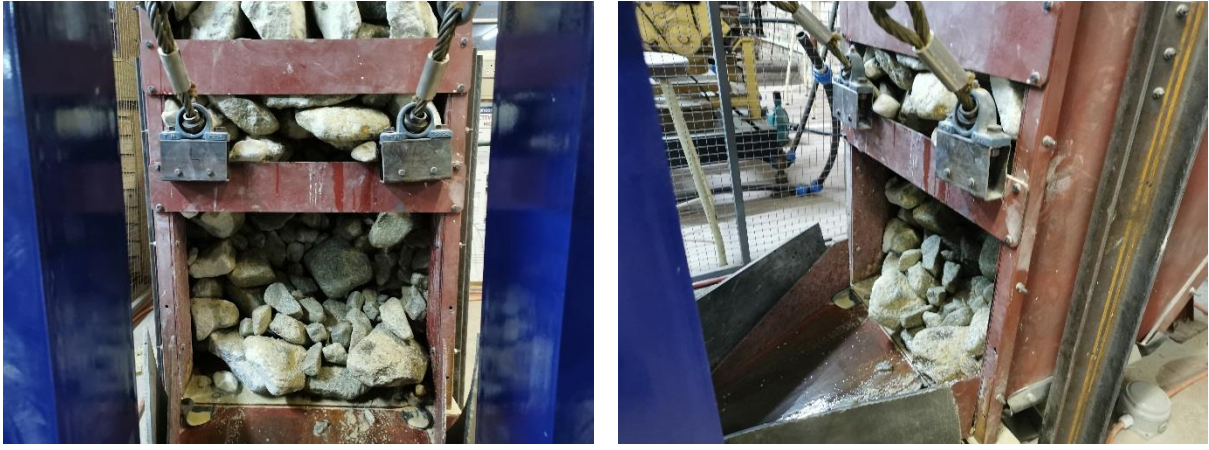


Figure 6-63: Blockage created for the constant load test where the steel cables are used for unblocking a wet interlocking blockage.



Figure 6-64: Representation of a successful unblocking of the wet interlocking blockage by using a constant load method with the steel cables.

Figure 6-65 represents the constant load test setup for the hammer operation where water was introduced to the top of the scaled chute. Figure 6-66 represents the wet interlocking blockage created for the test. The excitation unbalance was set to 64% and the machine was operated at a frequency of 18.25 Hz. The hammer was turned into the blockage and the constant load test was conducted. A few rocks fell out while turning the hammer in between runs and also when operating. The unblocking of the blockage was unsuccessful after 10 set of runs and the blockage after 10 runs can be seen in Figure 6-67.



Figure 6-65: Representation of test setup for the fatigue based test where the hammer is used for unblocking a wet interlocking blockage.

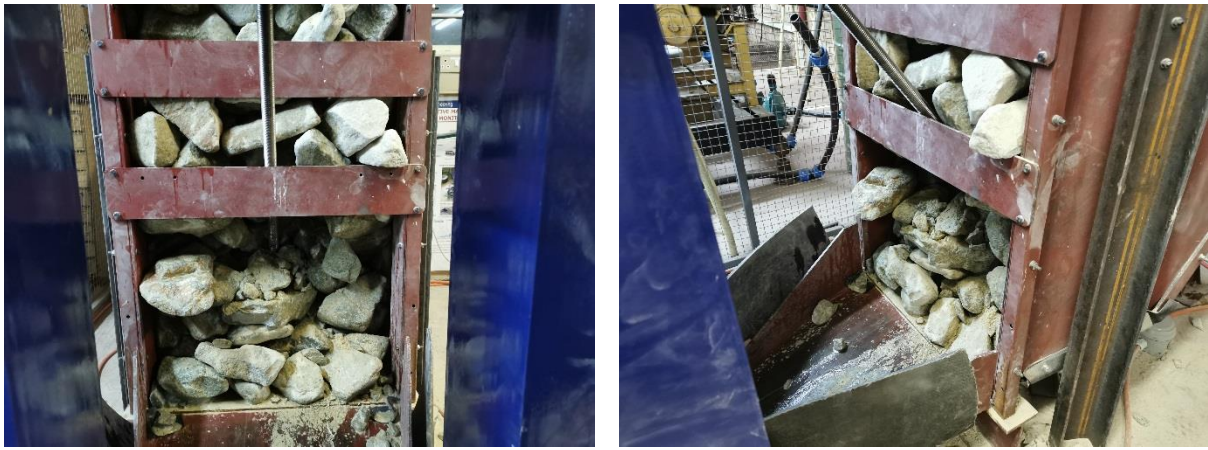


Figure 6-66: Blockage created for the constant load test where the hammer is used for unblocking a wet interlocking blockage.



Figure 6-67: Representation of the blockage after 10 consecutive runs.

Table 6.20 summarize the results obtained for the two constant load tests conducted for unblocking a wet interlocking blockage.

Table 6.20: Summary of the constant load tests for unblocking wet interlocking blockages.

Test no.	VSD input frequency [Hz]	Unblocking test result
Steel cables	20.25	Successful after 17 runs
Hammer	18.25	Unsuccessful after 10 runs

6.11 Conclusion and discussion of results

This chapter served to compare the predicted and measured responses, dynamic forces and natural frequencies for two operational conditions. The two operational conditions investigated were the stand-alone machine and when the steel cables are caught in a blockage. The predicted and measured responses for the stand-alone machine did not correlate very well but the predicted and measured natural frequencies showed a better correlation. As for the machine when the steel cables are caught in a blockage, the predicted and measured responses correlated well but the predicted and measured natural frequencies showed a larger difference. The response and dynamic forces of the hammer operation were measured in order to determine whether the machine is operating in a safe manner and does not exceed the rubber mounts' limits.

The steel cables were tested at three different frequencies for the unblocking of an interlocking blockage and was partially successful at two of the tests. The hammer was tested at one frequency for the unblocking of an interlocking blockage and was partially successful at one of the two tests conducted. For both the steel cables and hammer, the partial unblocking of an interlocking blockage occurred at an excitation motor unbalance of 77% and higher.

The steel cables were tested at one frequency for the unblocking of a cemented blockage and was partially successful for both of the tests conducted. The hammer was tested at one frequency for the unblocking of a cemented blockage and was partially successful at one of the two tests conducted. For both the steel cables and hammer, the partial unblocking of a cemented blockage occurred at an excitation motor unbalance of 50% and higher.

A constant load method was applied where either the steel cables or hammer were tightened in between consecutive runs. This method was successful at unblocking a blockage for the hammer operation but not for the steel cables. This method was also tested where water was added to the blockage to reduce friction between the rocks. The addition of water to the blockage led to a successful unblocking with steel cables but no unblocking occurred for the hammer.

The blockages were created at random and none of the blockages were the same which may be a possible reason why the machine was or was not successful for the different tests. The reason for conducting the few number of tests was that the tests were time and labour intensive. The tests were also dependent on laboratory and instrumentation availability which also presented a time constraint for conducting tests.

The system never exceeded the rubber mounts' limits for all the operation conditions even at an excitation motor unbalance of 94%, the highest tested unbalance.

7 CONCLUSIONS

Hang-ups and blockages occurring in ore passes of underground mines create problems in terms of production (and associated costs). A method needed to be designed to safely restore the flow after a blockage occurred. It was proposed to design a special machine to transfer vibration to a blockage in order to clear the flow in the ore pass. This machine also had to be built and experimentally evaluated.

Two concept designs were proposed to the mine and the first design was declined due to the financial impact and the second design was chosen to implement for this study. Mathematical models were developed to analyse the design of the proposed ore flow restore machine. This was regarded necessary to investigate whether the ore flow restore machine is capable of unblocking a blockage in an ore pass. Two three-degree-of-freedom mathematical models were developed to predict the dynamic displacements, dynamic forces and system natural frequencies for the ore flow restore machine. The first mathematical model was developed for the machine when the steel cables are not attached and the second mathematical model was developed for the machine when the steel cables are caught in a blockage. These mathematical models were implemented in a computer program, MATLAB®.

A Finite Element Analysis (FEA) approach was used to analyse whether the design is free of structural resonance. The results revealed that the structural natural frequency, driven by the elasticity of the machine, is well above the operating frequency of the exciter motors. An FEA approach was also used to determine the dynamic material stresses of the design when operating with and without steel cables. The design was deemed acceptable and safe from failure for normal operational conditions, therefore the machine was built and experimentally evaluated.

The input parameters required for the computer program were characterised. These parameters include machine rigid body mass, position of centre of gravity of machine, machine rigid body Mass Moment of Inertia, global coordinates of machine mounts, exciter motor speed and unbalance characteristics, global coordinates of two exciter motors, angle of attachment of the exciter motors, steel cables combination stiffness and global coordinates of attachment point, and rubber mount dynamic properties. In addition, the sizes of the sample rocks used for experimental evaluation were also characterized.

A mathematical model was developed to characterise the horizontal stiffness and damping coefficients of the rubber mounts by means of a bump test. This model was implemented in MATLAB® using measured data as inputs. The horizontal dynamic properties of the rubber mounts were successfully characterized in-situ with a bump test. The vertical stiffness of the

rubber mounts was characterised in-situ by means of a bump test. The damping coefficients were characterised by means of the three-degree-of-freedom mathematical model and in-situ by means of a sweep test. The vertical dynamic properties of the rubber mounts were successfully characterised. The stiffness of the steel cables combination was characterised by comparing the predicted natural frequencies and in-situ measured natural frequencies. The theoretically calculated stiffness was deemed acceptable, for the predicted and measured natural frequencies corresponded well.

The constructed ore flow restore machine was partially successful in restoring the flow after a blockage occurred when only adjusting the excitation unbalance of the motors. However, successful unblocking of a blockage is possible by using a constant load method with the machine.

A limitation to the study was conducting only a small number of tests due to the tests being time and labour intensive. The tests were also dependent on laboratory and instrumentation availability which led to time constraints for conducting tests.

The underlying three-degree-of-freedom mathematical models for the ore flow machine were experimentally validated. The predicted response, transmitted forces and natural frequencies were compared to the corresponding measured values. This was done for the stand-alone machine, where the steel cables were removed from the machine, and for the machine when the steel cables are caught in a blockage.

It was found that the predicted magnitudes for these parameters differs to some extent with the measured values for both operating conditions. The experimental evaluation proved that the underlying mathematical models are reliable enough and could therefore aid in the further development of vibration ore flow restoring machinery for use in underground mines.

7.1 Suggestions for further study

Very small mount displacements were measured during the experimental evaluation phase compared to the designed displacement of 10 mm. The reason for this is that the damping ratios of the rubber mounts were underestimated for the design phase - manufacturers typically do not supply damping ratios. Although both the steel cables and hammer were partially successful at unblocking a blockage, larger displacement will lead to larger forces being exerted through the steel cables and hammer and possible more successful unblocking of blockages. It is recommended to further investigate the influence of larger mounts displacements on the functionality of the ore flow restore machine for both the steel cables and hammer. Other future possible work could be to investigate the influence of vibration

transferred directly onto the chute or boxfront and whether this would be a more sufficient method to unblock a blockage.

REFERENCES

- de Beer, M. The sizes of waste rock handled in a underground mine [e-mail correspondence]. 30 October 2018.
- Hadjigeorgiou, F. 2005. Ore pass practice in Canadian mines. *Journal of the Southern African Institute of Mining and Metallurgy*, 105(11):809-816.
- Hadjigeorgiou, J. & Lessard, J.F. 2007. Numerical investigations of ore pass hang-up phenomena. *International Journal of Rock Mechanics and Mining Sciences*, 44(6):820-834.
- Hadjigeorgiou, J. & Lessard, J.F. 2010. Strategies for restoring material flow in ore and waste pass systems. *International Journal of Mining, Reclamation and Environment*, 24(3):267-282.
- Rao, S.S. 2011. Mechanical vibrations: Upper Saddle River, N.J. : Prentice Hall, c2011. 5th ed.
- Stacey, T. & Swart, A. 1997. Investigation into drawpoints, tips orepasses and chutes. *Report to the safety in Mines Research Advisory Committee. Steffen, Robertson and Kirsten*, 1:112.
- Szwedzicki, T. 2007. Formation and removal of hang-ups in ore passes. *Transactions of the Institutions of Mining and Metallurgy, Section A: Mining Technology*, 116(3):139-145.
- Vo, T., Yang, H. & Russell, A.R. 2016. Cohesion and suction induced hang-up in ore passes. *International Journal of Rock Mechanics and Mining Sciences*, 87:113-128.
- Wu, A. & Sun, Y. 2008. Vibrating Ore-drawing Technology. *Granular Dynamic Theory and Its Applications*. Berlin, Heidelberg: Springer Berlin Heidelberg. p. 271-347).

APPENDIX A – MATLAB® COMPUTER PROGRAMS

Main program for stand-alone machine:

```
clc
clear all
close all
format long

global x1 x2 x3 z1 z2 z3 kx1 kx2 kz1 kz2 cx1 cx2 cz1 cz2 beta Ccz Ccx
zeta_z zeta_x m Jyy W r Fe me omega fr

% Mass Inputs
m = 310.35;
r = 0.3861351713;
W = m*9.81;
Jyy = m*r^2;

% Mount coordinates
x1 = -0.42060028;
x2 = 0.38645104;
x3 = -0.01707462;
x4 = -0.01707462;
x5 = -0.01707462;
z1 = -0.37375638;
z2 = -0.37375637;
z3 = -0.05876920;
z4 = 0.24821796;
z5 = 0.24821796;

% Dynamic stiffness of mounts
kx1 = 513322;
kx2 = 513322;
kz1 = 1822887;
kz2 = 1822887;

% Damping ratio of mounts
zeta_z = 0.09;
zeta_x = 0.049;

% Critical damping of mounts
Ccz = 2*sqrt((kz1+kz2)*m);
Ccx = 2*sqrt((kx1+kx2)*m);

% Damping coefficients of mounts
cz1 = ((zeta_z*Ccz)/2)*1;
cz2 = cz1;
cx1 = ((zeta_x*Ccx)/2)*1;
cx2 = cx1;

% Excitation motors
me = 0.032*0.5^2;
fr = 18.25;
omega = 2*pi*fr;
Fe = me*omega^2;
Fe_motors = Fe;
beta = 135*(pi/180);

% staticmoment x unbalance x amount
% operating frequency
% rotational velocity
% excitation force
% angle of motors
```

```

% ode inputs
y0 = [0 0 0 0 0 0];
domain = 0:0.003:70;

% run ode
[t,y] = ode23('vibration_Fu',domain,y0);

x = y(:,1);
dotx = y(:,2);

z = y(:,3);
dotz = y(:,4);

theta = y(:,5);
dottheta = y(:,6);

% Determine natural frequency of system
Natfreq

% Displacements at mounts
x1_dyn = x + z1*theta;
x2_dyn = x + z2*theta;
x4_dyn = x + z4*theta;
x5_dyn = x + z5*theta;
z1_dyn = z - x1*theta;
z2_dyn = z - x2*theta;
z4_dyn = z - x4*theta;
z5_dyn = z - x5*theta;

% Velocities at mounts
dotx1_dyn = dotx + z1*dottheta;
dotx2_dyn = dotx + z2*dottheta;
dotx4_dyn = dotx + z4*dottheta;
dotx5_dyn = dotx + z5*dottheta;
dotz1_dyn = dotz - x1*dottheta;
dotz2_dyn = dotz - x2*dottheta;
dotz4_dyn = dotz - x4*dottheta;
dotz5_dyn = dotz - x5*dottheta;

% Forces transmitted
Fz1_dyn = z1_dyn*kz1 + dotz1_dyn*cz1;
Fz2_dyn = z2_dyn*kz2 + dotz2_dyn*cz2;

Fx1_dyn = x1_dyn*kx1 + dotx1_dyn*cx1;
Fx2_dyn = x2_dyn*kx2 + dotx2_dyn*cx2;

F0 = vertcat((me*omega^2)*ones(20333,1),zeros(3001,1));

ddotx = ((-x*(kx1+kx2)) - (dotx*(cx1+cx2)) - (theta*(kx1*z1 + kx2*z2)) -
(dottheta*(cx1*z1+cx2*z2)) + F0.*sin(omega*t)*cos(beta))/m;
ddotz = ((-z*(kz1+kz2)) - (dotz*(cz1+cz2)) - (theta*(-kz1*x1 - kz2*x2)) -
(dottheta*(-cz1*x1-cz2*x2)) + F0.*sin(omega*t)*sin(beta))/m;
ddottheta = ((-x*(kx1*z1+kx2*z2)) - (dotx*(cx1*z1+cx2*z2)) - (z*(-kz1*x1 -
kz2*x2)) - (dotz*(-cz1*x1-cz2*x2)) - (theta*(kx1*z1^2 + kx2*z2^2 + kz1*x1^2
+ kz2*x2^2)) - (dottheta*(cx1*z1^2 + cx2*z2^2 + cz1*x1^2 + cz2*x2^2)) +
F0.*sin(omega*t)*cos(beta)*z3 - F0.*sin(omega*t)*sin(beta)*x3)/Jyy;

% Acceleration at mounts
ddotx1_dyn = ddotx + z1*ddottheta;

```

```

ddotx2_dyn = ddotx + z2*ddottheta;

ddotz1_dyn = ddotz - x1*ddottheta;
ddotz2_dyn = ddotz - x2*ddottheta;

% Transient operation
x1_dyn_m_transient = max(abs(x1_dyn(1:12000)));
x2_dyn_m_transient = max(abs(x2_dyn(1:12000)));
x4_dyn_m_transient = max(abs(x4_dyn(1:12000)));
x5_dyn_m_transient = max(abs(x5_dyn(1:12000)));

z1_dyn_m_transient = max(abs(z1_dyn(1:12000)));
z2_dyn_m_transient = max(abs(z2_dyn(1:12000)));
z4_dyn_m_transient = max(abs(z4_dyn(1:12000)));
z5_dyn_m_transient = max(abs(z5_dyn(1:12000)));

Fx1_dyn_m_transient = max(abs(Fx1_dyn(1:12000)));
Fx2_dyn_m_transient = max(abs(Fx2_dyn(1:12000)));

Fz1_dyn_m_transient = max(abs(Fz1_dyn(1:12000)));
Fz2_dyn_m_transient = max(abs(Fz2_dyn(1:12000)));

F_m_transient =
Fz1_dyn_m_transient+Fz2_dyn_m_transient+Fx1_dyn_m_transient+Fx2_dyn_m_trans
ient;

Tf_transient = (F_m_transient/Fe_motors)*100;

% Steady State operation
x1_dyn_m_ss = max(abs(x1_dyn(12001:20000)))
x2_dyn_m_ss = max(abs(x2_dyn(12001:20000)))
x4_dyn_m_ss = max(abs(x4_dyn(12001:20000)));
x5_dyn_m_ss = max(abs(x5_dyn(12001:20000)));

z1_dyn_m_ss = max(abs(z1_dyn(12001:20000)))
z2_dyn_m_ss = max(abs(z2_dyn(12001:20000)))
z4_dyn_m_ss = max(abs(z4_dyn(12001:20000)));
z5_dyn_m_ss = max(abs(z5_dyn(12001:20000)));

Fx1_dyn_m_ss = max(abs(Fx1_dyn(12001:20000)));
Fx2_dyn_m_ss = max(abs(Fx2_dyn(12001:20000)));

Fz1_dyn_m_ss = max(abs(Fz1_dyn(12001:20000)));
Fz2_dyn_m_ss = max(abs(Fz2_dyn(12001:20000)));

F_m_ss = Fz1_dyn_m_ss+Fz2_dyn_m_ss+Fx1_dyn_m_ss+Fx2_dyn_m_ss;

Tf_ss = (F_m_ss/Fe_motors)*100;

Plotting(t,x1_dyn,ddotx1_dyn,x2_dyn,
ddotx2_dyn,z1_dyn,ddotz1_dyn,z2_dyn,ddotz2_dyn)

```


Ode 23 subprogram for stand-alone machine:

```
function f = vibration_Fu(t,y)
global x1 x2 x3 z1 z2 z3 kx1 kx2 kz1 kz2 cx1 cx2 cz1 cz2 m Jyy beta Fe
omega
if t>61
    Fe = 0;
end
% First Order Differential Equations
f = zeros(6,1);

f(1) = y(2);
f(2) = ((-y(1)*(kx1+kx2)) - (y(2)*(cx1+cx2)) - (y(5)*(kx1*z1 + kx2*z2)) -
(y(6)*(cx1*z1+cx2*z2)) + Fe*sin(omega*t)*cos(beta))/m;
f(3) = y(4);
f(4) = ((-y(3)*(kz1+kz2)) - (y(4)*(cz1+cz2)) - (y(5)*(-kz1*x1-kz2*x2)) -
(y(6)*(-cz1*x1-cz2*x2)) + Fe*sin(omega*t)*sin(beta))/m;
f(5) = y(6);
f(6) = ((-y(1)*(kx1*z1+kx2*z2)) - (y(2)*(cx1*z1+cx2*z2)) - (y(3)*(-kz1*x1-
kz2*x2)) - (y(4)*(-cz1*x1-cz2*x2)) -
(y(5)*(kx1*z1^2+kx2*z2^2+kz1*x1^2+kz2*x2^2)) -
(y(6)*(cx1*z1^2+cx2*z2^2+cz1*x1^2+cz2*x2^2)) + Fe*sin(omega*t)*cos(beta)*z3
- Fe*sin(omega*t)*sin(beta)*x3)/Jyy;
end
```

Natural frequency subprogram for stand-alone machine:

```
function Natfreq
global x1 x2 z1 z2 kx1 kx2 kz1 kz2 m Jyy

K = [ (kx1+kx2) 0 (kx1*z1+kx2*z2);
      0 (kz1+kz2) (-kz1*x1-kz2*x2);
      (kx1*z1+kx2*z2) (-kz1*x1-kz2*x2) (kx1*z1^2+kx2*z2^2+kz1*x1^2+kz2*x2^2) ]

M = [m 0 0; 0 m 0; 0 0 Jyy]

[V,D] = eig(K,M)
omega_n = sqrt(D);
f_n = sqrt(D)/(2*pi)

[val,horisontal] = max(abs(V(1,:)));
[val,vertical] = max(abs(V(2,:)));
[val,rotational] = max(abs(V(3,:)));
f_n_horisontal = max(f_n(:,horisontal));
f_n_vertical = max(f_n(:,vertical));
f_n_rotational = max(f_n(:,rotational));

disp('Natural Frequencies:')
disp(['Horisontal mode = ',num2str(f_n_horisontal),'Hz'])
disp(['Vertical mode = ',num2str(f_n_vertical),'Hz'])
disp(['Rotational mode = ',num2str(f_n_rotational),'Hz'])

end
```

Subprogram to plot different graphs for stand-alone machine:

```
function Plotting(t,x1_dyn,ddotx1_dyn,x2_dyn,
ddotx2_dyn,z1_dyn,ddotz1_dyn,z2_dyn,ddotz2_dyn)

%Plot mount displacements - Steady state

figure(1)
subplot(2,1,2);plot(t(11670:20000),x1_dyn(11670:20000))
xlabel('$$$ Time \; (s) $$$','Interpreter','latex')
ylabel('$$$ Displacement \; \Delta x_1 \; [m] $$$','Interpreter','latex')

subplot(2,1,1);plot(t(11670:20000),ddotx1_dyn(11670:20000))
xlabel('$$$ Time \; (s) $$$','Interpreter','latex')
ylabel('$$$ Acceleration \; \Delta\ddot{x}_1 \; [m/s^2]
$$$','Interpreter','latex')

figure(2)
subplot(2,1,2);plot(t(11670:20000),x2_dyn(11670:20000))
xlabel('$$$ Time \; (s) $$$','Interpreter','latex')
ylabel('$$$ Displacement \; \Delta x_2 \; [m] $$$','Interpreter','latex')

subplot(2,1,1);plot(t(11670:20000),ddotx2_dyn(11670:20000))
xlabel('$$$ Time \; (s) $$$','Interpreter','latex')
ylabel('$$$ Acceleration \; \Delta\ddot{x}_2 \; [m/s^2]
$$$','Interpreter','latex')

figure(3)
subplot(2,1,2);plot(t(11670:20000),z1_dyn(11670:20000))
xlabel('$$$ Time \; (s) $$$','Interpreter','latex')
ylabel('$$$ Displacement \; \Delta z_1 \; [m] $$$','Interpreter','latex')

subplot(2,1,1);plot(t(11670:20000),ddotz1_dyn(11670:20000))
xlabel('$$$ Time \; (s) $$$','Interpreter','latex')
ylabel('$$$ Acceleration \; \Delta\ddot{z}_1 \; [m/s^2]
$$$','Interpreter','latex')

figure(4)
subplot(2,1,2);plot(t(11670:20000),z2_dyn(11670:20000))
xlabel('$$$ Time \; (s) $$$','Interpreter','latex')
ylabel('$$$ Displacement \; \Delta z_2 \; [m] $$$','Interpreter','latex')

subplot(2,1,1);plot(t(11670:20000),ddotz2_dyn(11670:20000))
xlabel('$$$ Time \; (s) $$$','Interpreter','latex')
ylabel('$$$ Acceleration \; \Delta\ddot{z}_2 \; [m/s^2]
$$$','Interpreter','latex')

end
```

Main program for machine and steel cable combination:

```
clc
clear all
close all
format long

global x1 x2 x3 x4 z1 z2 z3 z4 kx1 kx2 kcsx kz1 kz2 kcsz kcs cx1 cx2 cz1
cz2 beta gamma Ccz Ccx zeta_z zeta_x m Jyy W r omega fr E L d Fe me

% Mass inputs
m = 310.35+(2/3)*10.85;
r = 0.3861351713;
W = m*9.81;
Jyy = m*r^2;

% Mount coordinates
x1 = -0.42060028;
x2 = 0.38645104;
x3 = -0.01707462;
x4 = -0.01707462;
x5 = -0.01707462;
z1 = -0.37375638;
z2 = -0.37375637;
z3 = -0.05876920;
z4 = 0.24821796;
z5 = 0.24821796;

% Dynamic stiffness of mounts
kx1 = 513322;
kx2 = 513322;
kz1 = 1822887;
kz2 = 1822887;

% Cable and spring stiffness
E = 96E+09;
L = 0.3;
d = 0.016;

kveer = 525000*2;
kcable = ((E*0.410*d^2)/L)*2;
kcs = ((kveer*kcable)/(kveer+kcable));
gamma = 45*(pi/180);
kcsx = kcs*cos(gamma);
kcsz = kcs*sin(gamma);

% Damping ratio of mounts
zeta_z = 0.09;
zeta_x = 0.049;

% Critical damping of mounts
Ccz = 2*sqrt((kz1+kz2+kcsz)*m);
Ccx = 2*sqrt((kx1+kx2+kcsx)*m);

% Damping coefficients
cz1 = ((zeta_z*Ccz)/2)*1;
cz2 = cz1;
cx1 = ((zeta_x*Ccx)/2)*1;
cx2 = cx1;

% Excitation motors
```

```

me = 0.032*0.5*2;           %staticmoment x unbalance x amount
fr = 20.25;                 %operation frequency
omega = 2*pi*fr;           %rotational velocity
Fe = me*omega^2;           %excitation force
Fe_motors = me*omega^2;
beta = 135*(pi/180);       %angle of motors

% ode inputs
y0 = [0 0 0 0 0 0];
domain = 0:0.003:70;

% run ode
[t,y] = ode23('vibration_Fu',domain,y0);

x = y(:,1);
dotx = y(:,2);

z = y(:,3);
dotz = y(:,4);

theta = y(:,5);
dottheta = y(:,6);

F0 = vertcat((me*omega^2)*ones(20333,1),zeros(3001,1));

ddotx = ((-x*(kx1+kx2+kcsx)) - (dotx*(cx1+cx2)) - (theta*(kx1*z1 + kx2*z2
+ kcsx*z4)) - (dottheta*(cx1*z1+cx2*z2)) + F0.*sin(omega*t)*cos(beta))/m;
ddotz = ((-z*(kz1+kz2+kcsz)) - (dotz*(cz1+cz2)) - (theta*(-kz1*x1 - kz2*x2
- kcsz*x4)) - (dottheta*(-cz1*x1-cz2*x2)) + F0.*sin(omega*t)*sin(beta))/m;
ddottheta = ((-x*(kx1*z1+kx2*z2+kcsx*z4)) - (dotx*(cx1*z1+cx2*z2)) - (z*(-
kz1*x1 - kz2*x2 - kcsz*x4)) - (dotz*(-cz1*x1-cz2*x2)) - (theta*(kx1*z1^2 +
kx2*z2^2 + kz1*x1^2 + kz2*x2^2 + kcsx*z4^2 + kcsz*x4^2)) -
(dottheta*(cx1*z1^2 + cx2*z2^2 + cz1*x1^2 + cz2*x2^2)) +
F0.*sin(omega*t)*cos(beta)*z3 - F0.*sin(omega*t)*sin(beta)*x3)/Jyy;

% Determine natural frequencies of system
Natfreq

% Displacements at mounts
x1_dyn = x + z1*theta;
x2_dyn = x + z2*theta;
x4_dyn = x + z4*theta;
x5_dyn = x + z5*theta;
z1_dyn = z - x1*theta;
z2_dyn = z - x2*theta;
z4_dyn = z - x4*theta;
z5_dyn = z - x5*theta;

% Velocities at mounts
dotx1_dyn = dotx + z1*dottheta;
dotx2_dyn = dotx + z2*dottheta;
dotx4_dyn = dotx + z4*dottheta;
dotx5_dyn = dotx + z5*dottheta;
dotz1_dyn = dotz - x1*dottheta;
dotz2_dyn = dotz - x2*dottheta;
dotz4_dyn = dotz - x4*dottheta;
dotz5_dyn = dotz - x5*dottheta;

% Acceleration at mounts
ddotx1_dyn = ddotx + z1*ddottheta;

```

```

ddotx2_dyn = ddotx + z2*ddottheta;
ddotx4_dyn = ddotx + z4*ddottheta;
ddotz1_dyn = ddotz - x1*ddottheta;
ddotz2_dyn = ddotz - x2*ddottheta;
ddotz4_dyn = ddotz - x4*ddottheta;

% Force transmitted
Fz1_dyn = z1_dyn*kz1 + dotz1_dyn*cz1;
Fz2_dyn = z2_dyn*kz2 + dotz2_dyn*cz2;
Fx1_dyn = x1_dyn*kx1 + dotx1_dyn*cx1;
Fx2_dyn = x2_dyn*kx2 + dotx2_dyn*cx2;

% Transient operation
x1_dyn_m_transient = max(abs(x1_dyn(1:12000)));
x2_dyn_m_transient = max(abs(x2_dyn(1:12000)));
x4_dyn_m_transient = max(abs(x4_dyn(1:12000)));
x5_dyn_m_transient = max(abs(x5_dyn(1:12000)));

z1_dyn_m_transient = max(abs(z1_dyn(1:12000)));
z2_dyn_m_transient = max(abs(z2_dyn(1:12000)));
z4_dyn_m_transient = max(abs(z4_dyn(1:12000)));
z5_dyn_m_transient = max(abs(z5_dyn(1:12000)));

dispc_dyn_m_transient = sqrt(x4_dyn_m_transient^2 + z4_dyn_m_transient^2);

Fx1_dyn_m_transient = max(abs(Fx1_dyn(1:12000)));
Fx2_dyn_m_transient = max(abs(Fx2_dyn(1:12000)));
Fz1_dyn_m_transient = max(abs(Fz1_dyn(1:12000)));
Fz2_dyn_m_transient = max(abs(Fz2_dyn(1:12000)));

F_c_dyn_m_transient = (dispc_dyn_m_transient*kcs);

F_m_transient =
Fz1_dyn_m_transient+Fz2_dyn_m_transient+Fx1_dyn_m_transient+Fx2_dyn_m_trans
ient;

Tf_transient = (F_m_transient/Fe_motors)*100;

% Cable stress
cable_axcial_transient = (F_c_dyn_m_transient/2)/(kcable/2);
sigma_cs_m_transient = (cable_axcial_transient*E)/L;
sigmac_m_transient = (F_c_dyn_m_transient/2)/(0.405*d^2);

% Steady State operation
x1_dyn_m_ss = max(abs(x1_dyn(12001:20000)))
x2_dyn_m_ss = max(abs(x2_dyn(12001:20000)))
x4_dyn_m_ss = max(abs(x4_dyn(12001:20000)));
x5_dyn_m_ss = max(abs(x5_dyn(12001:20000)));

z1_dyn_m_ss = max(abs(z1_dyn(12001:20000)))
z2_dyn_m_ss = max(abs(z2_dyn(12001:20000)))
z4_dyn_m_ss = max(abs(z4_dyn(12001:20000)));
z5_dyn_m_ss = max(abs(z5_dyn(12001:20000)));

dispc_dyn_m_ss = sqrt(x4_dyn_m_ss^2 + z4_dyn_m_ss^2);

Fx1_dyn_m_ss = max(abs(Fx1_dyn(12001:20000)));
Fx2_dyn_m_ss = max(abs(Fx2_dyn(12001:20000)));
Fz1_dyn_m_ss = max(abs(Fz1_dyn(12001:20000)));
Fz2_dyn_m_ss = max(abs(Fz2_dyn(12001:20000)));

```

```

F_c_dyn_m_ss = (dispc_dyn_m_ss*kcs);

F_m_ss = Fz1_dyn_m_ss+Fz2_dyn_m_ss+Fx1_dyn_m_ss+Fx2_dyn_m_ss;

Tf_ss = (F_m_ss/Fe_motors)*100;

% Cable stress
cable_axcial_ss = (F_c_dyn_m_ss/2)/(kcable/2);
sigma_cs_m_ss = (cable_axcial_ss*E)/L;
sigmac_m_ss = (F_c_dyn_m_ss/2)/(0.405*d^2);

Plotting(t,x1_dyn,ddotx1_dyn,x2_dyn,
ddotx2_dyn,z1_dyn,ddotz1_dyn,z2_dyn,ddotz2_dyn)

```

Ode 23 subprogram for machine and steel cable combination:

```

function f = vibration_Fu(t,y)
global x1 x2 x3 x4 z1 z2 z3 z4 kx1 kx2 kcsx kz1 kz2 kcsz cx1 cx2 cz1 cz2 m
Jyy beta Fe omega
if t>61
    Fe = 0;
end
% First Order Differential Equations
f = zeros(6,1);

f(1) = y(2);
f(2) = ((-y(1)*(kx1+kx2+kcsx)) - (y(2)*(cx1+cx2)) - (y(5)*(kx1*z1 +
kx2*z2+kcsx*z4)) - (y(6)*(cx1*z1+cx2*z2)) + Fe*sin(omega*t)*cos(beta))/m;
f(3) = y(4);
f(4) = ((-y(3)*(kz1+kz2+kcsz)) - (y(4)*(cz1+cz2)) - (y(5)*(-kz1*x1-kz2*x2-
kcsz*x4)) - (y(6)*(-cz1*x1-cz2*x2)) + Fe*sin(omega*t)*sin(beta))/m;
f(5) = y(6);
f(6) = ((-y(1)*(kx1*z1+kx2*z2+kcsx*z4)) - (y(2)*(cx1*z1+cx2*z2)) - (y(3)*(-
kz1*x1-kz2*x2-kcsz*x4)) - (y(4)*(-cz1*x1-cz2*x2)) -
(y(5)*(kx1*z1^2+kx2*z2^2+kz1*x1^2+kz2*x2^2+kcsx*z4^2+kcsz*x4^2)) -
(y(6)*(cx1*z1^2+cx2*z2^2+cz1*x1^2+cz2*x2^2)) + Fe*sin(omega*t)*cos(beta)*z3
- Fe*sin(omega*t)*sin(beta)*x3)/Jyy;

end

```

Natural frequency subprogram for machine and steel cable combination:

```
function Natfreq
global x1 x2 x4 z1 z2 z4 kx1 kx2 kcsx kz1 kz2 kcsz m Jyy

K = [ (kx1+kx2+kcsx) 0 (kx1*z1+kx2*z2+kcsx*z4);
      0 (kz1+kz2+kcsz) (-kz1*x1-kz2*x2-kcsz*x4);
      (kx1*z1+kx2*z2+kcsx*z4) (-kz1*x1-kz2*x2-kcsz*x4)
      (kx1*z1^2+kx2*z2^2+kz1*x1^2+kz2*x2^2+kcsx*z4^2+kcsz*x4^2) ];

M = [m 0 0; 0 m 0; 0 0 Jyy];

[V,D] = eig(K,M);
omega_n = sqrt(D);
f_n = sqrt(D)/(2*pi);

[val,horizontal] = max(abs(V(1,:)));
[val,vertical] = max(abs(V(2,:)));
[val,rotational] = max(abs(V(3,:)));
f_n_horizontal = max(f_n(:,horizontal));
f_n_vertical = max(f_n(:,vertical));
f_n_rotational = max(f_n(:,rotational));

disp('Natural Frequencies:')
disp(['Horizontal mode = ',num2str(f_n_horizontal),' Hz'])
disp(['Vertical mode = ',num2str(f_n_vertical),' Hz'])
disp(['Rotational mode = ',num2str(f_n_rotational),' Hz'])

end
```

Subprogram to plot different graphs for machine and steel cable combination:

```
function Plotting(t,x1_dyn,ddotx1_dyn,x2_dyn,
ddotx2_dyn,z1_dyn,ddotz1_dyn,z2_dyn,ddotz2_dyn)

%Plotting

figure(1)
subplot(2,1,2);plot(t(11670:20000),x1_dyn(11670:20000))
xlabel('$$$ Time \; (s) $$$','Interpreter','latex')
ylabel('$$$ Displacement \; \Delta x_1 \; [m] $$$','Interpreter','latex')

subplot(2,1,1);plot(t(11670:20000),ddotx1_dyn(11670:20000))
xlabel('$$$ Time \; (s) $$$','Interpreter','latex')
ylabel('$$$ Acceleration \; \Delta\ddot{x}_1 \; [m/s^2]
$$$','Interpreter','latex')

figure(2)
subplot(2,1,2);plot(t(11670:20000),x2_dyn(11670:20000))
xlabel('$$$ Time \; (s) $$$','Interpreter','latex')
ylabel('$$$ Displacement \; \Delta x_2 \; [m] $$$','Interpreter','latex')

subplot(2,1,1);plot(t(11670:20000),ddotx2_dyn(11670:20000))
xlabel('$$$ Time \; (s) $$$','Interpreter','latex')
ylabel('$$$ Acceleration \; \Delta\ddot{x}_2 \; [m/s^2]
$$$','Interpreter','latex')

figure(3)
subplot(2,1,2);plot(t(11670:20000),z1_dyn(11670:20000))
xlabel('$$$ Time \; (s) $$$','Interpreter','latex')
ylabel('$$$ Displacement \; \Delta z_1 \; [m] $$$','Interpreter','latex')

subplot(2,1,1);plot(t(11670:20000),ddotz1_dyn(11670:20000))
xlabel('$$$ Time \; (s) $$$','Interpreter','latex')
ylabel('$$$ Acceleration \; \Delta\ddot{z}_1 \; [m/s^2]
$$$','Interpreter','latex')

figure(4)
subplot(2,1,2);plot(t(11670:20000),z2_dyn(11670:20000))
xlabel('$$$ Time \; (s) $$$','Interpreter','latex')
ylabel('$$$ Displacement \; \Delta z_2 \; [m] $$$','Interpreter','latex')

subplot(2,1,1);plot(t(11670:20000),ddotz2_dyn(11670:20000))
xlabel('$$$ Time \; (s) $$$','Interpreter','latex')
ylabel('$$$ Acceleration \; \Delta\ddot{z}_2 \; [m/s^2]
$$$','Interpreter','latex')

end
```


Bump test program

```
clear all
syms zeta omega_n
format long

y_1 = 0.02358986175;
y_2 = 0.017331327;
t_1 = 1.632813;
t_2 = 1.742188;
m = 310.35;
n = 1;

tau_d = t_2-t_1;
omega_d = (2*pi)/tau_d;

eqn1 = (y_2/y_1) == exp(zeta*omega_n*tau_d*n);
eqn2 = omega_d == (sqrt(1 - zeta^2))*omega_n;

[omega_n, zeta] = solve(eqn1,eqn2);
zeta_x = max(abs(double(zeta)))
omega_nx = max(double(omega_n))

f_nx = omega_nx/(2*pi)

k_1 = (omega_nx^2)*m*0.5
c_crit = 2*m*omega_nx;
c_1 = zeta_x*c_crit*0.5
```

APPENDIX B – PHOTOS OF EXPERIMENTAL WORK



Figure 7-1: Representation of the test setup for the second test frequency where steel cables are caught in a dry interlocking blockage.



Figure 7-2: Blockage created for the second test frequency where steel cables are caught in a dry interlocking blockage.



Figure 7-3: Representation of the test setup for the third test frequency where steel cables are caught in a dry interlocking blockage.



Figure 7-4: Blockage created for the third test frequency where steel cables are caught in a dry interlocking blockage.



Figure 7-5: Partial unblocking occurred at 20.25 Hz and an unbalance of 94 % for the third test frequency where steel cables are used for unblocking a dry interlocking blockage.



Figure 7-6: Representation of test setup for the second test where steel cables are caught in a cemented blockage.



Figure 7-7: Blockage created for the second test where cables are caught in a cemented blockage.



Figure 7-8: Partial unblocking for the second test, at 77 % excitation unbalance, where steel cables are used for unblocking a cemented blockage.



Figure 7-9: Blockage created for the second test where the hammer is for unblocking a dry interlocking blockage.



Figure 7-10: Representation of test setup for the second test where the hammer is used for unblocking a cemented blockage.



Figure 7-11: Blockage created for the second test where the hammer is used for unblocking a cemented blockage.



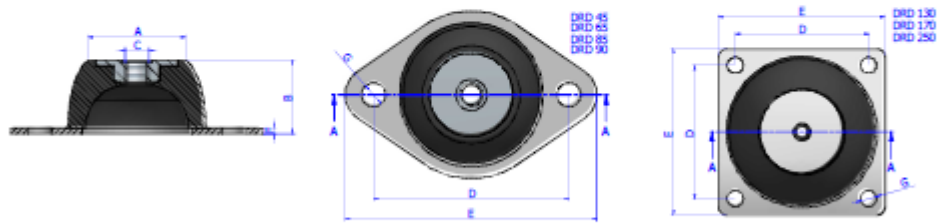
Figure 7-12: Small partial unblocking for the second test where the hammer is used for unblocking a cemented blockage at an excitation unbalance of 50 %.

APPENDIX C – RUBBER MOUNT SPECIFICATIONS



Rubber Metal anti vibration mounts DRD ANTI VIBRATION MOUNTS

DRAWINGS

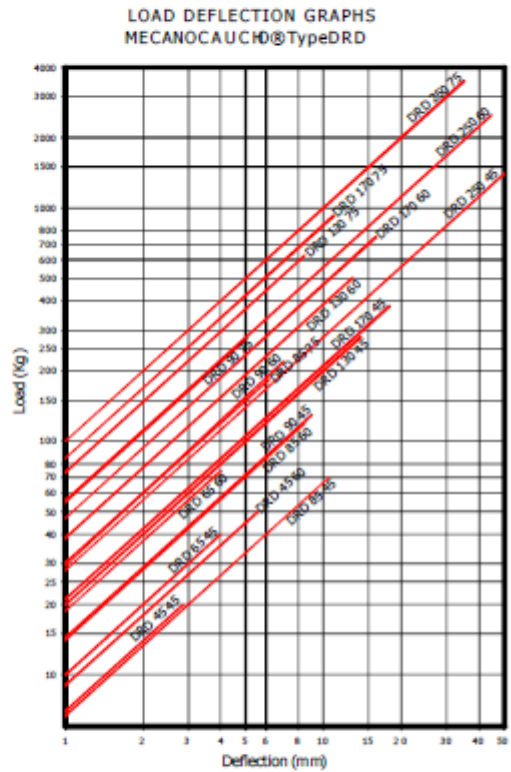
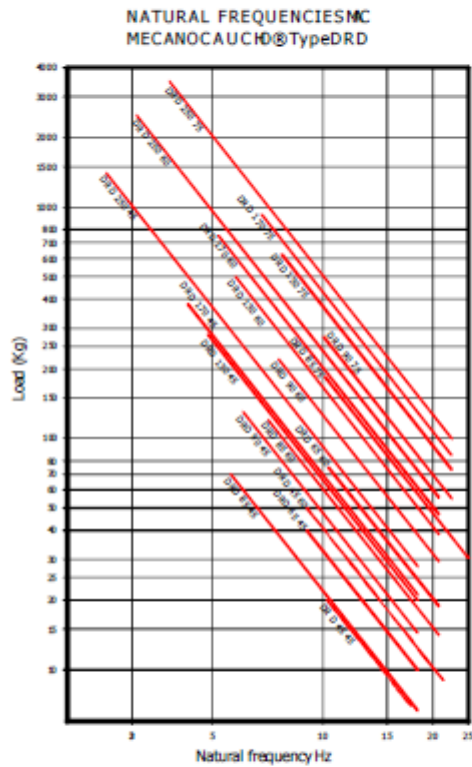


DIMENSIONS

Type	A (mm)	B (mm)	C (mm)	D (mm)	E (mm)	F (mm)	G (mm)	Weight (g/°)	Load (kg)	Shore	Code
DRD 45	33	25	M-8	66	85	2	8	70	20	45 Sh	175081
									50	60 Sh	175083
DRD 65	52	35	M-10	92	114	2,5	10,5	170	40	45 Sh	175001
									75	60 Sh	175002
DRD 85	52	40	M-10	110	136	3	11,5	303	75	45 Sh	175003
									120	60 Sh	175004
									185	75 Sh	175013
DRD 90	57,5	45	M-10	125	150	3	12,5	430	130	45 Sh	175021
									220	60 Sh	175022
									275	75 Sh	175023
DRD 130	78	63,5	M-12	120	150	5	14,5	1080	280	45 Sh	175031
									500	60 Sh	175032
									625	75 Sh	175033
DRD 170	100	84	M-16	160	200	4	14,5	2390	380	45 Sh	175036
									750	60 Sh	175037
									930	75 Sh	175038
DRD 250	187	158	M-24	250	310	6	18,5	10400	1400	45 Sh	175041
									2500	60 Sh	175042
									3150	75 Sh	175044


Rubber Metal anti vibration mounts DRD ANTI VIBRATION MOUNTS

Elastical properties




APPENDIX E – PERMISSION TO USE FIGURES FROM ARTICLES

Permission for Figure 1-3:



RightsLink®

Home
?
Email Support
Barend Meiring v



Numerical investigations of ore pass hang-up phenomena

Author: J Hadjigeorgiou, J.F. Lessard

Publication: International Journal of Rock Mechanics and Mining Sciences

Publisher: Elsevier

Date: September 2007

Copyright © 2006 Elsevier Ltd. All rights reserved.

Order Completed

Thank you for your order.

This Agreement between Mr. Barend Meiring ("You") and Elsevier ("Elsevier") consists of your license details and the terms and conditions provided by Elsevier and Copyright Clearance Center.

Your confirmation email will contain your order number for future reference.

License Number	5014820407513
License date	Feb 23, 2021

[Printable Details](#)

Licensed Content

Licensed Content Publisher	Elsevier
Licensed Content Publication	International Journal of Rock Mechanics and Mining Sciences
Licensed Content Title	Numerical investigations of ore pass hang-up phenomena
Licensed Content Author	J Hadjigeorgiou, J.F. Lessard
Licensed Content Date	Sep 1, 2007
Licensed Content Volume	44
Licensed Content Issue	6
Licensed Content Pages	15
Journal Type	S&T

Order Details

Type of Use	reuse in a thesis/dissertation
Portion	figures/tables/illustrations
Number of figures/tables/illustrations	1
Format	electronic
Are you the author of this Elsevier article?	No
Will you be translating?	No


About Your Work


Title	Design and Evaluation of an Ore Flow Restore Machine
Institution name	North West University of Potchefstroom
Expected presentation date	Mar 2021


Additional Data


Portions	Fig. 3. Screening technique at the dump points: (a) grizzly, (b) scalper, (c) mantles, (d) no screening. Located on page 3 of 15
----------	--


Permission for Figure 1-16:







Home


Help


Email Support


Barend Meiring ▼

SPRINGER NATURE

Vibrating Ore-drawing Technology

Publication: Springer eBook
 Publisher: Springer Nature
 Date: Jan 1, 2008

Copyright © 2008, Metallurgical Industry Press, Beijing and Springer-Verlag GmbH Berlin Heidelberg

Order Completed

Thank you for your order.

This Agreement between Mr. Barend Meiring ("You") and Springer Nature ("Springer Nature") consists of your license details and the terms and conditions provided by Springer Nature and Copyright Clearance Center.

Your confirmation email will contain your order number for future reference.

License Number 5014821126613

License date Feb 23, 2021

[Printable Details](#)

<div style="font-size: 0.8em; font-weight: bold; margin: 0;"> ▣ Licensed Content </div>	<div style="font-size: 0.8em; font-weight: bold; margin: 0;"> ▣ Order Details </div>
<p style="margin: 0; font-size: 0.8em;">Licensed Content Publisher Springer Nature</p> <p style="margin: 0; font-size: 0.8em;">Licensed Content Publication Springer eBook</p> <p style="margin: 0; font-size: 0.8em;">Licensed Content Title Vibrating Ore-drawing Technology</p> <p style="margin: 0; font-size: 0.8em;">Licensed Content Date Jan 1, 2008</p>	<p style="margin: 0; font-size: 0.8em;">Type of Use Theses/Dissertation academic/university or research institute</p> <p style="margin: 0; font-size: 0.8em;">Requestor type electronic</p> <p style="margin: 0; font-size: 0.8em;">Format figures/tables/illustrations</p> <p style="margin: 0; font-size: 0.8em;">Number of figures/tables/illustrations 1</p> <p style="margin: 0; font-size: 0.8em;">Will you be translating? no</p> <p style="margin: 0; font-size: 0.8em;">Circulation/distribution 1 - 29</p> <p style="margin: 0; font-size: 0.8em;">Author of this Springer Nature content no</p>
<div style="font-size: 0.8em; font-weight: bold; margin: 0;"> ▣ About Your Work </div>	<div style="font-size: 0.8em; font-weight: bold; margin: 0;"> ▣ Additional Data </div>
<p style="margin: 0; font-size: 0.8em;">Title Design and Evaluation of an Ore Flow Restore Machine</p> <p style="margin: 0; font-size: 0.8em;">Institution name North West University of Potchefstroom</p> <p style="margin: 0; font-size: 0.8em;">Expected presentation date Mar 2021</p>	<p style="margin: 0; font-size: 0.8em;">Portions Fig.9.7 The outline sketch of the structure and installation of ore-drawing machine of TZ type. Located on page 286</p>

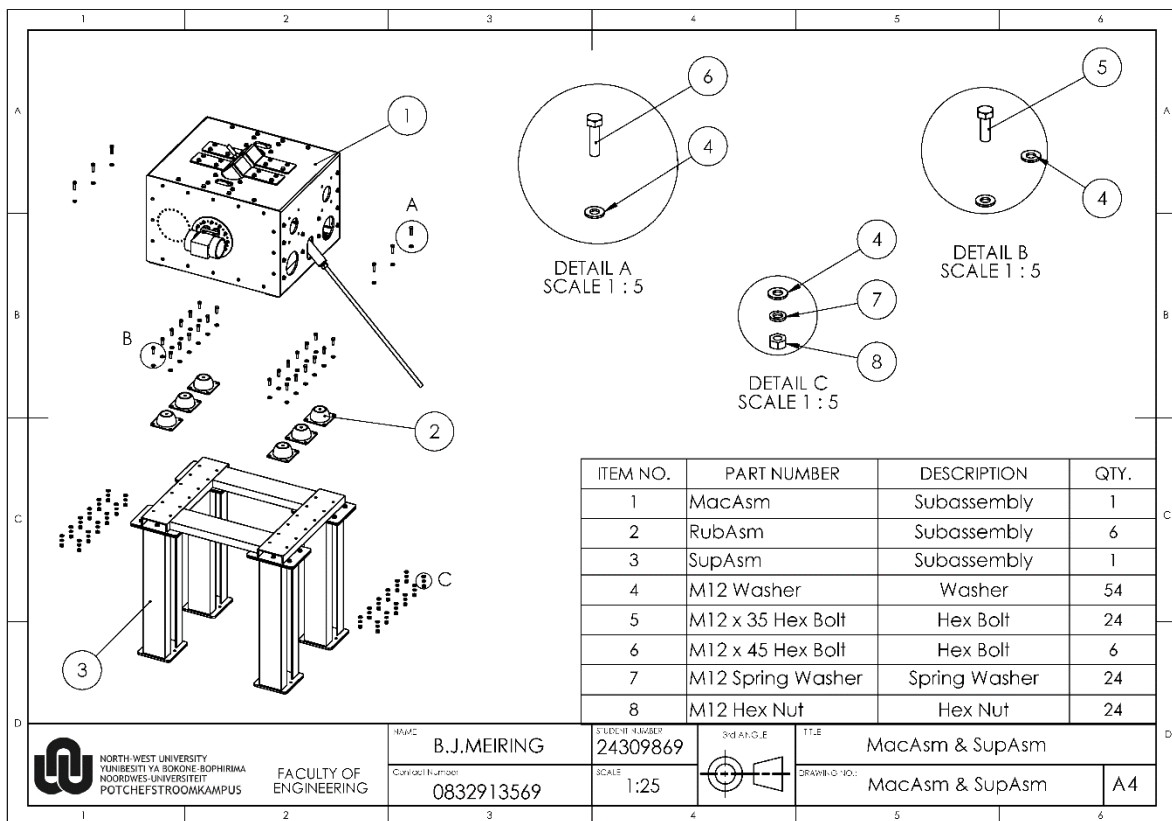
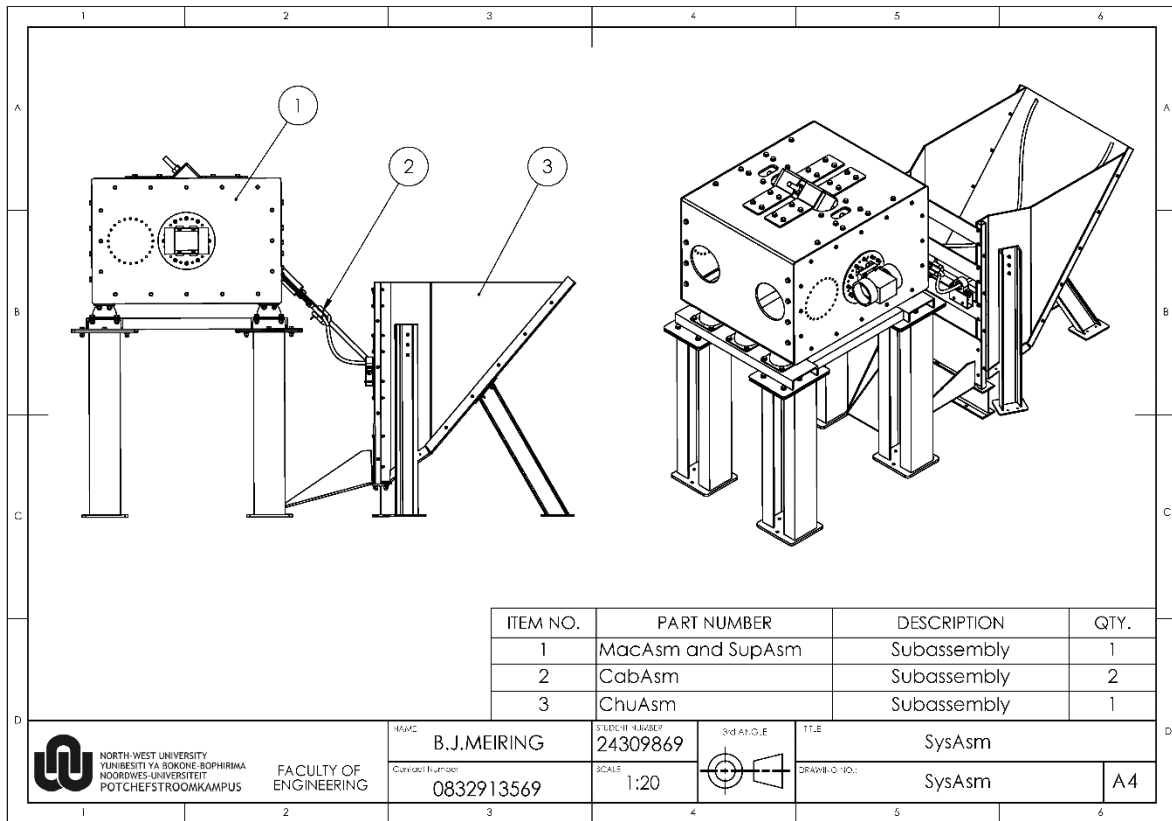
Permission for Figure 1-2, Figure 1-14 and Figure 1-15:

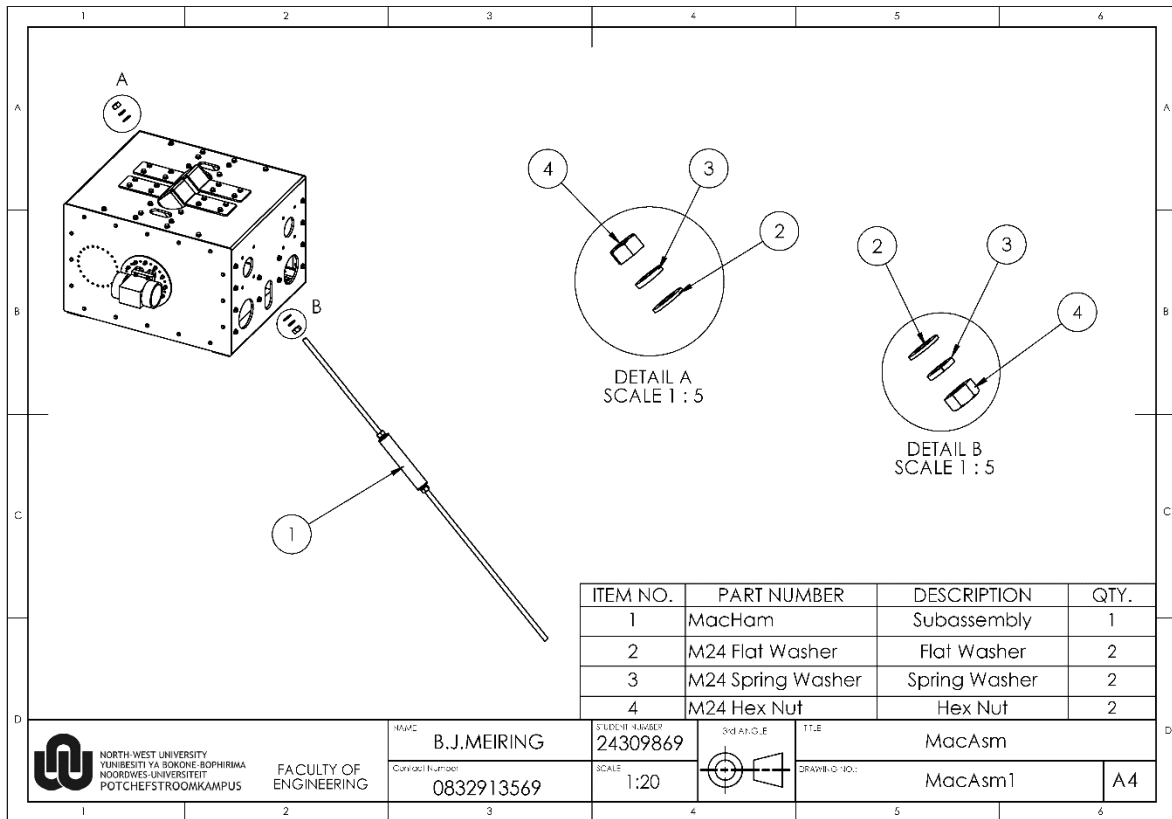
The screenshot shows the RightsLink interface for a specific work. At the top left is the Copyright Clearance Center logo and the RightsLink logo. On the top right are navigation links: Home, Help, Email Support, Sign in, and Create Account. The main content area displays the title "Formation and removal of hang-ups in ore passes" and the author "Author: T. Szwedzicki". Below this, it lists the publication "Mining Technology (Transactions of the Institutions of Mining and Metallurgy: Section A)", the publisher "Taylor & Francis", and the date "Date: Sep 1, 2007". A Taylor & Francis logo is also present. A note states "Rights managed by Taylor & Francis". Below the main content is a "Thesis/Dissertation Reuse Request" section with the text: "Taylor & Francis is pleased to offer reuses of its content for a thesis or dissertation free of charge contingent on resubmission of permission request if work is published." This section includes a "BACK" button and a "CLOSE" button. At the bottom, there is a footer with copyright information: "© 2021 Copyright - All Rights Reserved | Copyright Clearance Center, Inc. | Privacy statement | Terms and Conditions" and a comment: "Comments? We would like to hear from you. E-mail us at customercare@copyright.com".

Permission for Figure 1-1, all figures from Figure 1-4 to Figure 1-13:

The screenshot shows the RightsLink interface for a specific work. At the top left is the Copyright Clearance Center logo and the RightsLink logo. On the top right are navigation links: Home, Help, Email Support, Sign in, and Create Account. The main content area displays the title "Strategies for restoring material flow in ore and waste pass systems" and the author "Author: John Hadjigeorgiou, J.F. Lessard". Below this, it lists the publication "International Journal of Mining, Reclamation and Environment", the publisher "Taylor & Francis", and the date "Date: Sep 1, 2010". A Taylor & Francis logo is also present. A note states "Rights managed by Taylor & Francis". Below the main content is a "Thesis/Dissertation Reuse Request" section with the text: "Taylor & Francis is pleased to offer reuses of its content for a thesis or dissertation free of charge contingent on resubmission of permission request if work is published." This section includes a "BACK" button and a "CLOSE" button. At the bottom, there is a footer with copyright information: "© 2021 Copyright - All Rights Reserved | Copyright Clearance Center, Inc. | Privacy statement | Terms and Conditions" and a comment: "Comments? We would like to hear from you. E-mail us at customercare@copyright.com".

APPENDIX F – DETAILED DRAWINGS





NORTH WEST UNIVERSITY
YUNIBESITHI YA BOKONE-BOPHIRIMA
NOORDWES-UNIVERSITEIT
POTCHEFSTROOMKAMPUS

FACULTY OF
ENGINEERING

NAME: B.J.MEIRING
Contact Number: 0832913569

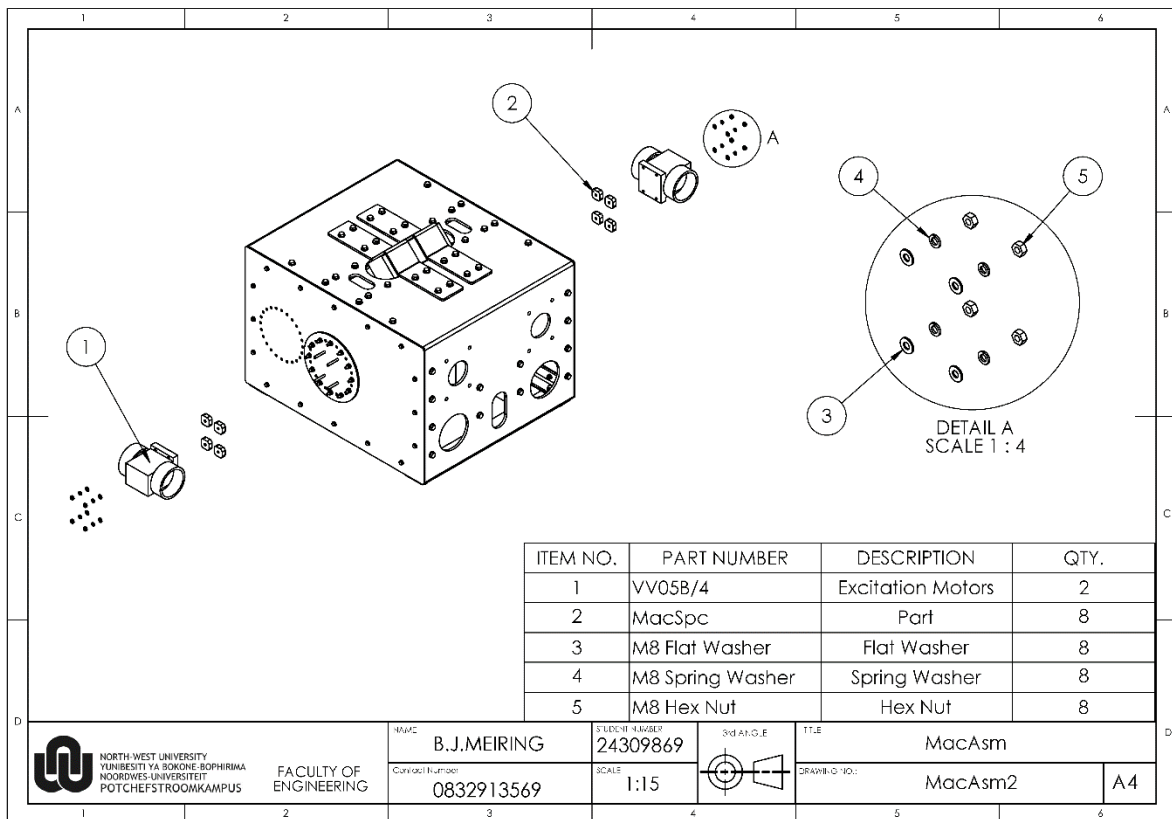
STUDENT NUMBER: 24309869
SCALE: 1:20



3rd ANGLE

TITLE: MacAsm
DRAWING NO.: MacAsm1

A4



NORTH WEST UNIVERSITY
YUNIBESITHI YA BOKONE-BOPHIRIMA
NOORDWES-UNIVERSITEIT
POTCHEFSTROOMKAMPUS

FACULTY OF
ENGINEERING

NAME: B.J.MEIRING
Contact Number: 0832913569

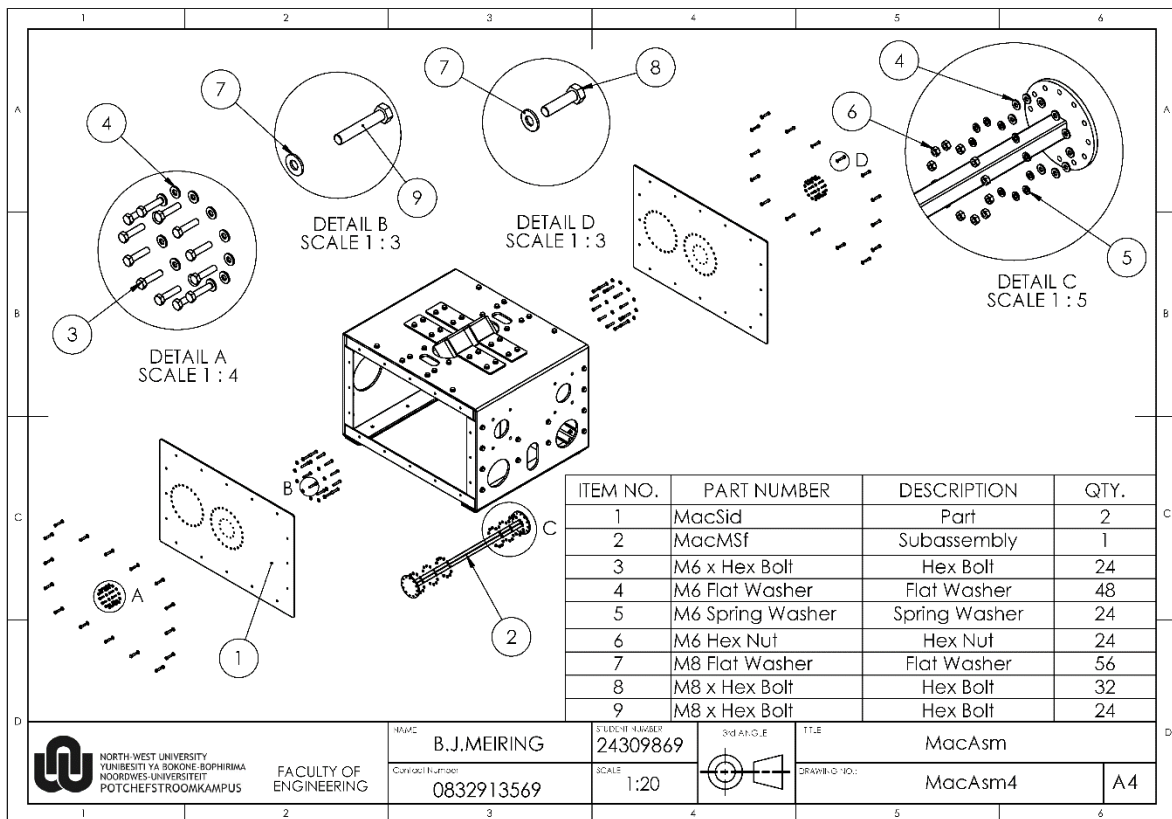
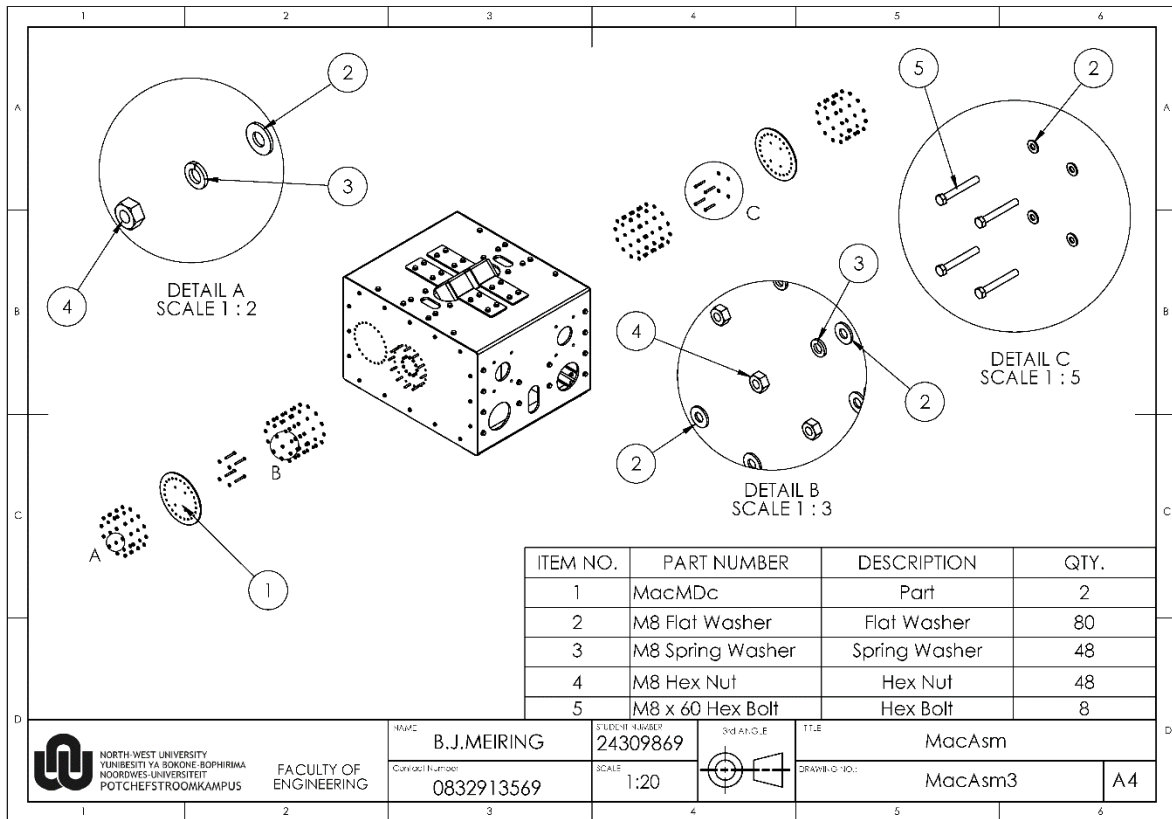
STUDENT NUMBER: 24309869
SCALE: 1:15



3rd ANGLE

TITLE: MacAsm
DRAWING NO.: MacAsm2

A4



ITEM NO.	PART NUMBER	DESCRIPTION	QTY.
1	MacTag	Part	1
2	MacSag	Part	2
3	MacBag	Part	1
4	33312040 X01	Hex Bolt	12
5	M12 Flat Washer	Flat Washer	32
6	M12 Spring Washer	Spring Washer	16
7	M12 Hex Nut	Hex Nut	16
8	M8 Flat Washer	Flat Washer	16
9	M8 Spring Washer	Spring Washer	16
10	M8 Hex Nut	Hex Nut	16
11	M12 x 50 Hex Bolt	Hex Bolt	4

NORTH WEST UNIVERSITY
 YUNIBESITHI YA BOKONE-BOPHIRIMA
 NOORDWES-UNIVERSITEIT
 POTCHEFSTROOMKAMPUS

FACULTY OF
 ENGINEERING

B.J.MEIRING
 Student Number: 24309869
 Contact Number: 0832913569

SCALE: 1:15

TITLE: MacAsm
 MacAsm5

A4

ITEM NO.	PART NUMBER	DESCRIPTION	QTY.
1	MacTag	Part	1
2	MacSag	Part	2
3	MacBag	Part	1
4	M12 x 40 Hex Bolt	Hex Bolt	12
5	M12 Flat Washer	Flat Washer	32
6	M12 Spring Washer	Spring Washer	16
7	M12 Hex Nut	Hex Nut	16
8	M8 Flat Washer	Flat Washer	16
9	M8 Spring Washer	Spring Washer	16
10	M8 Hex Nut	Hex Nut	16
11	M12 x 50 Hex Bolt	Hex Bolt	4

NORTH WEST UNIVERSITY
 YUNIBESITHI YA BOKONE-BOPHIRIMA
 NOORDWES-UNIVERSITEIT
 POTCHEFSTROOMKAMPUS

FACULTY OF
 ENGINEERING

B.J.MEIRING
 Student Number: 24309869
 Contact Number: 0832913569

SCALE: 1:15

TITLE: MacAsm
 MacAsm6

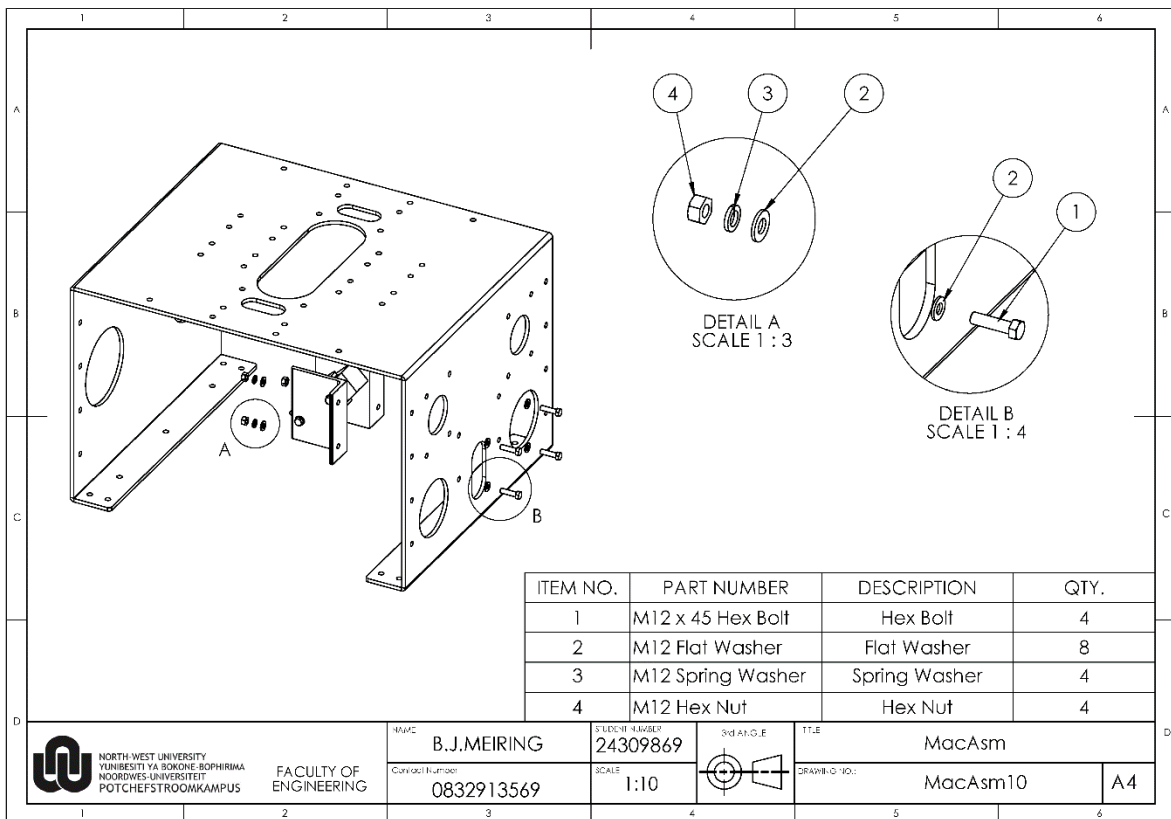
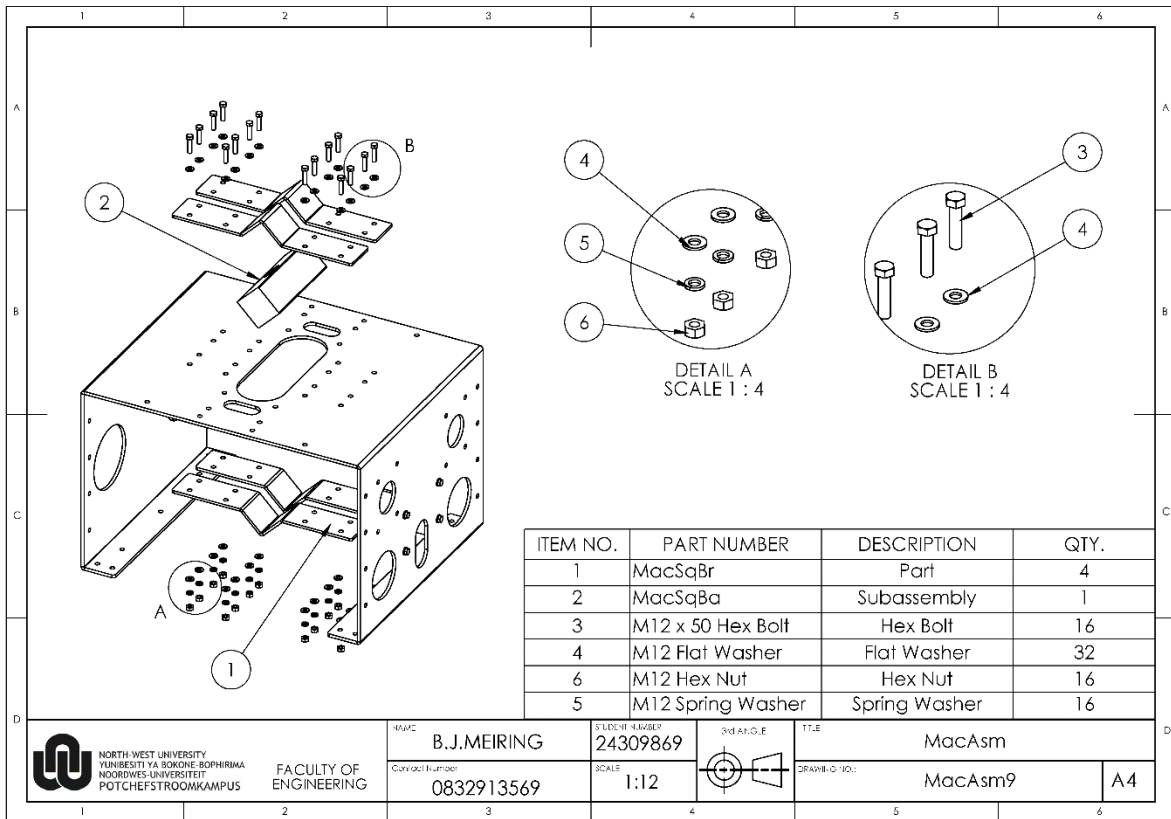
A4

ITEM NO.	PART NUMBER	DESCRIPTION	QTY.
1	MacU5f	Part	2

NORTH WEST UNIVERSITY YUNIBESITHI YA BOKONE-BOPHIRIMA NOORDWES-UNIVERSITEIT POTCHEFSTROOMKAMPUS	B.J.MEIRING <small>Course Number:</small> 0832913569	<small>STUDENT NUMBER</small> 24309869 <small>SCALE</small> 1:12	<small>3rd ANGLE</small> 	<small>TITLE</small> MacAsm MacAsm7	A4
	FACULTY OF ENGINEERING		<small>DRAWING NO.:</small>		

ITEM NO.	PART NUMBER	DESCRIPTION	QTY.
1	MacMBr	Part	2
2	M12 x 45 Hex Bolt	Hex Bolt	12
3	M12 Flat Washer	Flat Washer	24
4	M12 Spring Washer	Spring Washer	12
5	M12 Hex Nut	Hex Nut	12

NORTH WEST UNIVERSITY YUNIBESITHI YA BOKONE-BOPHIRIMA NOORDWES-UNIVERSITEIT POTCHEFSTROOMKAMPUS	B.J.MEIRING <small>Course Number:</small> 0832913569	<small>STUDENT NUMBER</small> 24309869 <small>SCALE</small> 1:10	<small>3rd ANGLE</small> 	<small>TITLE</small> MacAsm MacAsm8	A4
	FACULTY OF ENGINEERING		<small>DRAWING NO.:</small>		



Exploded view drawing of the MacAsm assembly. Callouts 1-8 identify the main components. Detail A shows a close-up of the hex bolt, flat washer, and spring washer assembly. Detail B shows a close-up of the hex nut, spring washer, and flat washer assembly.

ITEM NO.	PART NUMBER	DESCRIPTION	QTY.
1	MacShl	Part	1
2	MacSIaG	Part	2
3	MacSIaQ	Part	2
4	MacVBu	Part	1
5	M12 x 160 Hex Bolt	Hex Bolt	2
6	M12 Flat Washer	Flat Washer	4
7	M12 Spring Washer	Spring Washer	2
8	M12 Hex Nut	Hex Nut	2

NORTH WEST UNIVERSITY
 YUNIBESITHI YA BOKONE-BOPHIRIMA
 NOORDWES-UNIVERSITEIT
 POTCHEFSTROOMKAMPUS

FACULTY OF
 ENGINEERING

NAME: B.J.MEIRING
 STUDENT NUMBER: 24309869
 COURSE NUMBER: 0832913569

SCALE: 1:12

3rd ANGLE

TITLE: MacAsm
 DRAWING NO.: MacAsm11

A4

Exploded view drawing of the MacHam assembly. Callouts 1-6 identify the main components.

ITEM NO.	PART NUMBER	DESCRIPTION	QTY.
1	HamTRd	Part	1
2	HamHoB	Part	1
3	HamSBu	Part	2
4	M24 Flat Washer	Flat Washer	2
5	M24 Spring Washer	Spring Washer	2
6	M24 Hex Nut	Hex Nut	2

NORTH WEST UNIVERSITY
 YUNIBESITHI YA BOKONE-BOPHIRIMA
 NOORDWES-UNIVERSITEIT
 POTCHEFSTROOMKAMPUS

FACULTY OF
 ENGINEERING

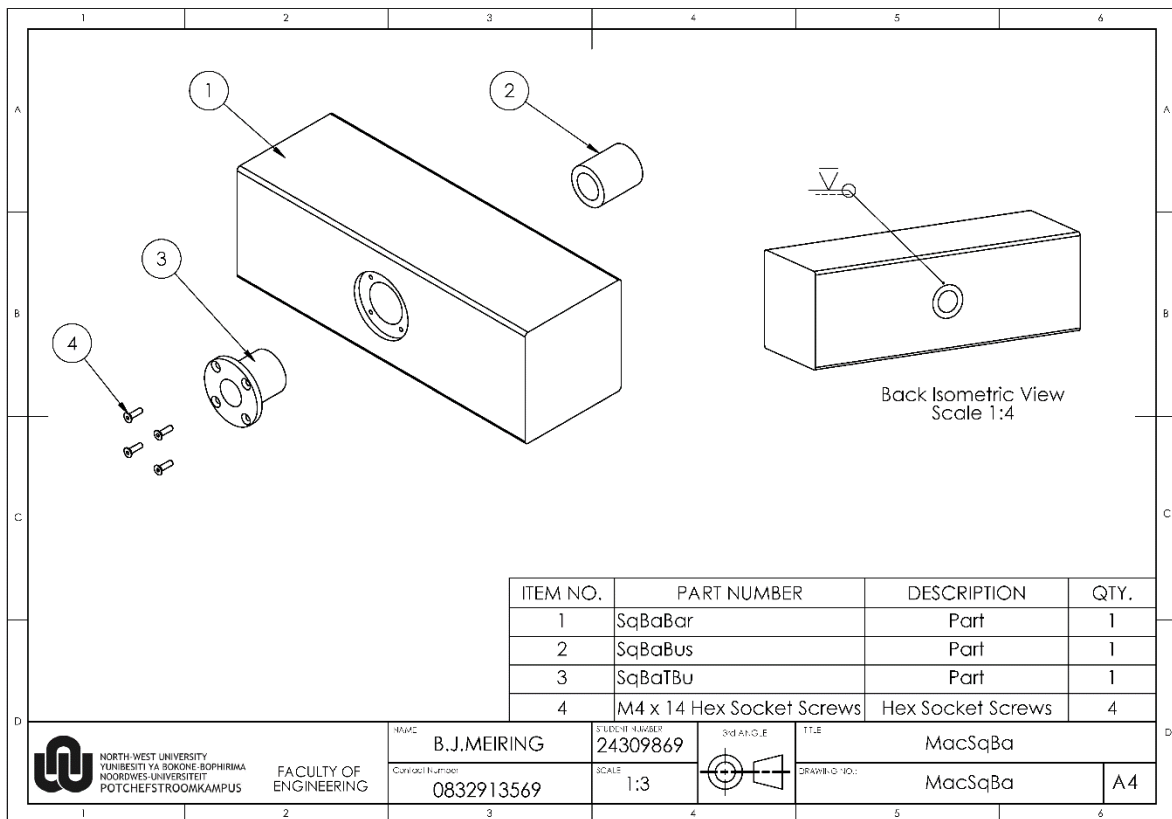
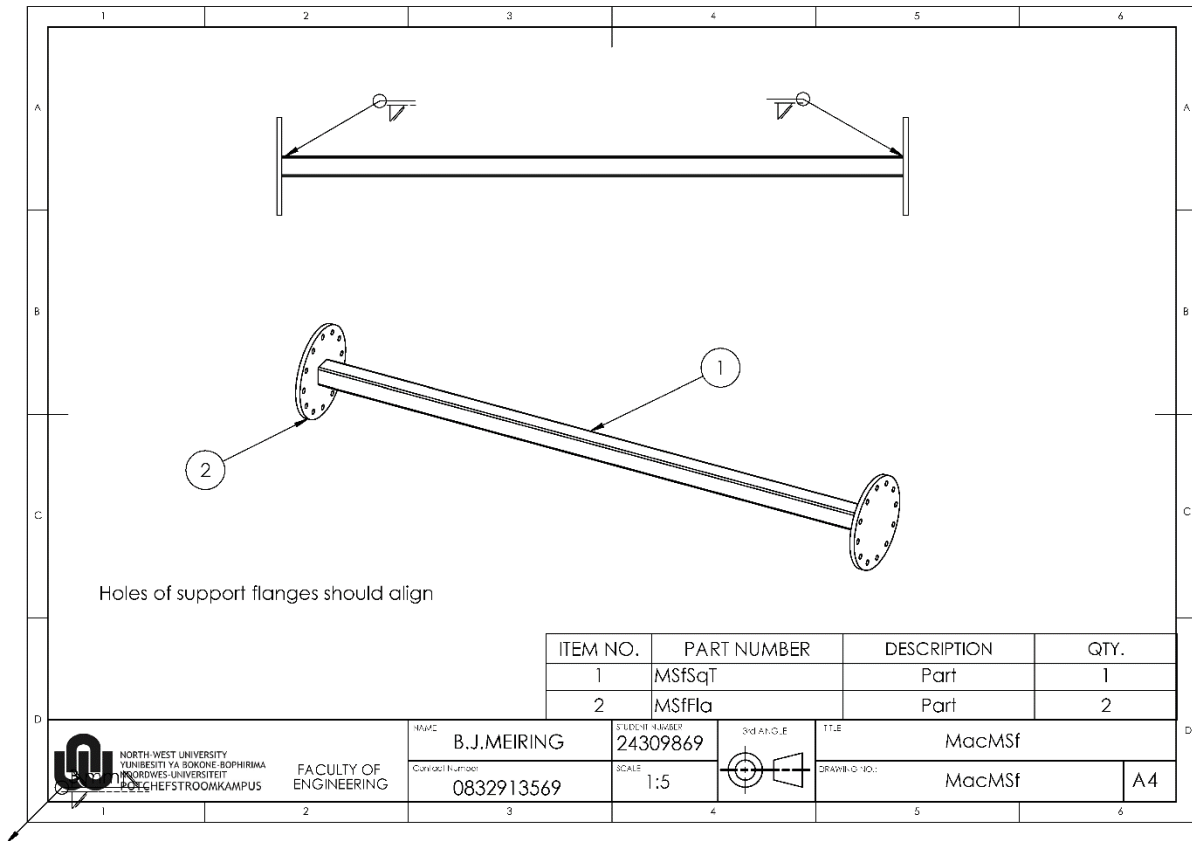
NAME: B.J.MEIRING
 STUDENT NUMBER: 24309869
 COURSE NUMBER: 0832913569

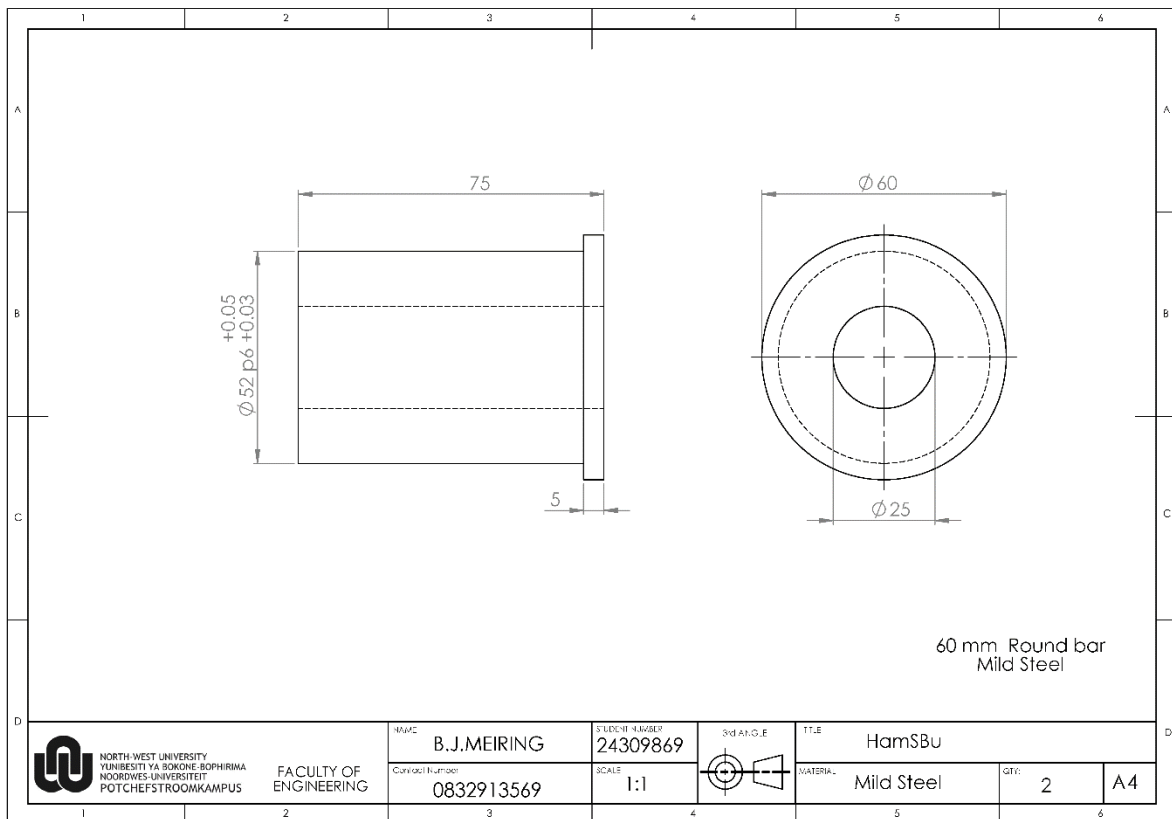
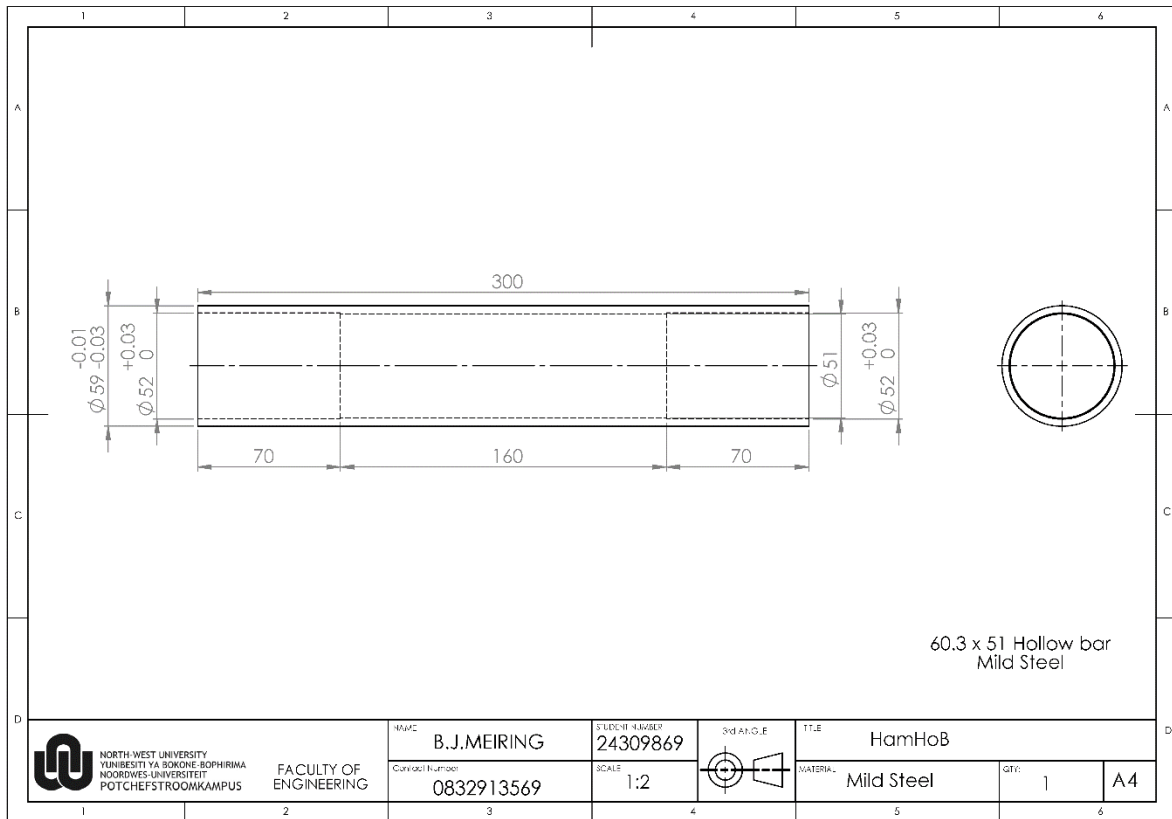
SCALE: 1:15

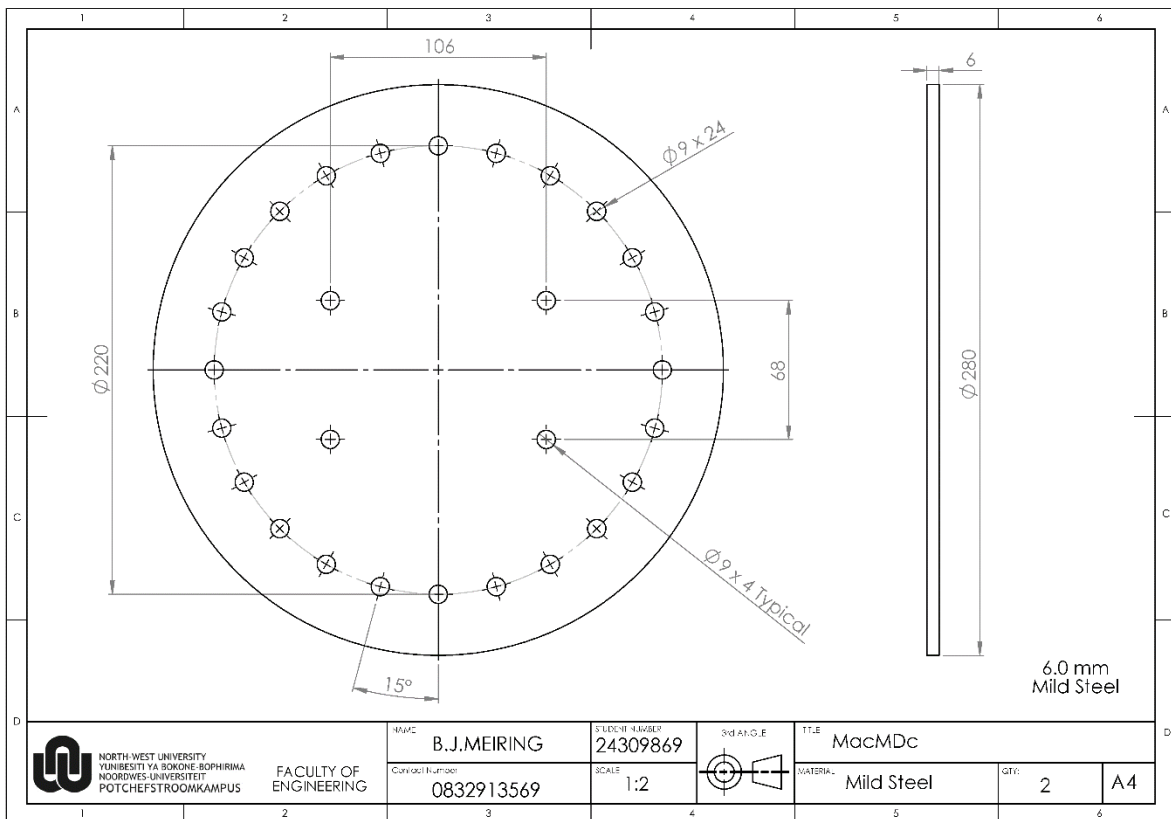
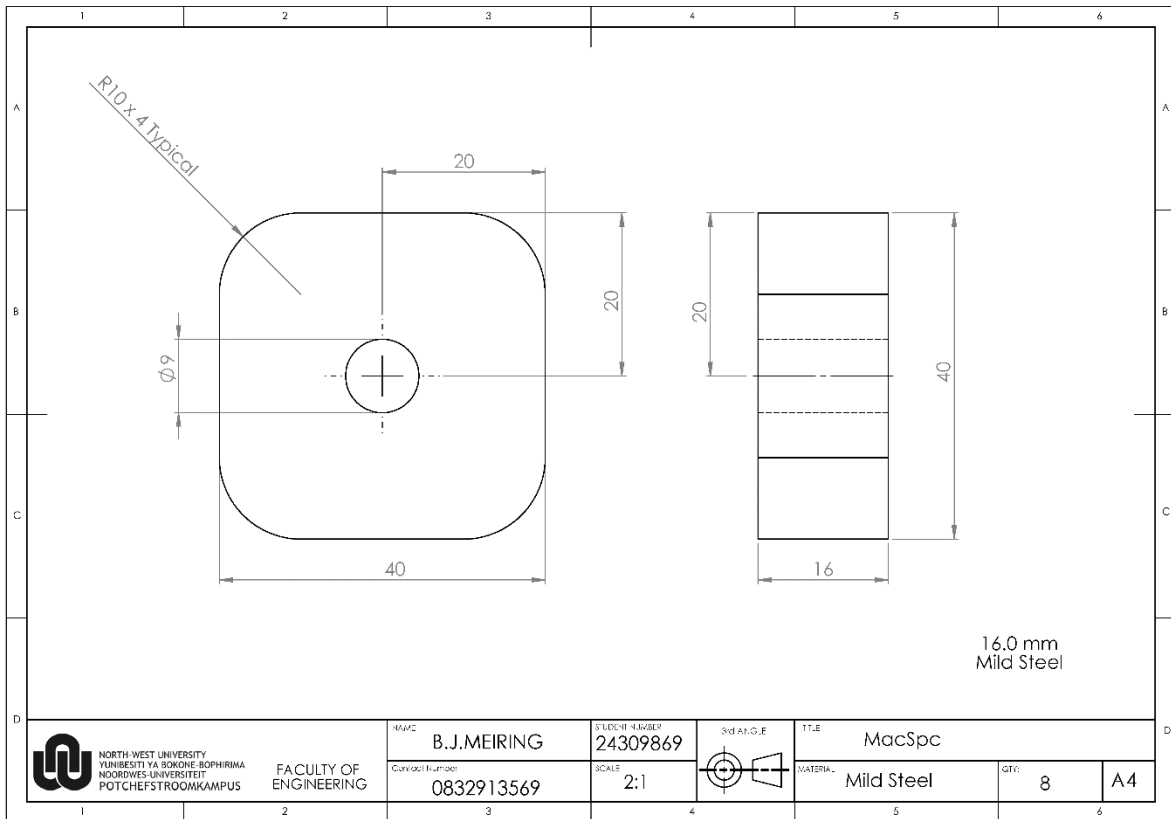
3rd ANGLE

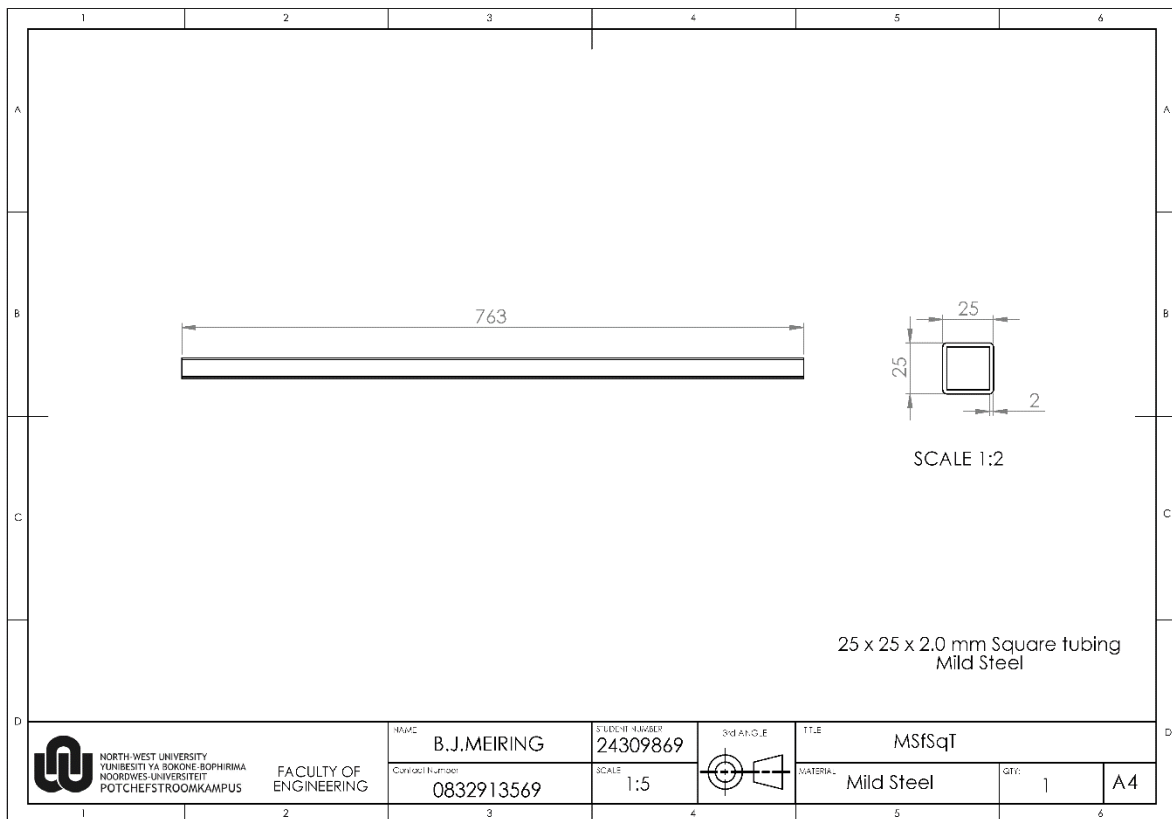
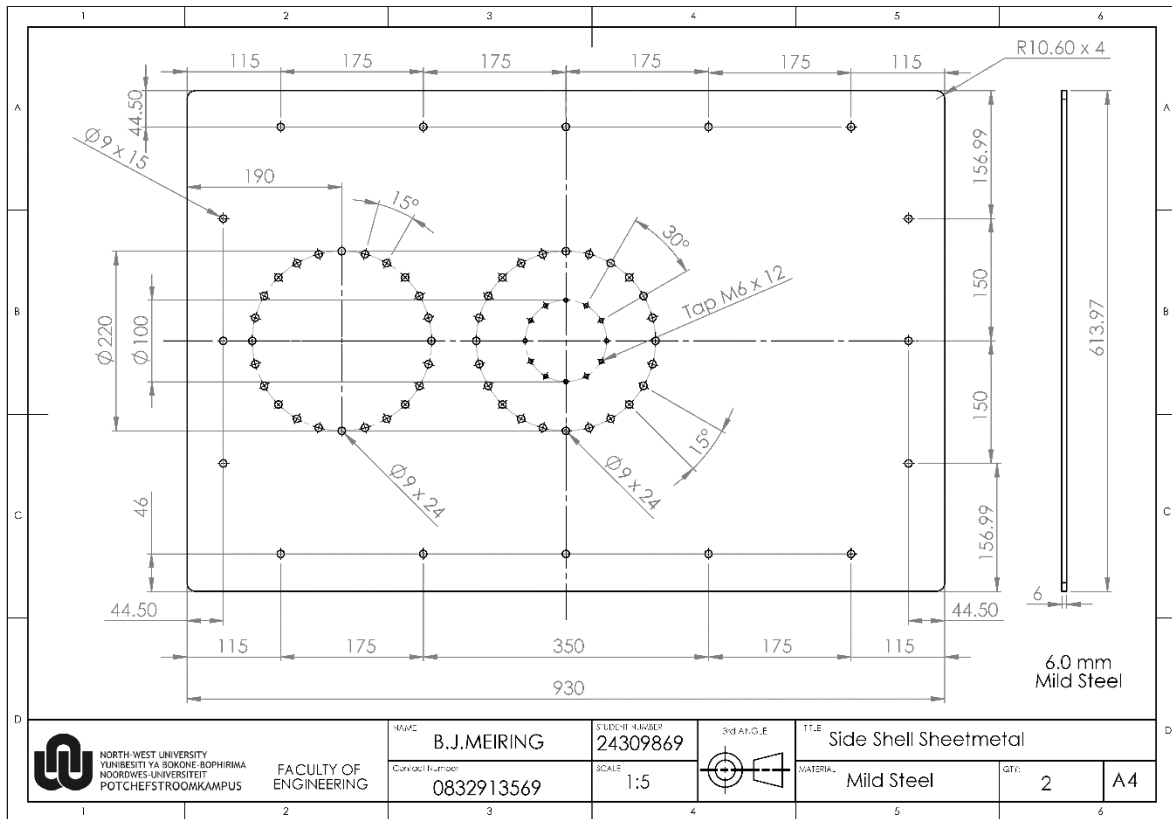
TITLE: MacHam
 DRAWING NO.: MacHam

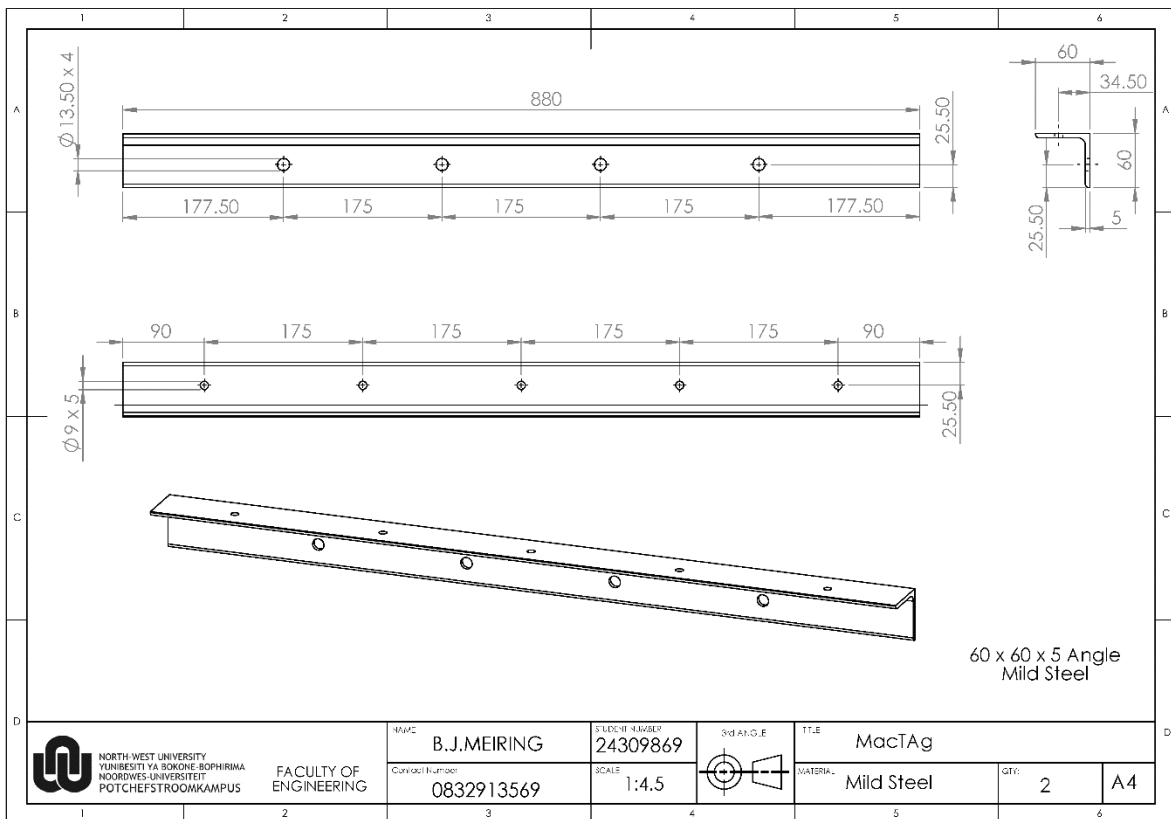
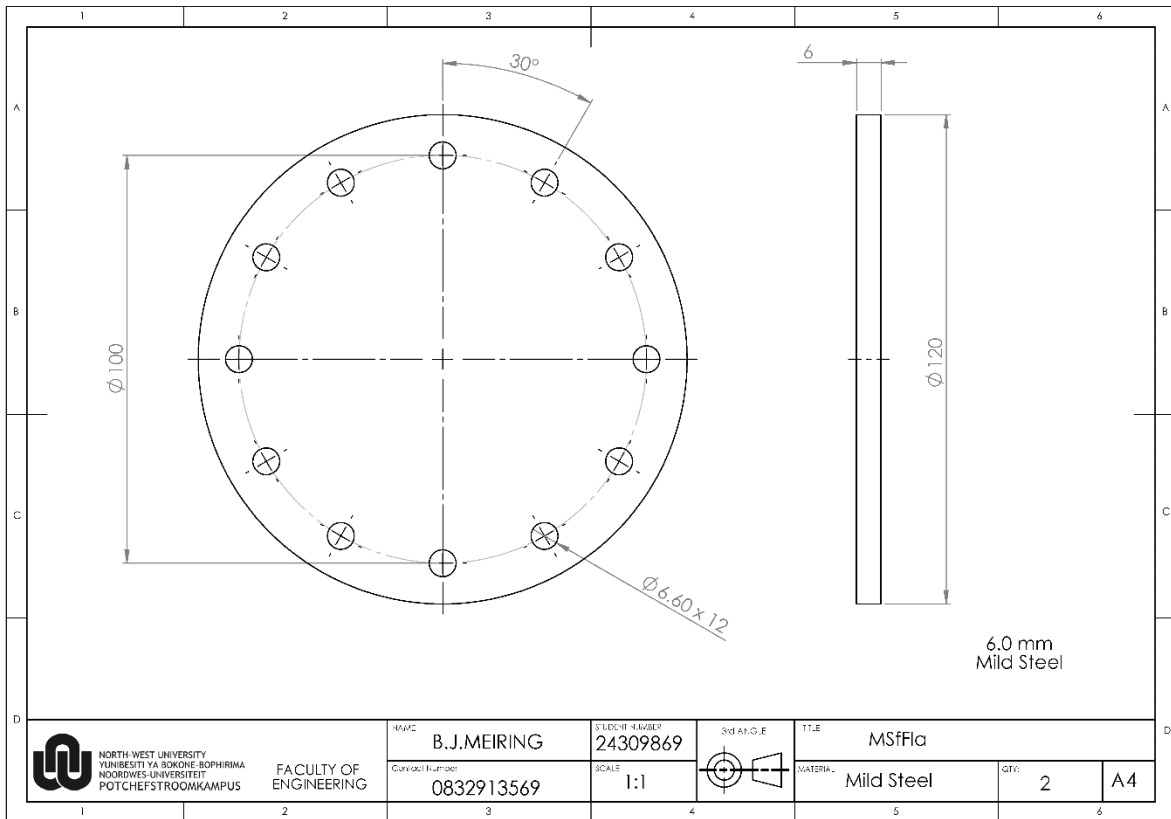
A4

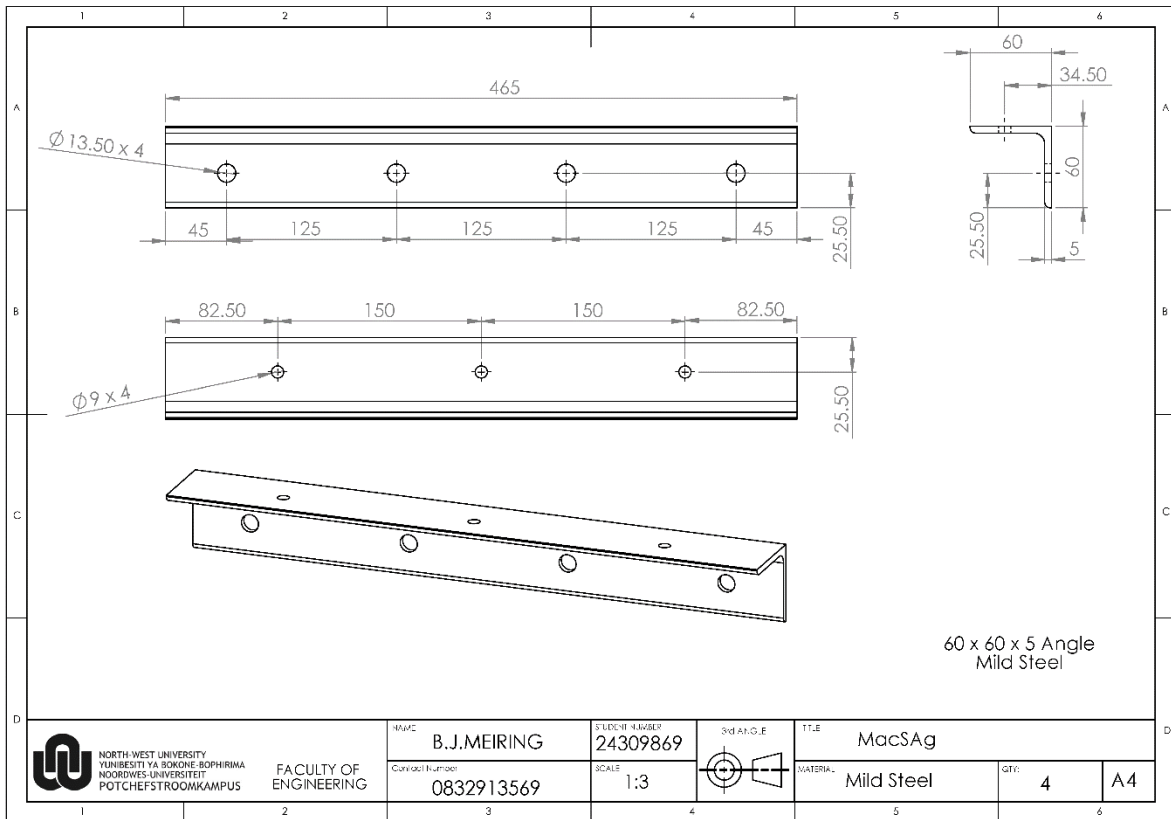












NORTH WEST UNIVERSITY
YUNIBESITHI YA BOKONE-BOPHIRIMA
NOORDWES-UNIVERSITEIT
POTCHEFSTROOMKAMPUS

FACULTY OF
ENGINEERING

NAME
B.J.MEIRING
Contact Number
0832913569

STUDENT NUMBER
24309869
SCALE
1:3

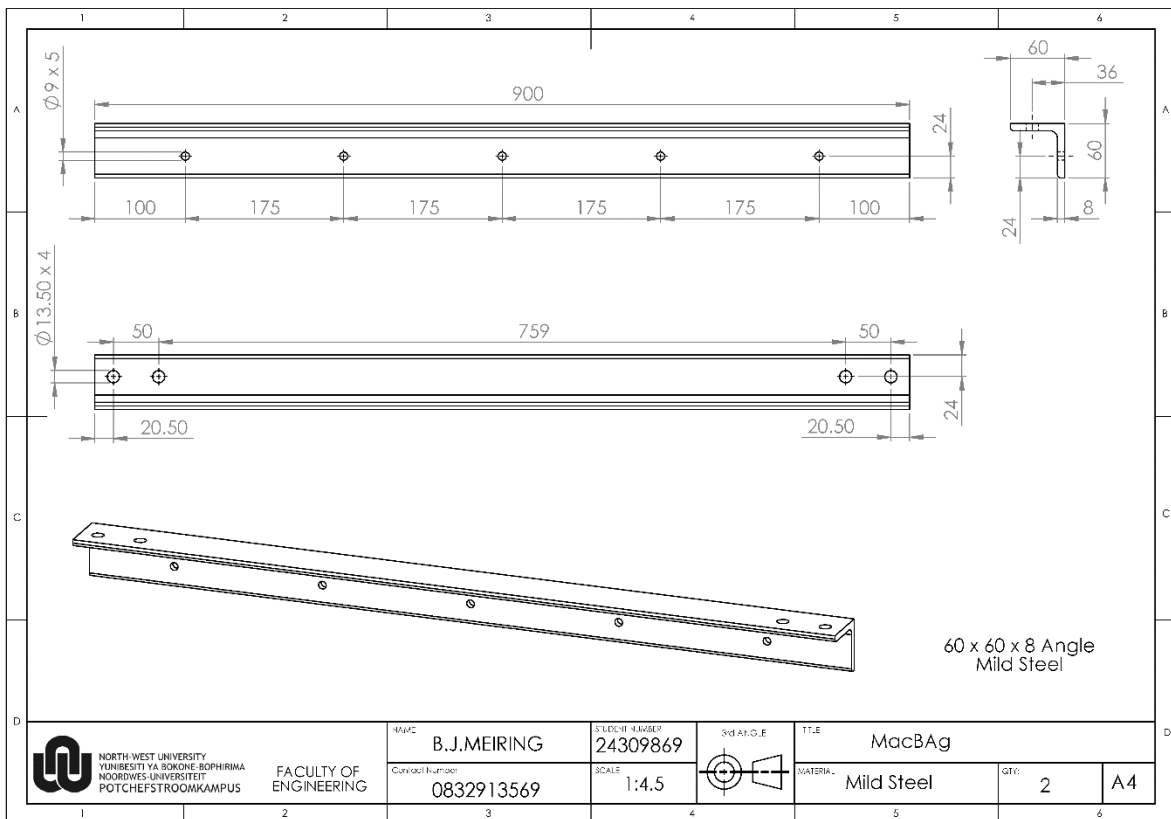


TITLE
MacSag

MATERIAL
Mild Steel

QTY
4

SIZE
A4



NORTH WEST UNIVERSITY
YUNIBESITHI YA BOKONE-BOPHIRIMA
NOORDWES-UNIVERSITEIT
POTCHEFSTROOMKAMPUS

FACULTY OF
ENGINEERING

NAME
B.J.MEIRING
Contact Number
0832913569

STUDENT NUMBER
24309869
SCALE
1:4.5

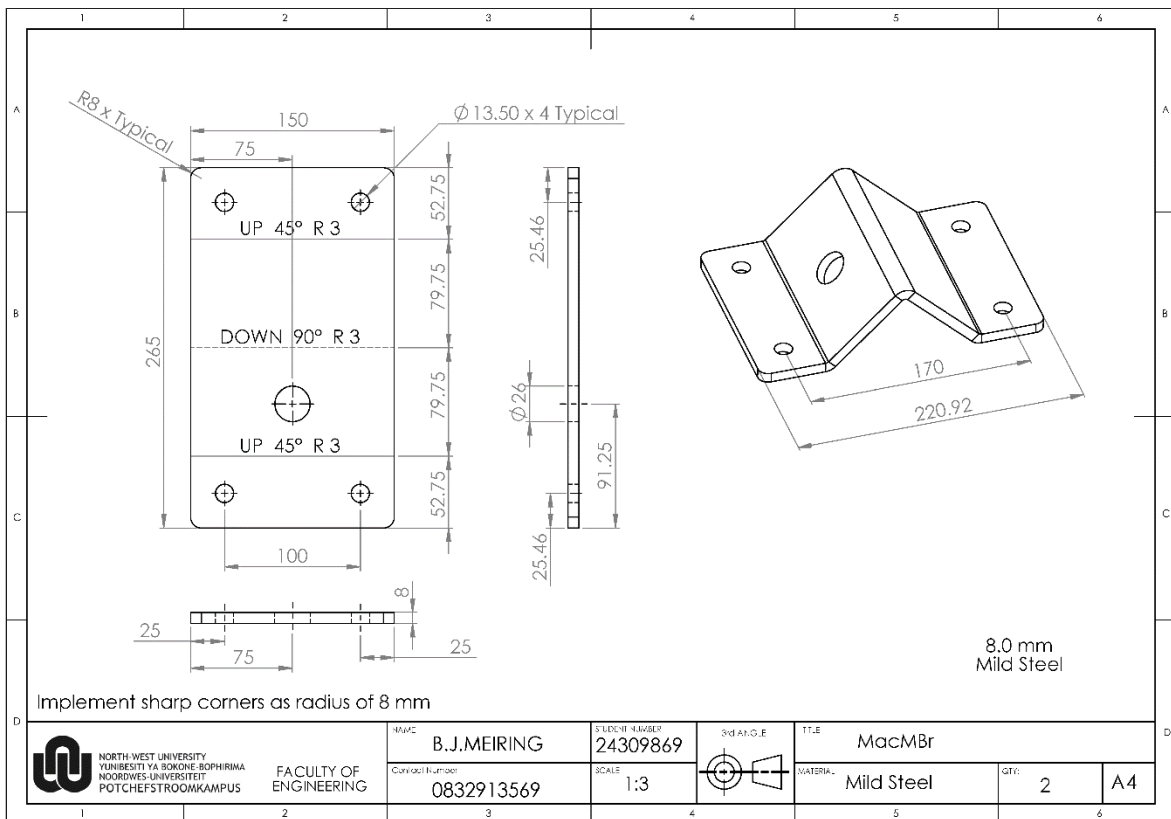
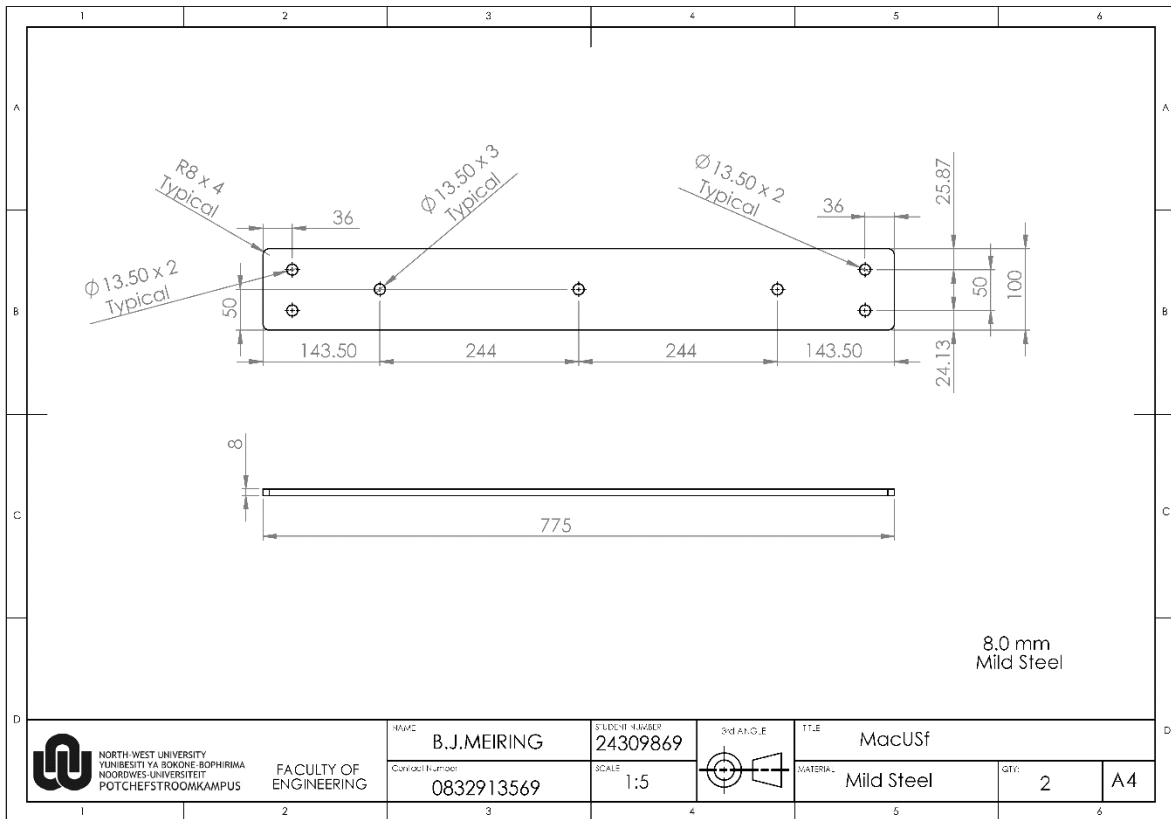


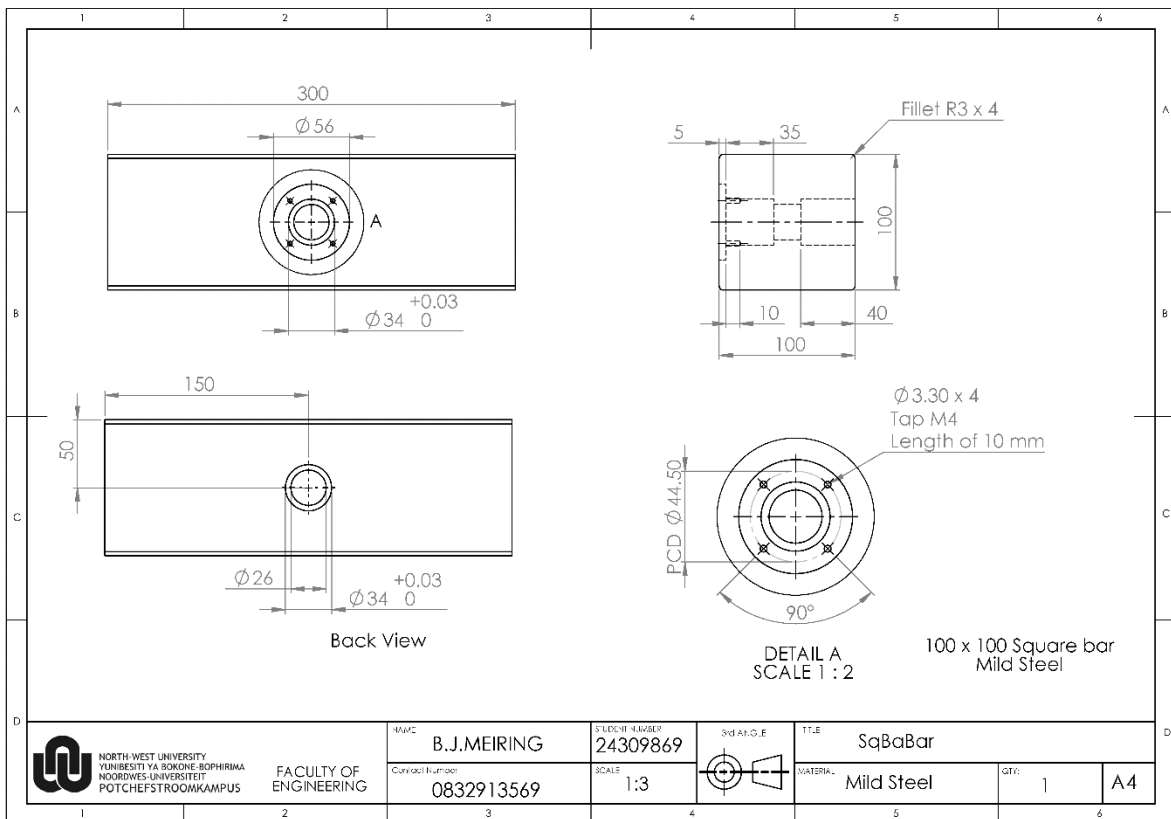
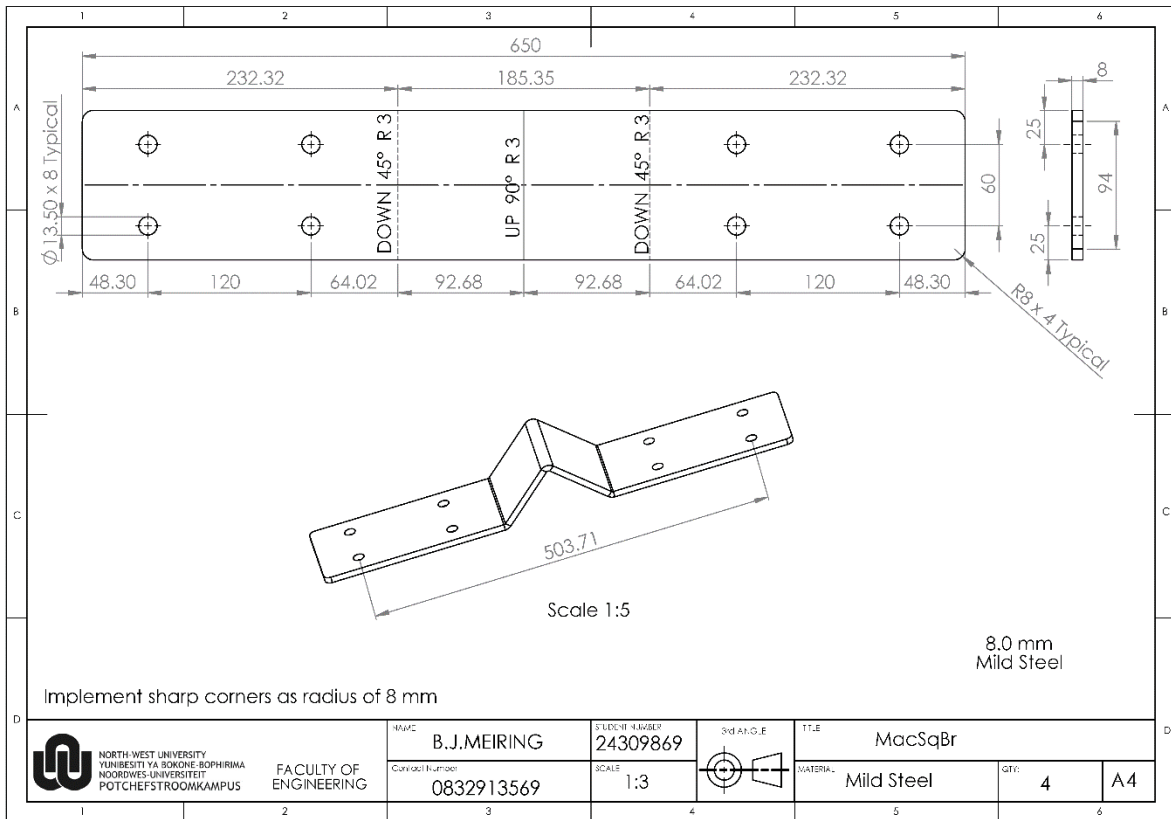
TITLE
MacBAg

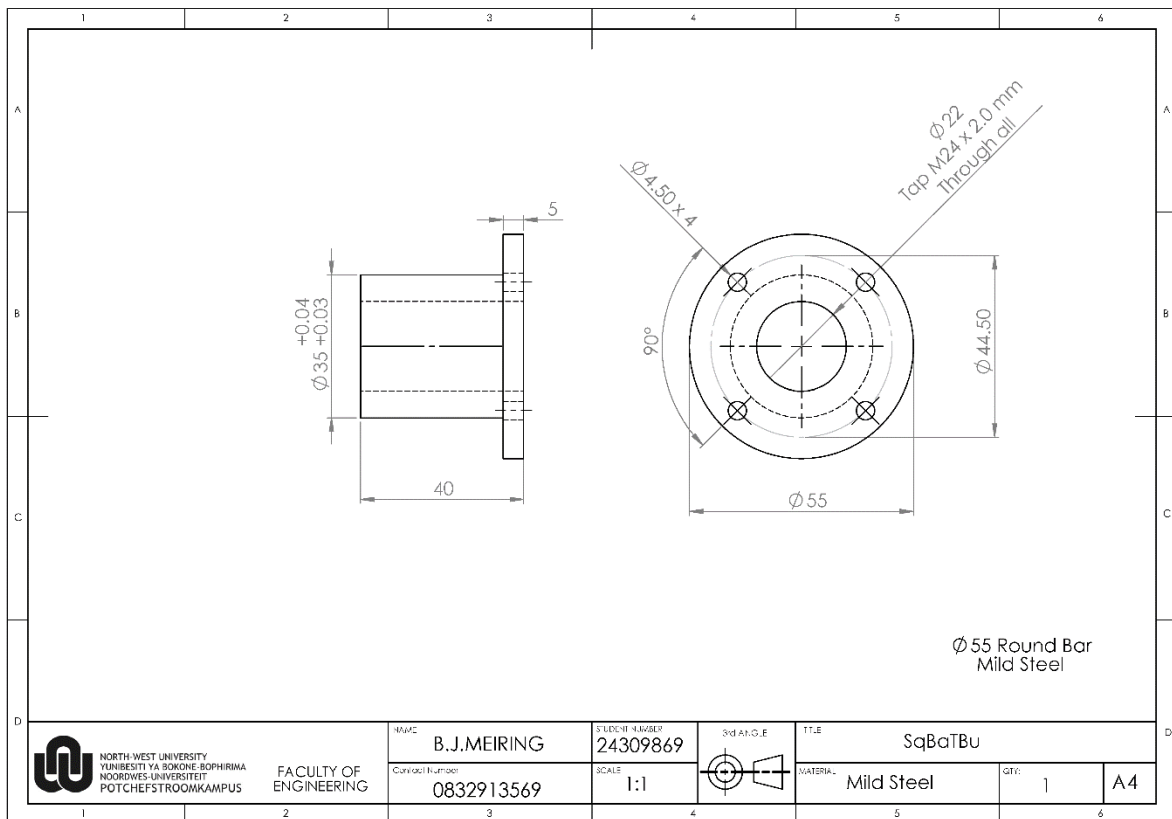
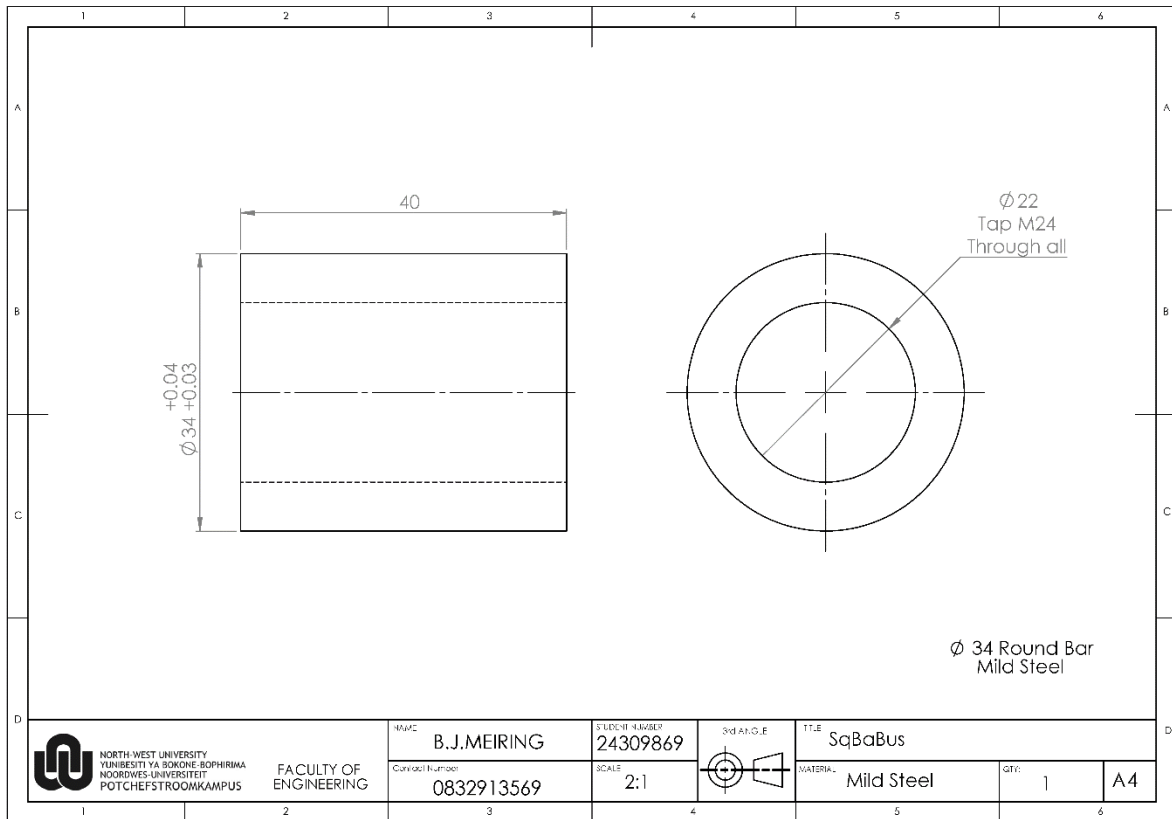
MATERIAL
Mild Steel

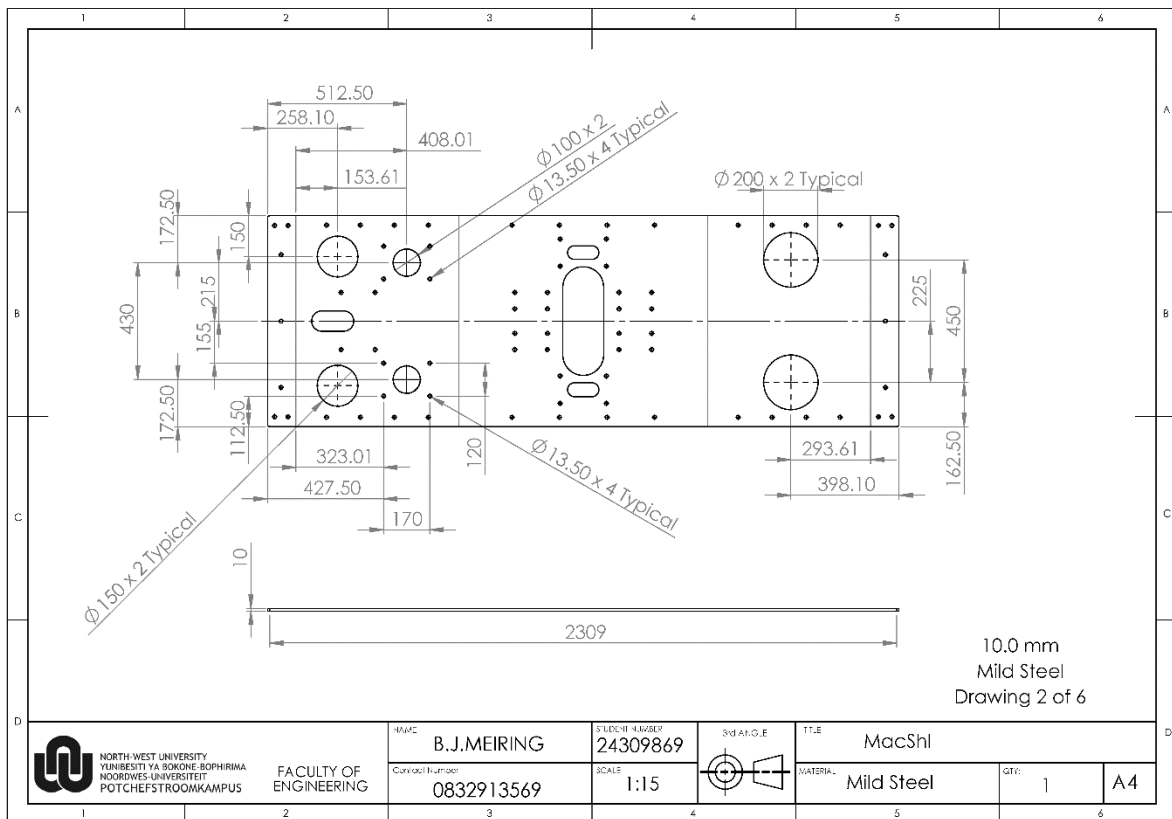
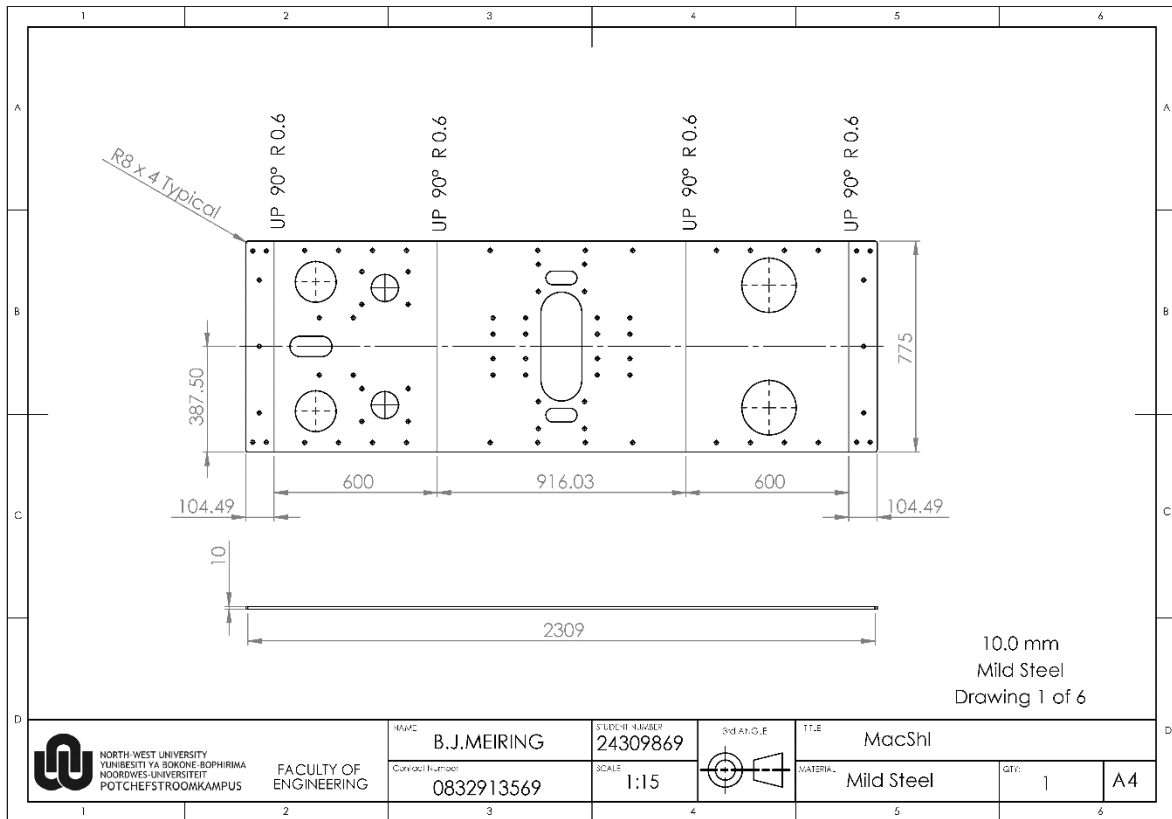
QTY
2

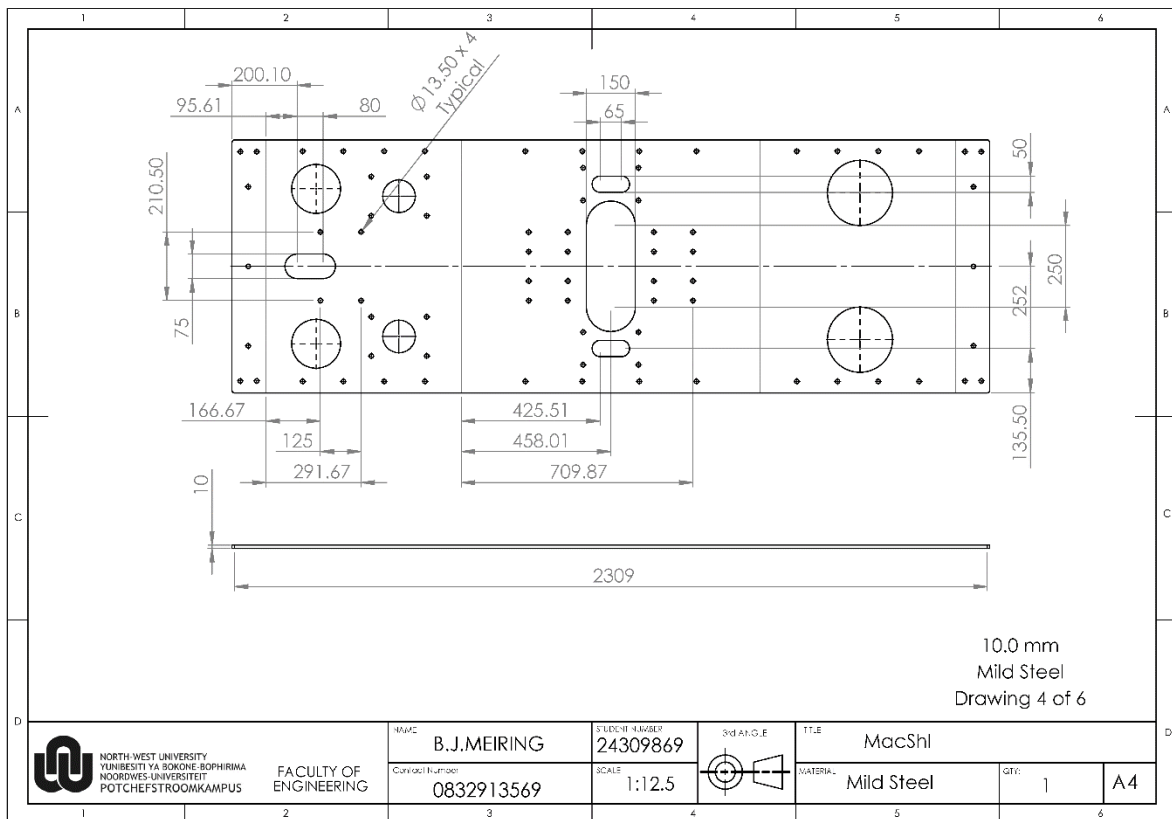
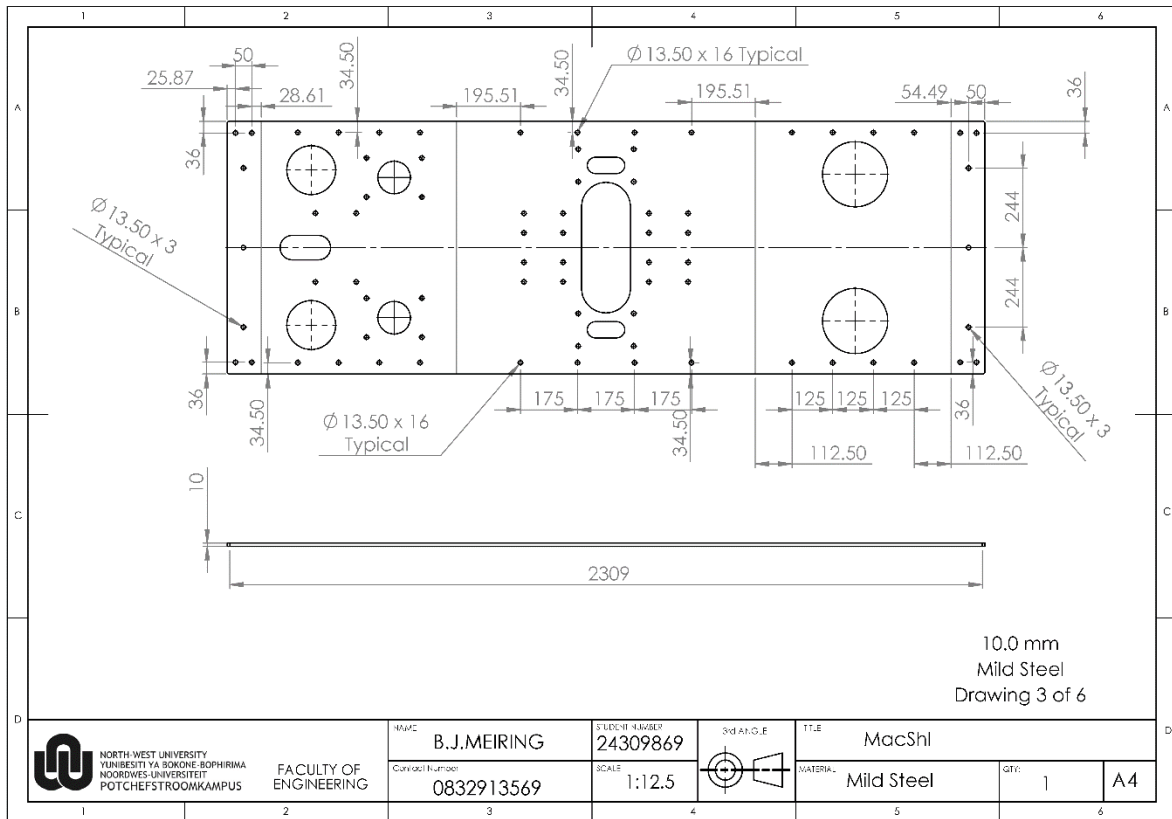
SIZE
A4

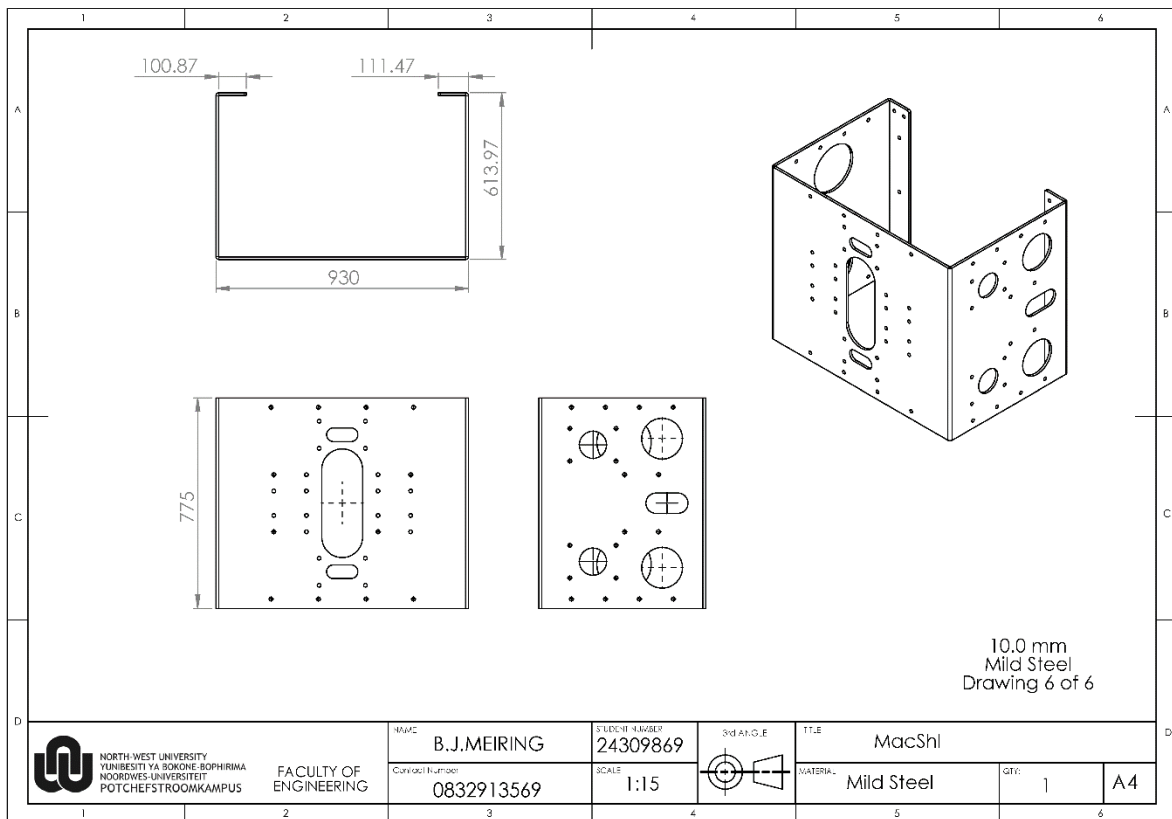
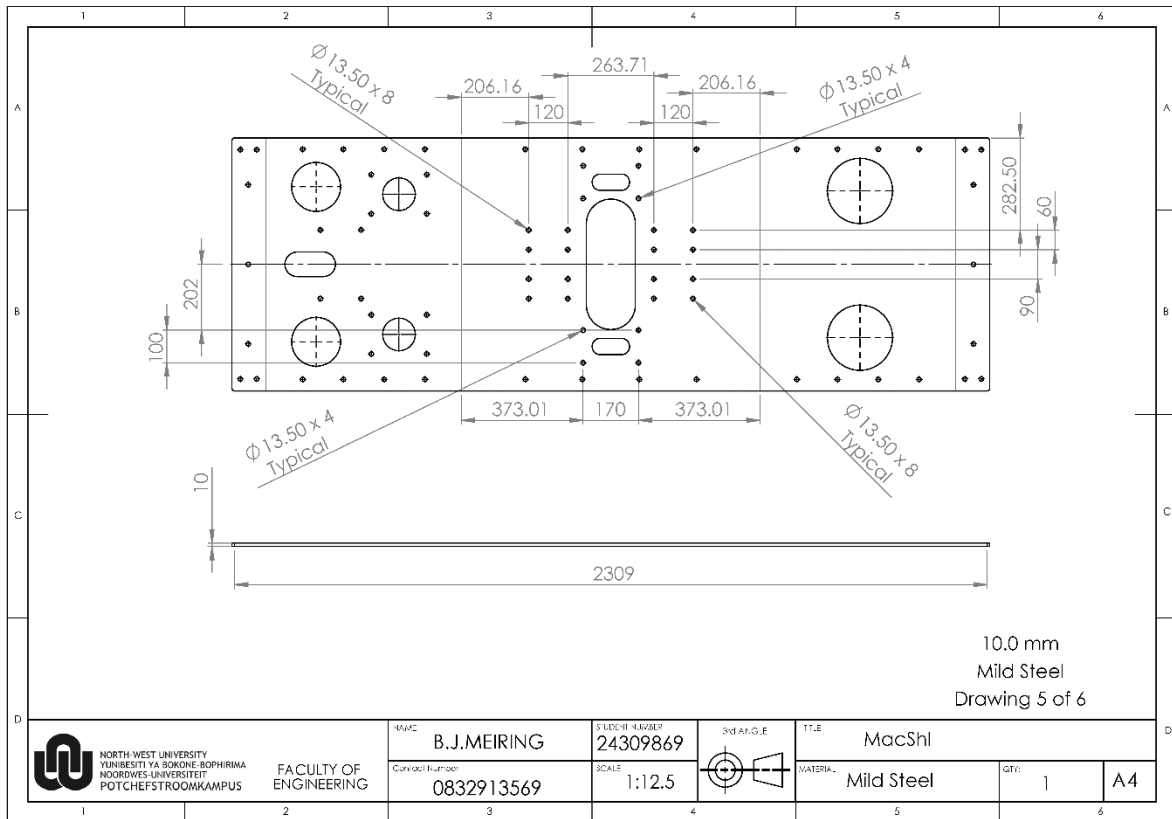


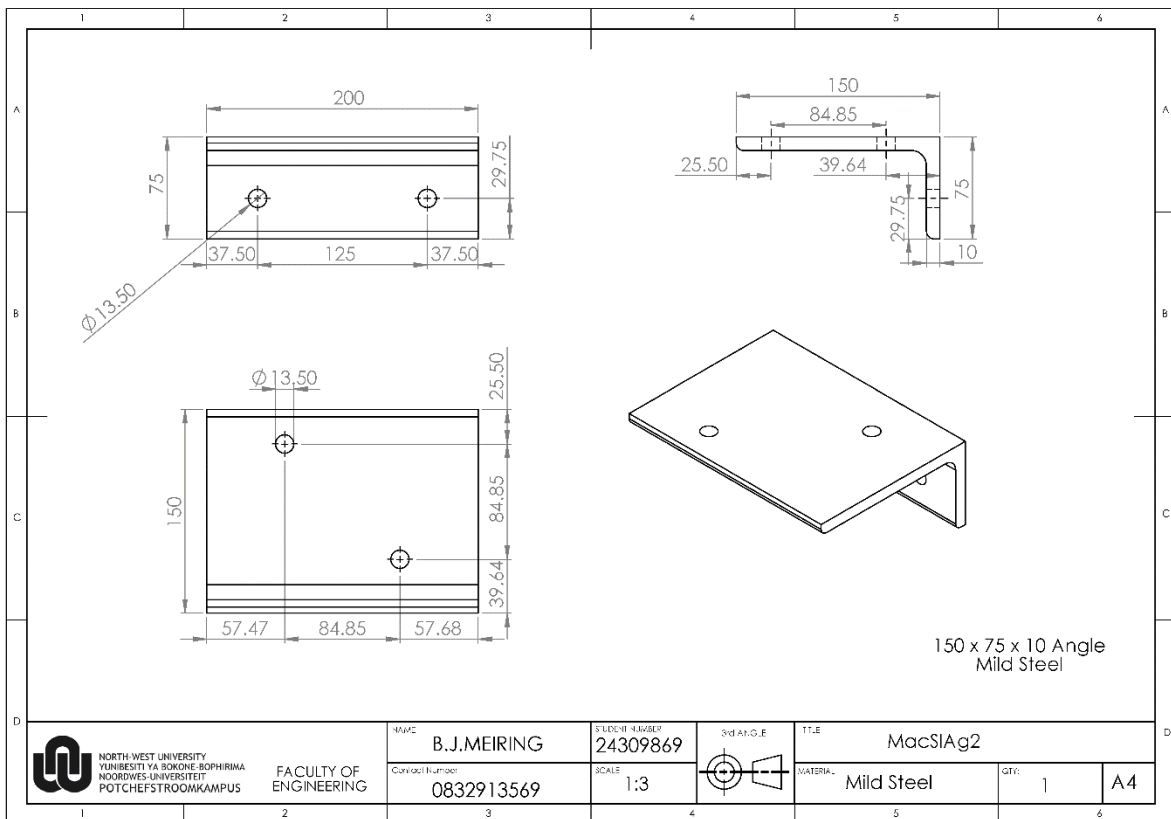
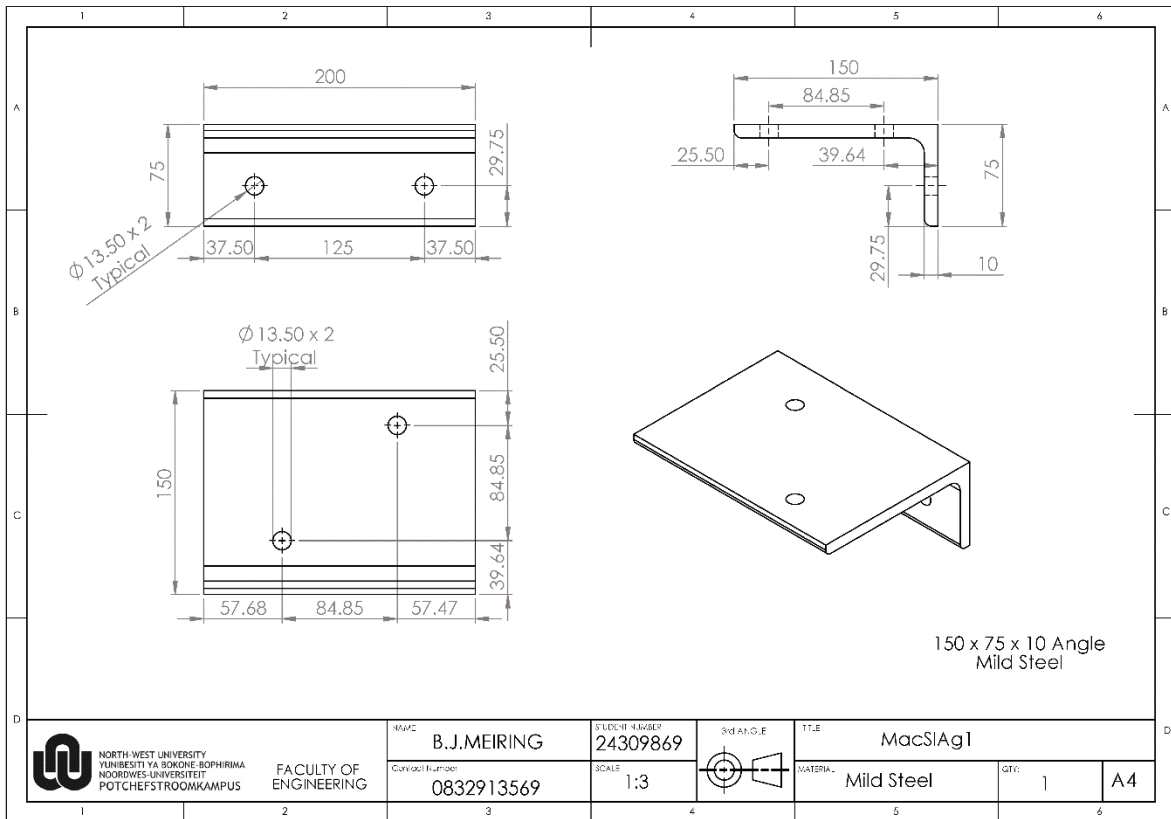


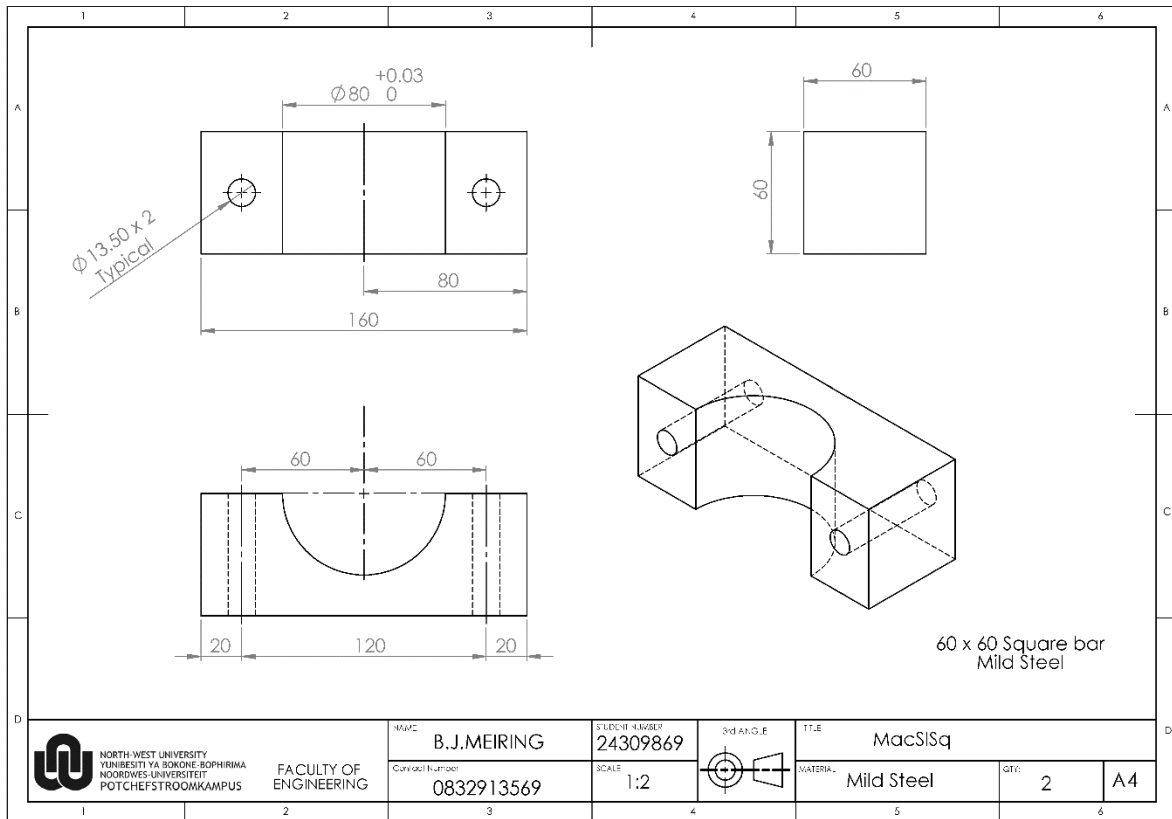












NORTH WEST UNIVERSITY
YUNIBESITHI YA BOKONE-BOPHIRIMA
NOORDWES-UNIVERSITEIT
POTCHEFSTROOMKAMPUS

FACULTY OF
ENGINEERING

NAME: B.J.MEIRING
Course Number: 0832913569

STUDENT NUMBER: 24309869
SCALE: 1:2

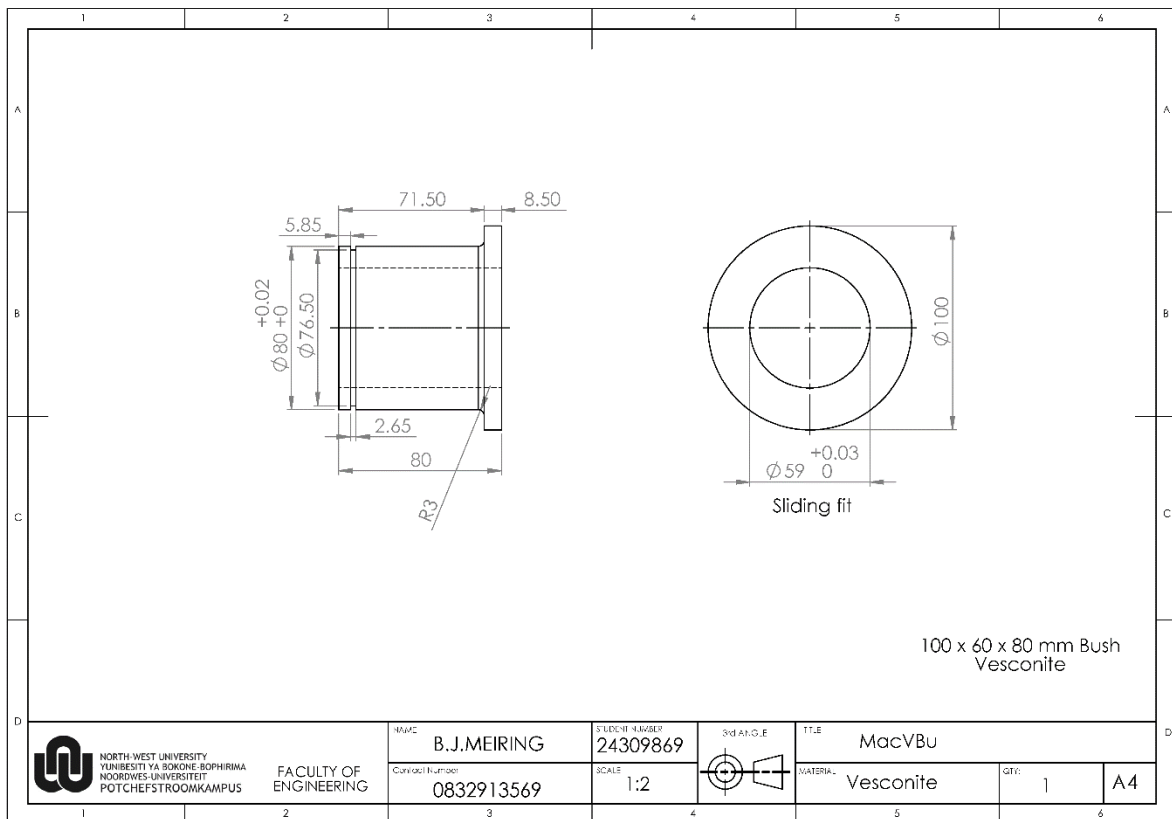


TITLE: MacSISq

MATERIAL: Mild Steel

QTY: 2

A4



NORTH WEST UNIVERSITY
YUNIBESITHI YA BOKONE-BOPHIRIMA
NOORDWES-UNIVERSITEIT
POTCHEFSTROOMKAMPUS

FACULTY OF
ENGINEERING

NAME: B.J.MEIRING
Course Number: 0832913569

STUDENT NUMBER: 24309869
SCALE: 1:2

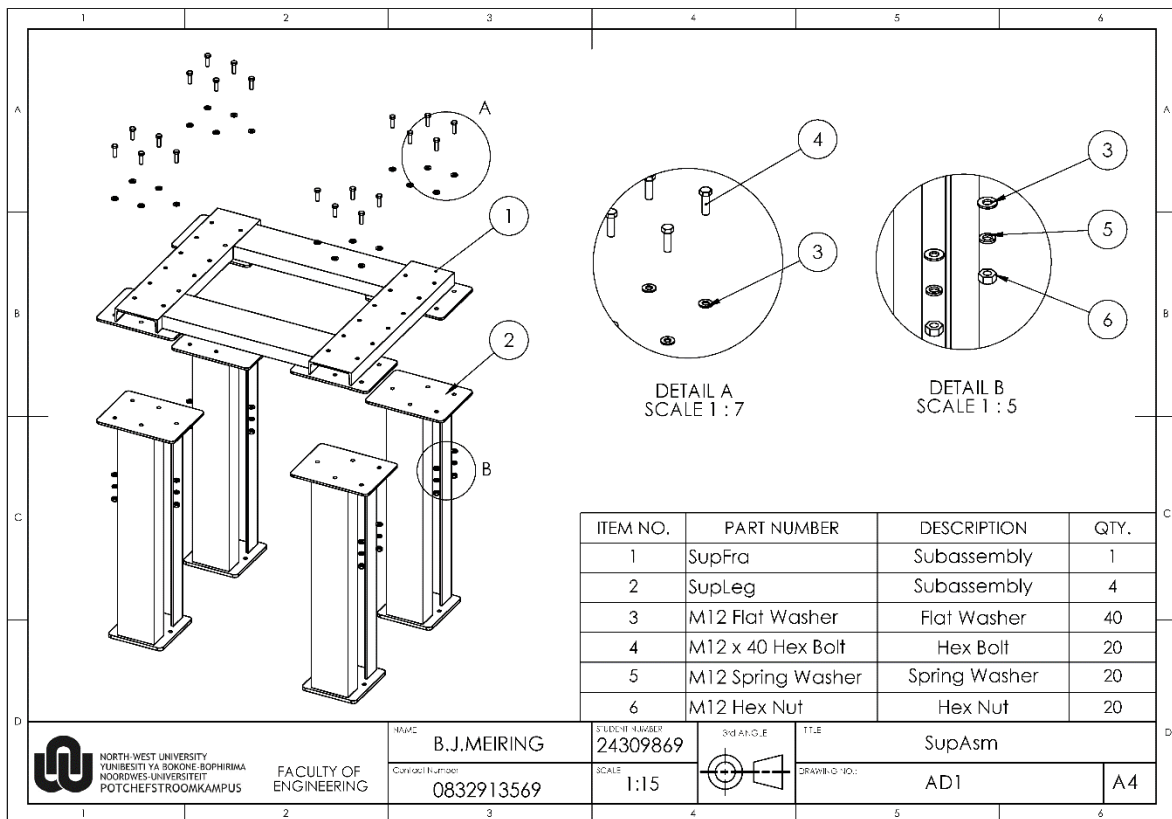
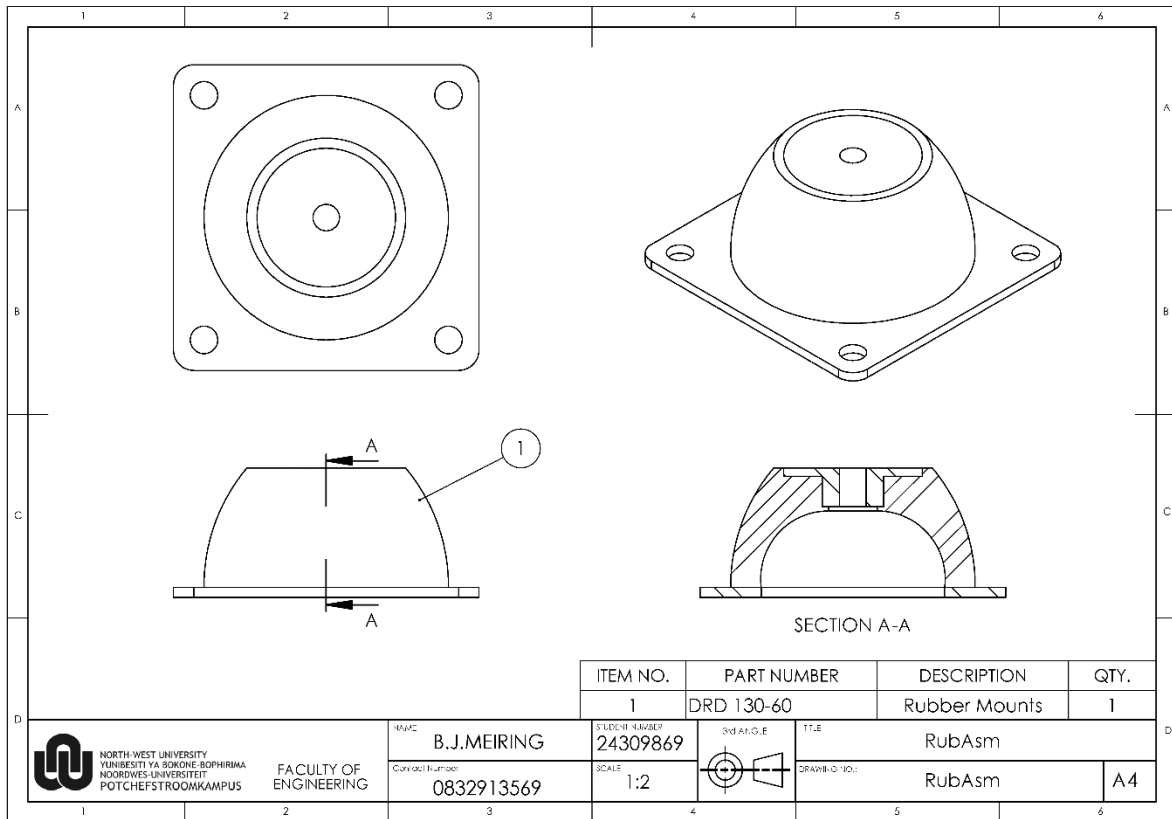


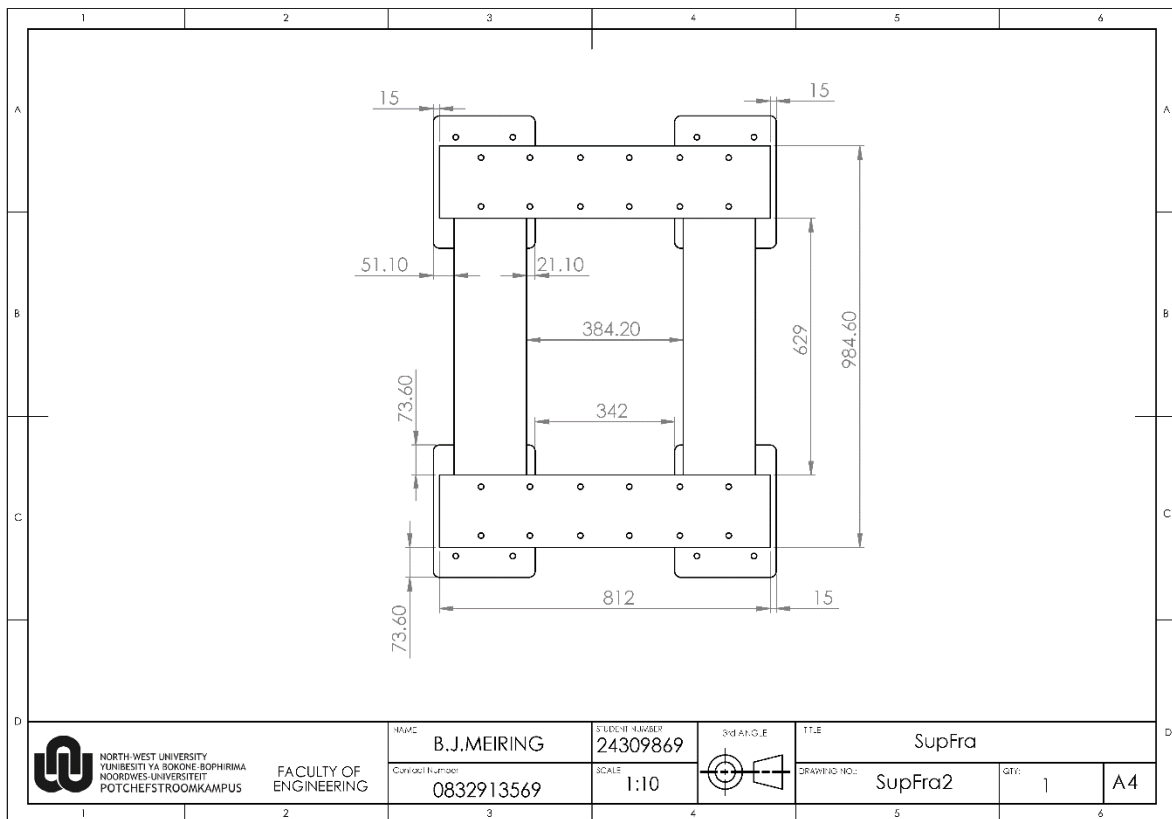
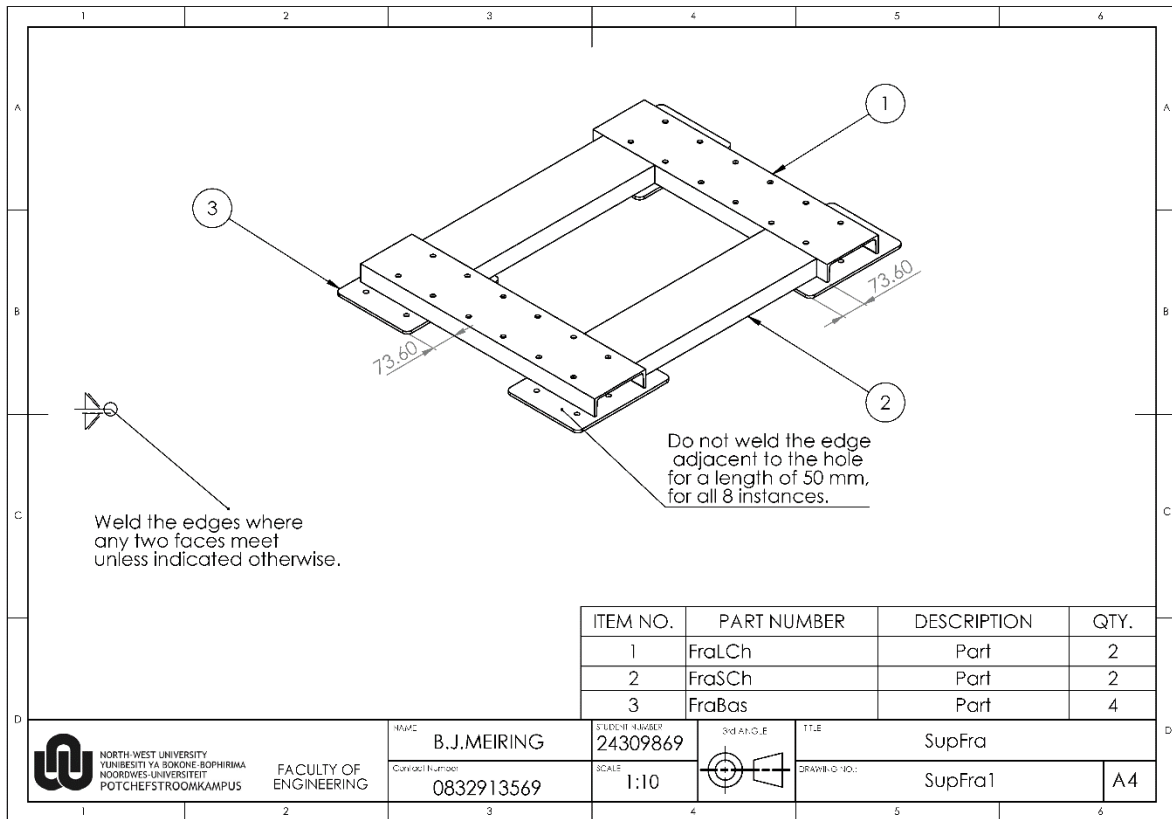
TITLE: MacVBu

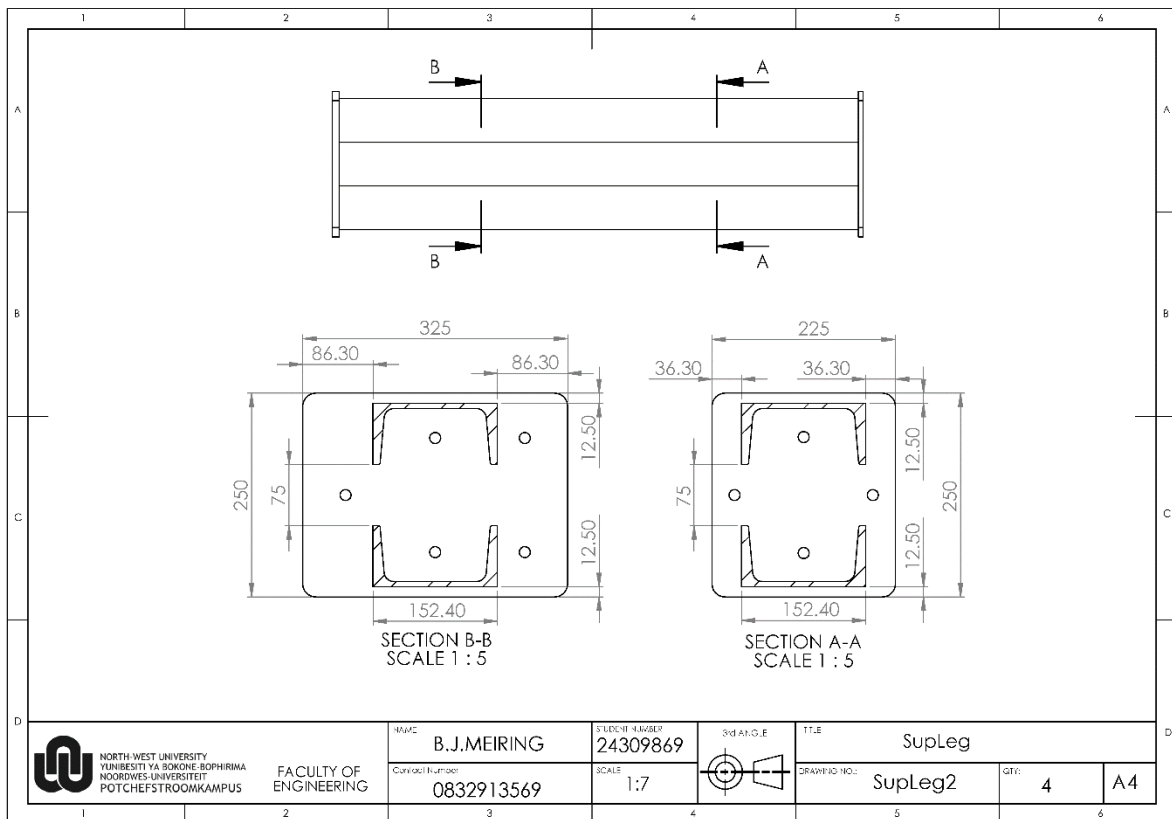
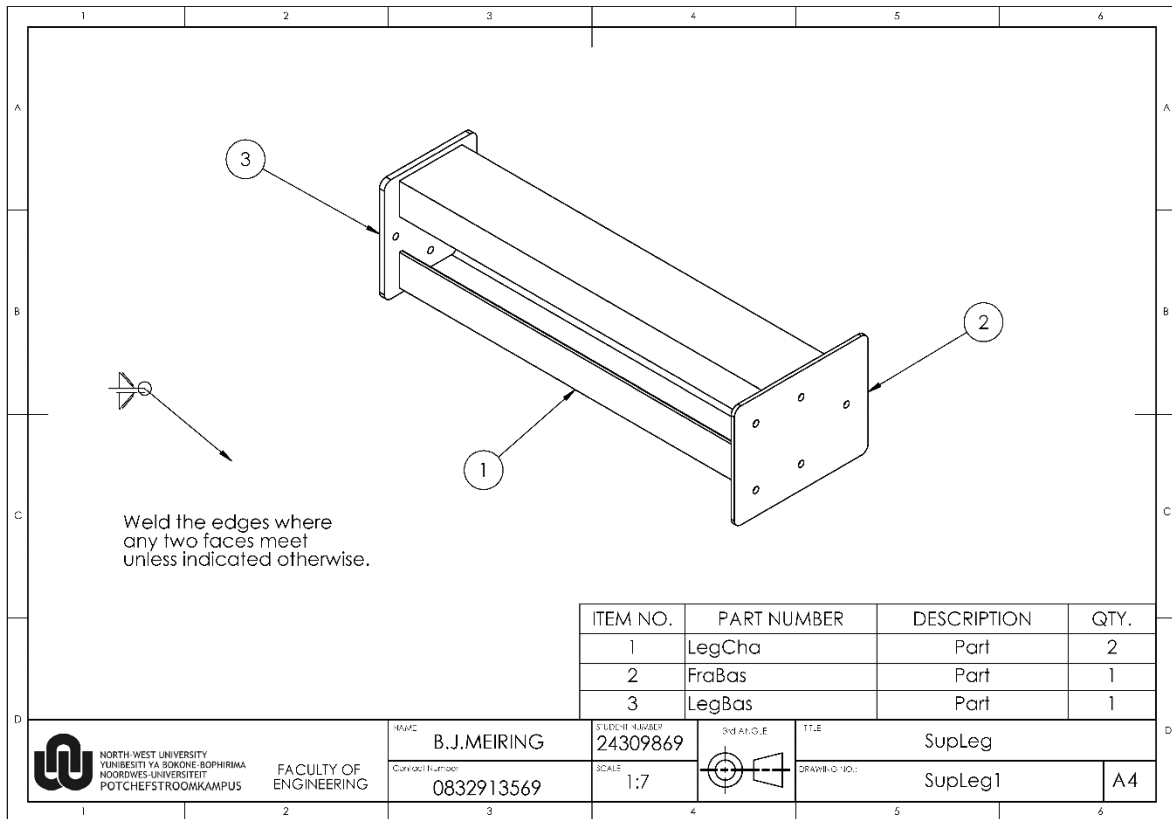
MATERIAL: Vesconite

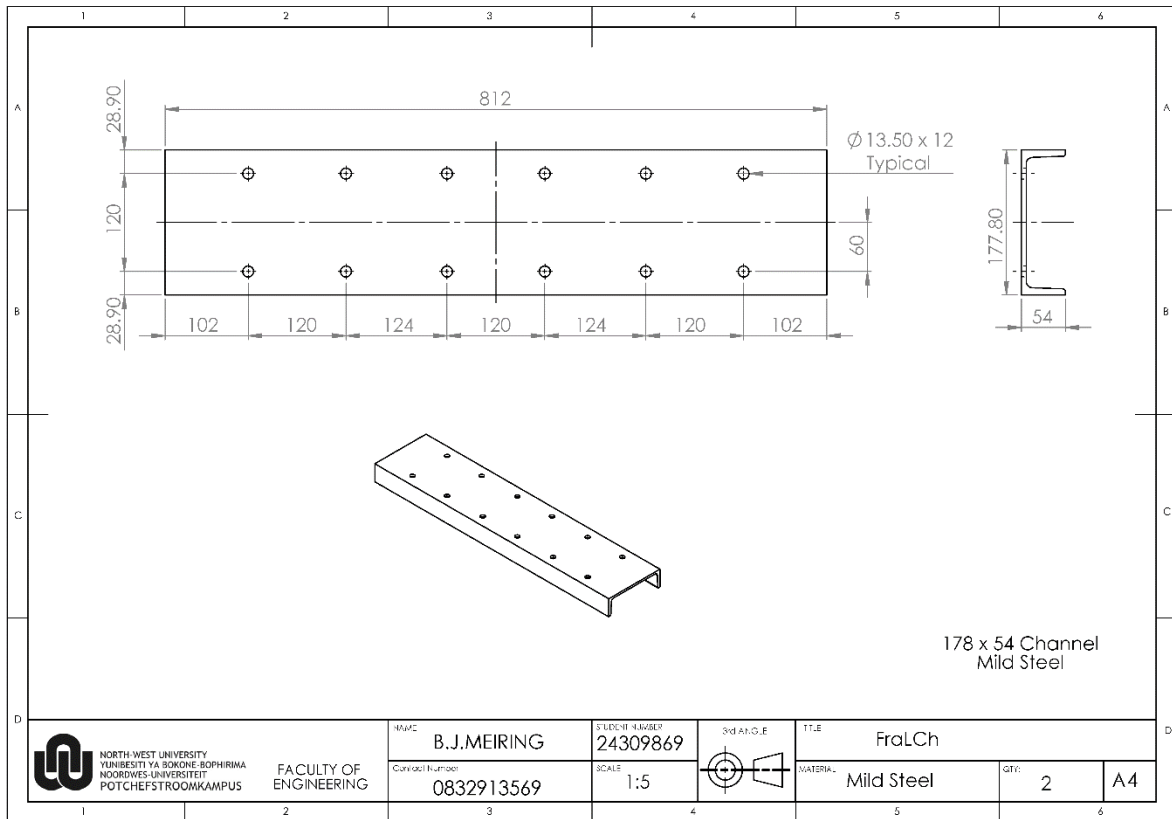
QTY: 1

A4









NORTH WEST UNIVERSITY
YUNIBESITHI YA BOKONE-BOPHIRIMA
NOORDWES-UNIVERSITEIT
POTCHEFSTROOMKAMPUS

FACULTY OF
ENGINEERING

NAME: **B.J.MEIRING**
Contact Number: **0832913569**

STUDENT NUMBER: **24309869**
SCALE: **1:5**

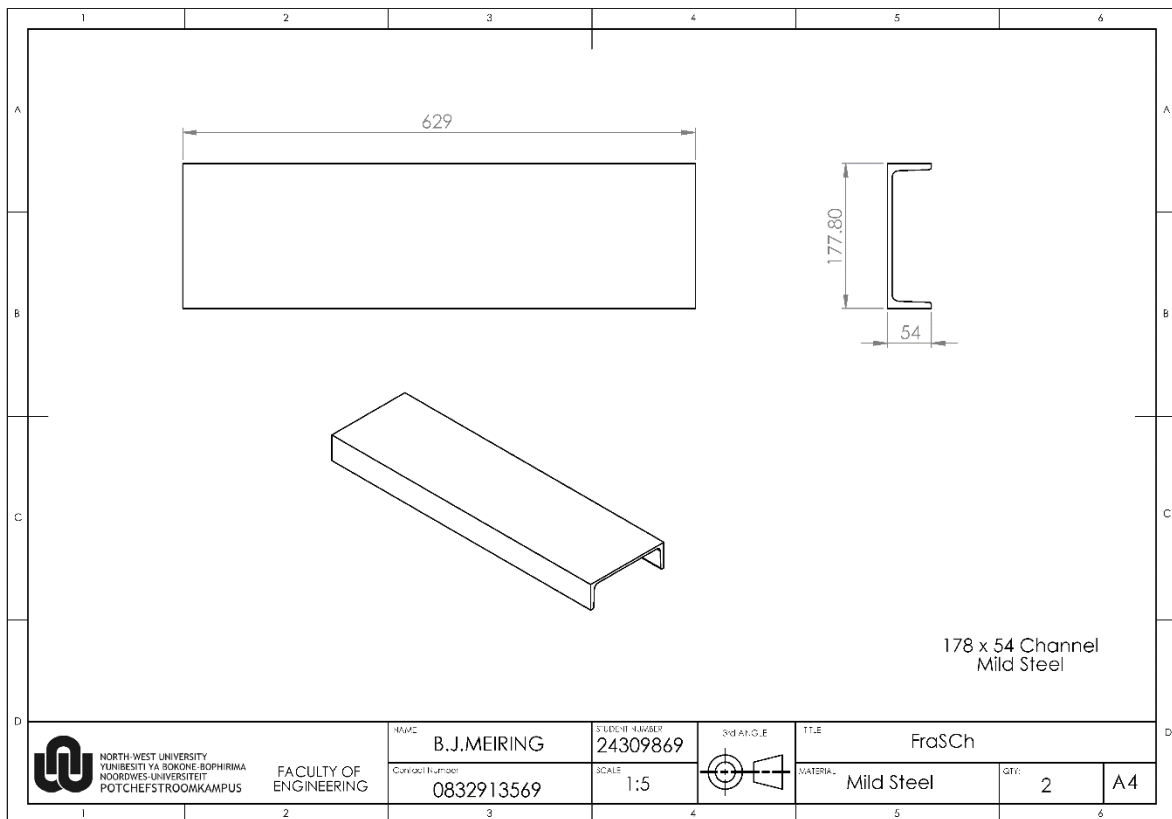


TITLE: **FraLCh**

MATERIAL: **Mild Steel**

QTY: **2**

A4



NORTH WEST UNIVERSITY
YUNIBESITHI YA BOKONE-BOPHIRIMA
NOORDWES-UNIVERSITEIT
POTCHEFSTROOMKAMPUS

FACULTY OF
ENGINEERING

NAME: **B.J.MEIRING**
Contact Number: **0832913569**

STUDENT NUMBER: **24309869**
SCALE: **1:5**

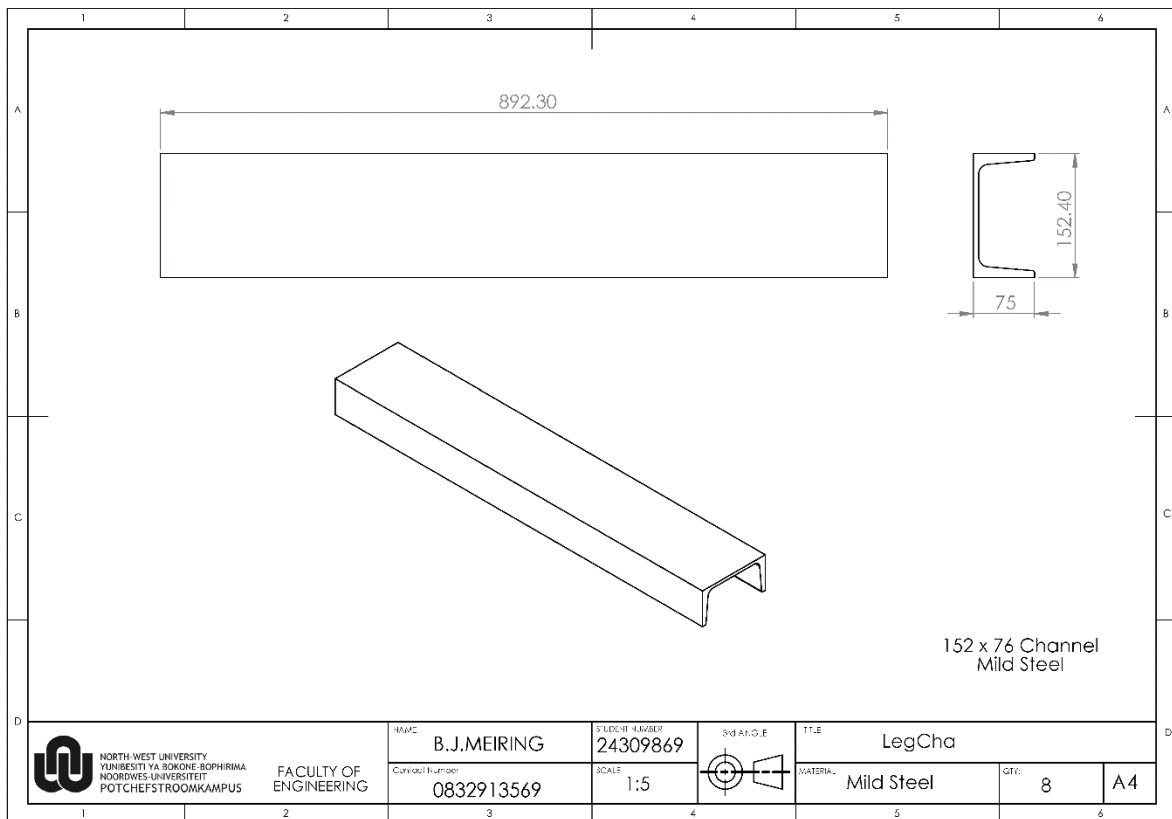
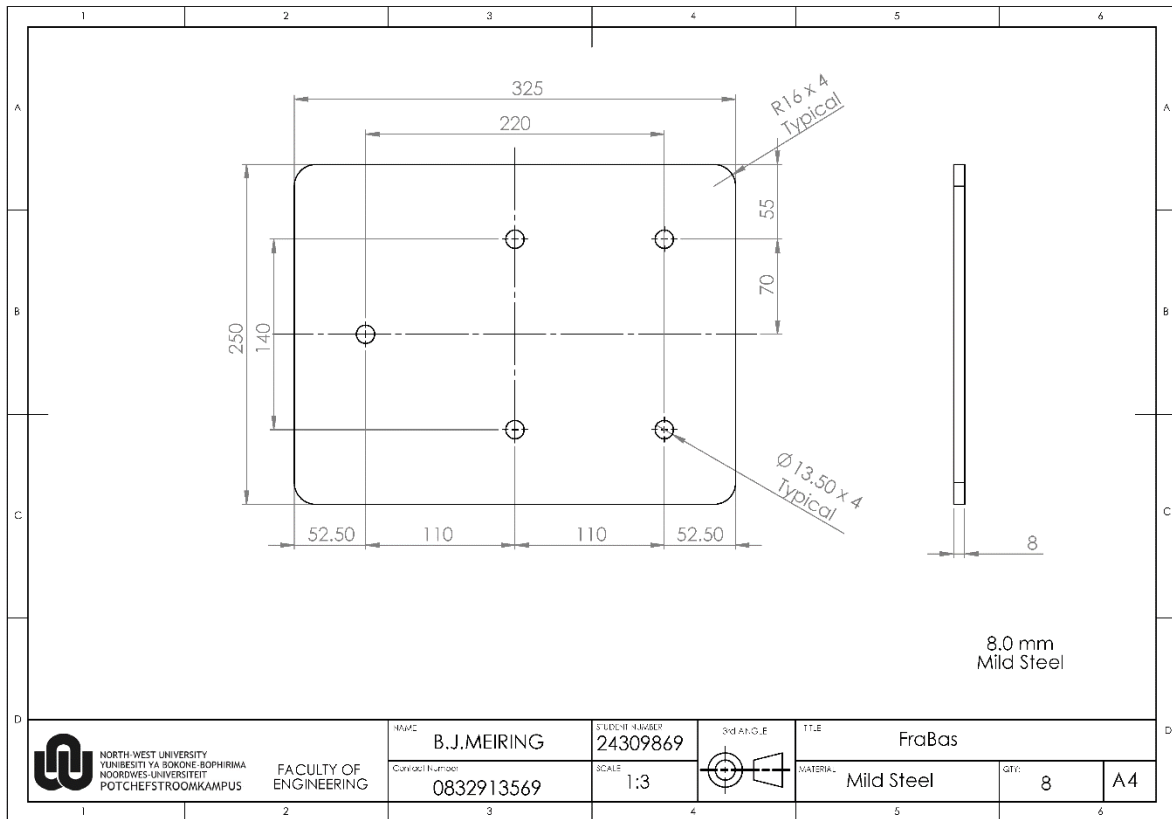


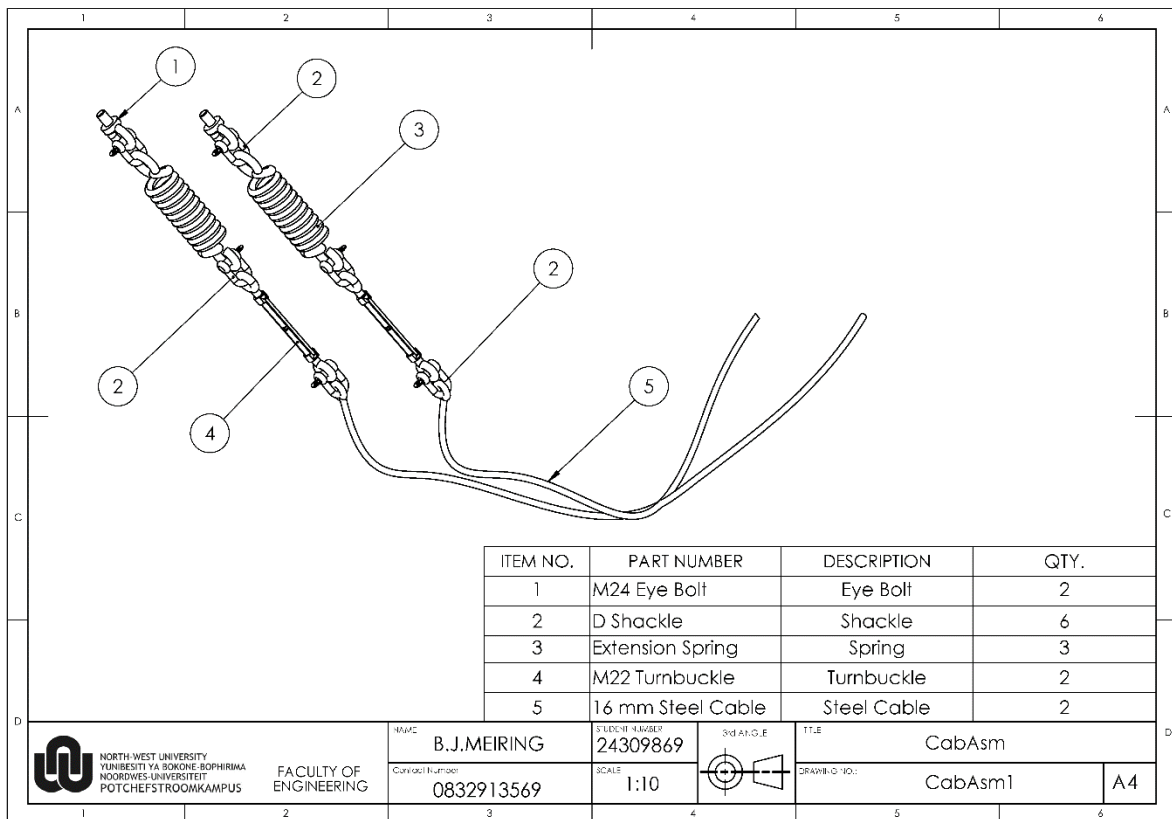
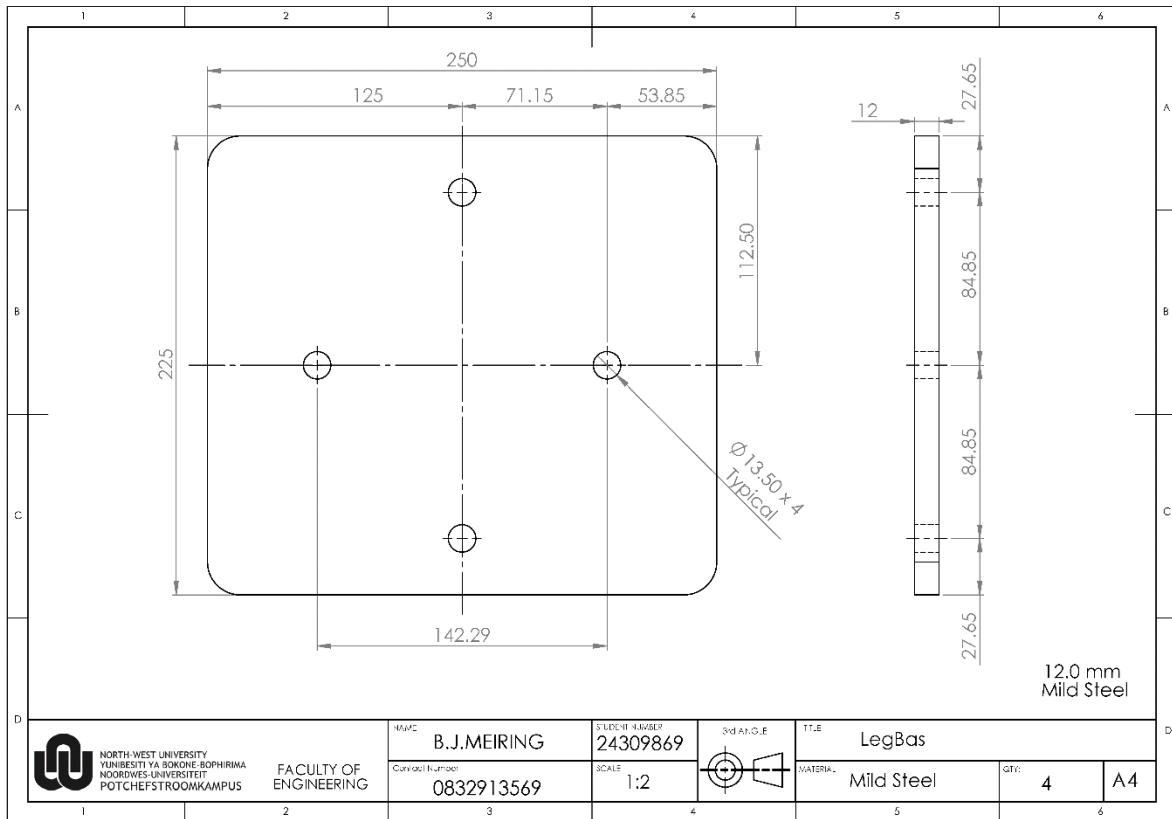
TITLE: **FraSCh**

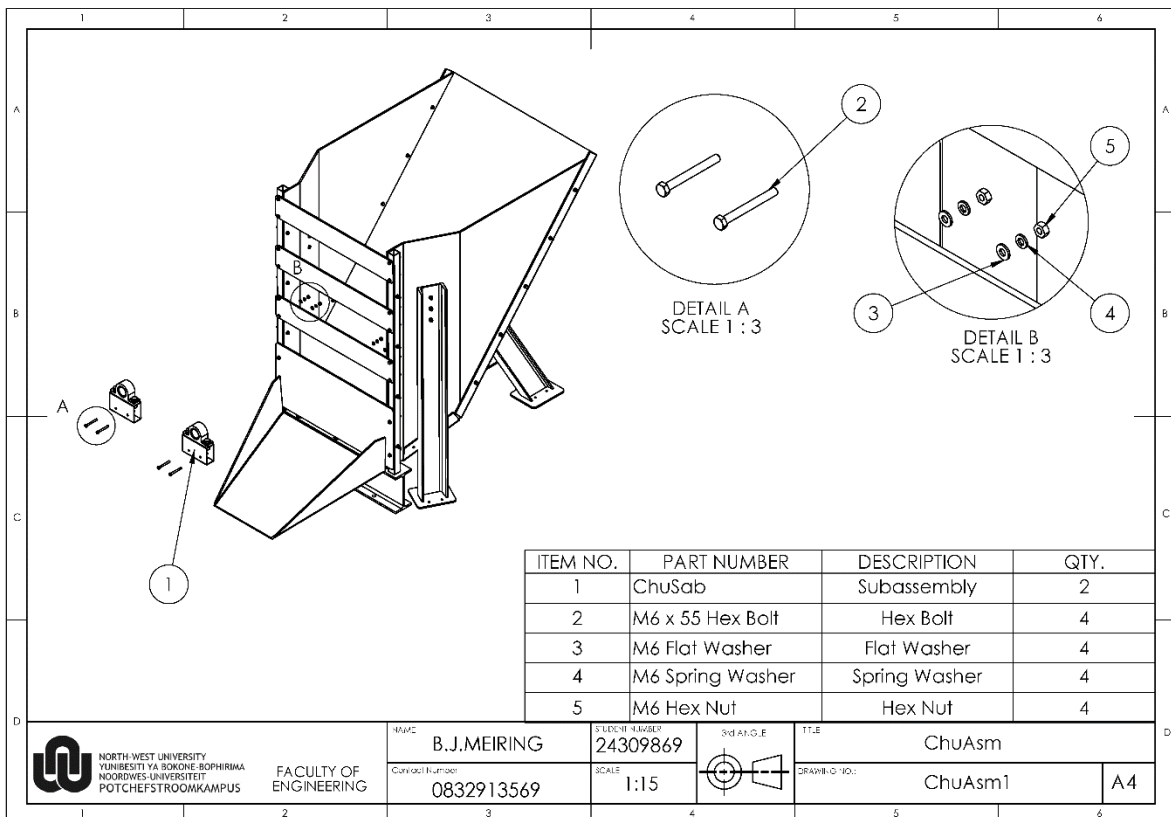
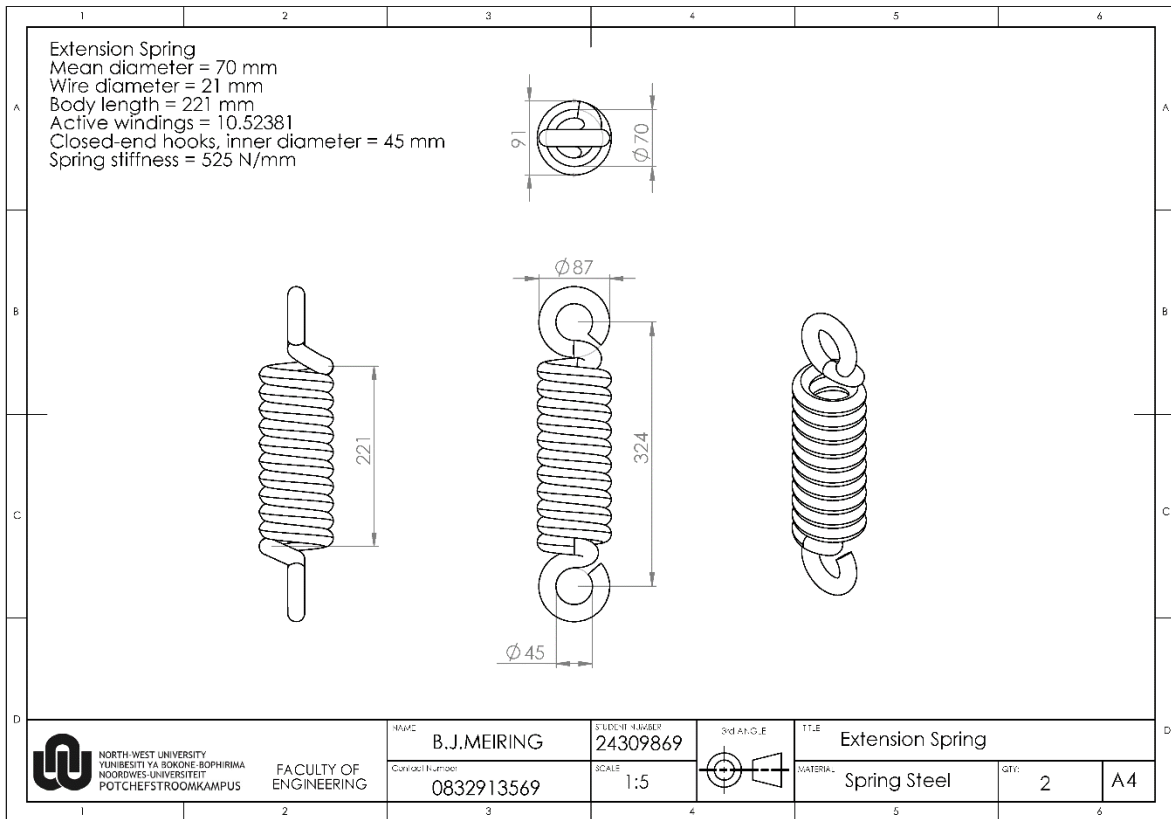
MATERIAL: **Mild Steel**

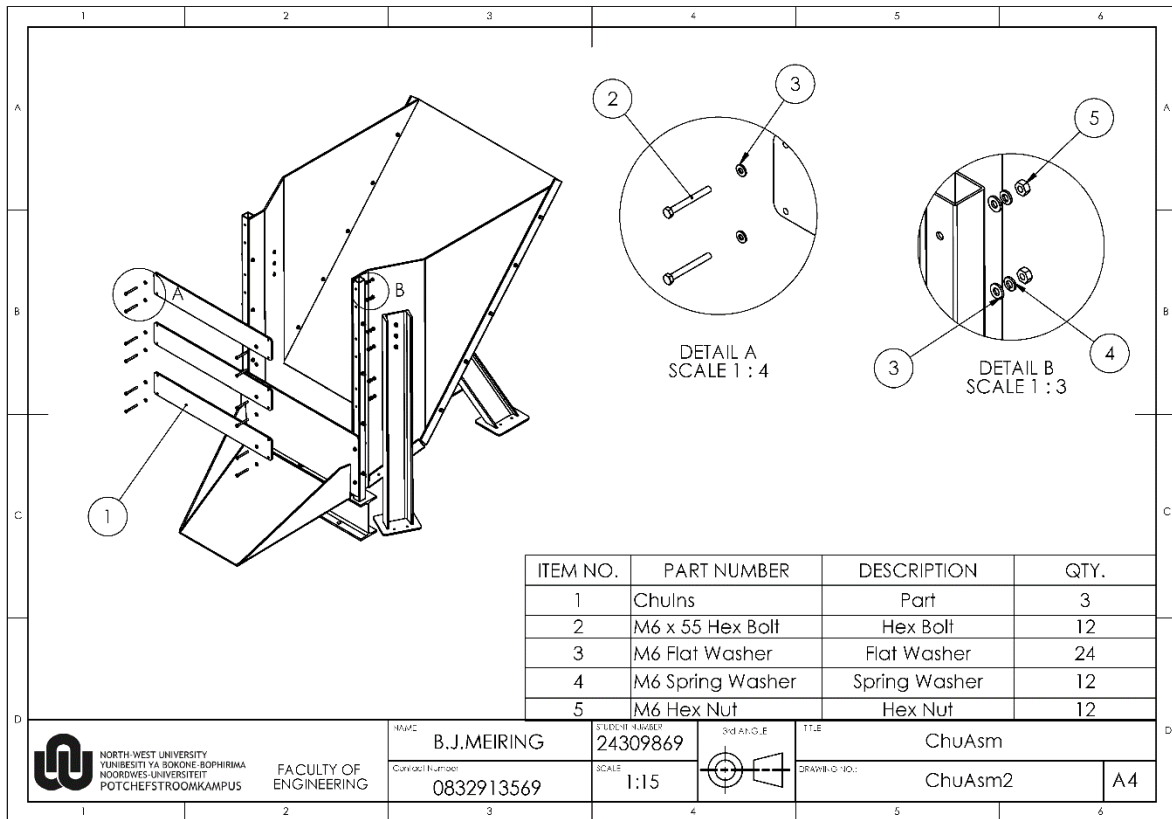
QTY: **2**

A4









NORTH WEST UNIVERSITY
YUNIBESITHI YA BOKONE-BOPHIRAMA
NOORDWES-UNIVERSITEIT
POTCHEFSTROOMKAMPUS

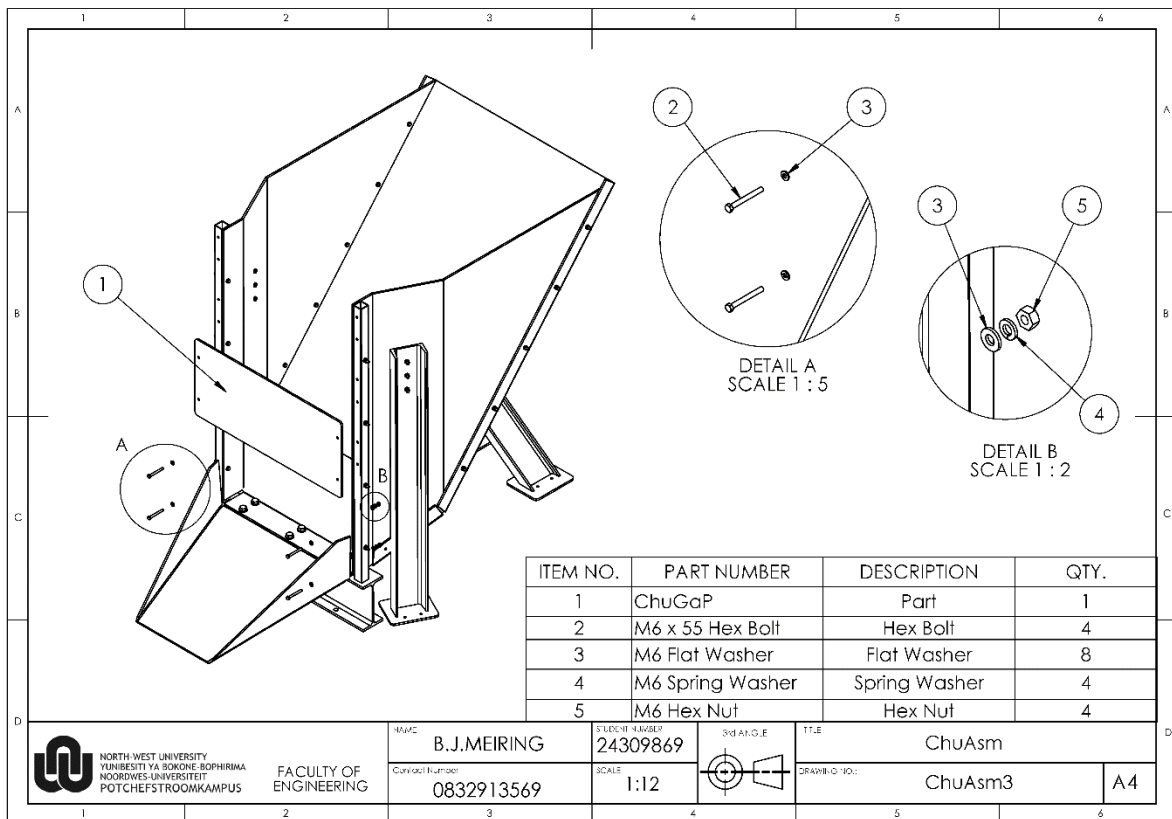
FACULTY OF
ENGINEERING

NAME: B.J.MEIRING
Course Number: 0832913569

STUDENT NUMBER: 24309869
SCALE: 1:15



TITLE: ChuAsm
DRAWING NO.: ChuAsm2 A4



NORTH WEST UNIVERSITY
YUNIBESITHI YA BOKONE-BOPHIRAMA
NOORDWES-UNIVERSITEIT
POTCHEFSTROOMKAMPUS

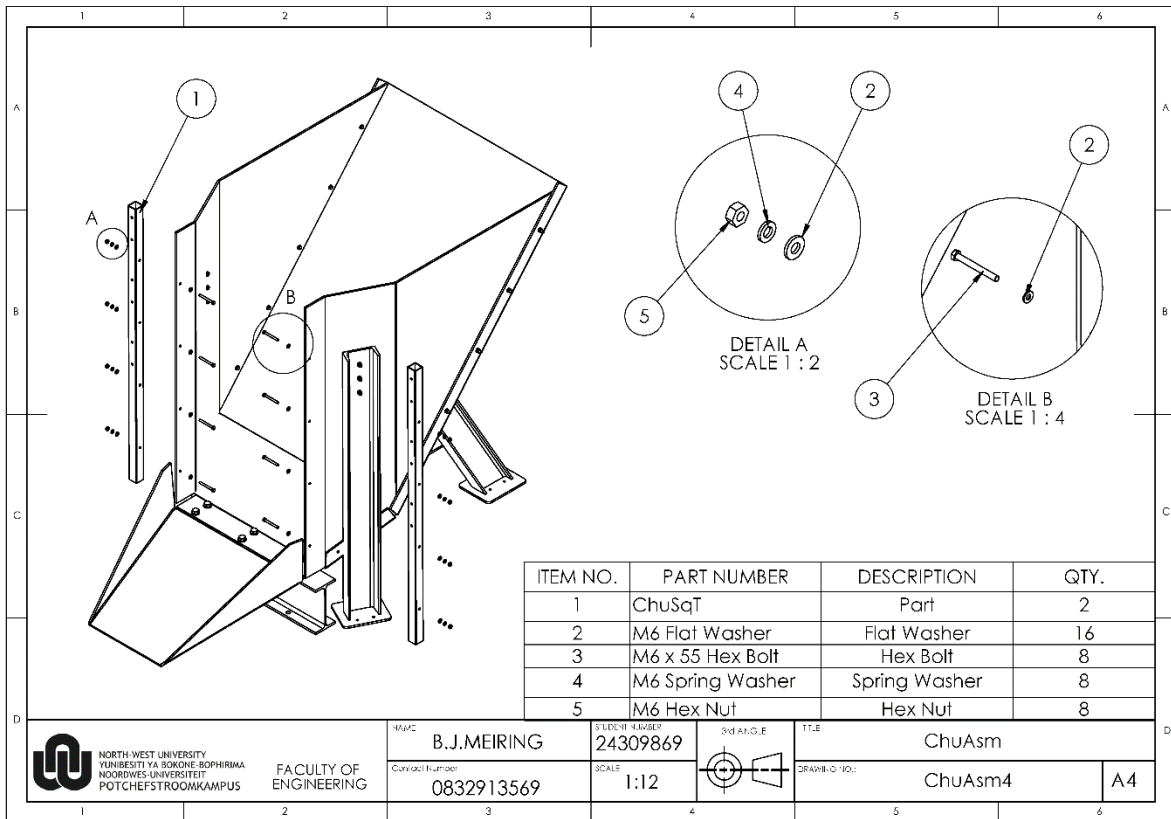
FACULTY OF
ENGINEERING

NAME: B.J.MEIRING
Course Number: 0832913569

STUDENT NUMBER: 24309869
SCALE: 1:12



TITLE: ChuAsm
DRAWING NO.: ChuAsm3 A4



NORTH WEST UNIVERSITY
YUNIBESITHI YA BOKONE-BOPHIRIMA
NOORDWES-UNIVERSITEIT
POTCHEFSTROOMKAMPUS

FACULTY OF
ENGINEERING

NAME

B.J.MEIRING

STUDENT NUMBER
24309869

3rd ANGLE

TITLE

ChuAsm

Contact Number

0832913569

SCALE

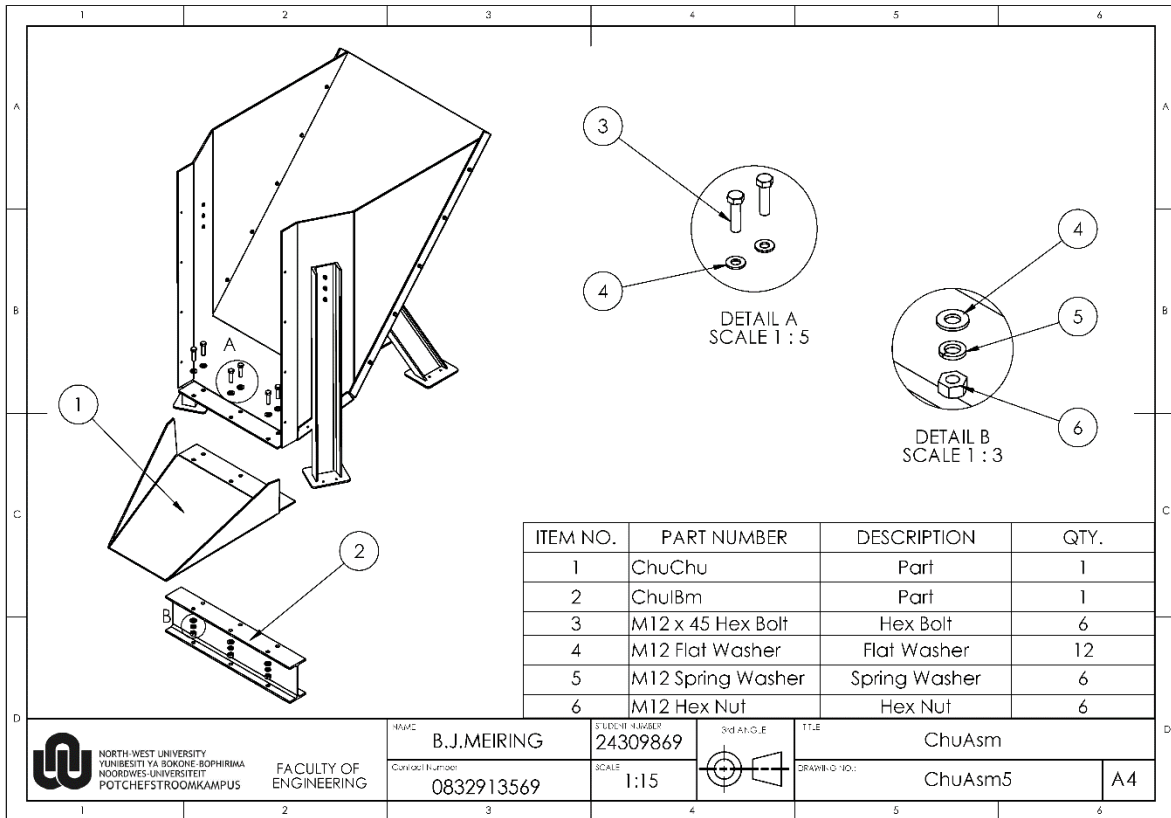
1:12

3rd ANGLE

DRAWING NO.

ChuAsm4

A4



NORTH WEST UNIVERSITY
YUNIBESITHI YA BOKONE-BOPHIRIMA
NOORDWES-UNIVERSITEIT
POTCHEFSTROOMKAMPUS

FACULTY OF
ENGINEERING

NAME

B.J.MEIRING

STUDENT NUMBER
24309869

3rd ANGLE

TITLE

ChuAsm

Contact Number

0832913569

SCALE

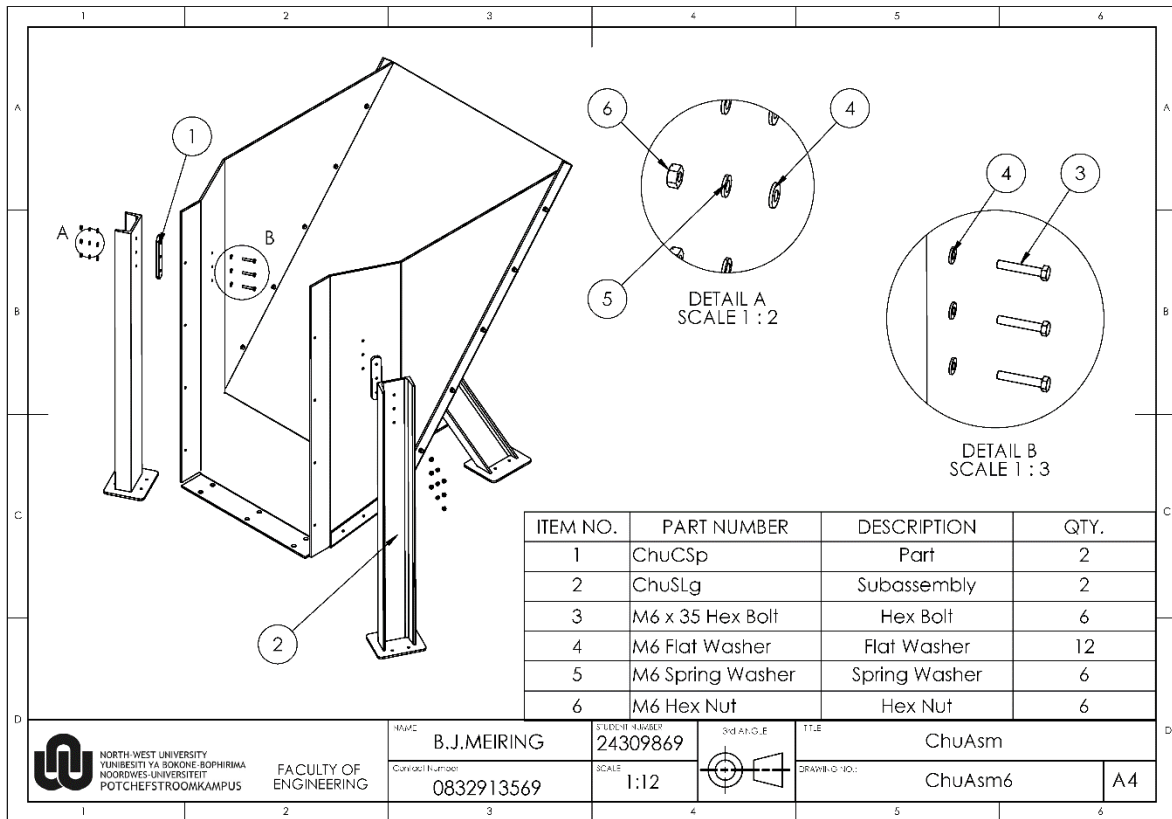
1:15

3rd ANGLE

DRAWING NO.

ChuAsm5

A4



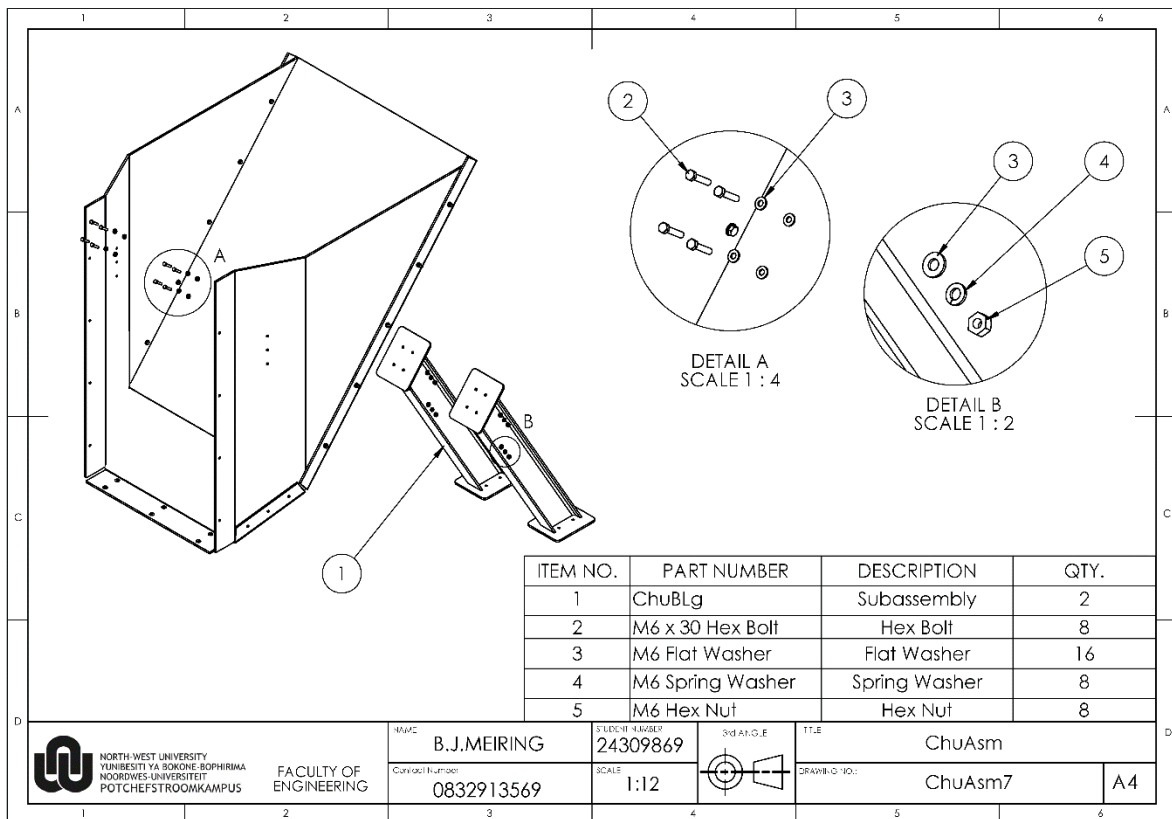
FACULTY OF ENGINEERING

NAME: B.J.MEIRING
Contact Number: 0832913569

STUDENT NUMBER: 24309869
SCALE: 1:12



TITLE: ChuAsm
DRAWING NO.: ChuAsm6 | A4



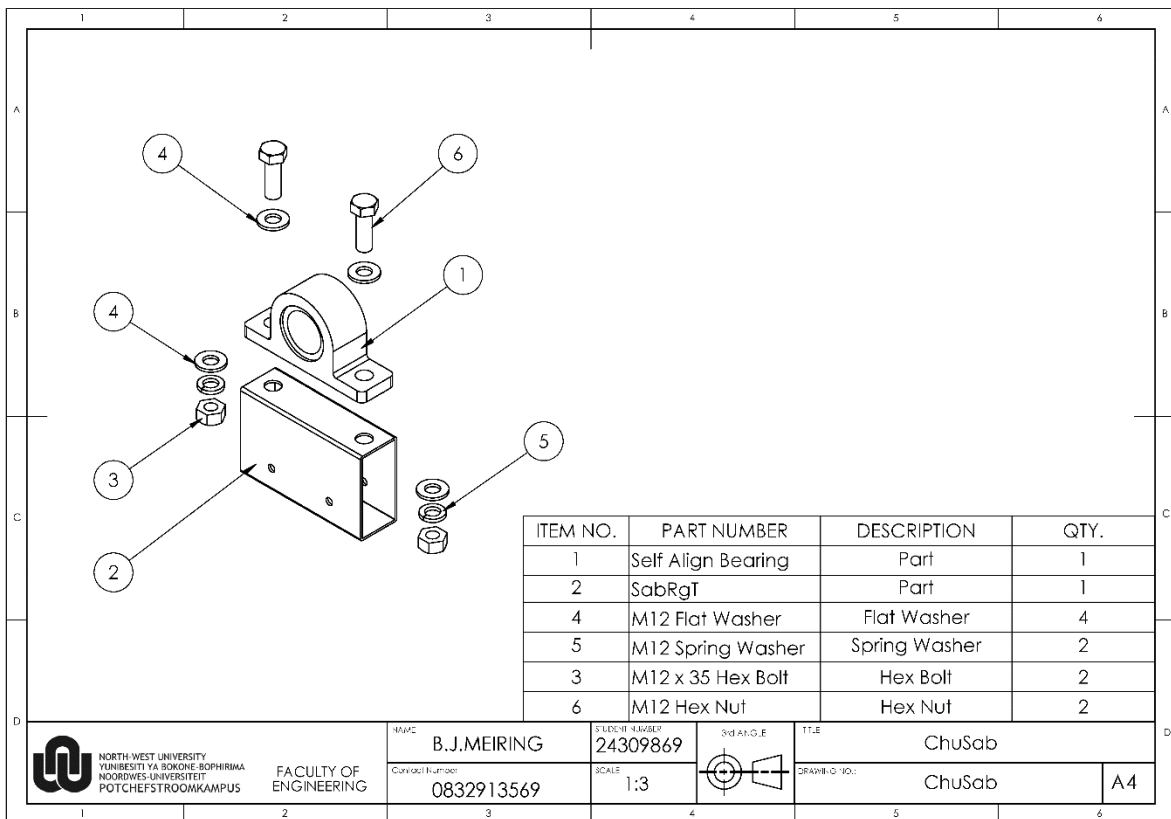
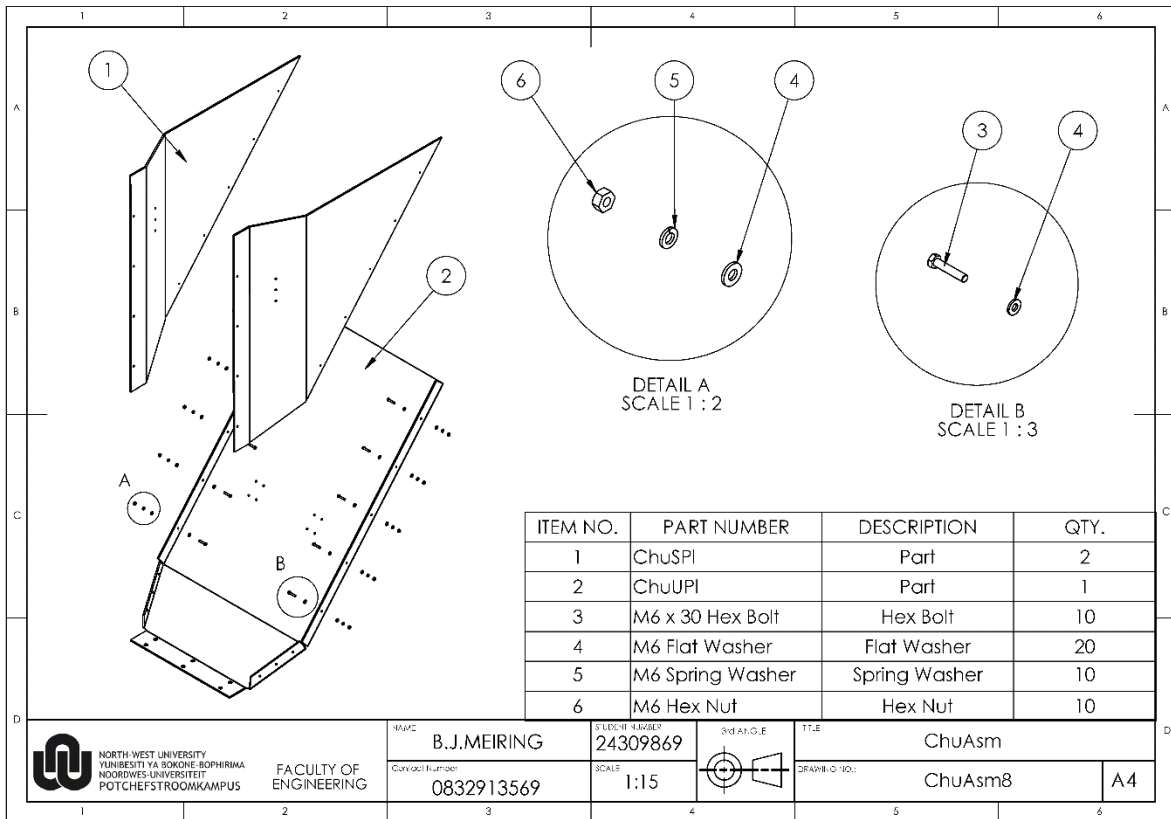
FACULTY OF ENGINEERING

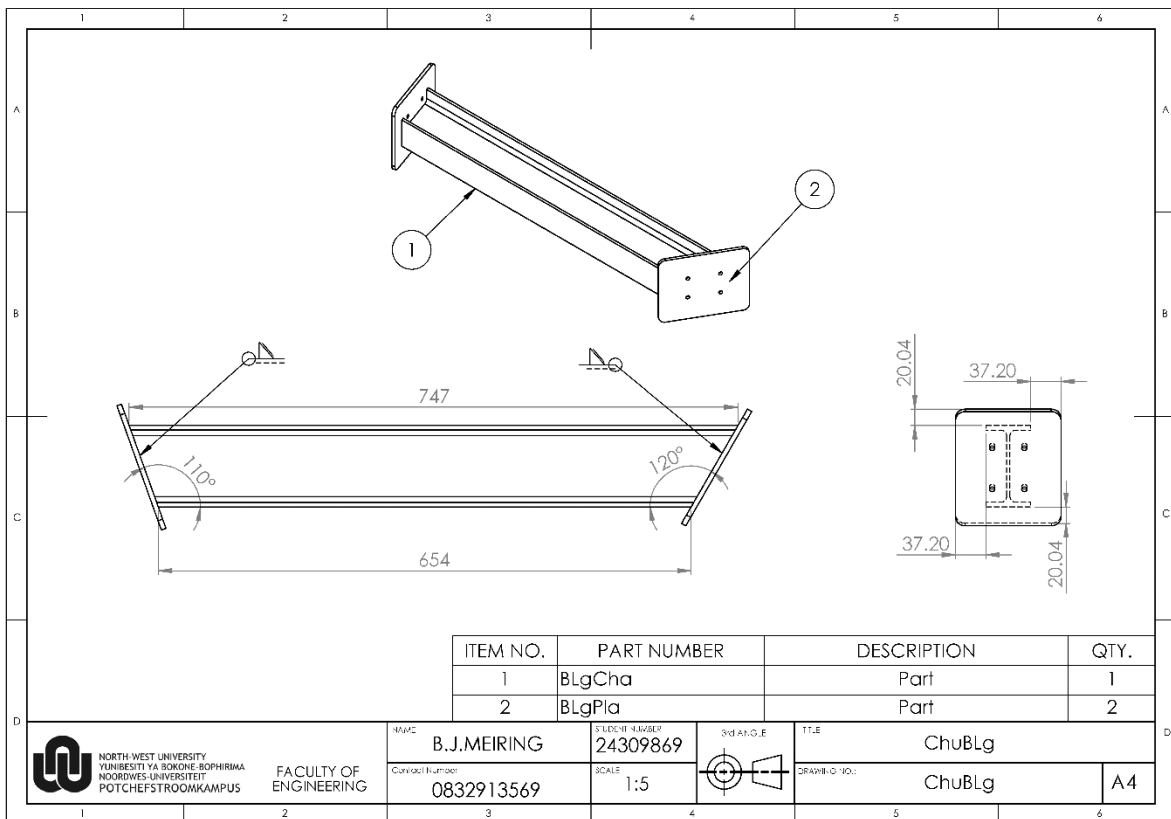
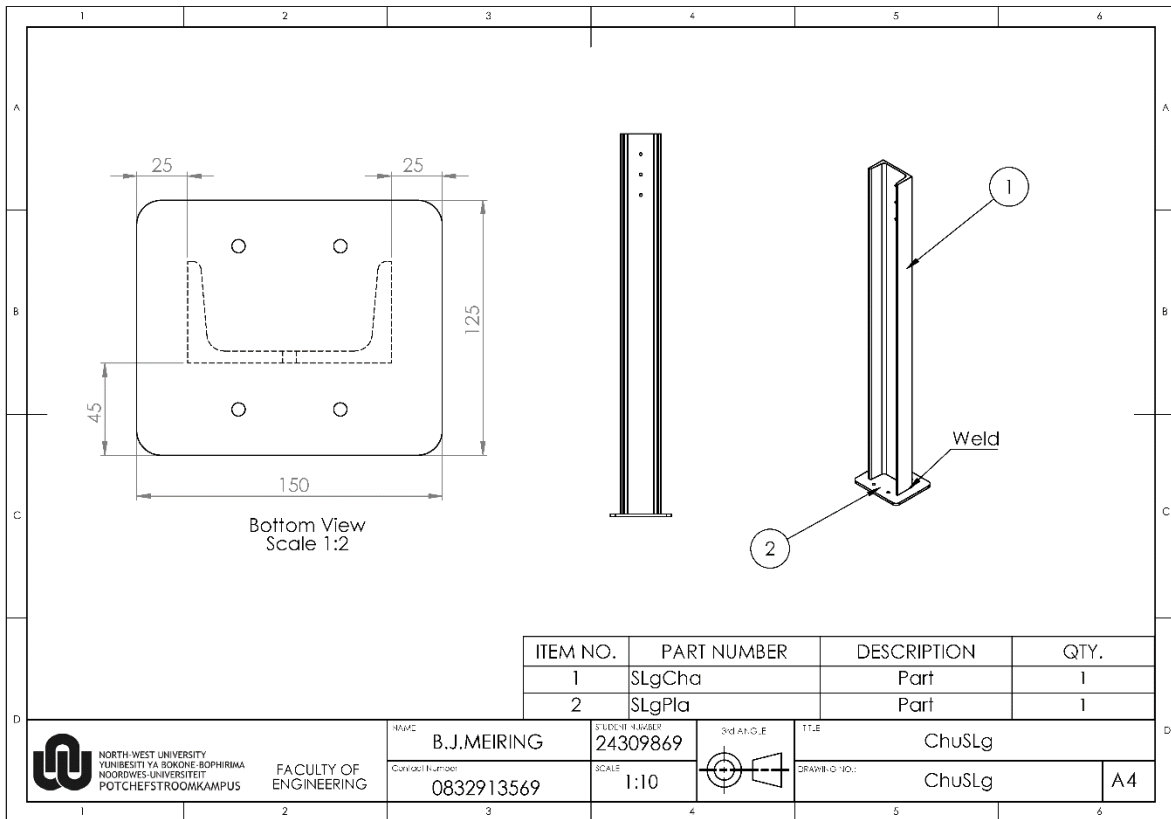
NAME: B.J.MEIRING
Contact Number: 0832913569

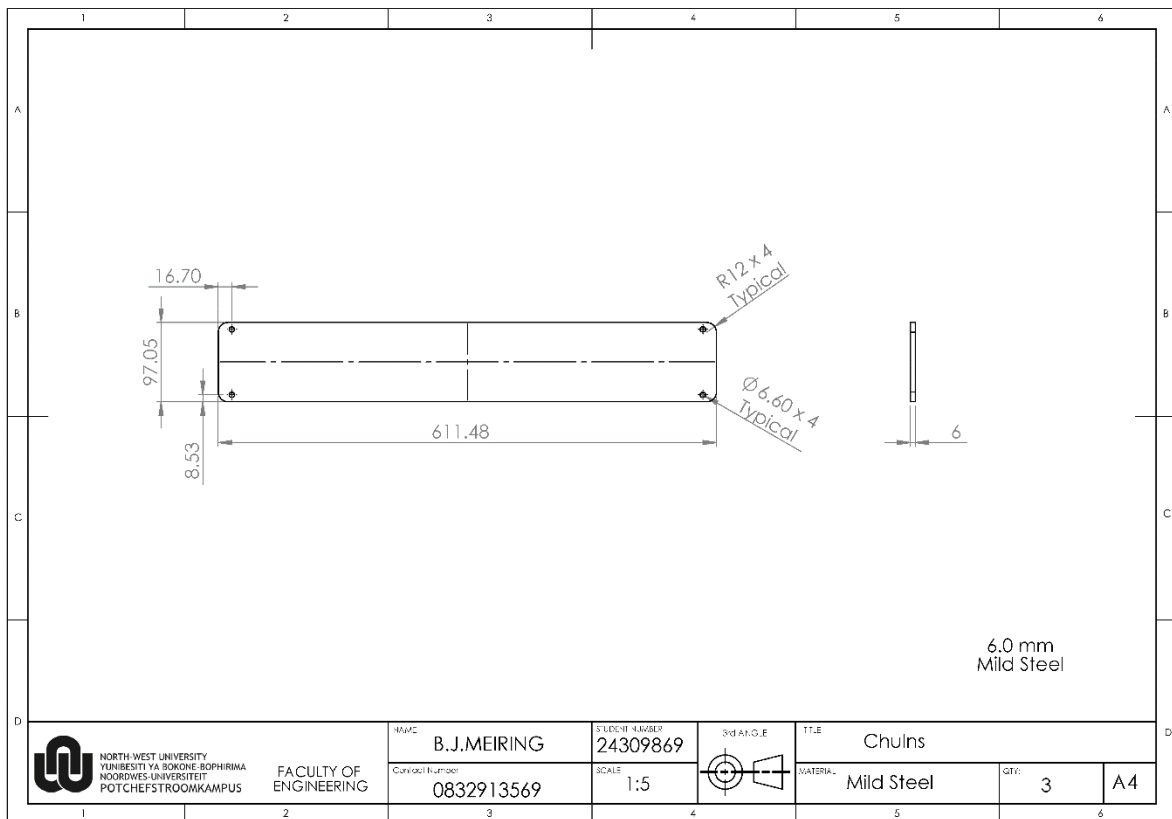
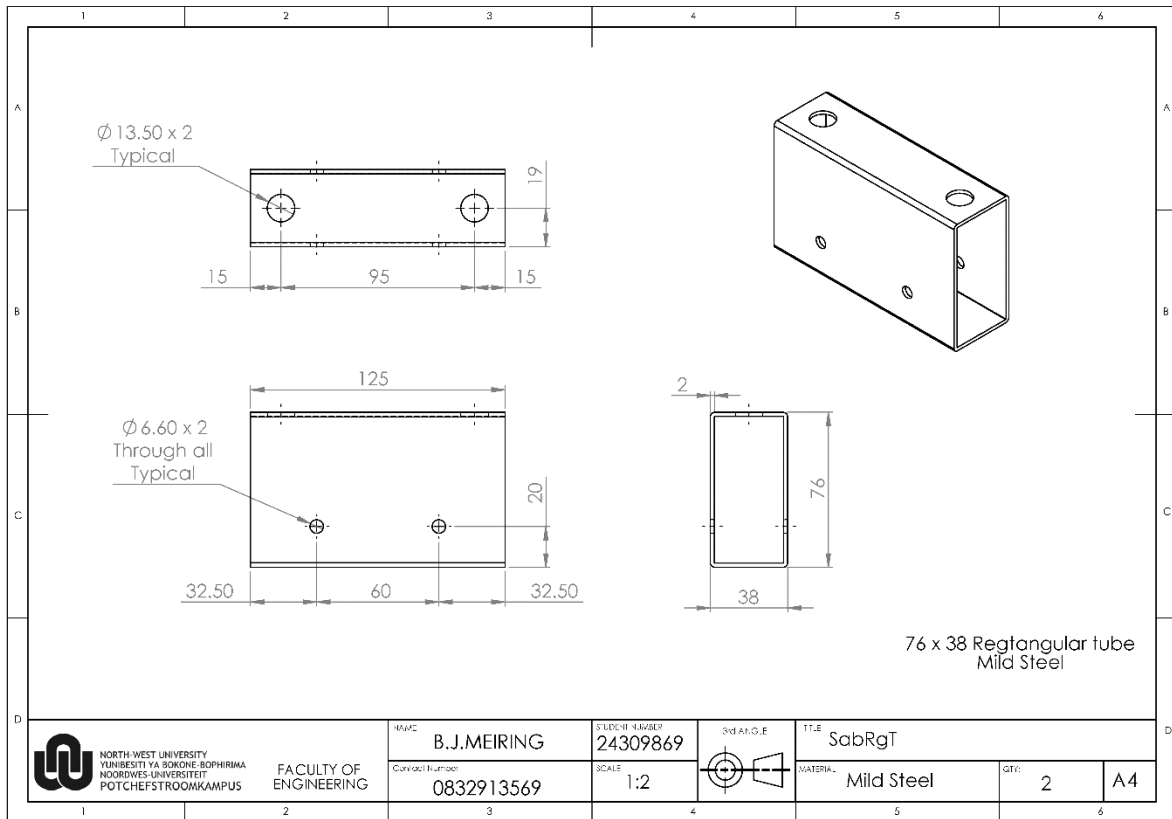
STUDENT NUMBER: 24309869
SCALE: 1:12

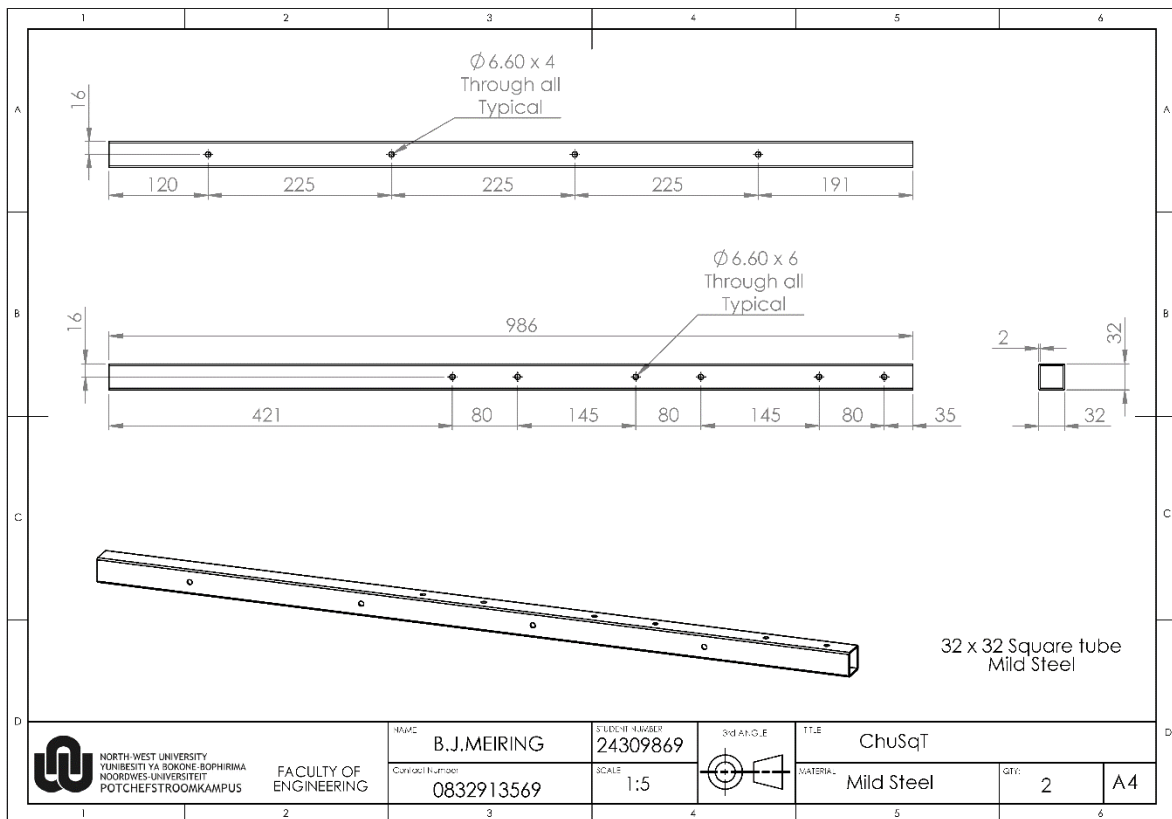
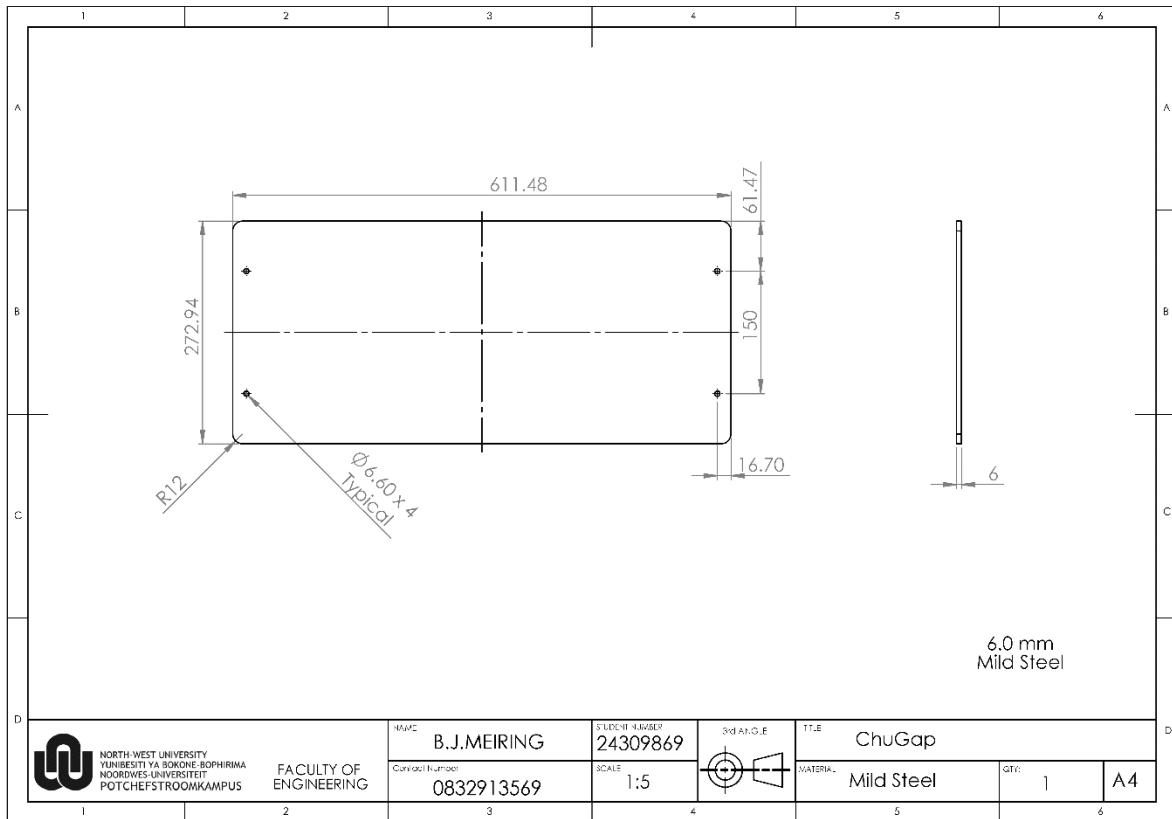


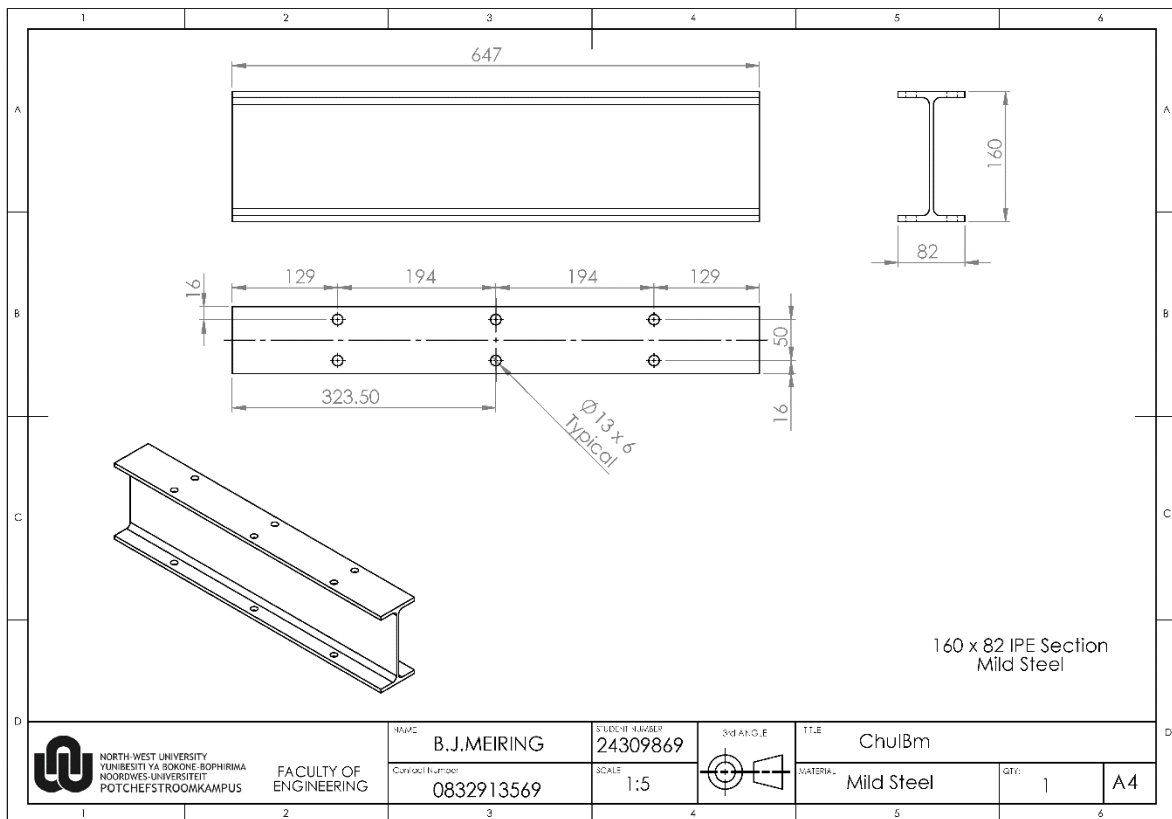
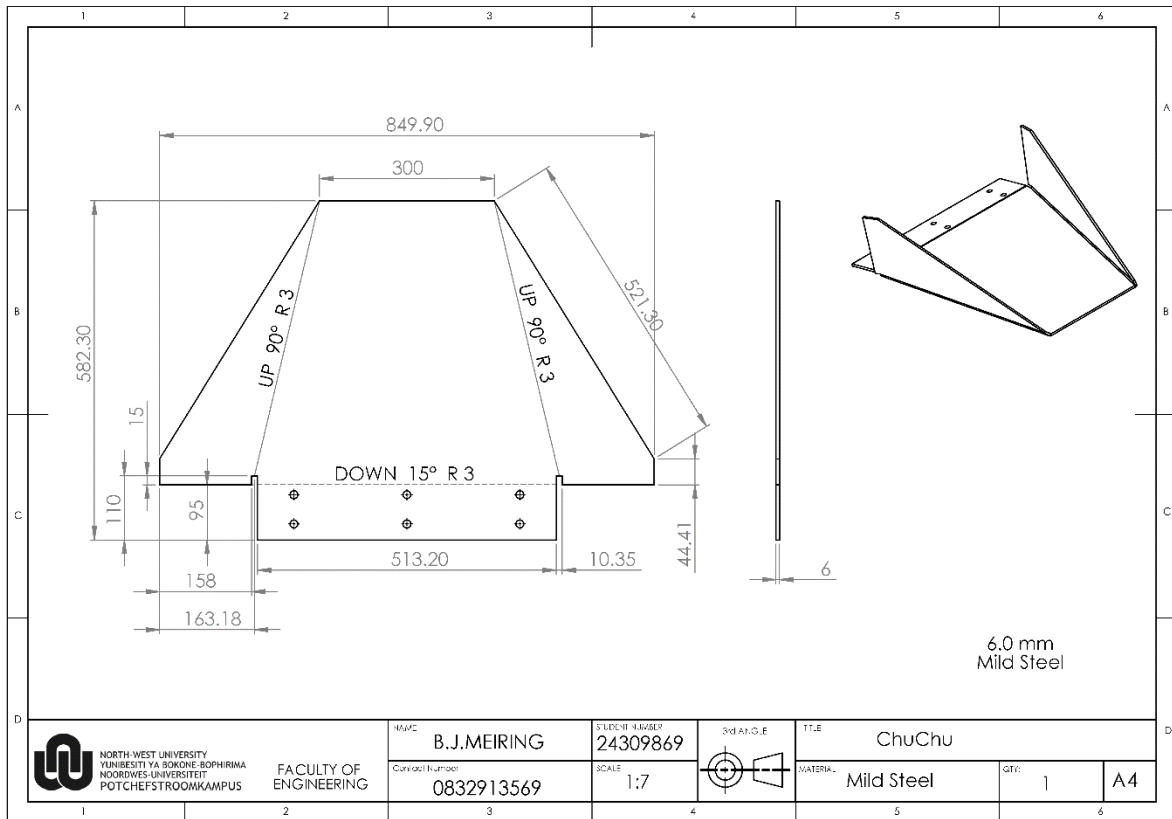
TITLE: ChuAsm
DRAWING NO.: ChuAsm7 | A4

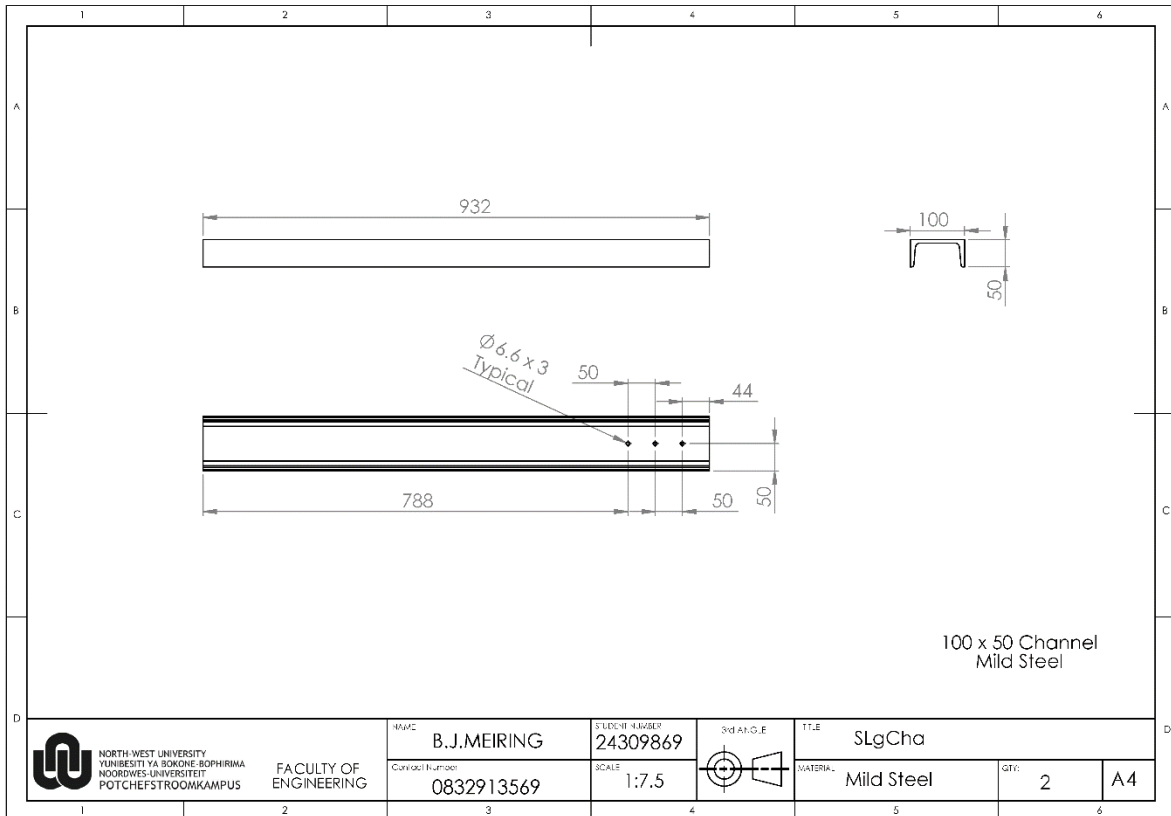
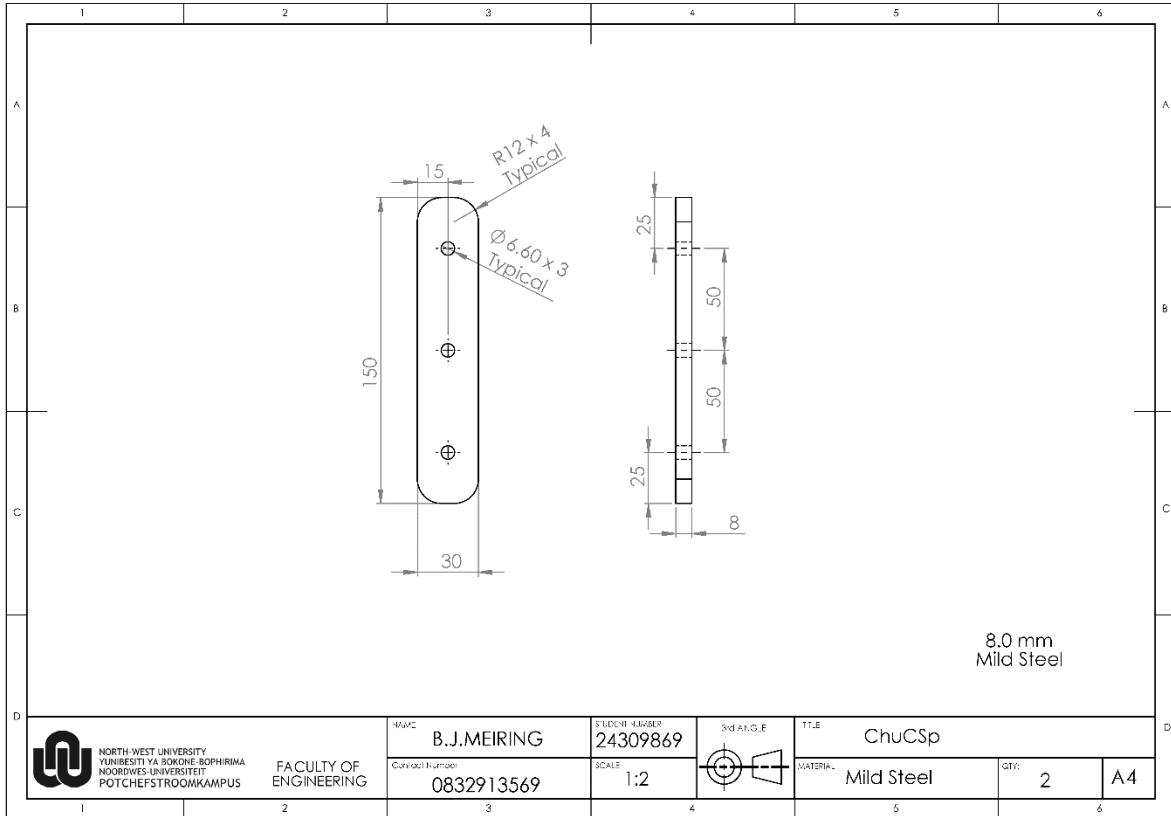


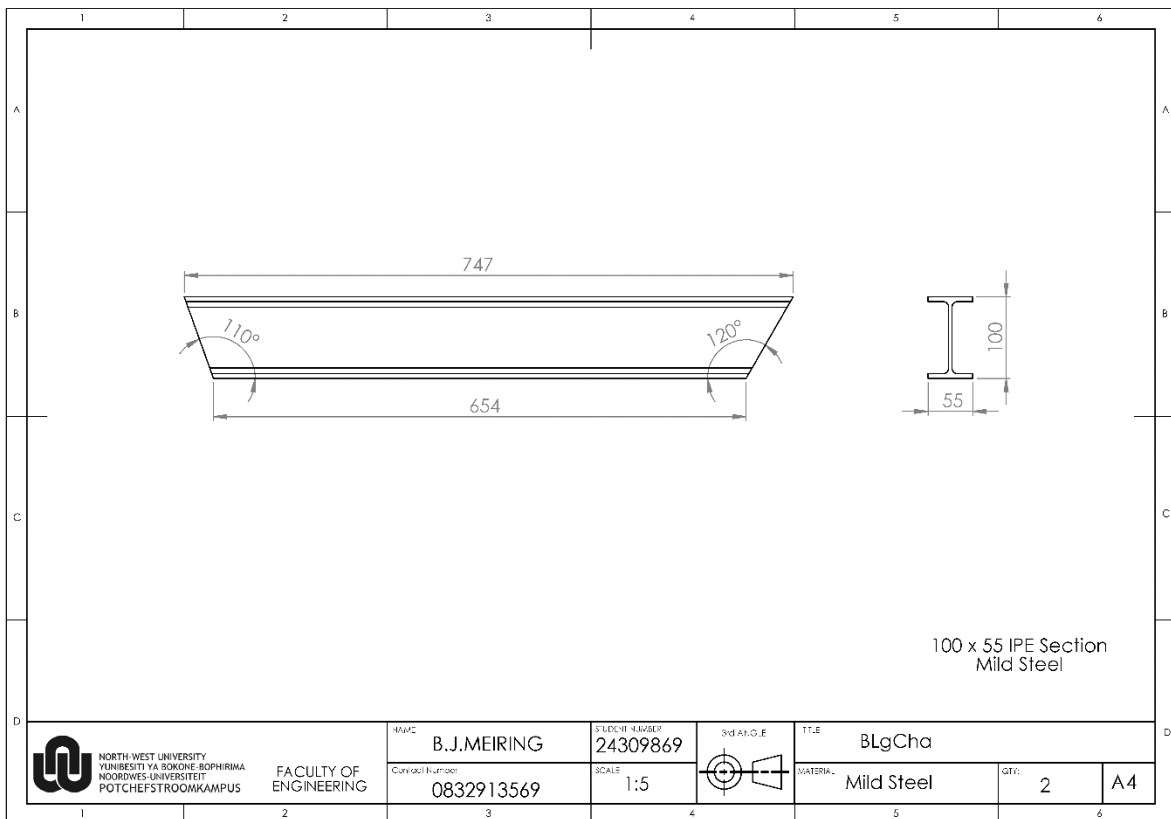
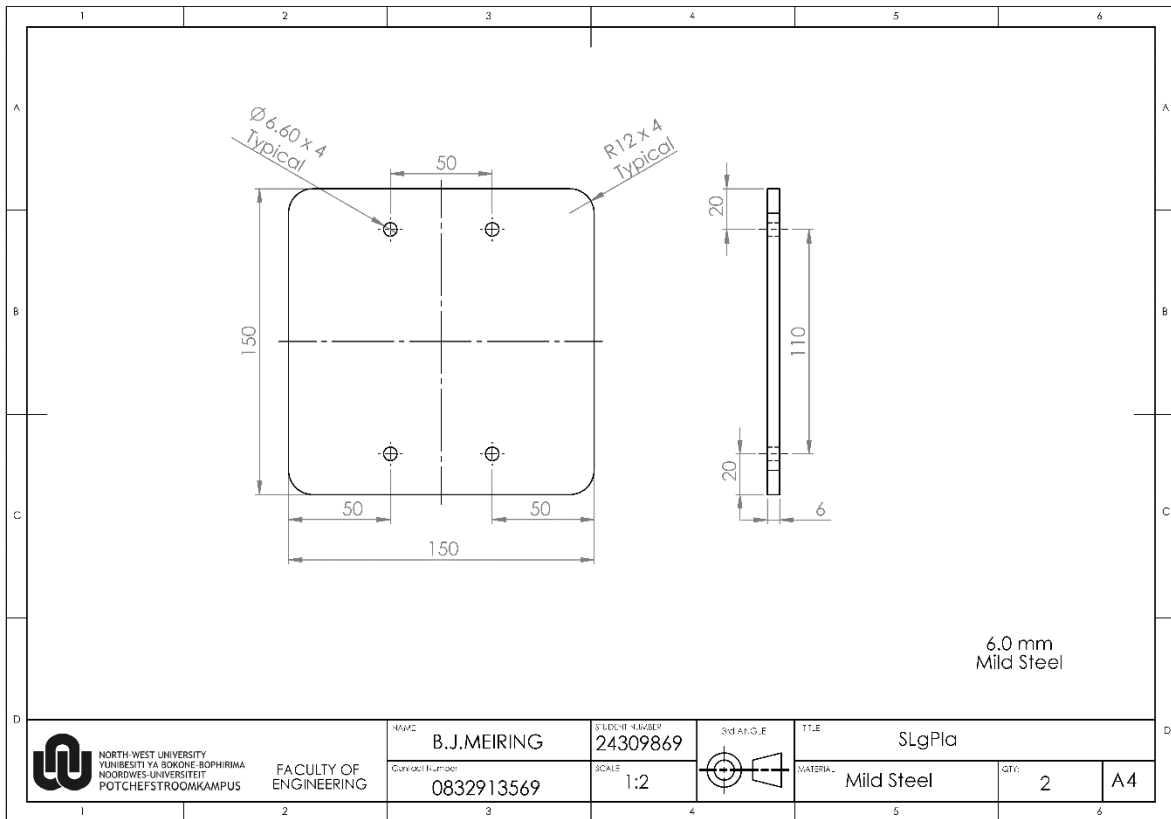


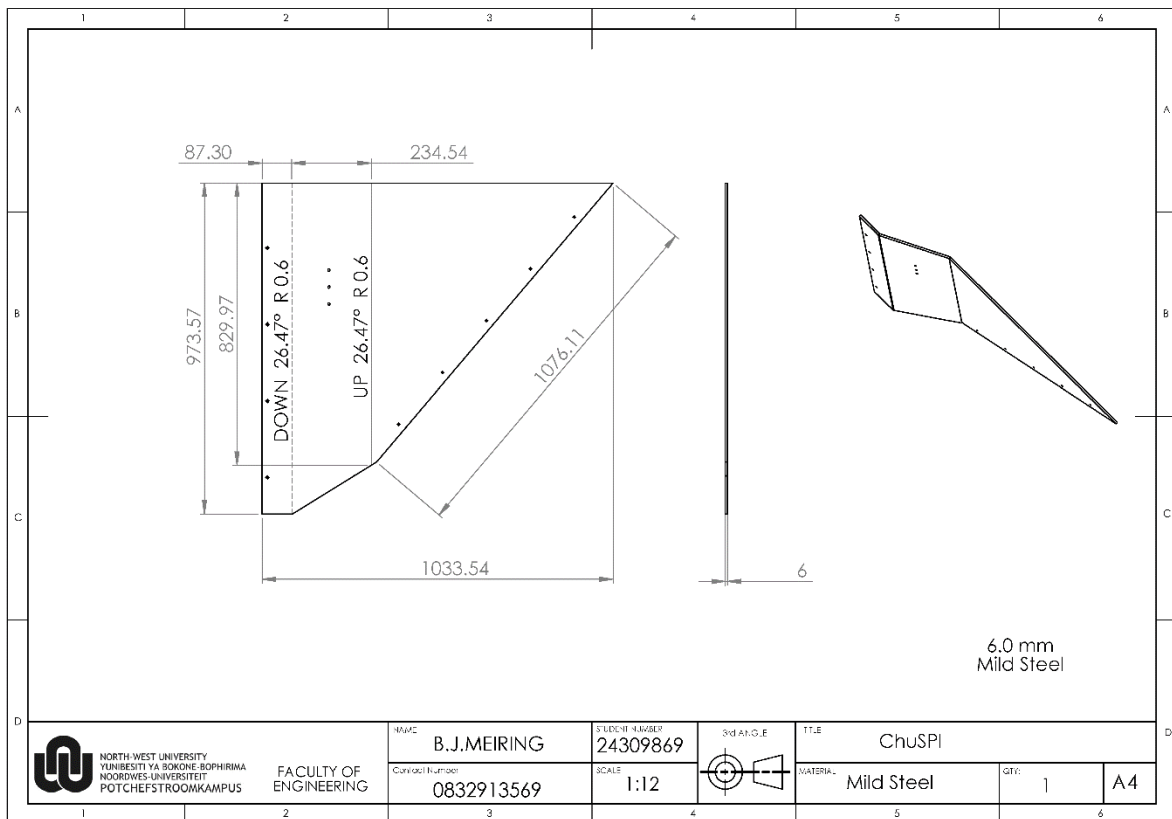
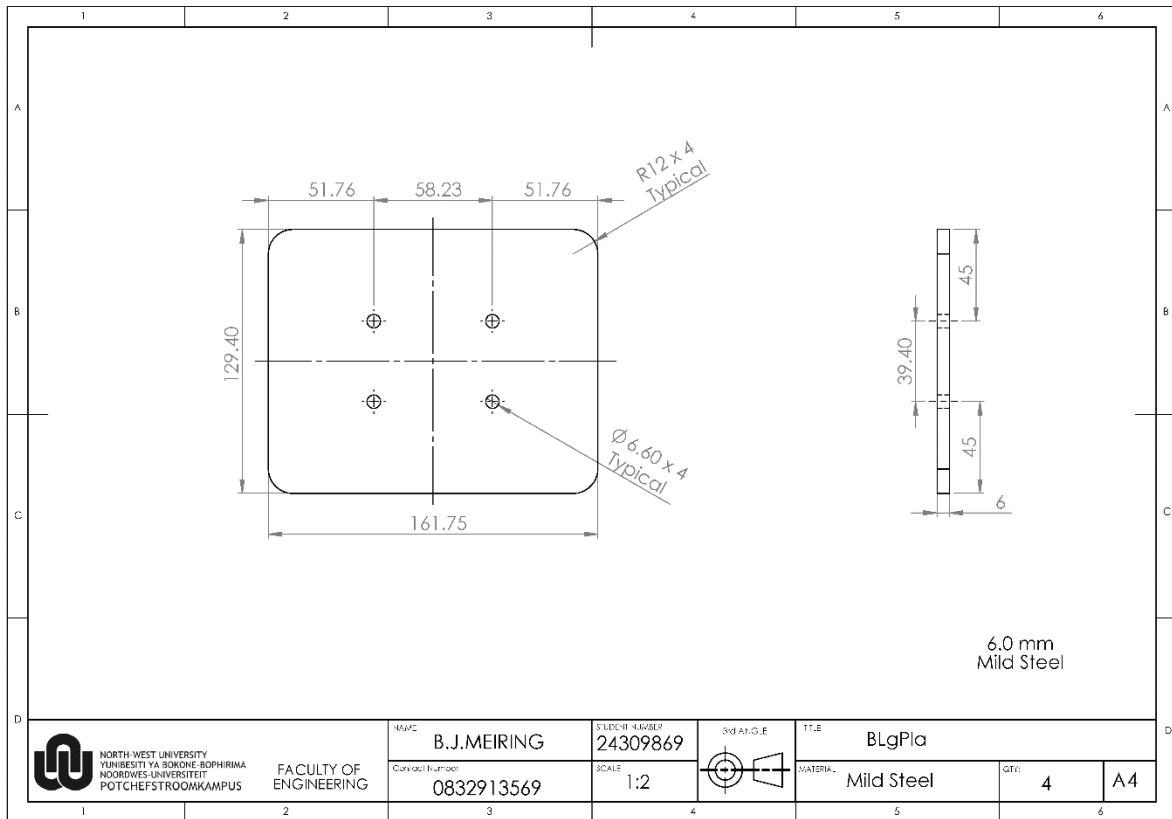


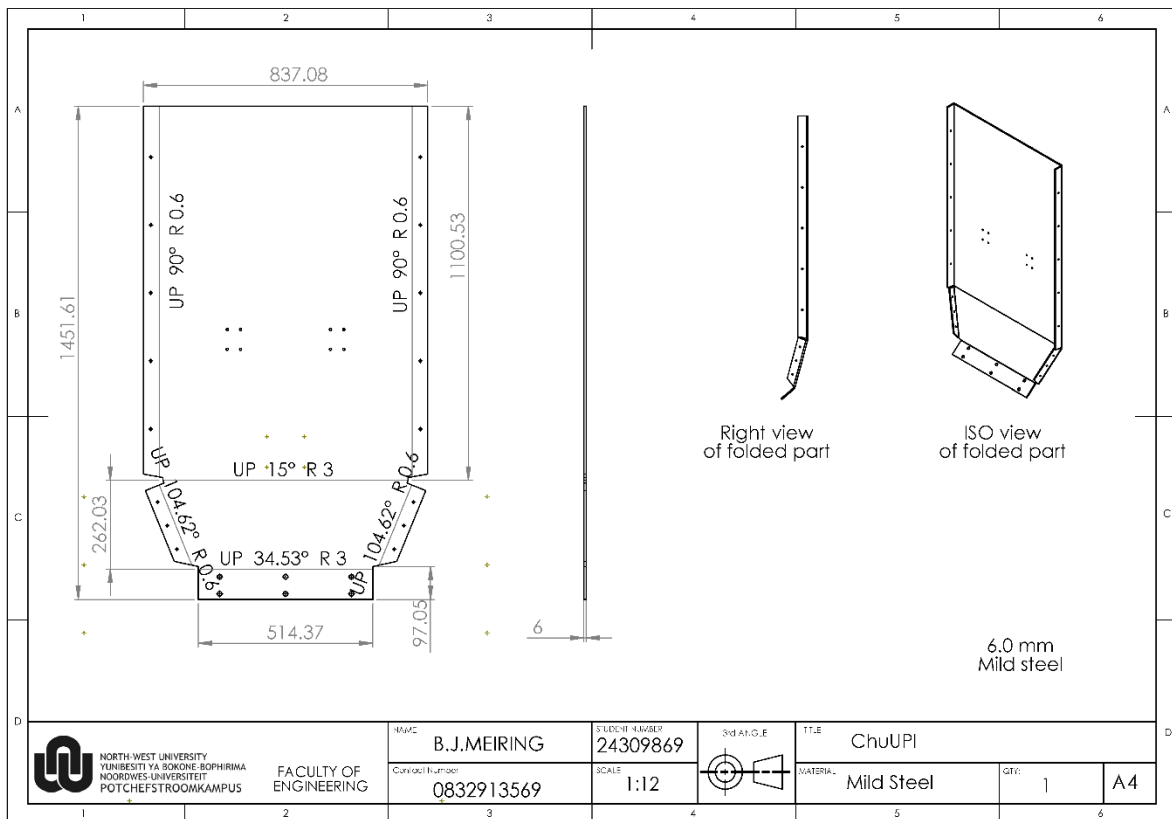
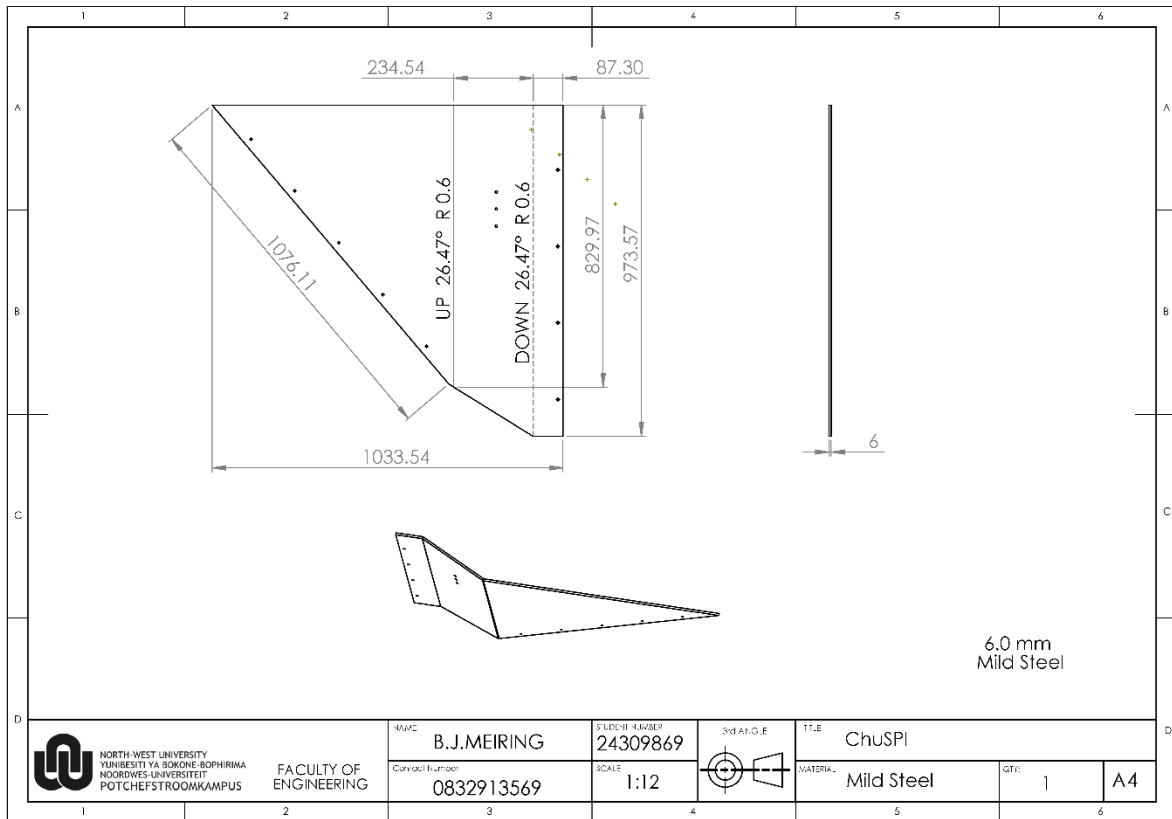












APPENDIX G – LANGUAGE EDITING DECLARATION

Christel Eastes
PO Box 21061
Noordbrug
2522
082 566 4229

25 May 2021

To whom it may concern:

DECLARATION: LANGUAGE EDITING

This letter serves as proof that the following document was submitted to the undersigned for language editing in May 2021:

Author: BJ (Barend) Meiring (24309869)

Document type: Dissertation submitted for the degree Magister in Mechanical Engineering at the North-West University.

Title: *Design and evaluation of a vibration ore flow restore machine.*

Final review comments and recommendations were communicated to the author on 25 May 2021.

Applying changes in order to arrive at a final, approved document remains the responsibility of the document author.

Yours sincerely


CHRISTEL EASTES
Potchefstroom